Aus der Abteilung
für Pädiatrische Hämatologie, Onkologie und Stammzelltransplantation
des Lehrstuhls für Kinder- und Jugendmedizin
Prof. Dr. Selim Corbacioglu
der Fakultät für Medizin
der Universität Regensburg

# Mechanism of the Multimodal Molecularly Targeted Therapy RIST in an *in Vitro* Model of Neuroblastoma

Inaugural – Dissertation
zur Erlangung des Doktorgrades
der Medizin

der
Fakultät für Medizin
der Universität Regensburg

vorgelegt von
Gina Penkivech

2024

Aus der Abteilung
für Pädiatrische Hämatologie, Onkologie und Stammzelltransplantation
des Lehrstuhls für Kinder- und Jugendmedizin
Prof. Dr. Selim Corbacioglu
der Fakultät für Medizin
der Universität Regensburg

# Mechanism of the Multimodal Molecularly Targeted Therapy RIST in an *in Vitro* Model of Neuroblastoma

Inaugural – Dissertation
zur Erlangung des Doktorgrades
der Medizin

der
Fakultät für Medizin
der Universität Regensburg

vorgelegt von
Gina Penkivech

2024

| | |
|---|---|
| Dekan: | Prof. Dr. Dirk Hellwig |
| 1. Berichterstatter: | Prof. Dr. Selim Corbacioglu |
| 2. Berichterstatter: | Prof. Dr. Tobias Pukrop |
| Tag der mündlichen Prüfung: | 23.01.2025 |

# Zusammenfassung

Das Neuroblastom ist der häufigste extrakranielle solide Tumor im Kindesalter. Die Prognose für Patienten mit refraktärem oder rezidiviertem Hochrisiko-Neuroblastom ist trotz intensiver multimodaler Therapieregime nach wie vor schlecht. Für intensiv vorbehandelte Patienten gibt es keine etablierten Therapieprotokolle für den Fall eines Rückfalls oder Therapieversagens, und es werden dringend neue therapeutische Optionen benötigt. Die multimodale, metronomisch angelegte RIST-Therapie kombiniert molekular zielgerichtete Medikamente (Rapamycin und Dasatinib) mit konventioneller Chemotherapie (Irinotecan und Temozolomid) und wurde in einer klinischen Phase-II-Studie (RIST-rNB-2011) untersucht. Die vielversprechenden Daten dieser klinischen Studie sind zum Zeitpunkt dieser Dissertation zur Veröffentlichung eingereicht worden. Ziel dieser Arbeit war es, in einem *in vitro* Modell des Neuroblastoms zu analysieren, ob eine MycN-Amplifikation zu einem Unterschied in der Ansprechbarkeit der RIST-Therapie führt. Zweitens zielte diese Arbeit darauf ab, ein tieferes Verständnis für die der RIST-Therapie zugrunde liegenden molekularen Mechanismen zu erlangen und bisher nicht bekannte therapierelevante Signalwege zu identifizieren.

In Apoptose-Assays mit Annexin V- und Propidiumiodid-Färbung und anschließender Fluorescence-Activated Cell Sorting-Analyse konnte gezeigt werden, dass RIST den programmierten Zelltod effizienter in MycN-amplifizierten (KELLY, LAN-5) als in MycN-nicht-amplifizierten (SK-N-SH, SK-N-AS) Neuroblastom-Zelllinien induziert. Durch RIST konnte in semiquantitativen Multiplex-Antikörper-Arrays, und basierend auf dem Status der Phosphorylierung definierter Zielproteine, eine erfolgreiche Hemmung von Schlüsselkomponenten innerhalb des PI3K/AKT/mTOR-Signalwegs sowie die Aktivierung von Tumorsuppressoren, wie der Phosphatase PTEN und der Proteinkinase GSK-3β, nachgewiesen werden. Weiterhin wurde durch RIST eine niedrigere Proteinexpression des molekularen Chaperons HSP60 und eine geringere Aktivierung des Tumor-fördernden Transkriptionsfaktors CREB sowie der Angiogenese-stimulierenden Proteinkinase WNK gezeigt. Diese Effekte der RIST-Therapie wurden insbesondere in MycN-amplifizierten Neuroblastom-Zelllinien im Vergleich zu MycN-nicht-amplifizierten Neuroblastom-Zelllinien deutlich, während die Hemmung der Src Kinase-Familie unabhängig vom MycN-Status zu sein scheint. Die hier vorgestellten Ergebnisse liefern wichtige Einblicke in die molekularen Mechanismen der RIST-Therapie und bilden die Grundlage für weitere Folgestudien zur dringend notwendigen Verbesserung der Therapie für Patienten mit refraktärem bzw. rezidiviertem Neuroblastom.

# Abstract

Neuroblastoma is the most common extracranial solid tumor of childhood, and the prognosis for patients with refractory or relapsed high-risk neuroblastoma remains dismal despite intensive multimodal therapy regimens. No established therapy protocols exist for heavily pre-treated patients in the case of relapse or treatment failure, and novel therapeutic options are urgently needed. The multimodal metronomically designed RIST therapy combines molecularly targeted drugs (rapamycin and dasatinib) with conventional chemotherapy (irinotecan and temozolomide) and has been evaluated in a clinical phase II trial (RIST-rNB-2011). The promising results of this trial have been submitted for publication at the time of this thesis publication. This study aimed to analyze whether the presence of a MycN amplification in neuroblastoma leads to a difference in responsiveness to the RIST therapy in an *in vitro* model of neuroblastoma. Secondly, this study aimed to gain a deeper understanding of the underlying molecular mechanisms and to identify previously unknown signaling pathways relevant to the RIST therapy.

RIST was shown to induce programmed cell death more efficiently in MycN-amplified (KELLY, LAN-5) than in MycN-non-amplified (SK-N-SH, SK-N-AS) neuroblastoma cell lines in apoptosis assays utilizing Annexin V- and propidium iodide staining followed by fluorescence-activated cell sorting analysis. In semiquantitative multiplex antibody arrays and based on the status of phosphorylation of defined target proteins, successful inhibition of key components within the PI3K/AKT/mTOR pathway, as well as activation of tumor suppressors, such as the phosphatase PTEN and the protein kinase GSK-3β, by RIST could be demonstrated. Furthermore, lower protein expression of the molecular chaperone HSP60 and lower activation of the tumor-promoting transcription factor CREB and the angiogenesis-stimulating protein kinase WNK were demonstrated after treatment with RIST. These effects of the RIST therapy were particularly evident in MycN-amplified neuroblastoma cell lines compared to MycN-non-amplified neuroblastoma cell lines. In contrast, inhibition of the Src kinase family appears to be independent of MycN status. The results presented here provide important insights into the molecular mechanisms of the RIST therapy and lay the groundwork for further follow-up studies urgently needed to improve therapy regimens for patients with refractory or relapsed high-risk neuroblastoma.

# I. Table of Contents

# II. Abbreviations

| | |
|---|---|
| 4E-BP1 | Eukaryotic translation initiation factor 4E-binding protein 1 |
| Abl | Ab elson murine leukemia viral oncogene homolog 1 |
| AKT (PKB) | Protein kinase B |
| ALK | Anaplastic lymphoma kinase |
| AMPK | 5' adenosine monophosphate-activated protein kinase |
| ATCC | American Type Culture Collection |
| AU | Arbitrary unit |
| AV | Annexin V |
| BCA | Bicinchoninic acid |
| Bcr-Abl | Philadelphia chromosome, fusion gene of Abelson Murine Leukemia Viral Oncogene Homolog 1 (ABL, chromosome 22) and breakpoint cluster region (BCR, chromosome 9) |
| BET | Bromodomain and extra-terminal motif |
| CAR-T cell | Chimeric antigen receptor T cell |
| CBP | CREB binding protein |
| CML | Chronic myeloid leukemia |
| CREB | Cyclic AMP response element-binding protein |
| CRISPR/Cas9 | Clustered Regularly Interspaced Short Palindromic Repeats/ Cas9 |
| CSC | Cancer stem cell |
| D | Dasatinib |
| DDX1 | Dead box helicase 1 |
| DMSO | Dimethyl sulfoxide |
| DNA | Deoxyribonucleic acid |
| DSMZ | Deutsche Sammlung von Mikroorganismen und Zellkulturen |
| ECACC | European Collection of Authenticated Cell Cultures |
| EDTA | Ethylenediaminetetraacetic acid |
| eIF4E | Eukaryotic translation initiation factor 4E |
| EMEM | Eagle's Minimal Essential Medium |
| ERK | Extracellular signal-regulated kinase |
| FACS | Fluorescence-activated cell sorting |
| FBS | Fetal bovine serum |
| FITC | Fluorescein isothiocyanate |
| FKBP | FK binding protein |
| FSC | Forward scatter |
| GD2 | Disialoganglioside GD2 |
| GPCR | G protein-coupled receptor |
| Grb2 | Growth factor receptor-bound protein 2 |
| GSK-3β | Glycogen synthase kinase 3β |
| HSP | Heat shock protein |
| I | Irinotecan |
| IAP | Inhibitor of apoptosis |
| $IC_{50}$ | Half-maximal inhibitory concentration |

| | |
|---|---|
| INRG | International Neuroblastoma Risk Group |
| INRGSS | International Neuroblastoma Risk Group Staging System |
| IRS-1 | Insulin receptor substrate 1 |
| ITT | Intention to treat |
| LOH | Loss of heterozygosity |
| MAPK | Mitogen-activated protein kinase |
| MNA | MycN-amplified |
| MNN | MycN-non-amplified |
| MSK | Mitogen-and stress-activated protein kinase |
| MTD | Maximum tolerated dose |
| MTIC | 5-(3-methyltriazen-1-yl) imidazole-4-carboxamide |
| mTOR | Mammalian target of rapamycin |
| mTORC 1/2 | Mammalian target of rapamycin complex 1/2 |
| NB | Neuroblastoma |
| NRAS | Neuroblastoma RAS viral oncogene homolog |
| NSCLC | Non-small-cell lung cancer |
| OS | Overall survival |
| PARP | Poly (ADP)-ribose polymerase |
| PBS | Phosphate-buffered saline |
| PCR | Polymerase chain reaction |
| PDK-1 | 3-phosphoinositide-dependent protein kinase-1 |
| Pen/Strep | Penicillin/ streptomycin |
| PFS | Progress-free survival |
| PI | Propidium iodide |
| PI3K | Phosphatidylinositol 3-kinase |
| $PIP_2$ | Phosphatidylinositol (4,5)-biphosphate |
| $PIP_3$ | Phosphatidylinositol (3,4,5)-triphosphate |
| PKA | Protein kinase A |
| PLK1 | Polo-like kinase 1 |
| PP | Per protocol |
| PP2A | Protein phosphatase 2A |
| PS | Phospholipid phosphatidylserines |
| PTEN | Phosphatase and tensin homolog |
| PTPN11 | Tyrosine-protein phosphatase non-receptor type 11 |
| R | Rapamycin |
| Raf | Rapidly accelerated fibrosarcoma |
| RAPTOR | Regulatory-associated protein of mTOR |
| Ras | Rat sarcoma protein |
| RHEB | Ras homolog enriched in brain |
| RICTOR | Rapamycin insensitive companion of mTOR |
| RIST therapy | Combinatorial therapy consisting of Rapamune® (rapamycin), Irinomedac® (irinotecan), Sprycel® (dasatinib), and Temomedac® (temozolomide) |
| RNA | Ribonucleic acid |
| ROS | Reactive oxygen species |
| RPMI | Roswell Park Memorial Institute medium 1640 |
| rpS6 | S6 Ribosomal protein |

| | |
|---|---|
| RSK | Ribosomal S6 kinase |
| RTK | Receptor tyrosine kinase |
| S6K1/2 | Ribosomal p70 S6 kinase 1/2 |
| SD | Standard deviation |
| Ser | Serine |
| SFK | Src family kinase |
| Src | Sarcoma kinase |
| SSC | Side scatter |
| T | Temozolomide |
| T-ALL | T-cell acute lymphoblastic leukemia |
| Thr | Threonine |
| TKI | Tyrosine kinase inhibitor |
| Tris-Buffer | Tris(hydroxymethyl)aminomethane buffer |
| TSC1/2 | Tuberous sclerosis 1/2 |
| TSC1-TSC2 | Tuberous sclerosis 1 and tuberous sclerosis 2 complex |
| Tyr | Tyrosine |
| WNK | With no lysine kinase |

# III. Figures

# IV. Tables

# 1. Introduction

## 1.1.Neuroblastoma

Neuroblastoma (NB) is an embryonal tumor derived from peripheral sympathetic nervous system precursor cells (1, 2). It is the most common extracranial solid tumor of childhood, accounting for approximately 6 to 10 % of pediatric malignancies with a predominant occurrence in infancy (3-6). It is also the most commonly fatal extracranial pediatric solid tumor (2). While overall long-term survival is nearly 80 %, patients with advanced disease (stage IV) have a substantially worse prognosis (5, 7). The median age at diagnosis is 19 months (1, 8). Almost half of the primary tumors arise in the adrenal gland, while others are found in the paraspinal ganglia in the abdomen, chest, or pelvic area (2, 4, 9). It is a heterogeneous tumor, and the exact etiology of NB is unknown. No consistent underlying environmental exposure or genetic abnormality has yet been identified; however, subsets of NB are frequently associated with gene alterations such as MycN amplification or segmental chromosome alterations (1, 8). NB mainly occurs sporadically. Only 1-2 % of all NB patients account for familial disease (5, 8). Germline mutations of the anaplastic lymphoma kinase (ALK) gene are detectable in a large proportion of familial NB and approximately 8 % of primary NB (10, 11). The disease spectrum ranges from complete tumor regression in a subset of NB with a unique metastatic pattern in infants (stage IVS) with minimal or no therapy (12, 13) to markedly metastatic, aggressive tumors with poor prognosis despite intensive multimodal therapy in older children (>12-18 months of age) (1, 2, 9). About half of all patients present with distant metastasis at the time of diagnosis (8, 9). These most commonly involve the bone marrow, bone, lymph nodes, and liver (8, 9). Symptoms of NB vary greatly depending on the location and extent of the disease, ranging from completely asymptomatic to severe symptoms such as organ dysfunction or paraplegia due to paraspinal location (8, 9).

Patients with NB are stratified into four risk groups according to the International Neuroblastoma Risk Group (INRG) classification system (very low, low, intermediate, and high-risk) based on several clinical and molecular features (14). These include disease stage as defined by the International Neuroblastoma Risk Group Staging System (INRGSS) (15), age at diagnosis, tumor pathology, MycN status, 11q aberration, and DNA ploidy (14).

The clinical course and prognosis are primarily determined by genetic alterations, especially MycN amplification and 1p deletion (8, 16-18). MycN is a proto-oncogene located within the region 2p24, which encodes a transcription factor that plays a role in the expression of a wide array of human genes (8, 19) and is associated with a dysregulation of the PI3K/AKT/mTOR pathway (20). When MycN is overexpressed, it leads to the deregulation of growth and proliferation, promotes cell survival, angiogenesis, and metastasis, and inhibits immune surveillance (21, 22). The prevalence of MycN amplification is about 22 % in all NB (2, 8). Furthermore, MycN amplification is associated with advanced disease, rapid tumor progression, and poor outcome, even in patients with otherwise favorable markers (age < 18 months, lower stage of disease, absence of unbalanced translocations) (16, 17).

Other genetic alterations associated with advanced disease stage and poor prognosis include deletion of 1p, deletion of 11q, and unbalanced gain of 17q (2, 8). Deletion of 1p or loss of heterozygosity (LOH), meaning the loss of normal function of the allele of one gene in a cell in which the other allele was already inactivated, is most commonly attributed to region 1p36. It is found in up to 35 % of NB and is strongly associated with MycN amplification and poor prognosis (2, 18, 23). Deletion of 11q (11q23) is detected in up to 44 % of NB (2, 23-26) and inversely correlates with MycN amplification and 1p deletion but is still associated with other high-risk features such as advanced-stage disease (23, 24, 26). In addition, it is associated with decreased survival and might serve as a prognostic marker in clinically high-risk NB lacking MycN amplification (2, 23, 24). An unbalanced gain of 17q is also associated with high-risk NB and poor outcome, whereas whole chromosome gains are found in more favorable NB subtypes (25, 27, 28).

Nearly half of all patients present with high-risk NB (22). These patients undergo multimodal therapy, including conventional chemotherapy, radiotherapy, surgery, high-dose chemotherapy with autologous stem cell rescue, and immunotherapy (8, 29-32). Unfortunately, despite intensive treatment, 5-year survival rates for these patients remain below 50 % (14, 22), with a reported 5-year survival rate below 20 % if relapse occurs (33, 34). Furthermore, children who are treated for high-risk disease or relapse often suffer severe treatment-related side effects, such as sensorineural hearing loss, cardiac toxicity, infertility, and second neoplasms (35). At the same time, these therapies only show limited efficacy (36). Therefore, this patient group urgently needs new therapeutic approaches that improve the prognosis and survival while not impairing quality of life. Knowledge of the underlying pathological mechanisms and aberrant tumor-specific pathways in recent years has led to the development of targeted therapies, such

as tyrosine kinase inhibitors (TKIs), inhibitors of the PI3K/AKT/mTOR pathway, and immunotherapy utilizing anti-GD2-antibodies (21, 22, 36). Chimeric antigen receptor (CAR)-T cell-based therapies are also currently being investigated (22, 36). Compared to conventional chemotherapy drugs that target all rapidly dividing cells, including healthy tissues, these targeted therapy approaches are thought to act specifically on defined individual components of the aberrantly activated signaling cascades. Thereby specific interventions can be made in the tumor metabolism, intending to make therapy more effective and tolerable. One of these new therapeutic approaches is the RIST therapy (37). Below, pathways, drugs, and rationale for the RIST therapy design are outlined.

## 1.2.The PI3K/AKT/mTOR Pathway

While many mutations and genetic aberrations are responsible for cancer development, most driver mutations leading to cancer development are associated with only a handful of signaling pathways (38). Two main pathways associated with aberrant cell survival are the PI3K/AKT/mTOR pathway and the MAPK/ERK pathway (38).

The phosphatidylinositol 3-kinase (PI3K)/ protein kinase B (AKT)/ mammalian target of rapamycin (mTOR) signaling pathway plays a crucial role in regulating cellular functions, cancer development, and progression. It is involved in regulating cell growth, survival, metabolism, and angiogenesis (39-41). Furthermore, dysregulation and aberrant activation of the PI3K/AKT/mTOR pathway contribute to cancer development (40, 41) as well as (primary, adaptive, and acquired) resistance to anticancer therapy (40). *Figure 1* outlines significant steps within the PI3K/AKT/mTOR pathway.

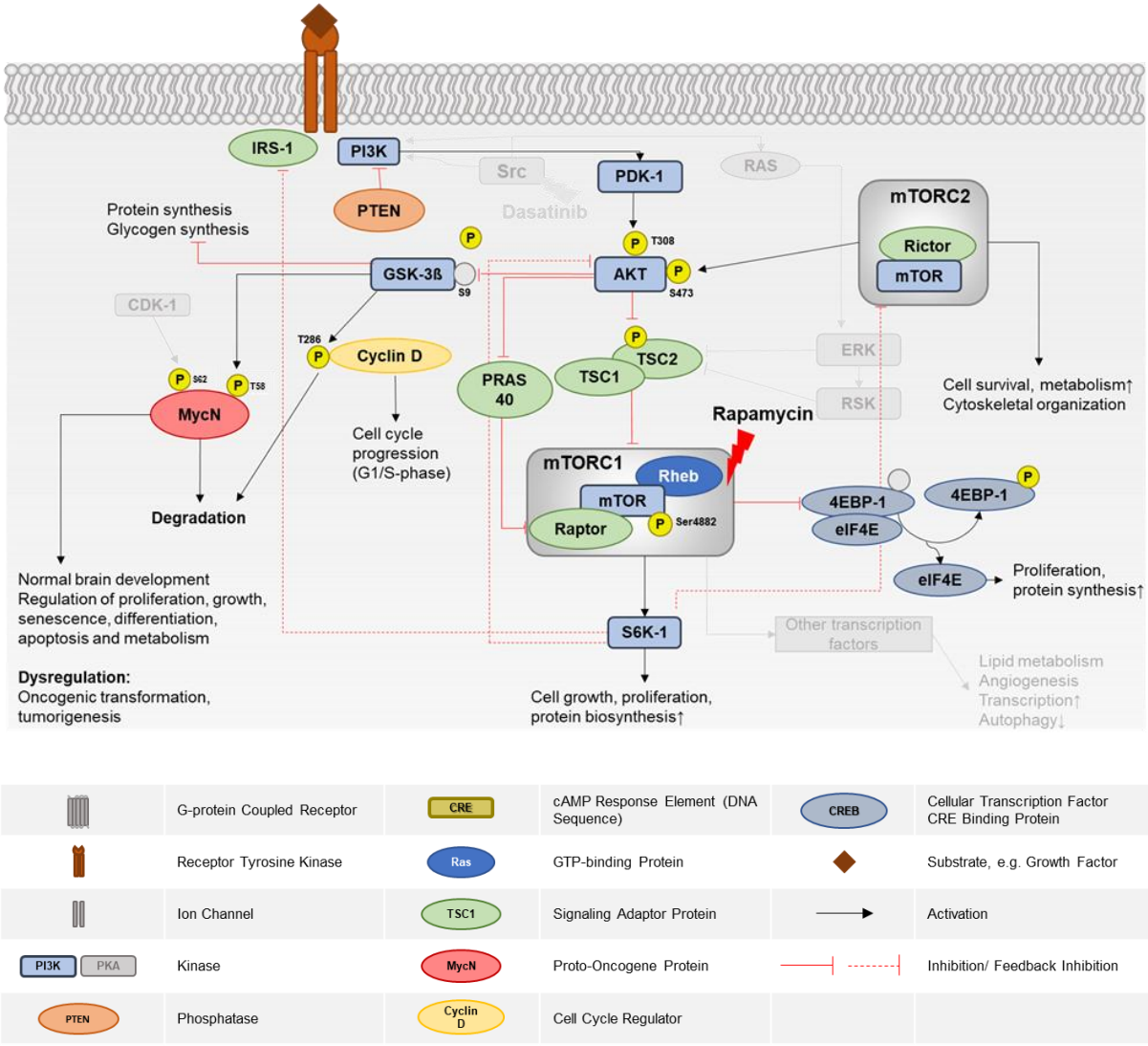


**Figure 1: PI3K/AKT/mTOR Pathway *(based on 42, 43-47)***

Illustration showing the relevant targets and mechanisms that are primarily affected by the pre-treatment rapamycin (R) within the RIST therapy.
Various ligands such as growth factors activate receptors on the cell surface (tyrosine kinase receptors, RTKs) and phosphatidylinositol 3-kinase (PI3K) is activated. PI3K converts phosphatidylinositol (4,5)-biphosphate ($PIP_2$) to phosphatidylinositol (3,4,5)-triphosphate ($PIP_3$) which recruits 3-phosphoinositide-dependent protein kinase-1 (PDK-1) and protein kinase B (AKT/ PKB). Phosphatase and tensin homolog (PTEN) negatively regulates the pathway by conversion of $PIP_2$ to $PIP_3$. AKT inhibits the tuberous sclerosis protein complex 1/2 (TSC complex 1/2) and proline-rich AKT substrate of 40 kDa (PRAS40), thereby disinhibiting the mammalian target of rapamycin complex 1 (mTORC1). mTORC1 in turn activates ribosomal protein S6 kinase (S6K1) and inhibits the eukaryotic translation initiation factor 4E-binding protein 1 (4EBP-1) by phosphorylation, thus releasing the eukaryotic translation initiation factor 4E (eIF4E). These events lead to translation initiation, protein biosynthesis, cell growth, and proliferation. The glycogen synthase kinase-3 beta (GSK-3β) phosphorylates the MyN proto-oncogene protein and Cyclin D, marking them for degradation. GSK-3β is inhibited by AKT via phosphorylation, leading to cell cycle progression and MycN stabilization. The pathway is regulated via several feedback loops (represented by dotted lines). The MAPK/ERK pathway can be triggered by several RTKs that are activated by growth factors and can activate the PI3K pathway directly or indirectly.
CDK-1: cyclin-dependent kinase 1, ERK: extracellular signal-regulated kinase, IRS-1: insulin receptor substrate 1, MAPK: mitogen-activated protein kinase, mTOR: mammalian target of rapamycin, mTORC1/2: mammalian target of rapamycin complex 1/2, Ras: rat sarcoma virus GTPase, Raptor: regulatory-associated protein of mTOR, Rheb: Ras homolog enriched in brain, Rictor: rapamycin-insensitive companion of mammalian target of rapamycin, RSK: ribosomal S6 kinase (p90-S6K), Src: sarcoma kinase.

Under physiologic conditions, PI3K is activated by various extracellular stimuli, including growth factors, certain hormones, or cytokines (39). PI3K catalyzes the phosphorylation of phosphatidylinositol (4,5)-biphosphate ($PIP_2$) to phosphatidylinositol (3,4,5)-triphosphate ($PIP_3$), a second messenger, that recruits a variety of lipid-binding domains of downstream targets, including AKT and 3-phosphoinositide-dependent protein kinase-1 (PDK-1) to the cell membrane (39-41, 48). The phosphatase and tensin homolog (PTEN) negatively regulates the activation of the PI3K/AKT/mTOR pathway by dephosphorylating $PIP_3$ to $PIP_2$, thus preventing the activation of downstream targets (39-41, 48).

AKT is the main target of PI3K and is phosphorylated at threonine 308 (Thr308) by PDK-1 (39, 41, 48). Additional phosphorylation at serine 473 (Ser473) by mammalian target of rapamycin complex 2 (mTORC2) is necessary to fully activate AKT (39, 41). Upon activation by mTORC2, AKT phosphorylates many downstream targets involved in but not limited to increased cell metabolism, cell cycle progression, cell proliferation, survival, and blockage of apoptosis (39). mTOR, therefore, functions as an activator of AKT via mTORC2-mediated phosphorylation of AKT Ser473 as well as a substrate to AKT via mTORC1 signaling (46). mTORC1 is viewed as the most important substrate in the downstream pathway of AKT (44) and will be the main focus in the section below.

The mTOR signaling cascade is a central regulator for cell growth, survival, protein biosynthesis, and cellular metabolism (43, 45, 46). Many other pathways converge into the mTOR signaling cascade or are tightly interconnected (43, 45). A wide array of signals, such as growth factors, nutrient supply, energy status, as well as stress signals, and hypoxia, are integrated through mTOR, subsequently triggering an appropriate cellular response, thereby balancing anabolic and catabolic processes in a cell in response to environmental conditions (45, 46, 49). In the absence of stress signals such as hypoxia, osmotic stress, heat shock, reactive oxygen species (ROS), or DNA damage (50), mTOR mediates the generation of proteins, lipids, and nucleotides by promoting anabolic processes in a nutrient-replete environment while turning off catabolic processes such as autophagy (45, 46, 49). On the contrary, in a nutrient-depleted environment, mTOR inhibits energy-intensive biosynthetic processes and upregulates autophagy (45, 46, 49), which is a self-degradation process by which proteins and cell organelles are recycled as an adaptive response to unfavorable conditions (51, 52). Therefore, it is crucial for cell survival and function and, when dysregulated, contributes to a wide array of diseases, including cancer (51, 52).

mTOR is a serine-threonine kinase and exists as a catalytic subunit of two complexes, mTOR complex 1 and 2 (mTORC1 and 2). mTORC 1 and 2 differ structurally, especially by their unique accessory proteins – regulatory-associated protein of mTOR (RAPTOR) in mTORC1 and rapamycin-insensitive companion of mTOR (RICTOR) in mTORC2 (45, 46, 49). The subunit composition distinguishes mTORC1 and 2 in their substrate specificity, functions, and their sensitivity to rapamycin (45, 46, 49). The key negative regulator of mTORC1 is the tuberous sclerosis 1 (TSC1) and tuberous sclerosis 2 (TSC2) complex (TSC1-TSC2) (45, 46, 49). Upon activation of the PI3K/AKT/mTOR pathway AKT phosphorylates and thereby inactivates TSC2 (49). Inhibition of TSC2 leads to disinhibition of the small G-protein Ras homolog enriched in brain (RHEB), which in turn activates mTORC1 (45, 46, 48, 49). Upon activation, mTORC1 phosphorylates ribosomal p70 S6 kinase 1/2 (S6K1/2) and, to a lesser extent, eukaryotic translation initiation factor 4E-binding protein 1 (4E-BP1) (47, 49, 53). To this date, S6K and 4E-BP1 are the primary known substrates downstream of mTOR (47, 49, 53).

Phosphorylation of 4E-BP1 releases eukaryotic translation initiation factor 4E (eIF4E), forming the eIF4E complex, thereby initiating translation (43, 45, 47, 49). Through phosphorylation (activation) of S6K1, mTOR regulates the translation of ribosomal proteins (43, 53). mTOR controls cell growth by promoting nucleotide and protein biosynthesis and activating the transcription of genes that encode various enzymes. In addition, by regulating proteins required for cell cycle progression, mTOR serves as a gatekeeper for progression from G1- to S-phase (43, 49).

Signals such as energy status and hypoxia also get integrated through mTORC1 in an AKT/TSC-dependent manner via 5’ adenosine monophosphate-activated protein kinase (AMPK) signaling (46, 49). In addition, through AKT/TSC complex-independent pathways, amino acids can activate mTOR via the Rag family of GTPases (46, 49).

Several negative feedback loops modulate mTOR function and the PI3K/AKT/mTOR pathway to maintain proper signaling via growth factors (see *Figure 1*). For example, S6K1 and mTORC1 mediate the downregulation of insulin receptor substrate 1 (IRS-1) by inducing its degradation and thus uncoupling the insulin receptor from PI3K and altering its location (46, 49, 54). S6K1 can also phosphorylate RICTOR, which may influence mTORC2 signaling to AKT, although its exact function remains inconclusive (55, 56). mTORC2 also limits PI3K

signaling by inducing the degradation of IRS-1 (46). Other feedback loops target growth factors or growth factor receptor-bound adaptors to limit growth factor signaling (46, 48).

Deregulation of the PI3K/AKT/mTOR pathway occurs in many human cancers (39, 44). Thus, its members present ideal targets for pharmaceutical intervention (39, 42, 44). Many components of the PI3K/AKT/mTOR signaling pathway, such as loss or inactivation of PTEN and other involved phosphatases, genetic alterations of PI3K, or mutations or amplifications of AKT, all lead to oncogenic activation of mTOR, promoting pro-survival and evasion of apoptosis, cell growth, enhanced proliferation drive, tumor progression as well as metabolic transformation (39, 42, 44). Several PI3K-, AKT-, and mTOR inhibitors have been developed and are tested in preclinical and clinical trials (42, 44).

The PI3K/AKT/mTOR pathway also plays a vital role in the development and progression of NB (41). *Opel et al.* show that AKT phosphorylation (p-AKT) as a surrogate for the activation of the PI3/AKT/mTOR pathway occurs in a large proportion of primary NB samples tested, indicating an activation of the PI3K/AKT/mTOR pathway *in vivo* (57). In these studies, activation of AKT also correlated with advanced disease stage, established negative prognostic factors such as MycN amplification, and was associated with poor outcome (57). *Iżycka-Świeszewska et al.* and *Johnsen et al.* also found evidence for the activation of the PI3K/AKT/mTOR pathway in almost all NB samples tested (58, 59).

Exactly how the PI3K/AKT/mTOR pathway is activated in NB remains mainly unclear (41). As described above, common mutations in adult cancers, such as loss of PTEN, rarely occur in NB (41). In a subset of NB, ALK mutations such as ALK F1174L lead to the overactivation of the PI3K/AKT/mTOR and MAPK/ERK pathways and potentiate the oncogenic activity of MycN (60). Activating ALK mutations are more common in advanced NB (61). Other receptor tyrosine kinases (RTKs) and their ligands have been implicated in playing a role in driving the overactivation of the PI3K/AKT/mTOR pathway as well (41, 57). While MycN itself contributes to the malignant behavior of NB by driving proliferation, angiogenesis, and self-renewal (20), the activated PI3K/AKT/mTOR pathway leads to the stabilization of MycN protein by negatively regulating glycogen synthase kinase 3β (GSK-3β) through inhibitory phosphorylation by AKT (19, 41, 48, 62) further contributing to the malignancy and progression of NB (41). Active GSK-3β phosphorylates MycN at Tyr58, marking it for degradation (19). Furthermore, mTORC1 also phosphorylates and thereby inhibits protein phosphatase 2A (PP2A), which enables the accumulation of active MycN (19).

While several therapeutical agents targeting the PI3K/AKT/mTOR pathway are being evaluated for use in NB treatment (20, 21, 36, 41, 63), targeting the transcription factor MycN directly proves difficult (20, 64, 65). Several studies have shown that inhibition of the PI3K/mTOR cascade can sensitize NB cells for chemotherapy-induced apoptosis (66), decrease angiogenesis (67), and PI3K/mTOR inhibitors themselves may cause apoptosis in NB (58, 62, 65, 68). *Schramm et al*. and others demonstrated that MycN-driven NB displayed activation of the mTOR pathway, suggesting mTOR inhibitors as a possible treatment option (58, 63, 64). Several studies show downregulation of MycN expression, MycN degradation, and NB growth inhibition *in vitro* and *in vivo* when treated with mTOR inhibitors (58, 62, 64, 65, 68). Furthermore, several of these studies displayed a greater sensitivity of MycN-amplified NB when treated with PI3K/mTOR inhibitors (58, 62, 64, 65, 68). Thus, MycN and the PI3K/mTOR pathway present attractive targets in treating high-risk NB (21, 63).

## 1.3. SRC Family Kinases and the MAPK/ERK Pathway

The mitogen-activated protein kinase (MAPK)/ extracellular signaling-regulated kinase (ERK) pathway plays a crucial role in cellular proliferation, differentiation, and survival (69). Aberrant regulation is common in many human types of cancers (69). Multiple stimuli, such as G-protein coupled receptor ligands or growth factors, activate the MAPK/ERK pathway (69). In a simplified model, as depicted in *Figure 2*, mitogens and growth factors bind to RTKs, leading to dimerization and assembly of a signaling complex (70, 71). Activated RTKs recruit kinases such as sarcoma kinase (Src) or PI3K, adaptor proteins such as growth factor receptor-bound protein 2 (Grb2), and docking proteins necessary for activating effector cascades (71). These events ultimately lead to the activation of the GTPase rat sarcoma virus GTPase (Ras) (69, 71, 72), which subsequently activates the rapidly accelerated fibrosarcoma protein kinase (Raf), a serine/threonine protein kinase (69, 71, 72).

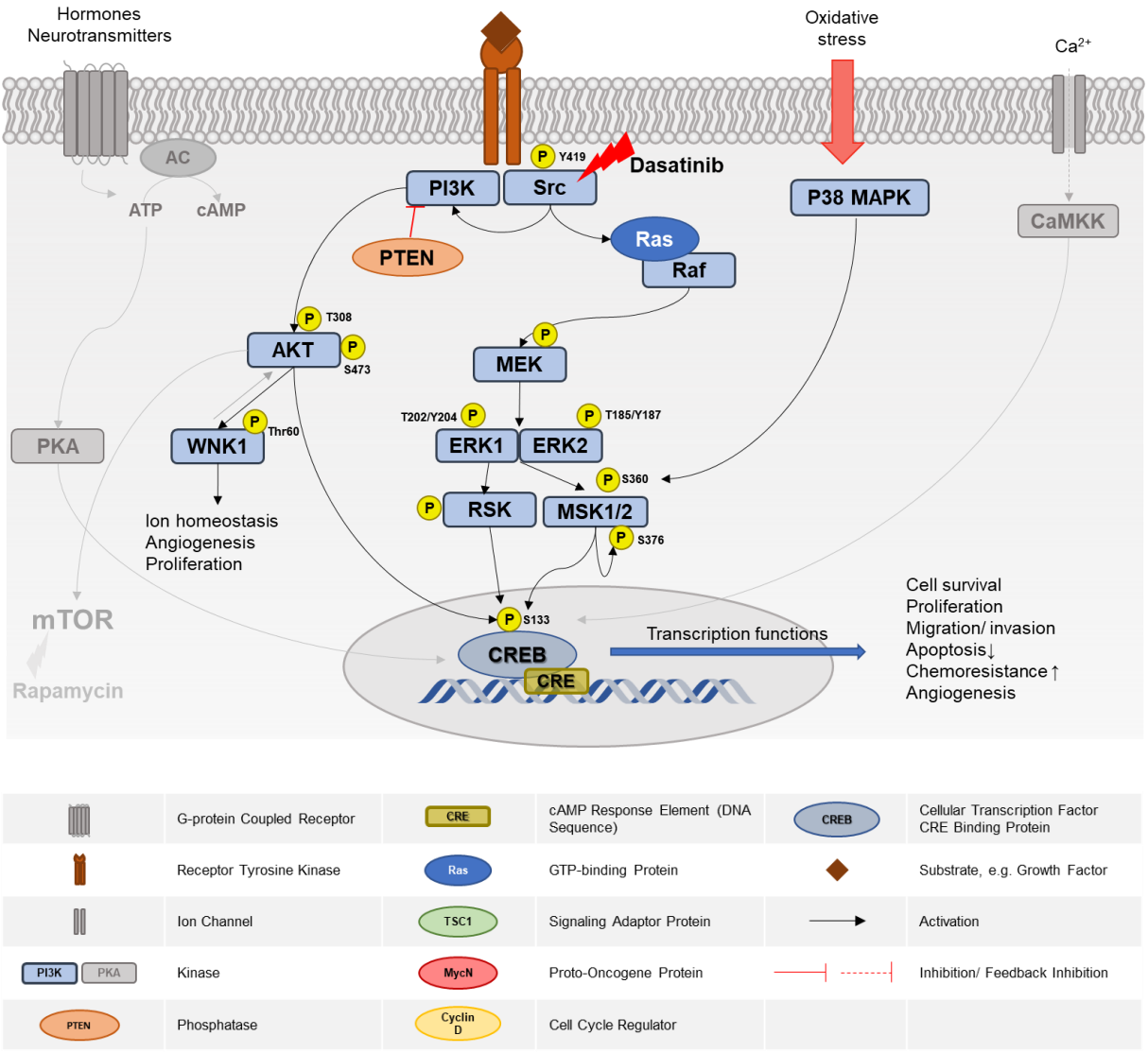


**Figure 2: MAPK/ERK Pathway (based on 73, 74, 75)**

Illustration showing the relevant targets and mechanisms that are affected by the pre-treatment dasatinib (D) within the RIST therapy.
Various ligands such as growth factors can bind to membrane-bound receptors such as receptor tyrosine kinases (RTKs). Upon ligand binding, RTKs dimerize and subsequently activate several downstream signaling cascades such as the PI3K/AKT or the MAPK/ERK pathway. Activation of the MAPK/ERK pathway via ligand binding leads to a series of phosphorylation events downstream including the phosphorylation of the extracellular signal-regulated kinases 1 and 2 (ERK 1/2). ERK 1/2 in turn activate mitogen and stress-activated protein kinases 1 and 2 (MSK 1/2) and p90 ribosomal s6 kinase (RSK) which then phosphorylate and activate cAMP response element-binding protein (CREB). Phosphatidylinositol 3-kinase (PI3K) is also able to activate CREB upon growth factor activation via the recruitment of protein kinase B (AKT/ PKB). Activation of CREB promotes cell survival, proliferation, and angiogenesis. Other stimulus-dependent CREB kinases leading to its activation include protein kinase A (PKA) and $Ca^{2+}$/ calmodulin-dependent protein kinase kinases (CaMKKs). Several non-receptor tyrosine kinases, such as sarcoma kinase (Src) and Src family kinases (SFK) participate in RTK signaling. Activated Src interacts directly with several downstream molecules such as the rapidly accelerated fibrosarcoma protein kinase (Raf), thereby stimulating the MAPK/ERK pathway.
AC: adenylyl cyclase, ATP: adenosine triphosphate, cAMP: cyclic adenosine monophosphate, CRE: cAMP response element, CREB: cAMP response element-binding protein, MEK (MAPKK): mitogen-activated protein kinase kinase, mTOR: mammalian target of rapamycin, p38 MAPK: p38 mitogen-activated protein kinase, PTEN: phosphatase and tensin homolog; Src: sarcoma kinase, Ras: rat sarcoma virus GTPase.

A series of phosphorylation events downstream within the MAPK cascade leads to phosphorylation and activation of ERK1 (Thr202/Tyr204) and ERK2 (Thr185/Tyr187) (69,

76). ERK then positively regulates gene expression by directly or indirectly phosphorylating several cytosolic and nuclear targets such as kinases and transcription factors (69, 72, 76). For example, ERK phosphorylates cytosolic signaling proteins such as the ribosomal S6 kinase (RSK) family and a family of RSK-related kinases, the mitogen- and stress-activated protein kinases (MSKs) (76-78). MSK 1 and 2 can be activated by ERK or p38 via sequential phosphorylation (77, 78). RSK and MSK phosphorylate several transcription factors, such as cyclic AMP response element-binding protein (CREB) at serine 133 (Ser133) (77, 78). Several other transcription factors regulated directly or indirectly via ERK include Myc. Phosphorylation of Myc by ERK leads to its stabilization (79). ERK phosphorylates several upstream mediators in a negative feedback loop manner and induces gene expression of several phosphatases and proteins that interfere with Raf-mediated activation (72).

Phosphorylation of CREB at Ser133 is thought to be a critical residue, and when phosphorylated in a stimulus-inducible manner, facilitates the binding of the transcriptional coactivator CREB binding protein (CBP), together with other modifications and co-activator proteins, subsequently triggering gene expression (74, 75, 80). Phosphorylation of CREB at Ser 133 occurs via several signaling pathways such as through stimulation of G protein-coupled receptors (GPCRs) via protein kinase A (PKA), $Ca^{2+}$-mediated activation as well as through growth factor signaling via RTKs and the MAPK/ERK pathway as well as via AKT, as described above (74, 75). Activation of CREB and CREB family transcription factors are implicated in neuronal survival under physiological conditions as well as in response to stimuli such as oxidative stress or hypoxia (74). While CREB is vital for essential cellular functions such as cell proliferation and cell cycle, survival, angiogenesis, and DNA repair, increased CREB expression and activation is associated with tumor progression and drug resistance, and downregulation has been shown to inhibit cell proliferation and invasion as well as induce apoptosis (75).

Several non-receptor tyrosine kinases, such as Src and Src family kinases (SFKs), play a role in mediating signal transduction (81, 82), participate in the signaling of many RTKs (81-84), and have been implicated in various downstream signaling cascades (83). Activated Src interacts with the RTKs but may also interact directly with downstream molecules such as Raf (83, 85), thereby stimulating the MAPK/ERK pathway (69, 71).

Aberrant activation of non-receptor tyrosine kinases such as Src has been implicated in tumor development, progression, and metastasis in many types of cancer (81, 84, 86). Interaction of

Src with aberrantly expressed or mutated RTKs can lead to constitutively increased Src activity, promoting proliferation and survival via the MAPK/ERK pathway and the PI3K/AKT pathway (81, 87). Increased Src activity has also been demonstrated in NB (88, 89). Inhibition of Src, e.g., via dasatinib, has shown antitumoral activity in various cancers (81, 90, 91) alone and in combination with other targeted drugs (90).

There is extensive crosstalk between the PI3K/AKT/mTOR pathway and the MAPK/ERK pathway implicating cross-inhibition as well as cross-activation, which has been reviewed elsewhere (92, 93). Targeting only one pathway may facilitate drug resistance via these mechanisms. The pathways also converge on several signaling targets, promoting cell survival and proliferation, such as Myc (92). Co-inhibition of these pathways may prove more effective in reducing tumor growth and reducing the risk of the development of drug resistance (92, 93).

## 1.4.The RIST Therapy

The RIST therapy is a multimodal metronomic therapy combining the biologics rapamycin (®Rapamune, R) and dasatinib (®Sprycel, D) with the chemotherapeutic agents irinotecan (®Irinomedac, I) and temozolomide (®Temomedac, T) (37, 94, 95).

The RIST therapy has been tested in a clinical setting in a randomized, non-blinded phase II study led by Prof. Dr. Selim Corbacioglu (RIST-rNB-2011, Clinical Trial.gov Identifier: NCT001467986) (37) and the results are currently under evaluation and prepared for publication.

The study aims to find out whether a therapeutic effect can be achieved with a pre-treatment consisting of molecularly active drugs (biologics) and subsequent treatment with "mild" chemotherapy as part of a metronomic therapy approach (37). The study hypothesizes that a combinatorial therapy of the abovementioned agents is superior to conventional chemotherapy alone by targeting oncogenic survival pathways (95). *Figure 3* shows the targets of the drugs used.

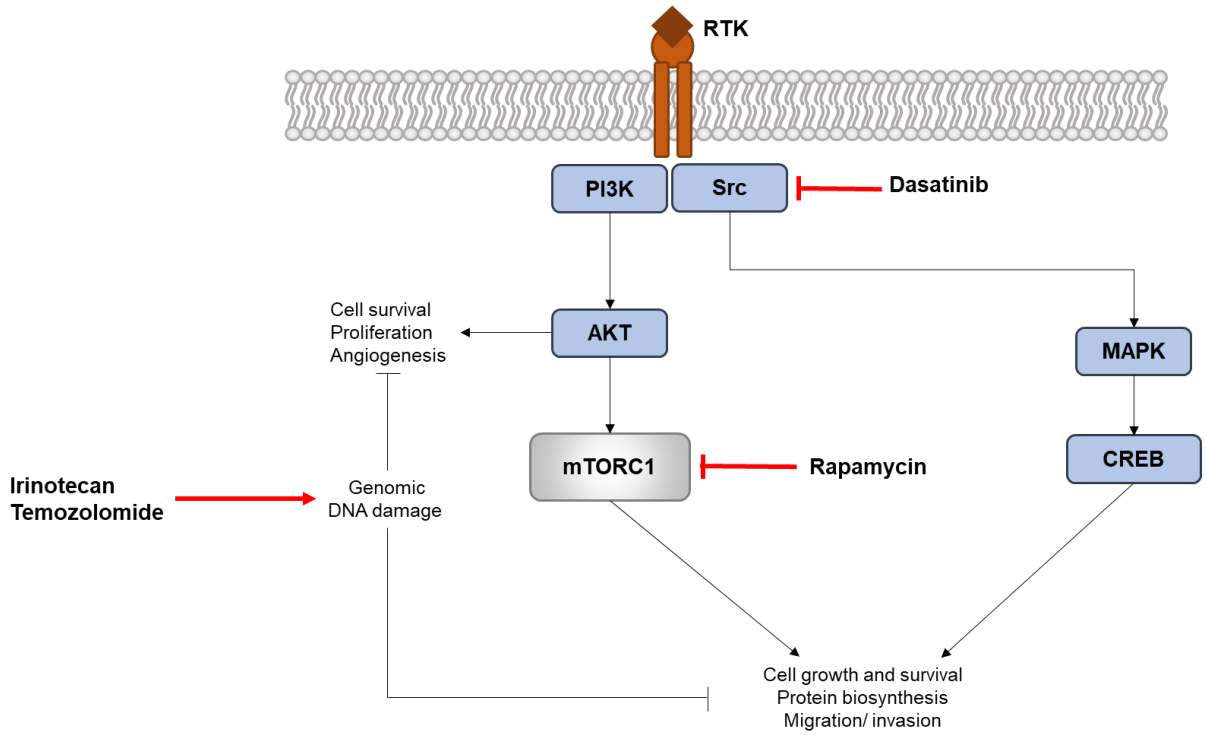


**Figure 3: Targets of the Drugs Used in the RIST Therapy (based on 129)**

Illustration of the molecular targets and mechanisms of action of the drugs used in the RIST therapy.
Rapamycin, an mTOR inhibitor, and dasatinib, a tyrosine kinase inhibitor (TKI), act together in inhibiting the PI3K/AKT/mTOR and MAPK/ERK pathway, thereby inhibiting cell growth and survival. Irinotecan, a topoisomerase I inhibitor, and temozolomide, an alkylating agent, lead to genomic DNA damage.
AKT: protein kinase B (PKB), CREB: cAMP response element-binding protein, MAPK: mitogen-activated protein kinase, mTORC1: mammalian target of rapamycin complex 1, PI3K: phosphatidylinositol 3-kinase, RTK: receptor tyrosine kinase, Src: sarcoma kinase.

### 1.4.1. Rapamycin

Rapamycin, produced by a strain of Streptomyces hygroscopicus, was initially reported to have antifungal properties (96, 97). Subsequent studies revealed potent immunosuppressant and antitumoral activity, which led to its use in preventing graft rejection in organ transplantation (96). Several rapamycin derivatives (rapalogs such as everolimus, temsirolimus) with improved pharmacokinetic properties while retaining the rapamycin backbone structure responsible for its function have been developed (98). The molecular mechanism underlying rapamycin's antifungal, antiproliferative, and immunosuppressive activities lay in its interaction with a family of intracellular binding proteins (FKBPs, most notably FKBP12). The rapamycin/FKBP12-complex binds directly to mTORC in an allosteric fashion, interfering with mainly the mTORC1-mediated signaling pathways leading to cell cycle arrest (in the G1 phase) and inhibition of proliferation (49, 96, 98).

*Johnsen et al.* were able to show that rapamycin was able to inhibit growth and induce apoptosis of NB *in vitro* and *in vivo* (58). Furthermore, *Bahmad et al.* showed that rapamycin could suppress proliferation, migration, and invasion in an NB cell line and inhibit self-replication through cancer stem/progenitor cells (CSC) (99). However, serial treatment was necessary to prevent the persistence of viable CSC populations. Therefore, a metronomic approach may successfully eradicate the CSC population and exhibit longer-lasting effects in reducing tumor burden (99).

### 1.4.2. Dasatinib

Dasatinib is an oral tyrosine kinase inhibitor (TKI), initially developed as a Bcr-Abl (Philadelphia chromosome)-kinase inhibitor. Along with many other receptor and non-receptor tyrosine kinases, dasatinib also targets Src and SFKs, which drive many different signaling pathways (90, 100-102). Aberrant SFK activity promotes survival, proliferation, and metastasis in many human cancers (81, 90). Dasatinib has been shown to induce cell cycle arrest in the G1 phase, cause apoptosis in several cancers, and inhibit metastatic dissemination (81, 90). *Timeus et al.* showed an anti-proliferative and anti-migratory effect of dasatinib in NB cell lines (103). *Vitali et al.* could show induction of apoptosis in several NB cell lines treated with dasatinib as well as partial anti-tumor effects in an orthotopic mouse model of NB (104).

### 1.4.3. Irinotecan

Irinotecan is an analog of the alkaloid camptothecin (105). It targets the DNA topoisomerase I and leads to DNA strand breaks and, subsequently, cell death (105). The metabolization of irinotecan occurs mainly in the liver via a carboxylesterase to various metabolites, including SN-38 (105), which is used in this study.

In various xenograft models of NB, an *in vivo* anticancer activity of irinotecan against NB could be shown (106-108). In following small clinical trials, however, irinotecan yielded mixed results with very limited efficacy as a single agent in treating refractory or relapsed NB but with manageable side effects (109-112).

### 1.4.4. Temozolomide

Temozolomide is an alkylating agent (113, 114). Its active metabolite is 5-(3-methyltriazen-1-yl) imidazole-4-carboxamide (MTIC), which causes methylation of guanine and adenine at several positions (most critical for its cytotoxic activity is methylation of position O6 of guanine) which in turn leads to disruption of DNA replication and apoptosis of the affected cells (113, 114). Limited data from clinical trials using temozolomide as a single agent show antitumoral activity of temozolomide in patients with refractory or relapsed heavily pretreated NB in up to 20% of patients while being generally well tolerated (115, 116).

### 1.4.5. Combination Therapy

Signaling networks are commonly dysregulated in oncogenesis (117). The development of targeted therapeutic agents against dysregulated oncogenic proteins has shown an improvement in cancer treatment. However, single-agent treatment has often demonstrated limited efficacy, partly due to feedback loops and crosstalk between signaling networks (117). Combination therapy, combining two or more therapeutic agents in a therapeutic regimen, has been well-established in cancer therapy (118, 119). Combinatorial treatment allows targeting multiple key pathway components for more efficient treatment compared to single-agent therapies (118, 119). Combining agents that target different pathways may also reduce the overall toxicity of the treatment and often work in an additive or synergistic manner; thus, lower drug doses are required, reducing the risk of undesired side effects (118). Additionally, targeting various pathways at once may also decrease the ability of cancer cells to develop escape mechanisms and may reduce (acquired) drug resistance (118, 119).

The combination of rapamycin and dasatinib has shown promising synergistic effects in an *in vitro* model of various breast cancer and non-small-cell lung cancer (NSCLC) cell lines (120, 121). Combining dasatinib with rapamycin was also shown to be able to block the negative feedback-loop activation of AKT due to mTOR inhibition by rapamycin in a breast cancer model (122). *Laukkanen et al.* recently showed a synergistic effect between AKT/mTORC1 inhibitors and dasatinib in xenograft and primary human T-cell acute lymphoblastic leukemia (T-ALL) (123). Rapamycin, combined with TKIs, has also been shown to overcome drug resistance (124, 125). In NB, the combination of an allosteric ALK inhibitor with rapamycin showed greater efficacy in inhibiting cell growth than either drug alone (126). *Bender et al.* could show that the treatment with the PI3K/mTOR inhibitor PI103 sensitized NB cells to the

following chemotherapy (66). Furthermore, *Kling et al.* recently showed that the combination of an allosteric mTOR inhibitor and a "bromodomain and extra-terminal motif (BET) inhibitor significantly suppressed NB cell growth and survival and reduced the expression of key component proteins of the activated mTOR translation pathway, along with suppression of MycN (127).

In the context of his dissertation, *J. Leister* was able to demonstrate a synergistic effect of rapamycin and dasatinib in three out of four NB cell lines used in the present study (128), and *Wätzig et al.* could also show a synergistic effect of this drug combination in several NB cell lines, including KELLY (129, 130).

Irinotecan and temozolomide were generally well tolerated and showed limited efficacy in treating high-risk refractory/ relapsed NB (rNB) as single agents. *Kushner et al.* treated 49 high-risk stage IV rNB patients with 5-day irinotecan and temozolomide in 3-to-5-week intervals in an outpatient setting with manageable side effects (131). Of 36 patients assessable for response, 33 % (12/36) showed disease regression, and an additional 42 % (15/36) showed stable disease during the length of the trial (131). *Bagatell et al.* conducted a phase II study with 55 patients with rNB and achieved an initial objective response rate of 15 % (8/55); an additional 53% (29/55) of patients achieved stable disease (132) despite substantially lower therapy intensity than administered in the trial of *Kushner et al*. Therapy was generally well tolerated, and several patients with stable disease or better outcome were able to carry on treatment for ten or more cycles in these trials (131, 132), which makes this combination a feasible therapy alternative in heavily pre-treated patients with high-risk rNB with manageable side effects and good quality of life (131). A modified therapy regime based on *Kushner et al.* served as the control arm of the RIST-rNB-2011 trial (37).

### 1.4.6. Metronomical Design

The metronomic therapy design is based upon frequent drug administration in comparatively low doses far below the maximum tolerated dose (MTD), thus reducing the necessity for prolonged therapy interruptions to allow for recovery from therapy-related toxicity (133, 134). It is theorized that such a drug administration schedule targets the tumor environment and angiogenesis (133-135). Such metronomic scheduling can lead to continuously sustained or even improved antitumor effects, allows for the combination of conventional chemotherapy with newer targeted anticancer drugs, antiangiogenic drugs, or other targeted therapies, reduces

the level of therapy-related toxicity, and thus may improve quality of life and may even prolong survival times compared to conventional MTD chemotherapy (133, 134). For example, long-term dasatinib treatment led to cardiac failure in a chronic myeloid leukemia (CML) rat model; however, these limitations were overcome by an intermittent treatment schedule (136). Similarly, improved tolerability while maintaining therapy effectiveness has been shown in CML patients treated with an intermittent dasatinib schedule (137). In addition, it has been shown that drug administration in a metronomic schedule may reduce or even overcome (acquired) drug resistance (133, 135).

The RIST therapy design offers heavily pre-treated patients with rNB a promising, tolerable therapeutic approach that can be administered in an outpatient setting and can reduce therapy-related toxicity for a better quality of life. Alternating courses of the molecularly targeted drugs rapamycin (Rapamune®, R) and dasatinib (Sprycel®, D or S) and the chemotherapeutics irinotecan (Irinomedac®, I) and temozolomide (Temomedac®, T) are administered in a metronomic design (*Figure 4*) (37, 95). Treatment consists of courses of R/S (4 days/week) followed by courses of I/T (5 days/week). Phase 1 is defined by alternating single courses of R/S and I/T respectively over the duration of eight weeks. Phase 2 is comprised of cycles consisting of two R/S followed by one I/T course over the duration of 12 weeks. In phase 3 and ongoing, additional R/S courses may be added to each cycle. The biologicals used aim to target multiple pathway targets to maximize efficacy, possibly reduce toxicity and development of drug resistance, and exert a potential synergistic or additive effect.

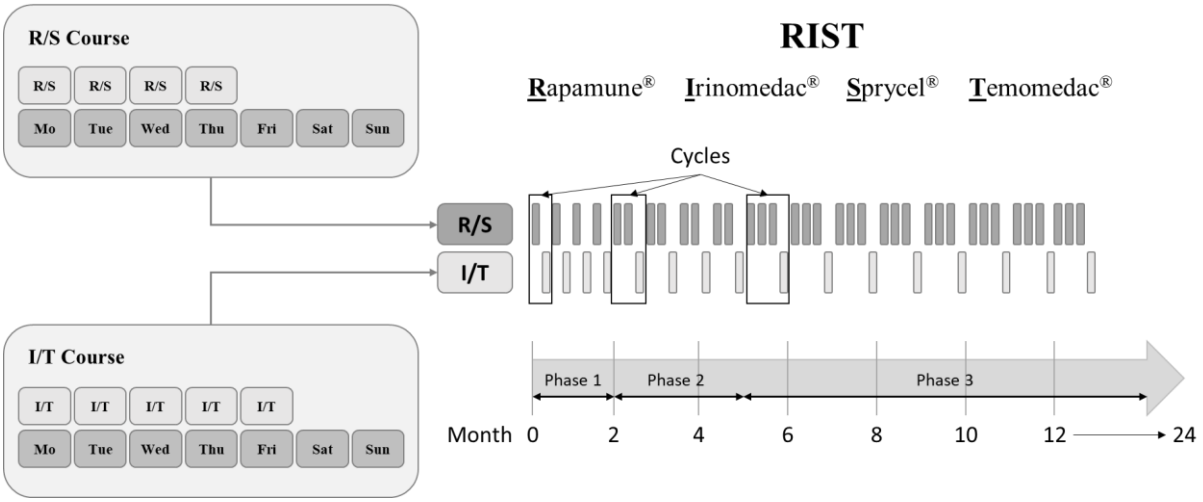


**Figure 4: Schematic Outline of the Clinical RIST Therapy Protocol**

Illustration of the RIST protocol as applied in the clinical setting. RIST treatment consists of courses of rapamycin (R) and dasatinib (S, derived from the trade name Sprycel®) (4 days/week) followed by irinotecan (I) and temozolomide (T) (5 days/week). Phase 1 consists of four cycles with alternating courses of R/S and I/T. Phase 2 is defined by four cycles comprised of two R/S courses followed by one I/T course. In subsequent phases additional R/S cycles may be given before one I/T course.

Cancer cells are thought to synchronize their cell cycle phases through pre-treatment with molecularly targeted drugs in a metronomic manner (94, 95). It is also suggested that pre-treatment with biologicals may trigger modulation of the tumor's microenvironment leading to improved therapeutic drug delivery (138). Thus, the time-optimized sequential treatment of molecularly targeted biologicals and chemotherapeutic agents or radiotherapy is thought to increase the sensitivity of cancer cells to chemo- or radiotherapy (95, 135, 138-140), even in already drug-resistant disease (135, 141), thus leading to improved outcome.

A pilot study of 21 patients showed promising results, with 12 (57 %) patients achieving complete remission, and 7 of those still in remission after a median follow-up of 148 weeks (142). In addition, the RIST therapy with sunitinib as a receptor tyrosine kinase inhibitor instead of dasatinib has been utilized successfully *in vitro* and *in vivo* in a study treating glioblastoma conducted by *Nonnenmacher et al*. (95). Additionally, despite the multitude of inhibitory effects, the profile of adverse effects of rapamycin and dasatinib, as well as the low-dose chemotherapeutics, remain relatively benign (94), and the RIST therapy can be administered in an outpatient setting, preserving the best possible quality of life for these patients.

## 1.5. Aim of this Study

This study aims to analyze in an *in vitro* model of NB if the combinatorial treatment of the molecularly targeted drugs rapamycin (an mTOR inhibitor) plus dasatinib (a TKI) (R+D) with chemotherapeutic drugs irinotecan plus temozolomide (I+T), as designed in the RIST therapy, has an advantage in treating NB with MycN amplification. The RIST therapy is based on the hypothesis that the pre-treatment with molecularly targeted agents will synchronize the cell cycle and sensitize cells for the following chemotherapy. Several studies have indicated greater sensitivity of MycN-amplified (MNA) cell lines toward mTOR inhibitors. Furthermore, research in our lab indicated greater sensitivity of MNA NB cell lines to the RIST therapy as well. By comparing four different NB cell lines with specific genetic markers, this study will analyze if NB cells with specific molecular characteristics show a better response to this targeted therapy than others by performing apoptosis assays (based on Annexin V/FITC (AV)- and propidium iodide (PI)-staining). In a second step, the study aims to identify therapy-relevant signaling pathways through which the RIST therapy inhibits tumor cell growth and whether predictive markers for treatment response can be determined utilizing semiquantitative multiplex antibody assays. The findings will allow for future more in-depth research into relevant targets using more refined methods such as Western blot analysis. In addition, these studies will provide the basis for future studies to further improve the RIST therapy approach in the long term (e.g., by using rapamycin analogs, etc.) and to possibly identify a driver seat mutation to predict which tumor entities will potentially respond to the RIST therapy.

# 2. Material and Methods

## 2.1. Material

### 2.1.1. Equipment, Software, Supplies, Chemicals, and Reagents

**Table 1: Equipment**

| Device | Manufacturer |
|---|---|
| Centrifuge, benchtop, ventilated/refrigerated 5810 R | Eppendorf |
| Centrifuge 5424 R | Eppendorf |
| Centrifuge Universal 320/320 R | Hettich Zentrifugen |
| $CO_2$ Incubator HERA Cell 240 | Heraeus |
| Flow Cytometer MacsQuant | Miltenyi Biotec |
| Gel electrophoresis chamber Biometra Compact | Analytic Jena |
| Integra Pipetboy acu 2 | Integra |
| ImageQuant LAS 4000 Mini | GE Healthcare |
| Laminar Flow Unit HERAsave | Heraeus |
| MacsQuant Chill Rack 50 | Miltenyi Biotec |
| Magnetic mixer with heating unit VMA-C4 | VWR |
| Microcentrifuge- Micro Star 17R | VWR |
| Microscope Nikon Eclipse TS100 | Nikon |
| Microscope Camera Nikon DS-Vil | Nikon |
| Multi-Pipette research 300 µl | Eppendorf |
| Neubauer cell counting chamber | Brand |
| Pipettes HandyStep ® | Brand |
| Pipettes Eppendorf research plus 10 µl, 100 µl, 200 µl, 1000 µl | Eppendorf |
| Scale | Kern EW |
| Spectrophotometer TECAN | Tecan |
| Thermocycler Biometra T Professional Basic Gradient | Analytik Jena |
| Vortex GvLab | Gilson |
| Waterbath GFL 1086 | Gesellschaft für Labortechnik |

**Table 2: Software**

| Software | Manufacturer |
|---|---|
| Adobe Photoshop CS6 | Adobe Inc. |
| EndNote ™20 | Clarivate |
| GraphPad Prism 9 | GraphPad Software Inc. |
| ImageStudio Lite Version 5.2 | LI-COR |
| MacsQuantify™ Software | Miltenyi Biotec |
| Microsoft 360 Excel, Word, Powerpoint | Microsoft Corporation |
| NIS Elements Imaging Software | Laboratory Imaging |

**Table 3: Supplies**

| Supplies | Manufacturer |
|---|---|
| Cell culture flasks 75 $cm^2$ | BD Biosciences |
| Cell culture flasks, collagen-coated 75 $cm^2$ | Biocoat |
| Cell culture plates 6 well | Falcon Corning |
| Cell culture plates 6 well, collagen-coated | Falcon Corning |
| Cryo Tubes 2.0 ml | Sarstedt |
| Eppendorf Tubes® 0.5 ml, 1.5 ml, 2.0 ml | Eppendorf |
| Falcon® tubes 50 ml, 15 ml | Sarstedt |
| Falcon® 60 mm TC-treated Cell culture dish | Corning |
| Falcon® 60 mm TC-treated Cell culture dish, collagen-coated | Corning |
| Fast Read 102® Cell Counting Slides | Biosigma |
| Multi-Step pipette tips 12.5 ml | Brand |
| Pasteur pipettes, glass 230 mm | VWR, Roth |
| Pipette tips with filter (Biosphere®Filter Tips) | Sarstedt |
| Pipette tips without filter 10 µl, 20 µl, 200 µl, 1000 µl | Gilson, Biosphere |
| Pipette tips 5 ml, 10 ml, 12.5 ml | Brand, Eppendorf |
| Sample tubes 5 ml | Sarstedt |
| Serological pipettes 2 ml, 5 ml, 10 ml, 25 ml, 50 ml | Sarstedt |

**Table 4: Chemicals and Reagents**

| Substance, Catalog Number (#) | Manufacturer |
|---|---|
| 2-Propanol | Chemicals Distribution Universität Regensburg |
| Agarose (peqGOLD Universal-A) (#35-1020) | VWR |
| Annexin V-FITC Kit (#130-092-052) | Miltenyi Biotec |
| Aprotinin (#A6279) | Sigma Aldrich |
| BC Assay Protein Quantification Kit (#UP40840A) | Uptima |
| DMSO, Hybri-Max™, sterile-filtered (#D2650) | Sigma Aldrich |
| Dulbecco's Phosphate Buffered Saline (PBS) | Sigma Aldrich |
| EMEM Cell Culture Media | BioWhittaker |
| Ethanol Rotipuran | Carl Roth |
| Fetal Bovine Serum (FBS) (#S0415) | Biochrom |
| Gibco™ RPMI 1640 with phenol red, without glutamine | Gibco Life Technologies |
| Gibco™ RPMI 1640 without phenol red | Gibco Life Technologies |
| Ham's F12 Cell Culture Medium | Biochrom |
| L-glutamine (L-Glyn), 200 mM | Gibco Life Technologies |
| Leupeptin (#1167) | Tocris |
| MACSQuant Calibration Beads (#130-093-607) | Miltenyi Biotec |
| MACSQuant Running Buffer (#130-111-562) | Miltenyi Biotec |
| MACSQuant Storage Solution (#130-092-748) | Miltenyi Biotec |
| MACSQuant Washing Solution (#130-092-749) | Miltenyi Biotec |
| MEM NEAA (Non-Essential Amino Acids) | Gibco Life Technologies |
| PathScan® Akt Signaling Antibody Array Kit (#9474) | CST |
| PathScan® RTK Signaling Antibody Array Kit (#7982) | CST |
| PCR Mycoplasma Test Kit I/C (PromoKine) | PromoCell |
| Penicillin/Streptomycin (Pen/Strep, 10,000 U/ml) | Biochrom |
| Pepstatin (#1190) | Tocris |
| Propidium iodide solution (PI) (#P4864) | Sigma Aldrich |
| Proteome Profiler™ Array Human Phospho-Kinase Array Kit (#ARY003B) | R&D Systems |
| Sodium azide ($NaN_3$) 5% | Merck |
| Sodium citrate ($C_6H_5Na_3O_7$) 0,1% | Merck |

| | |
|---|---|
| Staurosporine (#1285) | Tocris |
| Trypan Blue | BioWhittaker |
| Trypsin 0.05%/ EDTA 0.02% in PBS | Biochrom |

### 2.1.2. Cell Culture

*Table 5* lists the NB cell lines used, their phenotype in cell culture, as well as the source. *Figure 5* shows light microscopic images of the cell lines used in culture. *Table 6* lists relevant genetic markers of the NB cell lines used.

All cell lines were cultured in 75 $cm^2$ culture flasks in the respective growth medium listed below and incubated at 37°C and a $CO_2$ content of 5%.

**Table 5: Neuroblastoma Cell Lines**

| Name | Origin | Phenotype in cell culture | Source |
|---|---|---|---|
| KELLY | derived from human brain tissue of an NB patient (143) | neuronal cells, round to fusiform, adherent, grow in mono- and multilayers, with polar neuritic processes | ECACC (#92110411) |
| LAN-5 | derived from a bone marrow metastasis of NB of a 0.4-year-old boy (144, 145) | polymorph cells, adherent, grow in monolayers and small clusters | DSMZ (#ACC673) |
| SK-N-SH | derived 1970 from a bone marrow metastasis of NB of a 4-year-old female with prior treatment (145-147) | epithelial morphology, adherent | ATCC (#HTB-11) |
| SK-N-AS | Derived from a bone marrow metastasis of NB of a 6-year-old girl with prior treatment (145, 148) | neuroblasts with epithelial morphology, adherent | ATCC (#CRL-2137) |

ATCC: American Type Culture Collection, ECACC: European Collection of Authenticated Cell Cultures, DSMZ: Deutsche Sammlung von Mikroorganismen und Zellkulturen, NB: neuroblastoma.

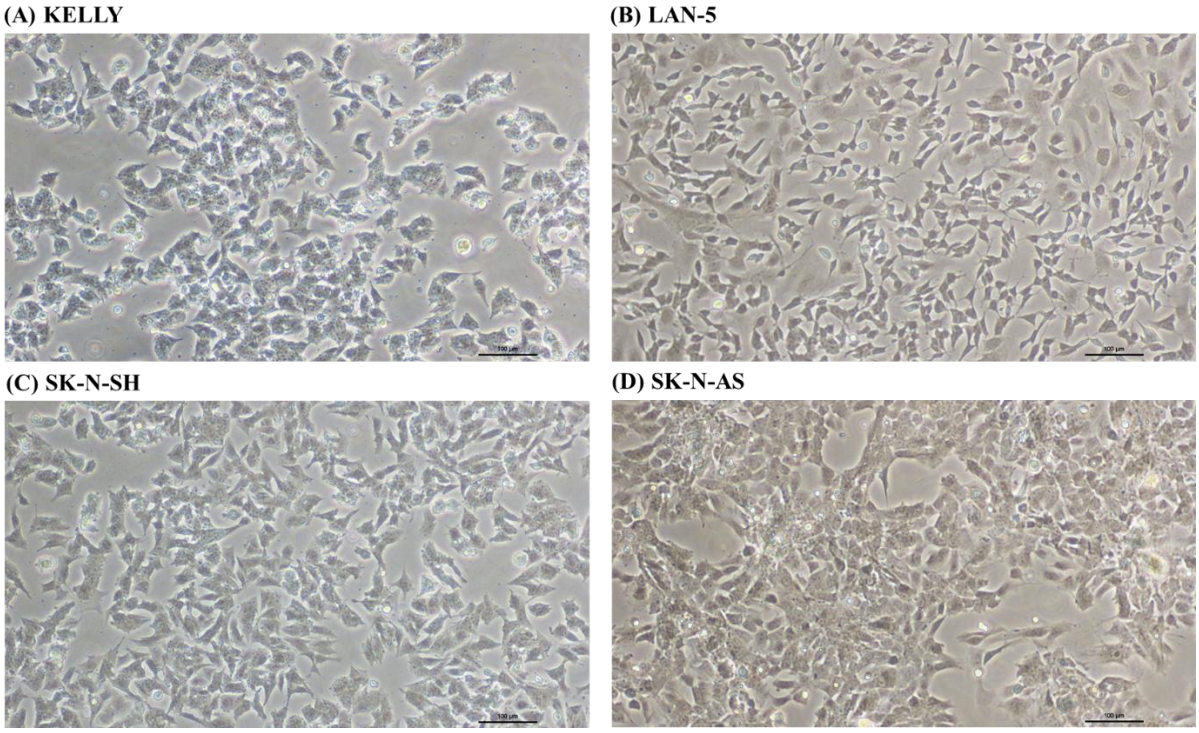


**Figure 5: Light Microscopic Images of Neuroblastoma Cell Lines in Culture**

Light microscopic images of the cell lines used at 10x magnification. **(A)** KELLY (MNA), **(B)** LAN-5 (MNA), **(C)** SK-N-SH (MNN), **(D)** SK-N-AS (MNN). MNA: MycN-amplified, MNN: MycN-non-amplified. The scale bar represents 100 µm.

**Table 6: Neuroblastoma Cell Lines and Their Genetic Characteristics**

| NB cell line | MycN amplification | 1pdel | ALK mutation | 11q23del | 17q gain | p53 or p73 mutation | NRAS mutation |
|---|---|---|---|---|---|---|---|
| KELLY | + (100-600-fold) (145, 149, 150) | + (LOH p21.3-pter; loss p36.32; gain p36.33) (151) | F1174L (Gain of function) (10, 151) | + (151) | + (151) | P177T (Loss of function) (151) | - (152) |
| LAN-5 | + (50-200-fold) (24, 145, 149, 150) | + (Loss p33-pter) (24, 145, 151) | R1275Q (Gain of function) (151, 153, 154) | - (24, 151) | + (151) | - (151, 155) | - (152) |
| SK-N-SH | - (24, 145, 147) | - (24, 145, 151) | F1174L (10, 11, 151, 153, 154) | - (24, 151) | + (11, 151) | - (151, 155) | - (152) |
| SK-N-AS | - (24, 145, 149) | + (Loss p36.22-36.32) (24, 145, 151) | - (10, 11, 151, 153, 154) | + (24, 151) | + (151) | H168R (151, 155) (Loss of function) del of p73 (1p36.33) (145, 156) | Q61K (152) |

ALK: anaplastic lymphoma kinase, del: deletion, LOH: loss of heterozygosity, NB: neuroblastoma, NRAS: neuroblastoma RAS viral oncogene homolog.

#### 2.1.2.1. Cell Culture Media and Reagents

**Table 7: Medium Preparation**

| | |
|---|---|
| KELLY and LAN-5: | 1x RPMI 1640 with phenol red, 15% FBS, 2 mM L-glutamine, 1% Pen/Strep |
| SK-N-SH and SK-N-AS: | Ham's F12/EMEM 1:1 with phenol red, 10% FBS, 1% Pen/Strep |
| Cryo-conservation: | FBS 10% DMSO |

DMSO: dimethyl sulfoxide, EMEM: Eagle's Minimal Essential Medium, FBS: fetal bovine serum, Pen/Strep: penicillin/streptomycin, RPMI 1640: Roswell Park Memorial Institute medium 1640.

All growth media were freshly prepared one to two times per month and stored at 4°C.

Medium for cryo-conservation was always freshly prepared directly before intended use.

### 2.1.3. Pharmaceutical Drugs

**Table 8: Pharmaceutical Drugs Used to Treat Cells**

| Name, Catalog Number (#) | Manufacturer |
|---|---|
| Dasatinib (#D-3307) | LC Laboratories |
| Rapamycin (#R-5000) | LC Laboratories |
| SN-38 (active metabolite of irinotecan) (#2684) | Tocris |
| Temozolomide (#2226-10) | BioVision |

All pharmaceutical drugs were dissolved according to the respective data sheet in dimethyl sulfoxide (DMSO) as vehicle, aliquoted, and stored at -20°C. The dissolved substances were frozen and thawed a maximum of 10 times in order to prevent any resulting impairment of effect. After thawing and during the preparation of the various necessary dilution steps, aliquots were vortexed thoroughly to ensure that a solution with an evenly distributed substance concentration was available for further use.

## 2.2.Methods

### 2.2.1. Cell Culture, Passaging, and Seeding

NB cells were cultured in the appropriate medium of the respective cell line (see *Section 2.1.2.1*) in 75 $cm^2$-cell culture flasks in a humidified atmosphere at 37°C and 5 % $CO_2$ in an incubator. All working steps were conducted under sterile conditions in a laminar flow hood to prevent contamination. All work surfaces and materials were disinfected with 70 % isopropanol before use, and only sterilized or autoclaved culture medium, pipette tips, and consumable materials were used. All solutions were brought to room temperature by leaving the solutions to sit at room temperature before use or using a 37°C warming bath. For the cell line SK-N-SH, collagen-coated culture flasks were used.

Cells were passaged approximately twice a week. For this, the confluence of cells was regularly assessed under the microscope and passaged when reaching a confluence of 70 to 100 %. In case of insufficient confluence, only a medium change was performed. The quality of cells was ensured by frequently assessing their morphology under the microscope and regularly performing mycoplasma tests.

To passage cells, the medium was first removed, and cells were washed with 10 ml of phosphate-buffered saline (PBS). This was done to remove residual fetal bovine serum (FBS), which would result in the inhibition of the trypsin and prevent detachment of the cell layer from the bottom of the cell culture flask. Subsequently, trypsinization followed (2 ml of trypsin-EDTA per T75 bottle) at room temperature (cell lines KELLY, LAN-5, SK-N-AS) for approximately five minutes. In the case of the cell line SK-N-SH, it was necessary to incubate the culture flasks in the incubator at 37°C for the duration of trypsinization (3 to 5 minutes) to ensure the detachment of cells. When cells visibly detached from the bottom of the culture flasks, the trypsinization was stopped by adding 10 ml of fresh FBS-containing medium to prevent irreversible cell damage due to prolonged contact with trypsin. Finally, the culture flasks were thoroughly rinsed with medium, and cells were isolated by pipetting the cell suspension up and down. Then, cells were resuspended in fresh culture medium and reseeded into new culture flasks according to the split ratios suggested in the respective data sheets.

For seeding into culture dishes for experiments, cells were detached from the culture flasks as described above and resuspended in 10 ml fresh medium. Cells were counted (see *Section*

*2.2.3*), and a batch containing the required number of cells was prepared in the appropriate amount of medium. Before seeding, cells were carefully mixed by pipetting up and down to ensure an even cell distribution. Seeding was done using a serological pipette. For 6-well tissue culture plates (growth area 9.6 $cm^2$), $0.5x10^6$ cells per well in 1 ml medium were seeded. For cell culture-treated dishes (growth area 21 $cm^2$), $2x10^6$ cells were seeded per dish in 5 ml medium.

### 2.2.2. Freezing and Thawing of Cells

Surplus cells were frozen during a low passage number to prepare a seeding stock. Frozen cells were stored in liquid nitrogen in FBS containing 10% of the cryoprotective agent DMSO. The freezing medium was prepared right before use as directed above and stored at 4°C until needed. Cells then were gently detached as described above using the protocol for subculturing cells (see *Section 2.2.1*). Afterward, cells were resuspended in the appropriate medium, and cell number and viability were determined using a hemacytometer and Trypan Blue exclusion according to the protocols described below (see *Section 2.2.3*). Cells were then centrifuged at 300 x g and 4°C for 5 minutes. The supernatant was decanted without disturbing the cell pellet. The pellet was then resuspended in the appropriate amount of cold freezing medium. Aliquots of the cell suspension were dispensed into cryogenic storage vials at a cell number of $2x10^6$ cells per cryo-vial, suspended in a volume of 1.5 ml. To maintain a homogenous cell suspension, cells were gently mixed. Cells then were slowly frozen by reducing the temperature at approximately 1°C per minute using the controlled rate cryo-freezing container “Mr. Frosty”. Alternatively, cryo-vials were placed in an isopropanol chamber and stored at -80°C overnight. For long-term storage, cryo-vials were subsequently placed in a liquid nitrogen tank.

When thawing cells, the cell suspension was immediately resuspended in an appropriate pre-warmed medium to thaw the cells with minimal stress. Afterward, the cell suspension was centrifuged at 300 x g and 20°C for 5 minutes. The supernatant was then decanted without disturbing the cell pellet. This step was repeated if necessary to ensure that as much freezing medium containing DSMO as possible was removed. Cells then were gently resuspended in the appropriate medium, transferred into 75 $cm^2$ culture flasks, and stored in the incubator.

### 2.2.3. Determining Cell Count in the Fast Read 102® Hemacytometer

To determine the number of cells, cells were first detached from the cell culture flasks as outlined above (see *Section 2.2.1*). Then 10 µl of cell suspension were diluted with Trypan Blue solution to a ratio of 1:10 to 1:20, depending on the expected cell count.

Trypan Blue exclusion is a rapid assay to determine the viability of cells accurately. Damaged cells are taking up Trypan Blue, meaning it can travel into cells through damaged membranes. Positively stained cells are considered non-viable and are excluded from the cell count. An aliquot of the cell suspension is pipetted into the Fast Read-Chamber. Depending on cell number and distribution of the cells, 3 to 6 squares were counted. Subsequently, the cell number was calculated using the following formula:

Cell number = average of cell counts per square

x volume of cell suspension (2-5 ml)

x dilution factor (10 or 20)

x chamber factor $10^4$.

The chamber factor is calculated as follows: Because of the defined height of the chamber, a three-dimensional space of defined size is created. In the used chambers, the height equals 0.1 mm. Therefore, the assessed volume in one square is 0.1 $mm^3$ (0.1 µl). Through multiplication per square with $10^4$ (10,000), the cell count per ml (1 ml = $10^4$ µl) is determined.

### 2.2.4. Mycoplasma Test

To exclude mycoplasma contamination in the cell lines, the PromoKine PCR Mycoplasma Test KIT I/C was used, which utilizes polymerase chain reaction (PCR) detection of mycoplasma DNA in the cell culture supernatant. The procedure was performed according to the protocol of the test kit. After performing PCR, the PCR products were mixed with loading buffer, transferred to a 1.5 %-agarose gel containing GelRed, and electrophoresis was performed at 100 V for 30 minutes. The DNA bands were visualized using UV light. A positive mycoplasma sample shows a distinct band at 265 to 278 bp. The internal control DNA should show a distinct band at 479 bp in every lane, indicating a successfully performed PCR. In regularly performed mycoplasma tests, no positive bands were detected for the cell lines in use.

### 2.2.5. *In Vitro* RIST Therapy

To assess the efficacy of the RIST therapy in MNA- versus MycN-non-amplified (MNN) cell lines, an *in vitro* model of NB with two MNA cell lines, KELLY and LAN-5, and two MNN cell lines, SK-N-SH and SK-N-AS, was established.

In extensive preliminary studies, the half-maximal inhibitory concentration ($IC_{50}$) values for single and combination drug treatment were established by *J. Leister* (128) and in further internal lab studies by *M. Matthes*. The drug concentrations applied in this study can be found in *Table 9* below.

**Table 9: Drug Concentrations Used for Combinatorial Treatment Rapamycin Plus Dasatinib and Irinotecan Plus Temozolomide and RIST Treatment in Different NB Cell Lines**

| Cell line | Rapamycin | Dasatinib | Irinotecan (SN-38) | Temozolomide |
|---|---|---|---|---|
| KELLY | 2 µM | 5 µM | 1.5 nM | 250 µM |
| LAN-5 | 0.1 µM | 1 µM | 0.3 nM | 35 µM |
| SK-N-SH | 0.2 µM | 0.1 µM | 1.3 nM | 100 µM |
| SK-N-AS | 0.1 µM | 5 nM | 6.7 nM | 200 µM |

For clarity, SN-38 is used synonymously with irinotecan (I) and will be referred to as irinotecan (I) in the following.

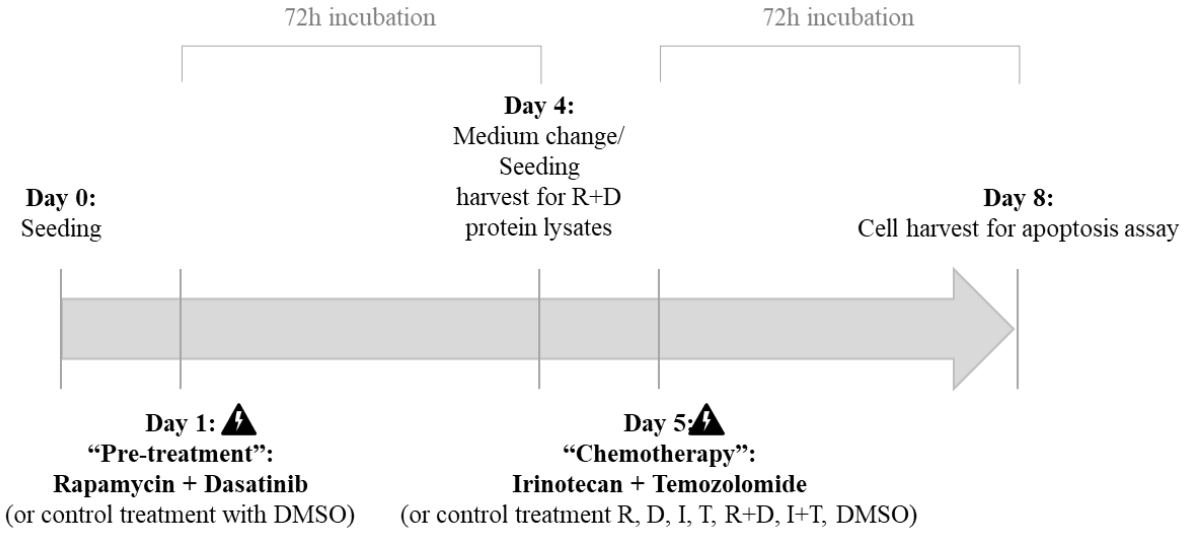


**Figure 6: Schematic Outline of the in Vitro RIST Therapy (based on 129, 130)**

Illustration of the RIST protocol as applied in the laboratory setting. Cells were seeded and 24 hours later (day 1) rapamycin plus dasatinib (R+D) at concentrations listed in *Table 9* or control treatment (DMSO vehicle in the maximum concentration as applied in the drug treatment) was administered. After 72 hours (day 4) medium was changed followed by 24 hours of rest before applying chemotherapeutic drugs irinotecan plus temozolomide (I+T) at concentrations listed in *Table 9*. Cells were harvested after 72 hours (day 8), and apoptosis assays were performed. For phosphorylation assays, cells were only treated with R+D or control treatment (DMSO vehicle), harvested on Day 4, and further processed.
D: dasatinib, DMSO: dimethyl sulfoxide, I: irinotecan, R: rapamycin, T: temozolomide.

For the *in vitro* RIST therapy (*Figure 6)*, cells were first plated by seeding 0.5 x $10^6$ cells per well in 6-well plates (apoptosis assays, Proteome Profiler™ arrays) or 2 x $10^6$ cells per cell culture-treated dish (PathScan® arrays), respectively.

After 24 hours (day 1), R+D treatment was administered at concentrations listed in *Table 9.* As a control, cells were treated with vehicle (DMSO) alone in the maximum concentration as applied in the drug treatment.

After 72 hours (day 4), a medium change was performed, followed by 24 hours of rest before treatment with the chemotherapeutic agents I+T at concentrations listed in *Table 9.* In addition, cells for single-drug treatments (R, D, I, and T) and the combinatorial treatments with two drugs, R+D and I+T, were seeded in 6-well plates with 0.5 x $10^6$ cells per well on day 4 and treated with single-drug treatment (R, D, I or T) or combinatorial treatment consisting of R+D or I+T after 24 hours of rest, in concentrations listed above in *Table 9.* As a control, cells were treated with vehicle (DMSO) alone in the maximum concentration as applied in the drug treatment. Cells were harvested after 72 hours (day 8), and the following assays were performed. Each treatment was done in triplicates.

For apoptosis assays, cells were treated with the complete *in vitro* RIST therapy, as well as the individual drugs R, D, I, and T, the drug combinations R+D and I+T, as well as controls treated with vehicle (DMSO) only. For the apoptosis assays, 0.5 x $10^6$ cells per well were seeded in 6-well plates.

For the Proteome Profiler™ arrays and PathScan® arrays, cells were treated with R+D or as control with vehicle (DMSO) in concentrations as applied in the drug treatment only.

### 2.2.6. Apoptosis Assay Annexin V/FITC- and Propidium Iodide-Staining

Fluorescence-activated cell sorting (FACS) analysis using the MacsQuant Flow Cytometer by Miltenyi Biotec was used to evaluate apoptosis induction in drug- and control-treated cells. Flow cytometric analysis is based on measuring light scatter and fluorescence when cells pass a laser beam perpendicular to the sample flow. To analyze, cells are labeled with a dye, if necessary, suspended in a liquid (sheath fluid) and then passed in a laminar flow by a focused monochromatic light beam (e.g., 488 nm). When cells pass through the laser beam, the resulting scattered light can be used to record various measured variables. Scattered light that is diffracted at a narrow angle to the laser beam is detected as forward scatter (FSC), and scattered light at right angles (90°) as side scatter (SSC). The FSC describes a rough measure for the cell size; SSC depends on the cell's inner structure and is influenced by granularity, dyes, and pre-treatment of cells before analysis (157). Depending on the size, granularity, and staining of the cells, a specific scattering of the light and characteristic emission of the dye can be measured with suitable photodetectors. The emitted light is directed into emission detectors and detected via photomultipliers. Light is separated using interference filters/band-pass filters according to the emission spectrum (e.g., for MacsQuant FL1 (B1): 525 nm, FL2 (B2): 585 nm, FL3 (B3): 655-730 nm) and detected (158). Adequate compensation methods must be used to correct an overlap of the emission spectrum of the dyes used. Cells stained with a fluorescence dye can be quantified as events and further analyzed using specialized software.

Apoptosis is a process in which a cell actively participates in its destructive processes (159). This process is characterized by a series of specific morphological changes, including loss of plasma membrane asymmetry and integrity, condensation of the nucleus and cytoplasm, and internucleosomal cleavage of the DNA (159, 160). In most eukaryotic viable cells, there are phospholipid phosphatidylserines (PS) located in the cytosolic leaflet of the plasma membrane

but not the outer leaflet (159, 161, 162). These phosphatidylserines are negatively charged (161). If a cell is undergoing apoptosis, PS redistribution from the inner to the outer leaflet of the membrane occurs in the early stages of apoptosis (160, 163)*;* thus, PS is exposed to the external cellular environment. In necrosis or late stages of apoptosis, PS becomes widely accessible due to the disruption of membrane integrity (163).

Annexin V (AV) is a 35 kDa phospholipid-binding protein with a high affinity to PS in the presence of physiological concentrations of calcium ($Ca^{2+}$) (162). It binds to the exposed PS of apoptotic cell surfaces (160, 162). AV can be conjugated to fluorochromes such as fluorescein isothiocyanate (FITC) (160, 162) (while retaining its high affinity to PS) and can therefore be used as a sensitive probe for flow cytometric analysis of cells undergoing apoptosis. Fluorochrome FITC emission with an emission maximum of ~520 nm is detected in fluorescence channel 1 (FL-1/MacsQuant Analyzer B1) (158, 164). Double staining with AV and PI to confirm (early) apoptosis vs. necrosis (162) has been widely used. As mentioned above, PS translocation precedes the loss of complete disruption of membrane integrity found in the later stages of apoptosis and necrosis. PI intercalates between base pairs of double-stranded nucleic acids and thus can be used as a marker of necrotic/late apoptotic cells that have lost membrane integrity (165). DNA-bound PI is detected at a fluorescence emission maximum of 610-620 nm and can therefore be detected in FL-2 (MacsQuant Analyzer B2) (158, 164). When combining staining with fluorescent FITC-labeled AV (AV/ FITC) with a staining protocol for cell viability, such as PI, cells in the early and late stages of apoptosis/ necrosis can be identified. *Figure 7* illustrates a simplified model of determining cell viability via the AV/FITC- and PI-staining.

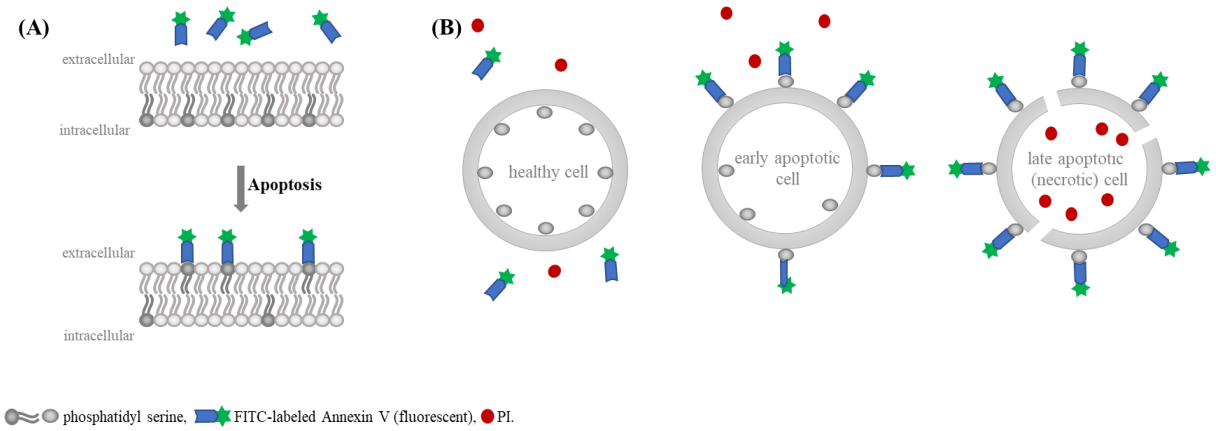


**Figure 7: Schematic Diagram Showing Detection of Apoptosis With Annexin V/Fluorescein Isothiocyanate and Propidium Iodide**

**(A)** Schematic diagram showing the loss of membrane asymmetry of cells undergoing apoptosis. Phosphatidylserines (PS) become exposed in the outer leaflet which results in the binding of fluorescein isothiocyanate (FITC)-labeled Annexin V (AV). (**B)** Schematic diagram showing the uptake of AV and/or propidium iodide (PI) depending on the stage cells are in. Healthy, live cells appear AV-/PI-, early apoptotic cells appear AV+/PI-, and late apoptotic cells appear AV+/PI+.

Viable cells will take up neither PI nor AV due to their intact phospholipid membrane and are therefore negative for AV and PI (no PI/ no AV*)*. Cells in the early stages of apoptosis have lost their membrane asymmetry and expose PS in the outer leaflet of their membrane, thus taking up AV. Still, cell membrane integrity is intact, so no PI uptake occurs. Therefore, cells in early apoptosis are negative for PI uptake but are highly positive for AV (no or low PI/ high AV). Cells in late apoptosis (high PI/ high AV) or undergoing necrosis (low AV/ high PI) have lost their membrane integrity and therefore take up PI *(Table 10)*. Distinguishing between late apoptosis and necrosis is not reliably possible. *In vivo*, apoptotic cells would be phagocytized by macrophages or neighboring cells; however, this does not happen in culture conditions (166, 167). Those cells will undergo so-called secondary necrosis, which includes membrane rupture and, thus, PI-uptake. It is not possible to reliably differentiate between late apoptotic and necrotic cells. In the final results, therefore, it was distinguished between live and dead (apoptotic/ necrotic) cells.

**Table 10: Cell Populations Stained With Annexin V/Fluorescein Isothiocyanate and Propidium Iodide**

| | AV/FITC | PI |
|---|---|---|
| **(Early) apoptotic cells** | positive | negative |
| **(Late) apoptotic/ necrotic cells** | positive | positive |
| **Viable cells** | negative | negative |

AV: Annexin V, FITC: fluorescein isothiocyanate, PI: propidium iodide

The Annexin V/FITC Kit by Miltenyi Biotec was used to conduct the apoptosis assay. The binding buffer was prepared according to kit instructions and stored at 4°C until use. For protocol, an established protocol from the laboratory was used.

For the assay, 0.5 x $10^6$ cells were seeded in 6-well plates and treated as described in *Section 2.2.5*. As apoptosis control (AV/FITC positive), cells were treated on "day 8" with 1 µM staurosporine in 0.5 ml medium and incubated for 4 hours at 37°C. As necrosis control, (PI positive) cells were treated with 0.5 ml 70% ethanol and incubated for 30 minutes at 37°C. Longer incubation time resulted in complete cell death and the inability to harvest cells for measurement via FACS (all cells discarded with supernatant); thus, the reduced incubation time was chosen for ethanol treatment.

For the harvest of cells, the medium was aspirated, and cells were washed with 2 ml PBS per well. Subsequently, trypsinization followed (0.5 ml of trypsin-EDTA per well) in the incubator at 37°C for the duration of trypsinization (3 to 5 minutes) to ensure detachment of cells. When cells visibly detached from the bottom of the wells, the trypsinization was stopped by adding 0.5 ml of FACS buffer solution. Wells were carefully but thoroughly rinsed by pipetting solution up and down to ensure all cells were aspirated. The solution was then transferred to FACS tubes and centrifuged at 160 x g for 5 minutes at 4°C. The supernatant was discarded. The washing step was repeated twice with 2 ml PBS per FACS tube. Subsequently, 100 µl binding buffer was added to each tube, and cell pellets were thoroughly resuspended. Then 5 µl AV/FITC was added, mixed well, and cells were incubated at room temperature in the dark wrapped in aluminum foil. Then 5 µl of PI solution and 400 µl binding buffer per tube were added, thoroughly mixed, and stored in a MacsQuant Chill Rack during analysis. Analysis was done immediately by flow cytometry using the MacsQuant Flow Cytometer by Miltenyi Biotec.

Initially, careful compensation was done to eliminate the emission overlap of the dyes used. Per tube, 20,000 events were recorded for each tube. The following plots were generated using proper controls:

1. FSC vs. SSC with a gate for cells for further analysis, separating them from debris

2. AV/FITC vs. PI with gates for the following populations:

    a. AV-/PI- (live cells)

    b. AV +/PI- (early apoptotic cells)

    c. AV +/ PI + (late apoptotic cells)

    d. AV-/PI+ (necrotic cells)

The following were used as controls: untreated, unstained cells, untreated cells stained with AV/FITC only, and untreated cells stained with PI only to set up initial compensations and quadrants. As controls during experiments, control (DMSO vehicle)-treated cells served as live control, cells treated with staurosporine as apoptosis control, and cells treated with ethanol as necrosis control.

Additionally, a summary report for each sample was calculated, stating the percentage of cells for each gate for further analysis. Each drug and drug combination were done in triplicates, and each experiment was repeated independently three times for each cell line. The recorded data were analyzed using the MacsQuantify™ software and Microsoft Excel. Results were grouped into live (no PI/no AV) and dead/apoptotic cells (AV and/or PI positive) for final analysis.

Statistical analysis was done using the software GraphPad Prism. Results were entered as the number of apoptotic (AV and/or PI positive) cells. First, each treatment (R+D, I+T, RIST) was compared to their respective control (DMSO)-treated population within each cell line. Data sets were assessed for normality. A visual analyzation using a Q-Q plot was done (data not shown) and two normality tests were performed to cross-validate results. Using more than one normality test can provide a more comprehensive understanding of whether a given data set follows a normal distribution. The Shapiro-Wilk test and the Anderson-Darling test were performed because they are regarded as the most powerful among the available normality tests. These two tests were chosen to receive the most robust results. The Shapiro-Wilk test is widely

used and accommodates very small sample size, whereas the Anderson-Darling test is less well-known, however can be more powerful for smaller sample sizes.

In the data groups tested, all but one data set followed a normal data distribution. In one case (LAN-5, group R+D), the Shapiro-Wilk Test did not find a normal distribution, however the Anderson-Darling test did. The Q-Q plot visually appeared slightly skewed, so a non-Gaussian distribution was assumed for more robust results as normality tests with small sample sizes are limited in their power.

To analyze each individual treatment group within each cell line compared to the respective control group, a t-test was performed for each group. Results were plotted in a bar plot with standard deviation (SD) values. A Gaussian distribution (parametric test) was assumed for all data sets but the LAN-5 population treated with R+D. For this particular group a non-parametric Mann-Whitney U test was performed as the requirement of normal distribution for the t-test was not met. Regarding standard deviations, constant standard deviations were not assumed for determining p values because three independent experiments with triplicates were performed for each drug or drug combination, so an unpaired t-test with Welch's correction with a two-tailed p-value was performed. In case of the one set with a non-Gaussian distribution, a Mann-Whitney test with a two-tailed p-value was performed.

To compare the effect of the therapy between the different cell lines, data was normalized. To do this, the data of each treatment group was computed as a percentage of the respective control group mean (which was set as 100 %). Then, in case of the S+T and RIST groups which showed a Gaussian distribution for all data sets, a one-way ANOVA was performed. No equal SD was assumed because data sets were from different populations and pooled from the independent experiments per cell line and treatment group, so Brown-Forsythe and Welch ANOVA tests were performed. For the following multiple comparison tests, Dunnet T3 (recommended, when n <50/group according to Prism) was performed. In the case of the R+D treatment group comparison, which included the data set of LAN-5 with a non-Gaussian distribution, a Kruskall-Wallis non-parametric test was performed instead. For the following multiple comparison tests, Dunn's test was performed. P values are reported as 0.12 (ns), 0.33 (*), 0.002 (**), <0.001 (***).

### 2.2.7. Preparation of Protein Lysates and PathScan® and Proteome Profiler™ Arrays

To assess which pathways and targets are affected by the RIST therapy, the Proteome Profiler™ Human Phospho-Kinase Array Kit, the PathScan® Akt Signaling Antibody Array Kit, and the PathScan® RTK Signaling Antibody Array Kit were used. These arrays allow the parallel determination of relative protein phosphorylation levels of many kinases and targets at once to gain insight into which targets are affected by a particular therapy. Thus, relevant targets and pathways can be narrowed down, and results can be verified using Western blot analysis, for example.

Arrays are based on the sandwich immunoassay principle. Capture and control antibodies have been spotted on nitrocellulose membranes. Cell lysates are incubated on the array, arrays are washed, and biotinylated detection antibodies are applied in a second step. Finally, streptavidin-conjugated chemiluminescent reagents are applied to make the reaction visible, producing a signal at each spot corresponding to the amount of phosphorylated protein bound. The signal intensity can then be quantified using image analysis software.

To prepare protein lysates for the Proteome Profiler™ Human Phospho-Kinase Arrays, cells of the cell lines KELLY (MNA) and SK-N-AS (MNN) were seeded into 6-well plates and treated with R+D and, as control, vehicle (DMSO) as described above (see *Section 2.2.5*). One 6-well plate of vehicle (DMSO)-treated cells and one 6-well plate of cells treated with R+D were prepared for each cell line. The medium was aspirated, and wells were thoroughly rinsed with PBS. All buffers were prepared fresh right before use according to the Proteome Profiler™ Human Phospho-Kinase Array (Chemiluminescent Readout) Kit to prepare and analyze the protein lysates.

To prepare protein lysates for the PathScan® Arrays, cells of the cell lines KELLY (MNA), LAN-5 (MNA), SK-N-SH (MNN), and SK-N-AS (MNN) were seeded into cell-culture-treated dishes and treated with R+D or vehicle (DMSO) only, as described above (see *Section 2.2.5*). For each cell line, one cell culture-treated dish (growth area 21 $cm^2$) with vehicle (DMSO)-treated cells as control and one cell culture-treated dish (growth area 21 $cm^2$) with cells treated with R+D were prepared. To prepare and analyze the samples, the PathScan® AKT Signaling Antibody Array Kit (Chemiluminescent Readout) and the PathScan® RTK Signaling Antibody Array Kit (Chemiluminescent Readout) were used. All

buffers were prepared fresh right before use according to the test kit instructions. Protein lysates were prepared according to the test kits.

A bicinchoninic acid assay (BC Assay Protein Quantification Kit, Uptima) was performed for the determination of protein concentrations of cell lysates. The BCA assay allows a colorimetric detection and quantification of total protein, known as the BCA method (168). It is based on the reduction of $Cu^{2+}$ to $Cu^{+}$ by tripeptides and larger polypeptides in an alkaline medium containing sodium potassium tartrate (biuret reaction) (168). Protein forms a blue-to-violet chelate complex with cupric ions. The intensity and color produced are proportional to the amount of protein present. BCA is a selective colorimetric detection reagent that reacts with $Cu^{+}$ formed in the first reaction step. As a result, a purple-colored complex is formed ($Cu^{2+}$ + 2 BCA →BCA-$Cu^{+}$-complex). The formed complex is water-soluble and exhibits a linear absorbance at 562 nm with increasing protein concentrations and thus can be measured using colorimetric techniques (168). A standard curve was prepared with albumin dissolved in Tris-Buffer 50 mM in concentrations from 0 mg/ml (Tris-Buffer only) up to 1 mg/ml. Protein lysates were also plated in triplicates. Per well, 10 µl standard or protein lysate was plated, and 200 µl BCA was added to each well using a multi-well-pipette. Then 200 µl BCA solution (prepared as instructed) was added to each well using a multi-well pipette and incubated at 37°C for 30 minutes. Then colorimetric analysis followed using the spectrophotometer TECAN.

Protein lysates were stored at -80°C until ready to use. To perform arrays, lysates were gently thawed and kept on ice prior to use per instruction. 300 µg lysate per array set was used as suggested in the test kit for the Proteome Profiler™ Human Phospho-Kinase Arrays. 75 µg lysate per array set was used as indicated in the test kit for the PathScan® Arrays. Arrays were prepared according to the test kit and then exposed with the ImageQuant LAS 4000 Mini for a maximum time of 10 minutes. Various images were taken for further analysis at 1, 3, 5, and 10 minutes. For the final analysis, images with the exposure time of 10 minutes (Proteome Profiler™ Arrays), and 3, and 5 minutes (PathScan® Arrays) were used. Care was taken that corresponding arrays of treated and control cells were exposed for the same amount of time to ensure comparability.

Images were analyzed using the image analysis software ImageStudio Lite Version 5.2 by LI-COR. Signal values were then exported to a spreadsheet file for further analysis in Microsoft Excel. An average background signal using the negative control spots as

background value was subtracted from each target spot value. Results were then analyzed by comparing the absolute signal intensity values, and the relative change in phosphorylation (in %) between drug- and control-treated cells was calculated. Graphical analysis was performed using GraphPad Prism.

For graphical analysis, the absolute signal intensity values for each target spot were entered into Prism and graphed. A visual descriptive analysis was then performed as only two values per target were available per array. To compare the same target across multiple arrays and across cell lines, the relative change in phosphorylation of the R+D-treated cell population in regard to the corresponding control-treated cells was calculated and entered into Prism and graphed followed by a visual and descriptive analysis.

# 3. Results

## 3.1. Induction of Apoptosis

### 3.1.1. Assessment of Pre-Treatment With Rapamycin Plus Dasatinib in Neuroblastoma Cell Lines

To assess the pre-treatment of NB cells with the molecularly targeted combination therapy consisting of R+D, apoptosis assays applying the AV/PI-binding assay were performed using two MNA NB cell lines, KELLY and LAN-5, and two MNN NB cell lines, SK-N-SH and SK-N-AS. Cells were seeded and after 24 hours treated with a combination of R+D at IC50 concentrations, as shown in *Table 9*. As a control, cells were treated with vehicle (DMSO) in concentrations as applied in the drug treatment. After 72 hours, cells were harvested, AV/FITC, in combination with PI-staining was performed, and the numbers of apoptotic (early apoptosis: no PI/high AV, late apoptosis: high PI/high AV, necrosis: high PI/no AV) and living (no PI/no AV) cells were determined using FACS analysis according to the protocol outlined in the section *Material and Methods*. Results were grouped into live (no PI/no AV) and dead/apoptotic cells (AV and/or PI positive) for final analysis as described above.

All control-treated cells showed a viability of > 99 % for all cell lines in all independent experiments, and the amount of necrosis (high PI/no AV) in all experiments was below 3 % except for the cell line LAN-5 (data not shown). One R+D data point of the cell line LAN-5 had to be omitted due to a technical error. All other data sets were complete. The mean amount of necrosis for LAN-5 was about 10 %. These values were attributed to already dead cells at the time of FACS analysis. *Figure 8* shows that the R+D treatment induced apoptosis to a varying degree compared to control (DMSO)-treated cells in all cell lines.

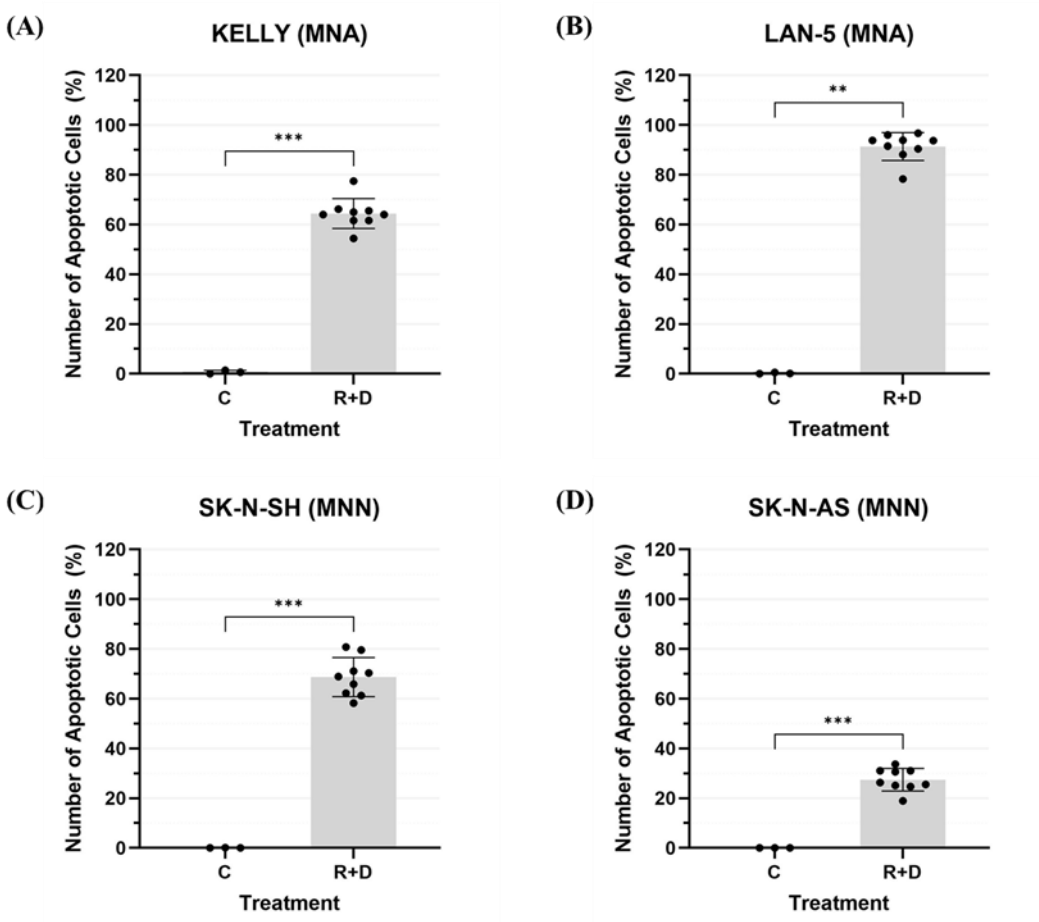


**Figure 8: Induction of Apoptosis in Neuroblastoma Cell Lines After Molecularly Targeted Pre Treatment Compared to Control (DMSO)-Treated Cells**

Annexin V (AV)- and propidium iodide (PI)-based fluorescence-activated cell sorting (FACS) analysis evaluating live (no PI/no AV) and apoptotic (AV and/or PI positive) cell numbers 72 hours after combinatorial treatment with rapamycin plus dasatinib (R+D) at $IC_{50}$ concentrations (as shown in *Table 9*) compared to control (DMSO)-treated cells in MycN-amplified (MNA) neuroblastoma (NB) cell lines KELLY **(A)** and LAN-5 **(B)**, and MycN-non-amplified (MNN) NB cell lines SK-N-SH **(C)** and SK-N-AS **(D)**. Data represents 3 independent experiments for each cell line (n=3) performed with one control per experiment and molecularly targeted treatment performed in triplicates. Displayed are the numbers of apoptotic cells (in %) after (control-) treatment. Data sets were assessed for normality followed by a t-test or Mann-Whitney test for each set as described in *Material and Methods.*
C: control, MNA: MycN-amplified, MNN: MycN-non-amplified, R+D: rapamycin plus dasatinib. P values are reported as 0.002 (**), < 0.001 (***).

In order to compare the effect of R+D treatment among the cell lines, the values were calculated as percentages of their respective control mean as described in *Material and Methods*.

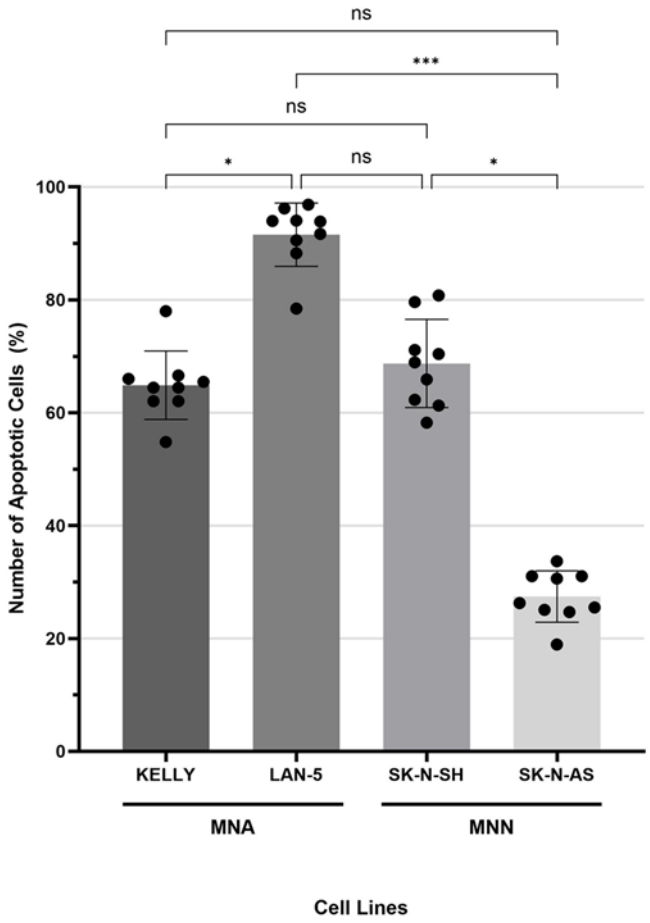


**Figure 9: Induction of Apoptosis in Neuroblastoma Cell Lines After Molecular Targeted Pre-Treatment**

Annexin V (AV)- and propidium iodide (PI)-based fluorescence-activated cell sorting (FACS) analysis evaluating live (no PI/no AV) and dead (AV and/or PI positive) cell numbers 72 hours after combinatorial treatment with rapamycin plus dasatinib (R+D) at $IC_{50}$ concentrations (as shown in *Table 9*) in MycN-amplified (MNA) neuroblastoma (NB) cell lines KELLY and LAN-5, and MycN-non-amplified (MNN) NB cell lines SK-N-SH and SK-N-AS. Data represents 3 independent experiments for each cell line (n=3) performed in triplicates. Displayed is the percentage (%) of apoptotic cells in respect to their individual controls after R+D treatment for each cell line. Data was assessed for normality followed by a Kruskall-Wallis non-parametric test as described in *Material and Methods.*
MNA: MycN-amplified, MNN: MycN-non-amplified, ns: not significant. P values are reported as 0.12 (ns), 0.33 (*), < 0.001 (***).

In comparison, *Figure 9* shows that in the MNA cell line KELLY, 64 % (*SD* = 6 %), and in the MNA cell line LAN-5, 91 % (*SD* = 6 %), of cells were AV- and/or PI-positively stained after treatment with R+D. These results were overall greater than the apoptosis induction in the MNN cell line SK-N-AS with only 27 % (*SD* = 5 %) of AV- and/or PI-positively stained cells after R+D treatment. However, there was no statistically significant difference between the MNA cell line KELLY and the MNN cell line SK-N-AS performing the Kruskall-Wallis test. The MNN cell line SK-N-SH showed 87 % (*SD* = 8 %) of AV- and/or PI-positively stained cells after R+D treatment and thus showed no significant difference in the induction of apoptosis

compared to the MNA cell lines KELLY and LAN-5. However, the treatment with R+D induces significantly more apoptosis in the MNN cell line SK-N-SH than in the MNN cell line SK-N-AS.

### 3.1.2. Assessment of Chemotherapeutic Treatment With Irinotecan Plus Temozolomide in Neuroblastoma Cell Lines

To assess the conventional chemotherapy consisting of the active metabolite of I (SN-38) and T in MNA and MNN NB cell lines, the two MNA cell lines, KELLY and LAN-5, and the two MNN NB cell lines, SK-N-SH and SK-N-AS, were seeded, incubated for 24 hours, and then treated with a combination of I+T for 72 hours at $IC_{50}$ concentrations as shown in *Table 9*. As a control, cells were treated with vehicle (DMSO) in concentrations as applied in the drug treatment.

After 72 hours, cells were harvested, AV/FITC-, in combination with PI-staining was performed, and the numbers of apoptotic (early apoptosis: no PI/high AV, late apoptosis: high PI/high AV, necrosis: high PI/no AV) and living (no PI/no AV) cells were determined using FACS analysis according to the protocol outlined in the section *Material and Methods*. Results were grouped into live (no PI/no AV) and dead/apoptotic cells (AV and/or PI positive) for final analysis as described in *Material and Methods*.

All control-treated cells showed a viability of > 99 % for all cell lines in all independent experiments, and the amount of necrosis (high PI/ no AV) in all experiments was below 3 % except for the cell line LAN-5 (data not shown). The mean amount of necrosis for LAN-5 was about 6 %. These values were attributed to already dead cells at the time of FACS analysis.

The I+T treatment induced apoptosis in all cell lines to a varying degree compared to control (DMSO)-treated cells, as shown in *Figure 10.*

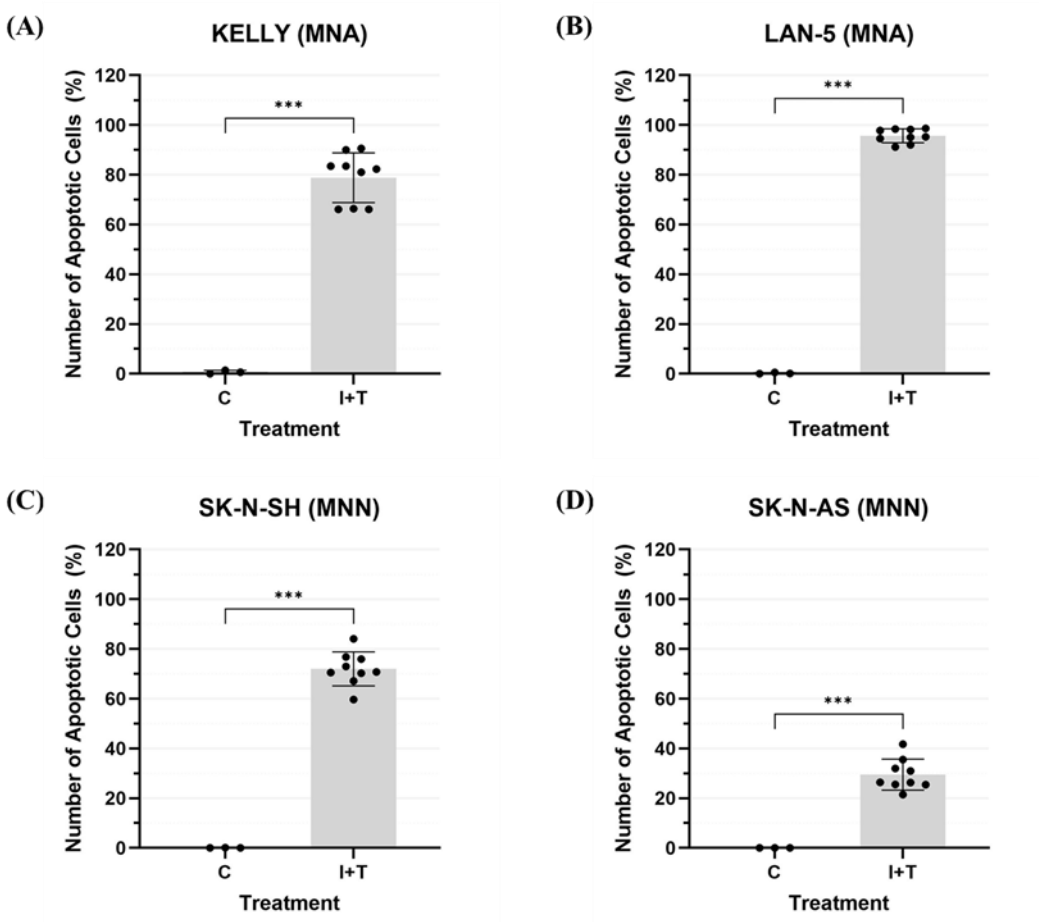


**Figure 10: Induction of Apoptosis in Neuroblastoma Cell Lines After Conventional Chemotherapy Treatment Compared to Control (DMSO)-Treated Cells**

Annexin V (AV)- and propidium iodide (PI)-based fluorescence-activated cell sorting (FACS) analysis evaluating live (no PI/no AV) and apoptotic (AV and/or PI positive) cell numbers 72 hours after conventional chemotherapy combination treatment with irinotecan plus temozolomide (I+T) at $IC_{50}$ concentrations (as shown in *Table 9*) compared to control (DMSO)-treated cells in MycN-amplified (MNA) neuroblastoma (NB) cell lines KELLY **(A)** and LAN-5 **(B)**, and MycN-non-amplified (MNN) NB cell lines SK-N-SH **(C)** and SK-N-AS **(D)**. Data represents 3 independent experiments for each cell line (n=3) performed with one control per experiment and chemotherapy treatment performed in triplicates. Displayed are the numbers of apoptotic cells after (control-) treatment. Data sets were assessed for normality followed by a t-test for each set as described in *Material and Methods.*
C: control, I+T: irinotecan plus temozolomide, MNA: MycN-amplified, MNN: MycN-non-amplified. P values are reported as < 0.001 (***).

In order to compare the effect of I+T treatment among the cell lines, the values were calculated as percentages of their respective control mean as described in *Material and Methods*.

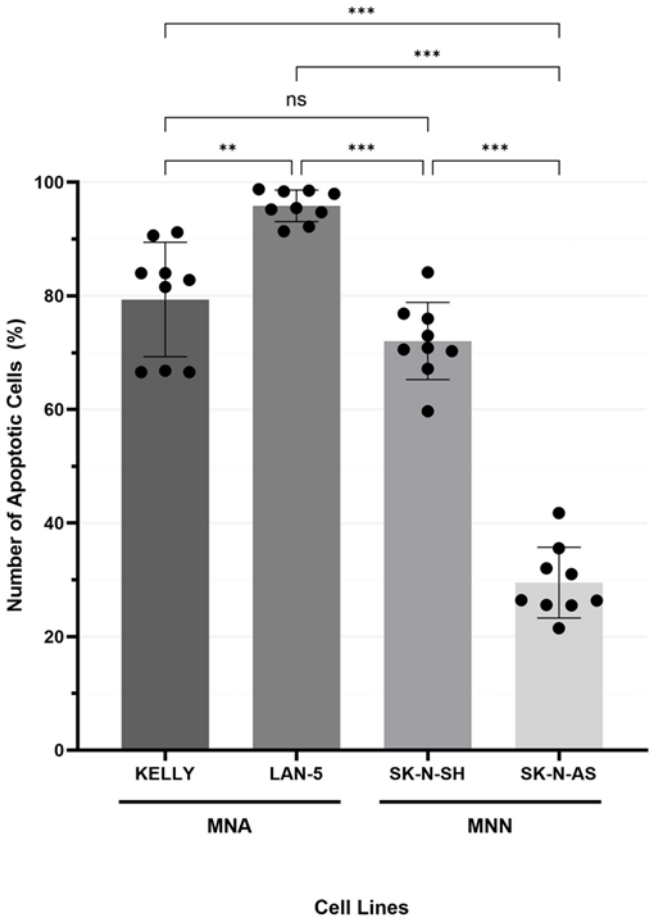


**Figure 11: Induction of Apoptosis in Neuroblastoma Cell Lines After Conventional Chemotherapy Treatment**

Annexin V (AV)- and propidium iodide (PI)-based fluorescence-activated cell sorting (FACS) analysis evaluating live (no PI/no AV) and apoptotic (AV and/or PI positive) cell numbers 72 hours after conventional chemotherapy combination treatment with irinotecan plus temozolomide (I+T) at $IC_{50}$ concentrations (as shown in *Table 9*) in MycN-amplified (MNA) neuroblastoma (NB) cell lines KELLY and LAN-5, and MycN-non-amplified (MNN) NB cell lines SK-N-SH and SK-N-AS. Data represents 3 independent experiments for each cell line (n=3) performed with one control per experiment and chemotherapy treatment performed in triplicates. Displayed is the percentage (%) of apoptotic cells in respect to their individual controls after I+T treatment. Data was assessed for normality and a One-Way Anova test was performed as described in *Material and Methods*.
MNA: MycN-amplified, MNN: MycN-non-amplified, ns: not significant. P values are reported as 0.12 (ns), 0.002 (**), < 0.001 (***).

In the MNA cell lines KELLY and LAN-5, 79 % (*SD* = 10 %) and 96 % (*SD* = 3 %) of all cells, respectively, were AV- and/or PI-positively stained after I+T treatment as shown in *Figure 11*. These results were significantly greater than the apoptosis induction in the MNN cell line SK-N-AS with 29 % (*SD* = 6 %) AV- and/ or PI-positively stained cells after treatment. On the other hand, the MNN cell line SK-N-SH showed 72 % (*SD* = 7 %) AV- and/ or PI-positively stained cells after treatment and thus showed only slightly lower numbers compared to the MNA cell line KELLY. Again, there is a greater induction of apoptosis after chemotherapy treatment in the MNN cell line SK-N-SH than in the MNN cell line SK-N-AS.

### 3.1.3. Assessment of the RIST Treatment in Neuroblastoma Cell Lines

To assess the RIST treatment combining the pre-treatment of R+D with the conventional chemotherapy treatment I+T (as shown in *Figure 6*) in MNA and MNN NB cell lines, the two MNA cell lines, KELLY, and LAN-5, and the two MNN NB cell lines, SK-N-SH and SK-N-AS, were seeded and incubated for 24 hours. First, cells were pre-treated with R+D for 72 hours, then the medium was changed, and after an additional 24 hours, the chemotherapeutic I+T treatment was added for 72 hours. All drugs were applied in $IC_{50}$ concentrations, as shown in *Table 9*. As a control, cells were treated with vehicle (DMSO) in concentrations as applied in the drug treatment.

After 72 hours, cells were harvested, AV/FITC-, in combination with PI-staining was performed, and the numbers of apoptotic (early apoptosis: no PI/high AV, late apoptosis: high PI/high AV, necrosis: high PI/no AV) and living (no PI/no AV) cells were determined using FACS according to the protocol outlined in the section *Material and Methods*. Results were grouped into live (no PI/no AV) and dead/apoptotic cells (AV and/or PI positive) for final analysis as described above.

All control-treated cells showed a viability of > 99 % for all cell lines in all independent experiments. The amount of necrosis (high PI/ no AV) in all experiments for cell lines KELLY and SK-N-AS was below 1 %. Cell lines LAN-5 and SK-N-SH showed higher values at 5 % for SK-N-SH and 8 % for LAN-5 (data not shown), respectively. These values were attributed to already dead cells at the time of FACS analysis. Due to a technical error, two RIST data points for SK-N-SH had to be omitted from the analysis.

As shown in *Figure 12*, the treatment with the complete RIST therapy protocol induced apoptosis in all cell lines to a varying degree compared to control (DMSO)-treated cells.

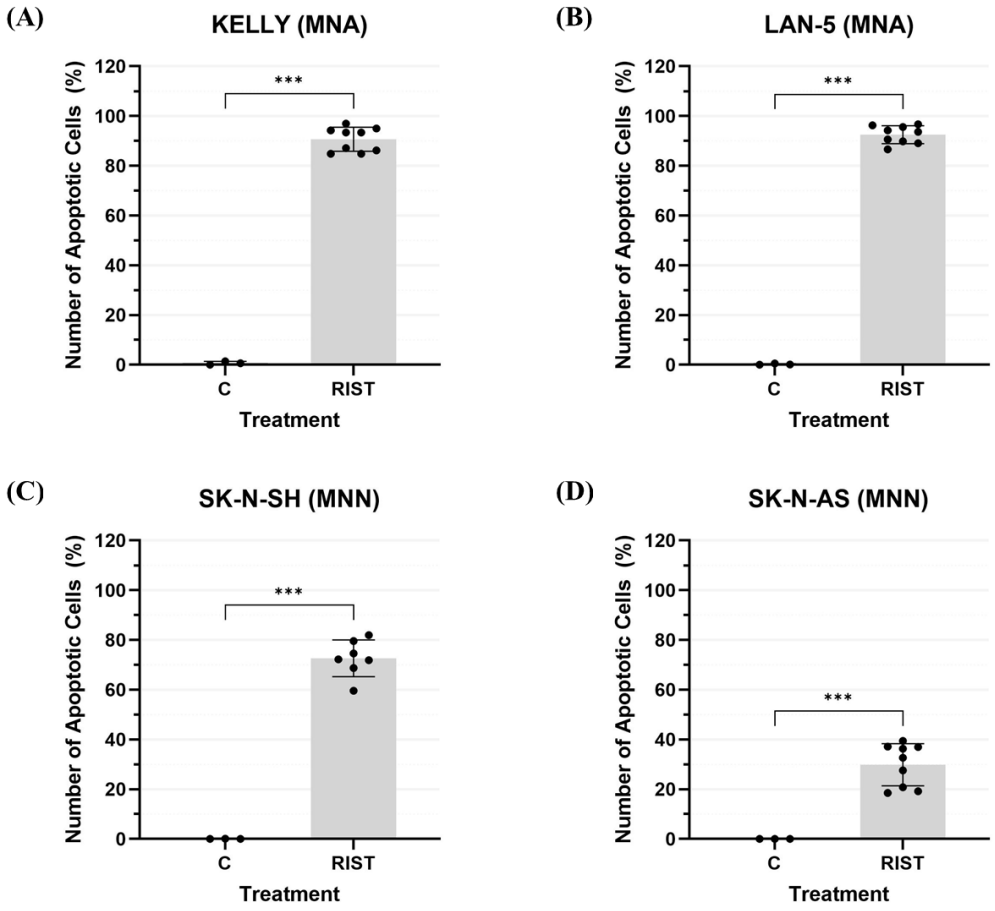


**Figure 12: Induction of Apoptosis in Neuroblastoma Cell Lines After RIST Treatment Compared to Control (DMSO)-Treated Cells**

Annexin V (AV)- and propidium iodide (PI)-based fluorescence-activated cell sorting (FACS) analysis evaluating live (no PI/no AV) and apoptotic (AV and/or PI positive) cell numbers after RIST treatment (as shown in *Figure 6*) at $IC_{50}$ concentrations (as shown in *Table 9*) compared to control (DMSO)-treated cells in MycN-amplified (MNA) neuroblastoma (NB) cell lines KELLY **(A)** and LAN-5 **(B)**, and MycN-non-amplified (MNN) NB cell lines SK-N-SH **(C)** and SK-N-AS **(D)**. Data represents 3 independent experiments for each cell line (n=3) performed with one control per experiment and RIST treatment performed in triplicates. Displayed are the numbers (in %) of apoptotic cells after (control-) treatment. Data sets were assessed for normality followed by a t-test for each set as described in *Material and Methods*.
C: control, MNA: MycN-amplified, MNN: MycN-non-amplified. P values are reported as < 0.001 (***).

In order to compare the effect of RIST treatment among the cell lines, the values were calculated as percentages of their respective control mean as described in *Material and Methods*.

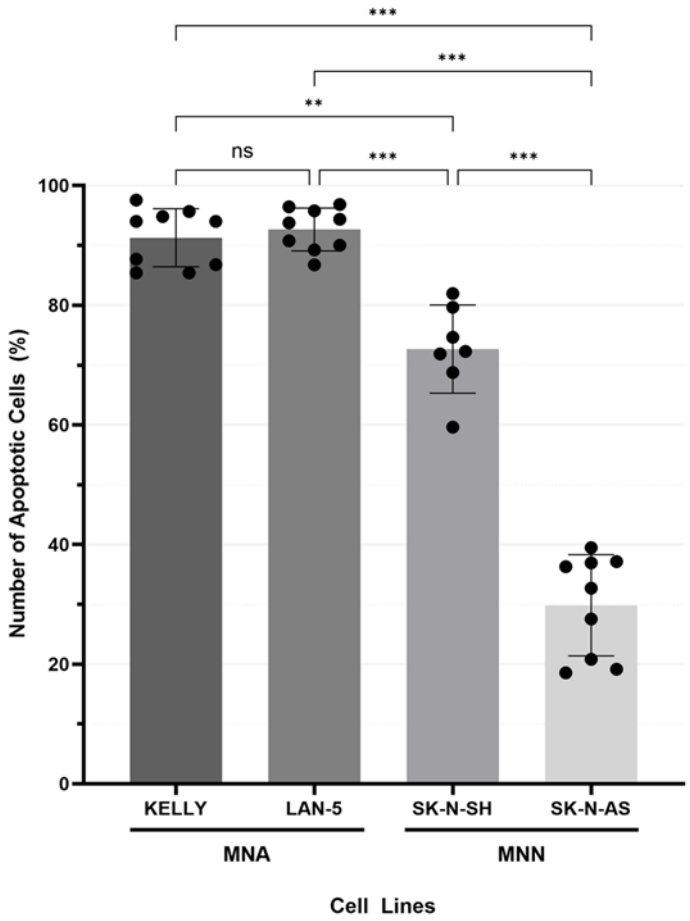


**Figure 13: Induction of Apoptosis in Neuroblastoma Cell Lines After RIST Treatment**

Annexin V (AV)- and propidium iodide (PI)-based fluorescence-activated cell sorting (FACS) analysis evaluating live (no PI/no AV) and apoptotic (AV and/or PI positive) cell numbers after RIST treatment (as shown in *Figure 6*) at $IC_{50}$ concentrations (as shown in *Table 9*) in MycN-amplified (MNA) neuroblastoma (NB) cell lines KELLY and LAN-5, and MycN-non-amplified (MNN) NB cell lines SK-N-SH and SK-N-AS. Data represents 3 independent experiments for each cell line (n=3) performed in triplicates. Displayed is the percentage (%) of apoptotic cells in respect to their individual controls after RIST treatment. Data sets were assessed for normality and a One-Way Anova test was performed as described in *Material and Methods*.
MNA: MycN-amplified, MNN: MycN-non-amplified, ns: not significant. P values are reported as 0.12 (ns), 0.002 (**), < 0.001 (***).

As seen in *Figure 13*, in the MNA cell line KELLY, 91 % (*SD* = 5 %), and in the MNA cell line LAN-5, 92 % (*SD* = 4 %) of cells were AV- and/ or PI-positively stained after treatment. These results were significantly greater than the apoptosis induction in the MNN cell lines SK-N-SH with 73 % (*SD* = 7 %) and SK-N-AS, which showed 30 % (*SD* = 8 %) of AV- and/ or PI-positively stained cells after treatment. There was no significant difference in the induction of apoptosis between the two MNA cell lines KELLY and LAN-5. However, there was a significantly greater induction of apoptosis in the MNN cell line SK-N-SH than in the MNN cell line SK-N-AS.

Taken together, the RIST therapy protocol showed greater efficacy regarding the induction of apoptosis in MNA cell lines KELLY and LAN-5 compared to the MNN cell lines SK-N-SH and SK-N-AS.

## 3.2.Phosphorylation Status Profiling

An approach using multi-well antibody signaling arrays was used to identify pathways and targets responsible for the greater efficacy of the RIST therapy in MNA compared to MNN NB cell lines. These arrays allow the parallel determination of relative protein phosphorylation levels of many signaling nodes and downstream targets at once in an efficient way, narrowing down relevant targets to be verified using more refined methods such as Western blot analysis.

These arrays are based on a sandwich immunoassay principle for detecting signaling proteins that have undergone phosphorylation. R+D-treated and control (DMSO vehicle)-treated cells were compared, and absolute pixel density (signal intensity) values were graphed to analyze phosphorylation status before and after R+D treatment for each cell line. Relative phosphorylation (%) of R+D- compared to control-treated cells for each target was calculated to identify differences between cell lines.

First, one Profiler™ Array per cell line was performed for the cell lines KELLY (MNA) and SK-N-AS (MNN), which allows the simultaneous detection of the relative phosphorylation levels of 43 different signaling and effector proteins and two related total proteins. Two independent PathScan® RTK Signaling Arrays, which allow the detection of the phosphorylation status of 28 tyrosine kinases and 11 signaling nodes (pathway components that route received signals through a variety of pathways and in turn can regulate a number of different effectors to elicit a particular response), and two independent PathScan® AKT Signaling Arrays, analyzing 16 signaling nodes predominantly belonging to the AKT signaling network, were done for all cell lines used in this study (MNA: KELLY, LAN-5; MNN: SK-N-SH, SK-N-AS). These specific arrays were chosen as they allowed the analysis of targets taking part in the PI3K/AKT/mTOR and MAPK/ERK pathways. As outlined above (see *Sections 1.2 and 1.3*), these pathways are critical in cell signaling, regulating cell growth and cell cycle, proliferation, survival, as well as protein biosynthesis, and are directly targeted by the RIST therapy model. Additionally, the PathScan® Arrays were also used to verify findings from the

Proteome Profiler™ arrays. R+D-treated cells and vehicle (DMSO)-treated cells in concentrations as applied in the drug treatment were assessed for each cell line. Cells were seeded and after 24 hours treated with a combination of R+D at $IC_{50}$ concentrations, as shown in *Table 9*. As a control, cells were treated with vehicle (DMSO) in concentrations as applied in the drug treatment. After 72 hours, cells were harvested, protein lysates were prepared, and arrays were performed as outlined above (see *Section 2.2.7*).

The quality of the arrays was first assessed, considering well-stained positive control spots as well as true non-stained negative control spots and even staining of the individual target spots relevant to the following analysis to ensure reliable results. All Proteome Profiler™ arrays were used for further analysis. All PathScan® arrays for the cell line KELLY (MNA) were of good quality and used in further analysis. One PathScan® RTK Signaling Array and one PathScan® AKT Signaling Array had to be omitted due to low and uneven staining quality for the LAN-5 (MNA) and SK-N-SH (MNN) cell lines, respectively. One of each PathScan® array had to be omitted from further analysis for the cell line SK-N-AS (MNN). Array target maps, array layout, and complete array data of the arrays used can be found in the supplementary section (*Appendix, Figure 44-68*). *Figures 14* and *15* show exemplary arrays of the MNA NB cell line KELLY and the MNN NB cell line SK-N-AS, respectively. The difference in intensity of staining in control (DMSO vehicle)-treated in comparison to R+D-treated cells within the different cell lines is seen and can be further analyzed.

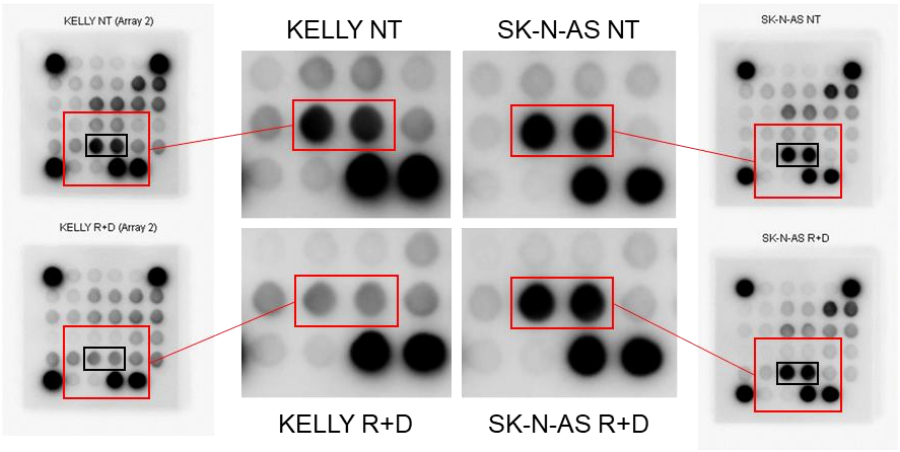


**Figure 14: Exemplary PathScan® AKT Signaling Arrays of the Neuroblastoma Cell Lines KELLY and SK-N-AS, Target Spot for Phosphatase and Tensin Homolog at Serine 380**

Exemplary PathScan® AKT Signaling Arrays (##9474) by Cell Signaling Technology for the MycN-amplified (MNA) neuroblastoma (NB) cell line KELLY and the MycN-non-amplified (MNN) NB cell line SK-N-AS, comparing control (DMSO vehicle)-treated (NT) and rapamycin plus dasatinib (R+D)-treated cells, are shown. Target-specific capture antibodies have been spotted in duplicate onto nitrocellulose-coated glass slides and cell lysates of NT- and R+D-treated cells were incubated, followed by a biotinylated detection antibody cocktail. Streptavidin-conjugated reagents were used to visualize the bound detection antibody by chemiluminescence. Images were captured with the ImageQuant LAS 4000 Mini.
Relative phosphorylation levels in NT- and R+D-treated cells of phosphatase and tensin homolog (PTEN) at serine 380 (Ser380) are marked. A defined reduction in phosphorylation at Ser380 as a readout for PTEN activity is seen in R+D treated KELLY (MNA) cells but not in SK-N-AS (MNN) cells.

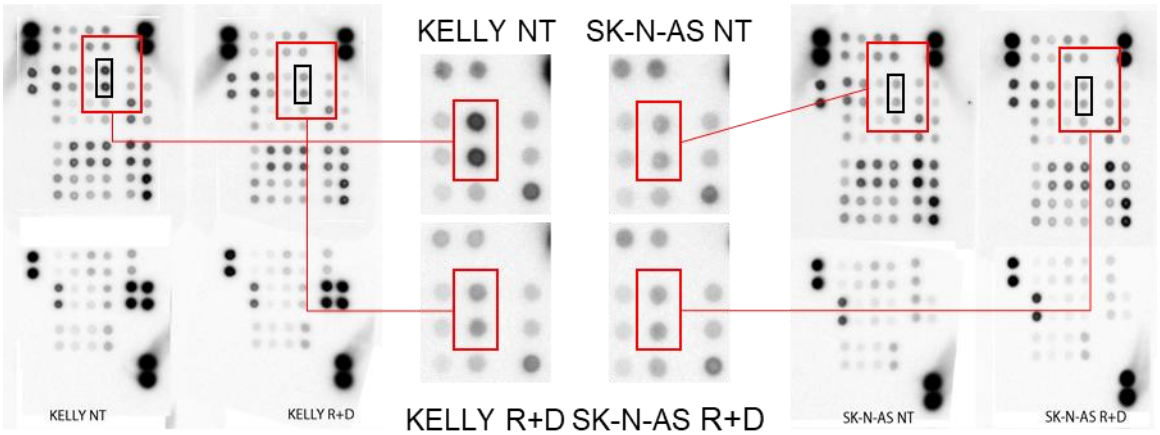


**Figure 15: Exemplary Proteome Profiler™ Human Phospho-Kinase Arrays of the Neuroblastoma Cell Lines KELLY and SK-N-AS, Target Spot for cAMP Response Element-Binding Protein at Serine 133**

Exemplary Proteome Profiler™ Human Phospho-Kinase Array Kit by R&D Systems (#ARY003B) for the MycN-amplified (MNA) neuroblastoma (NB) cell line KELLY and the MycN-non-amplified (MNN) NB cell line SK-N-AS, comparing control (DMSO vehicle)-treated (NT) and rapamycin plus dasatinib (R+D)-treated cells, are shown. Target-specific capture antibodies have been spotted in duplicate onto nitrocellulose-coated glass slides and cell lysates of NT- and R+D-treated cells were incubated, followed by a biotinylated detection antibody cocktail. Streptavidin-conjugated reagents were used to visualize the bound detection antibody by chemiluminescence. Images were captured with the ImageQuant LAS 4000 Mini.
Relative phosphorylation levels in NT- and R+D-treated cells of cAMP response element-binding protein (CREB) at serine 133 (Ser133) are marked. While CREB (Ser133) is noticeably stronger phosphorylated in untreated KELLY (KELLY NT) cells than in untreated SK-N-AS (SK-N-AS NT) cells, relative phosphorylation levels are noticeably reduced in the MNA cell line KELLY after R+D treatment but not in the MNN cell line SK-N-AS.

### 3.2.1. Greater Reduction in the Phosphorylation Status of Signaling Nodes in MycN-Amplified Neuroblastoma Cell Lines

The NB cell lines KELLY (MNA) and SK-N-AS (MNN) were used as the primary cell lines for the Proteome Profiler™ arrays because they represent an MNA cell line (KELLY) that responded to the RIST therapy versus an MNN cell line (SK-N-AS) with the least response to the RIST therapy applying the apoptosis assays (as described in *Chapter 3.1*) and so most significant differences in molecular changes were expected for these two cell lines.

When comparing changes induced by the combinatorial treatment of R+D compared to control (DMSO vehicle)-treated cells, it was notable that the molecularly targeted therapy induced distinctively greater changes in phosphorylation levels in the cell line KELLY than in SK-N-AS (*Appendix, Figure 47 and 48*).

Additionally, the phosphorylation levels in KELLY were more substantially reduced than in SK-N-AS, in which several target proteins even showed an increase in phosphorylation levels (*Appendix, Figure 47 and 48*). Similar trends, albeit less profound, could be seen when

comparing the PathScan® RTK (*Appendix, Figure 63, 64 and 68*) and PathScan® AKT (*Appendix, Figure 52, 53 and 57*) Signaling Array data.

In conclusion, the molecularly targeted treatment R+D reduced in higher quantity and quality the phosphorylation levels of signaling and effector proteins in the MNA cell line KELLY compared to the MNN cell line SK-N-AS.

As a side note, when only comparing vehicle (DMSO)-treated cell populations of the cell lines KELLY and SK-N-AS, phosphorylation levels of the 43 signaling and effector proteins were relatively similar across most targets. However, notable differences in phosphorylation levels (defined as a change of signal intensity by at least twofold) between those two cell lines were detected in three targets. Phosphorylation levels of CREB (Ser133) and three phosphorylation sites of p53 (Ser15, Ser46, Ser392) were noticeably greater in the cell line KELLY (MNA). In contrast, the phosphorylation level of AMPKalpha 1 (Thr183) was greater in the cell line SK-N-AS (MNN) (see *Appendix, Figure 44-48*).

### 3.2.2. Evidence for Greater Inhibition of mTOR Pathway in MycN-Amplified Neuroblastoma Cell Lines

#### 3.2.2.1. mTOR

The serine-threonine kinase mTOR exists as a catalytic subunit in two distinct complexes, mTORC1 and mTORC2 (45, 46, 49). mTORC 1 is activated by AKT (49).

Phosphorylation at serine 2448 (Ser2448) of mTOR may occur directly via AKT *in vitro* (169) but has recently been suggested to be a target of S6K1 rather than AKT (170). It is commonly used as a readout of mTOR activity, but the functional significance remains unclear (48, 169).

Change in phosphorylation of mTOR at Ser2448 after the treatment with R+D was analyzed for the MNA cell line KELLY and the MNN cell line SK-N-AS utilizing the Proteome Profiler™ Phospho-Kinase Array. *Figure 16* shows the phosphorylation status as absolute pixel density values (AU) after 72 hours of treatment with R+D compared to control (DMSO vehicle)-treated cells.

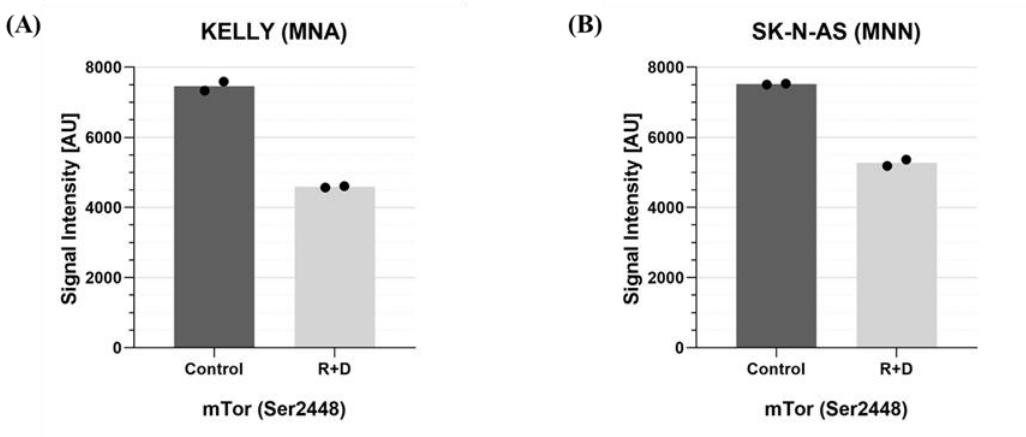


**Figure 16: Phosphorylation Status of Mammalian Target of Rapamycin in Control- and Rapamycin Plus Dasatinib-Treated Neuroblastoma Cell Lines**

Phosphorylation status of mammalian target of rapamycin (mTOR) at serine 2448 (Ser2448) after 72 hours of treatment with rapamycin plus dasatinib (R+D) compared to control (DMSO vehicle)-treated cells of the MycN-amplified (MNA) neuroblastoma (NB) cell line KELLY **(A)** and the MycN-non-amplified (MNN) NB cell line SK-N-AS **(B)** were analyzed utilizing the Proteome Profiler™ Human Phospho-Kinase Array by R&D Systems. Data represents one array with duplicate target spots for each cell line. DMSO: dimethyl sulfoxide. AU (arbitrary unit): absolute pixel density values, displayed bars are means.

The molecularly targeted combinatorial R+D treatment showed a marked decrease in phosphorylation at Ser2448 of mTOR in both cell lines tested (*Figure 16 A and B*). The reduction in phosphorylation is slightly greater in the MNA cell line KELLY than in the MNN cell line SK-N-AS, as shown in *Figure 17.*

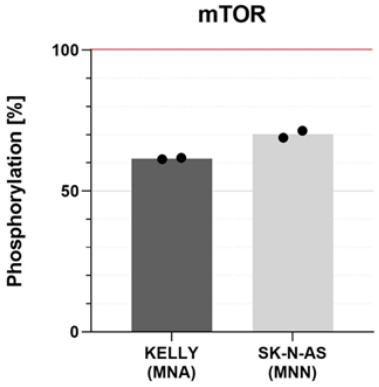


**Figure 17: Slightly More Reduced Serine 2448 Phosphorylation of Mammalian Target of Rapamycin in KELLY Compared to SK-N-AS Cells After Rapamycin Plus Dasatinib-Treatment**

Phosphorylation status (%) of mammalian target of rapamycin (mTOR) in rapamycin plus dasatinib (R+D)-treated cells relative to control (DMSO vehicle)-treated cells (100%, red line). Data represents one array with duplicate target spots for each cell line. DMSO: dimethyl sulfoxide, MNA: MycN-amplified, MNN: MycN-non-amplified. Displayed bars are means.

#### 3.2.2.2. PRAS40

PRAS40 is a component and a substrate of the mTORC1 and has been suggested to function as a negative regulator of mTORC1 (47, 48, 171). Upon phosphorylation at threonine 246 (Thr246) by activated AKT (47, 48, 171), it is thought that PRAS40 dissociates from the mTOR complex and thereby loses its ability to suppress mTOR signaling to its downstream targets S6K and 4E-BP1 (47, 48, 171). However, several other studies indicated that PRAS40 is necessary for mTORC1 activity and that its effects might be tissue-specific (171).

The change in phosphorylation of PRAS40 at Thr246 after the treatment with R+D was analyzed for the MNA cell lines KELLY and LAN-5 and the MNN cell lines SK-N-SH and SK-N-AS utilizing the PathScan® AKT Signaling Array. *Figure 18* shows the phosphorylation status as absolute pixel density values (AU) after 72 hours of treatment with R+D compared to control (DMSO vehicle)-treated cells.

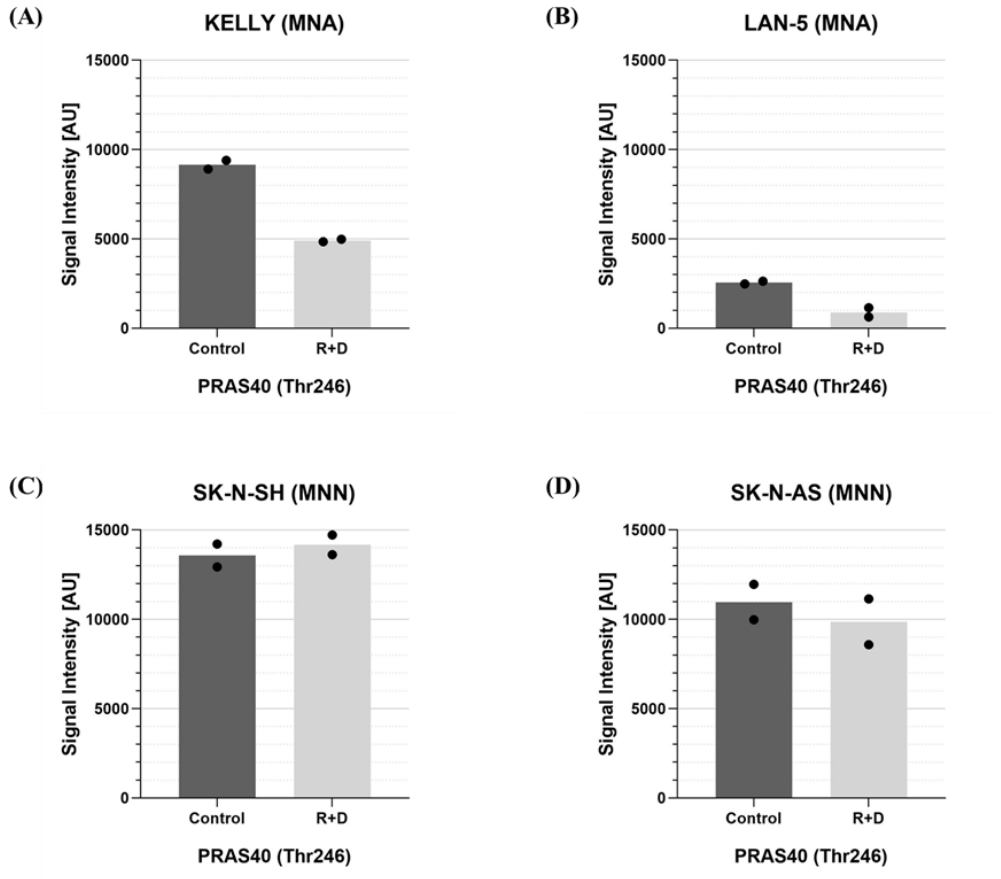


**Figure 18: Phosphorylation Status of Proline-Rich AKT Substrate of 40 kDa in Control- and Rapamycin Plus Dasatinib-Treated Neuroblastoma Cell Lines**

Phosphorylation status of proline-rich AKT substrate of 40 kDa (PRAS40) at threonine 246 (Thr246) after 72 hours of treatment with rapamycin plus dasatinib (R+D) compared to control (DMSO vehicle)-treated cells of the MycN-amplified (MNA) neuroblastoma (NB) cell lines KELLY **(A)** and LAN-5 **(B)**, and the MycN-non-amplified (MNN) NB cell lines SK-N-SH **(C)** and SK-N-AS **(D)** were analyzed utilizing the PathScan® AKT Signaling Array by Cell Signaling Technology. Data represents one array with duplicate target spots for each cell line. DMSO: dimethyl sulfoxide. AU (arbitrary unit): absolute pixel density values, displayed bars are means.

Treatment with R+D considerably reduced the phosphorylation of PRAS40 at Thr246 in both MNA cell lines tested (KELLY, LAN-5) (*Figure 18 A and B*). In contrast, no profound reduction in phosphorylation could be shown for the MNN cell lines (SK-N-SH, SK-N-AS) (*Figure 18 C and D*). In an independent PathScan® array, results for the MNA cell lines KELLY, and LAN-5 could be confirmed with similar results *(Appendix, Figure 69 A and B)*. No additional arrays for the cell lines SK-N-SH and SK-N-AS were available. The phosphorylation status of PRAS40 at Thr246 was also analyzed utilizing the Proteome Profiler™ Human Phospho-Kinase Array for the cell lines KELLY (MNA) and SK-NAS (MNN). While the overall reduction in phosphorylation of PRAS40 at Thr246 was less than in the PathScan® array, a reduction in phosphorylation after 72-hour treatment with R+D could

be confirmed for the MNA cell line KELLY, and again, no relevant decrease in phosphorylation occurred in the MNN cell line SK-N-AS (*Appendix, Figure 70 A and B*).

In conclusion, the molecularly targeted combinatorial R+D treatment leads to a decrease in phosphorylation of PRAS40 at Thr246 in MNA cell lines KELLY and LAN-5 but not in MNN cell lines SK-N-SH and SK-N-AS as depicted in *Figure 19.*

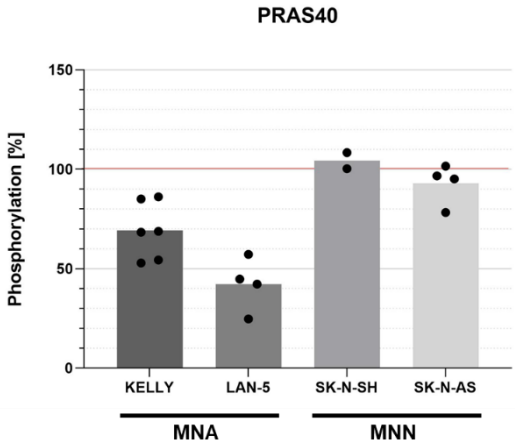


**Figure 19: Phosphorylation of Proline-Rich AKT Substrate of 40 kDa at Threonine 246 is More Reduced in MycN-Amplified Compared to MycN-non-Amplified Neuroblastoma Cell Lines After Rapamycin Plus Dasatinib-Treatment**

Phosphorylation status (%) of proline-rich AKT Substrate of 40 kDA (PRAS40) in rapamycin plus dasatinib (R+D)-treated cells relative to control (DMSO vehicle)-treated cells (100%, red line). Data represents three arrays for KELLY, two arrays each for LAN-5 and SK-N-AS, and one array for SK-N-SH, with duplicate target spots per array. DMSO: dimethyl sulfoxide, MNA: MycN-amplified, MNN: MycN-non-amplified. Displayed bars are means.

#### 3.2.2.3. mTORC1 Substrate p70 S6 Kinase, and S6 Ribosomal Protein

S6K1 is one of the main downstream targets of the PI3K/AKT/mTOR pathway (47, 49, 53). S6K1 phosphorylation at threonine 229 (Thr229) (by PDK-1) and threonine 229 (Thr389) (by mTORC1) are critical for its kinase activity (47, 53). Thr389 phosphorylation is known to be blocked by rapamycin (53). Phosphorylation sites threonine 421 and serine 424 (Thr421/Ser424) lie in a pseudo-substrate region and are thought to activate S6K1 by relieving pseudo-substrate suppression (53). While phosphorylation at this site contributes to activity, it does not appear to be critical (53).

The change in phosphorylation of S6K1 at phosphorylation sites Thr389, and Thr421/Ser424 after the treatment with R+D was analyzed for the MNA cell line KELLY and the MNN cell line SK-NAS utilizing the Proteome Profiler™ Human Phospho-Kinase Array. *Figure 20*

shows the phosphorylation status as absolute pixel density values (AU) after 72 hours of treatment with R+D compared to control (DMSO vehicle)-treated cells.

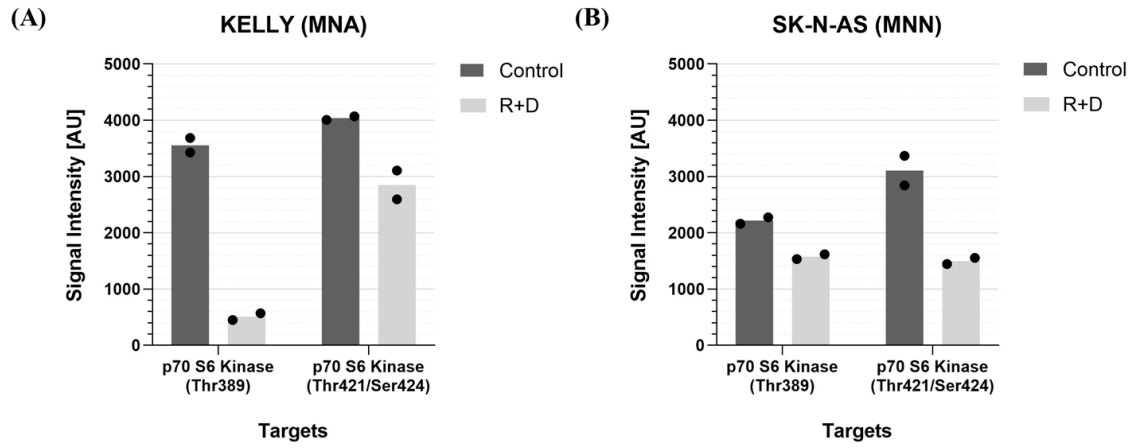


**Figure 20: Phosphorylation Status of p70 S6 Kinase in Control- and Rapamycin Plus Dasatinib-Treated Neuroblastoma Cell Lines**

Phosphorylation status of p70 S6 kinase (S6K) at threonine 389 (Thr389) and threonine 421/ serine 424 (Thr421/Ser424) after 72 hours of treatment with rapamycin plus dasatinib (R+D) compared to control (DMSO vehicle)-treated cells of the MycN-amplified (MNA) neuroblastoma (NB) cell line KELLY (**A)** and the MycN-non-amplified (MNN) NB cell line SK-N-AS **(B)** were analyzed utilizing the Proteome Profiler™ Human Phospho-Kinase Array by R&D Systems. Data represents one array with duplicate target spots for each cell line. DMSO: dimethyl sulfoxide. AU (arbitrary unit): absolute pixel density values. Displayed bars are means.

Treatment with R+D led to a noticeable reduction in phosphorylation at both phosphorylation sites in the MNA cell line KELLY as well as the MNN cell line SK-N-AS (*Figure 20 A and B*). Notably, a much greater reduction in phosphorylation at the primary rapamycin-sensitive phosphorylation site Thr389 occurred in the MNA cell line KELLY (*Figure 21 A*), whereas the reduction in phosphorylation at the unspecific site Thr421/Ser424 was greater in the MNN cell line SK-N-AS *(Figure 21 B)*. No independent confirmation arrays were available.

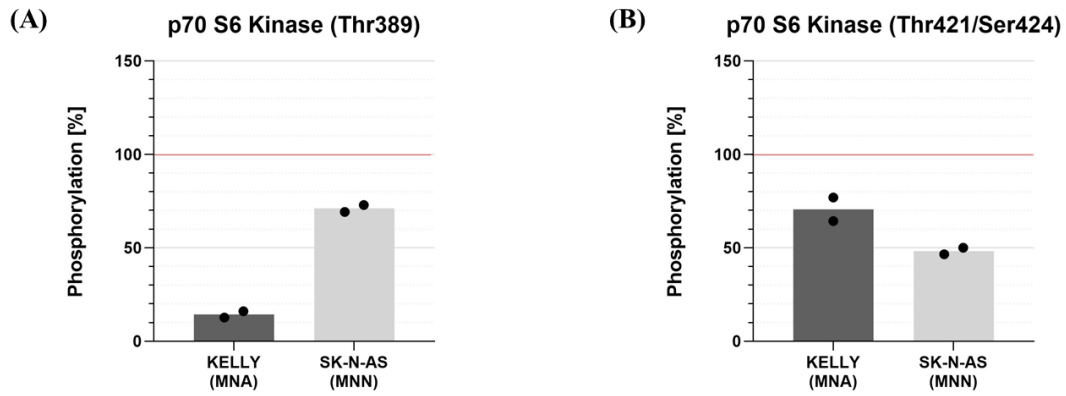


**Figure 21: Reduced Phosphorylation of p70 S6 Kinase at Threonine 389 in KELLY Compared to SK-N-AS Cells After Rapamycin Plus Dasatinib-Treatment**

Phosphorylation status (%) of p70 S6 Kinase (S6K) phosphorylation sites threonine 389 (Thr389) **(A)** and threonine 421/ serine 424 (Thr421/Ser424) **(B)** in rapamycin plus dasatinib (R+D)-treated cells relative to control (DMSO vehicle)-treated cells (100%, red line). Data represents one array with duplicate target spots for each cell line. DMSO: dimethyl sulfoxide, MNA: MycN-amplified, MNN: MycN-non-amplified. AU (arbitrary unit): absolute pixel density values. Displayed bars are means.

The PathScan® AKT Signaling Array was not utilized to analyze mTOR downstream targets as signals for Thr389 and Thr421/Ser424 were too weak to be analyzed reliably (data not shown).

S6 ribosomal protein (rpS6) is a substrate of S6K and has been used as a readout for mTOR activity (47). The phosphorylation sites serine 235 and serine 236 (Ser235/Ser236) represent two major phosphorylation sites responsible for its activation and are phosphorylated by S6K as well as RSK (53, 172).

The change in phosphorylation of rpS6 at Ser235/236 after treatment with R+D was analyzed for the MNA cell lines KELLY and LAN-5 and the MNN cell lines SK-N-SH and SK-N-AS utilizing the PathScan® RTK Signaling Array. *Figure 22 A-D* shows the phosphorylation status as absolute pixel density values (AU) after 72 hours of treatment with R+D compared to control (DMSO vehicle)-treated cells.

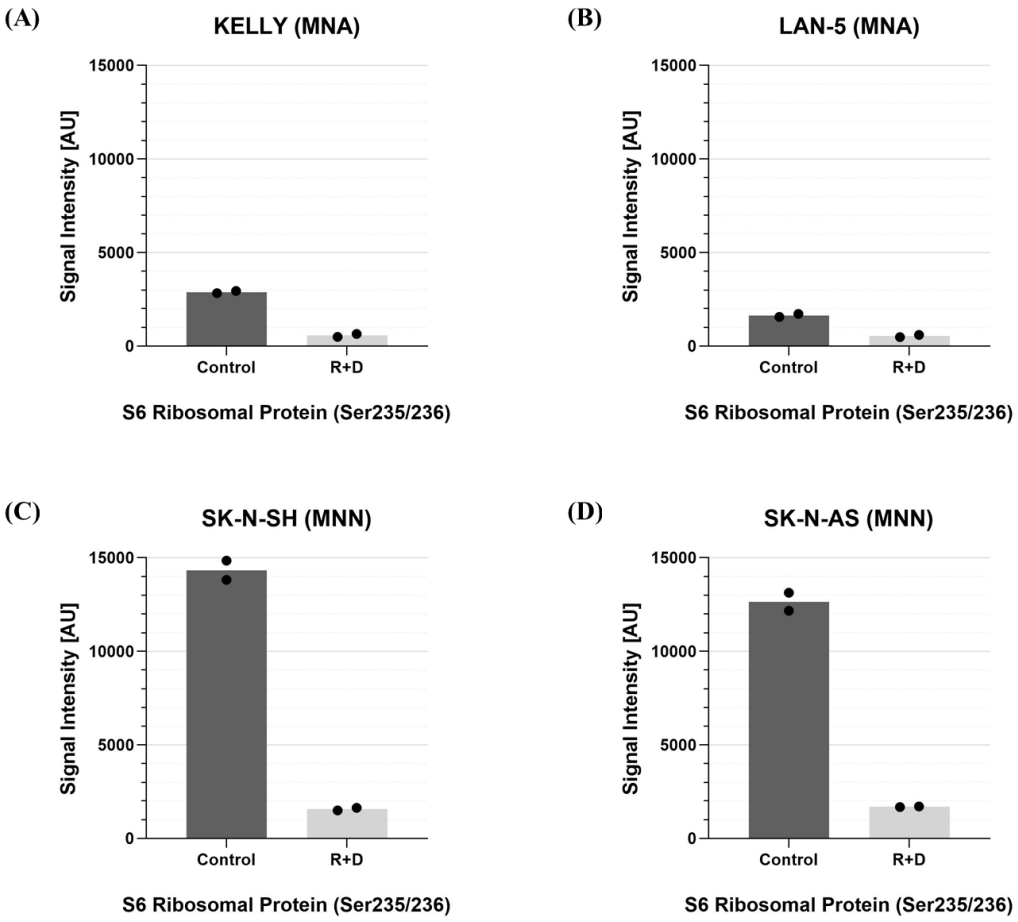


**Figure 22: Phosphorylation Status of S6 Ribosomal Protein at Serine 235/236 in Control- and Rapamycin Plus Dasatinib-Treated Neuroblastoma Cell Lines**

Phosphorylation status of S6 ribosomal protein (rpS6) at serine 235/236 (Ser235/236) after 72 hours of treatment with rapamycin plus dasatinib (R+D) compared to control (DMSO vehicle)-treated cells of the MycN-amplified (MNA) neuroblastoma (NB) cell lines KELLY **(A)** and LAN-5 **(B)**, and the MycN-non-amplified (MNN) NB cell lines SK-N-SH **(C)** and SK-N-AS **(D)** were analyzed utilizing the PathScan® RTK Signaling Array by Cell Signaling Technology. Data represents one array with duplicate target spots for each cell line. DMSO: dimethyl sulfoxide.AU: absolute pixel density values. Displayed bars are means.

Treatment with R+D showed a marked decrease in Ser235/236 phosphorylation levels in all cell lines tested, independent of MycN status (*Figure 23*). For the cell lines KELLY (MNA) and SK-N-SH (MNN), an independent second array was available, showing similar results, respectively (*Appendix, Figure 71 A and B*).

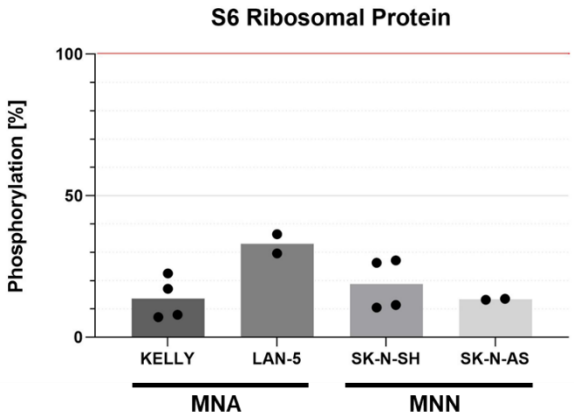


**Figure 23: Reduced Serine 235/236 Phosphorylation of S6 Ribosomal Protein in all Neuroblastoma Cell Lines After Rapamycin Plus Dasatinib Treatment**

Phosphorylation status (%) of S6 ribosomal protein (rpS6) in rapamycin plus dasatinib (R+D)-treated cells relative to control (DMSO vehicle)-treated cells (100%, red line). Data represents one array with duplicate target spots for LAN-5 (MNA) and SK-N-AS (MNN) and two arrays each for cell lines KELLY (MNA) and SK-N-SH (MNN). DMSO: dimethyl sulfoxide, MNA: MycN-amplified, MNN: MycN-non-amplified. Displayed bars are means.

Taken together, there is some evidence that the molecularly targeted combinatorial treatment R+D caused a greater reduction in phosphorylation at the rapamycin-sensitive S6K phosphorylation site Thr389 in the MNA cell line KELLY than in the MNN cell line SK-N-AS. In contrast, phosphorylation of rpS6 at Ser235/236 was equally reduced following R+D treatment in all cell lines, independent of MycN status.

#### 3.2.2.4. AKT

AKT, upstream of mTORC1, is the main target of PI3K and is phosphorylated at two key phosphorylation sites, threonine 308 (Thr308) and serine 473 (Ser473) (39, 41, 48). While Thr308 is phosphorylated as a direct downstream target of PI3K via PDK-1 (39, 41, 48), phosphorylation at Ser473 by mTORC2 is necessary to fully activate AKT (39, 48). Upon activation, AKT disinhibits mTORC1, thereby promoting increased cell metabolism, proliferation, survival, and blockage of apoptosis (48).

The change in phosphorylation of AKT at Thr308 and Ser473 after the treatment with R+D was analyzed for the MNA cell lines KELLY and LAN-5 and the MNN cell lines SK-N-SH and SK-N-AS utilizing the PathScan® RTK Signaling Array. *Figure 24* shows the phosphorylation status as absolute pixel density values (AU) after 72 hours of treatment with the combinatorial treatment R+D compared to control (DMSO vehicle)-treated cells.

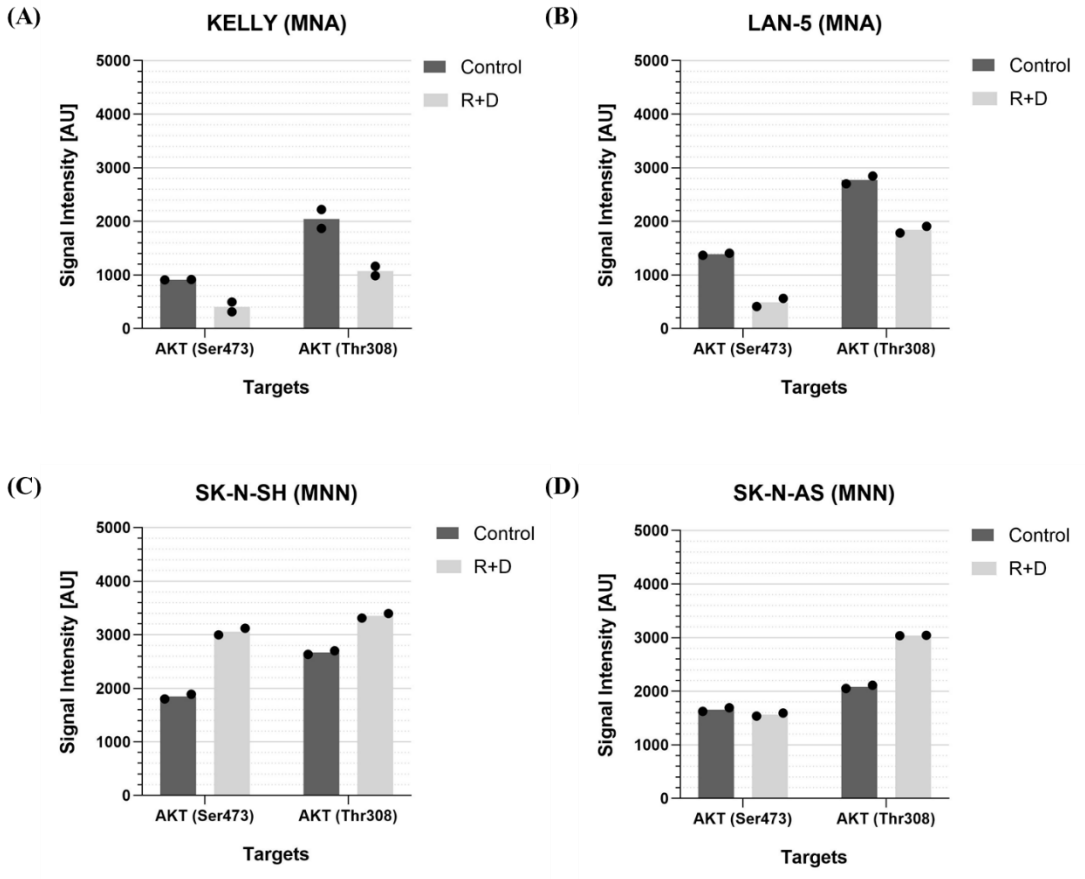


**Figure 24: Phosphorylation Status of Protein Kinase B (AKT) at Serine 473 and Threonine 308 in Control- and Rapamycin Plus Dasatinib-Treated Neuroblastoma Cell Lines**

Phosphorylation status of protein kinase B (AKT) at serine 473 (Ser473) and threonine 308 (Thr308) after 72 hours of treatment with rapamycin plus dasatinib (R+D) compared to control (DMSO-vehicle)-treated cells of the MycN-amplified (MNA) neuroblastoma (NB) cell lines KELLY **(A)** and LAN-5 **(B)**, and the MycN-non-amplified (MNN) NB cell lines SK-N-AS **(C)** and SK-N-AS **(D)** were analyzed utilizing the PathScan® RTK Signaling Array by Cell Signaling Technology. Data represents one array with duplicate target spots for each cell line.AU (arbitrary unit): absolute pixel density values. Displayed bars are means.

Treatment with R+D showed a noticeable decrease in phosphorylation of AKT at Thr308 and Ser473 in the MNA cell lines KELLY and LAN-5 (*Figure 24 A and B*). A second independent array performed for KELLY confirmed a reduction in phosphorylation at Thr308 but showed no profound changes at site Ser473 *(Appendix, Figure 72 A).* An additional array for Kelly also confirmed a decrease in phosphorylation at Thr308 and Ser473 (*Appendix, Figure 73 A)*. No further array was available for LAN-5.

Treatment with R+D showed a considerable increase in phosphorylation of AKT at Thr308 and Ser473 in the MNN cell line SK-N-SH (*Figure 24 C*). This could be confirmed in a second independently performed array, albeit to a lesser extent (*Appendix Figure 72 B*). In the cell line SK-N-AS (MNN), R+D treatment also led to a noticeable increase in phosphorylation of AKT

at Thr308 but no change at site Ser473 (*Figure 24 D*), whereas an independently performed array applying the Proteome Profiler™ array showed a decrease in AKT phosphorylation at both sites (*Appendix, Figure 73 B*).

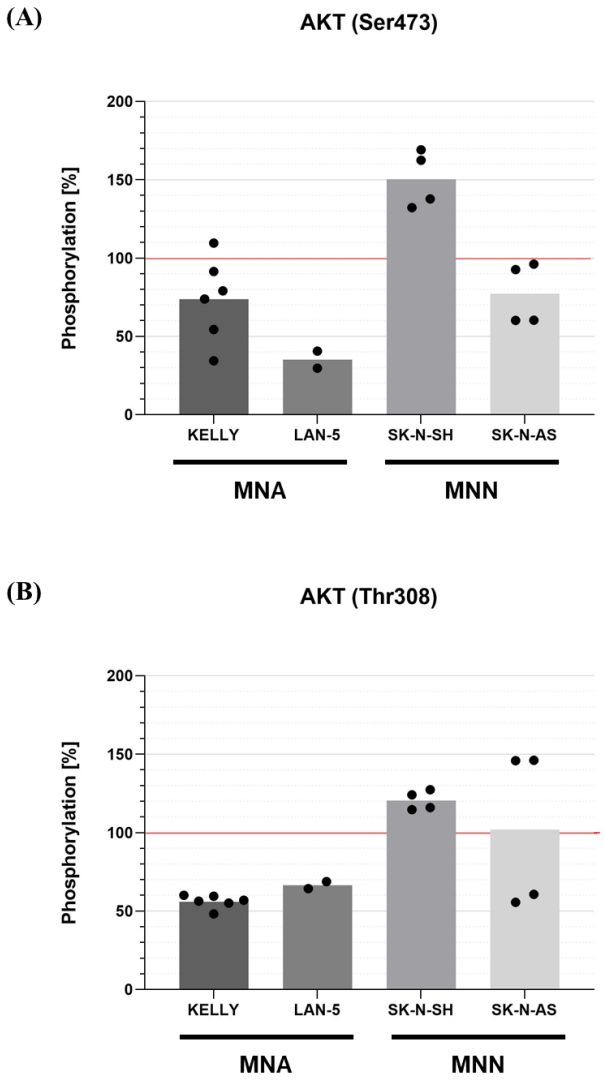


**Figure 25: Reduced Protein Kinase B (AKT) Phosphorylation at Threonine 308 in MycN-Amplified Compared to MycN-non-Amplified Neuroblastoma Cell Lines**

Phosphorylation status (%) of the protein kinase B (AKT) at serine 473 (Ser473) **(A)** and threonine 308 (Thr308) **(B)** in rapamycin plus dasatinib (R+D)-treated cells relative to control (DMSO-vehicle)-treated cells (100 %, red line). Data represents three arrays for KELLY, two arrays each for SK-N-SH and SK-N-AS, and one array for LAN-5 with duplicate target spots per array. DMSO: dimethyl sulfoxide, MNA: MycN-amplified, MNN: MycN-non-amplified. Displayed bars are means.

Taken together, *Figure 25* shows that treatment with the molecularly targeted combinatorial R+D treatment led to a decrease in phosphorylation of the key regulatory target AKT in MNA cell lines KELLY and LAN-5, however with a wide spread of results for KELLY at Ser473. Conversely, results in the MNN cell line SK-N-SH showed an increase in relative phosphorylation of AKT, whereas results in phosphorylation change for the MNN cell line SK-

N-AS remain inconclusive. While these results show a trend towards greater inhibition of AKT in MycN-amplified NB cell lines, results should be verified, especially regarding SK-N-AS.

#### 3.2.2.5. GSK-3β

The protein kinase GSK-3 is another key component within the complex regulation of the PI3K/AKT/mTOR pathway and is generally active (48). Upon activation of the PI3K/AKT/mTOR pathway, AKT phosphorylates GSK-3β at serine 9 (Ser9), thereby inhibiting its function (19, 48). Inhibition of AKT thereby should lead to activation of GSK-3β. It may also be inhibited due to phosphorylation by S6K (173). When activated, GSK-3β leads to the phosphorylation of several downstream targets, including MycN and cyclin D1, leading to their destabilization and degradation (19, 48, 62).

The change in phosphorylation of GSK-3β at Ser9 after the treatment with R+D was analyzed for the MNA cell lines KELLY and LAN-5, and the MNN cell lines SK-N-SH and SK-N-AS utilizing the PathScan® AKT Signaling Array. *Figure 26 A-D* shows the phosphorylation status as absolute pixel density values (AU) after 72 hours of treatment with the molecularly targeted combinatorial R+D treatment compared to control (DMSO vehicle)-treated cells.

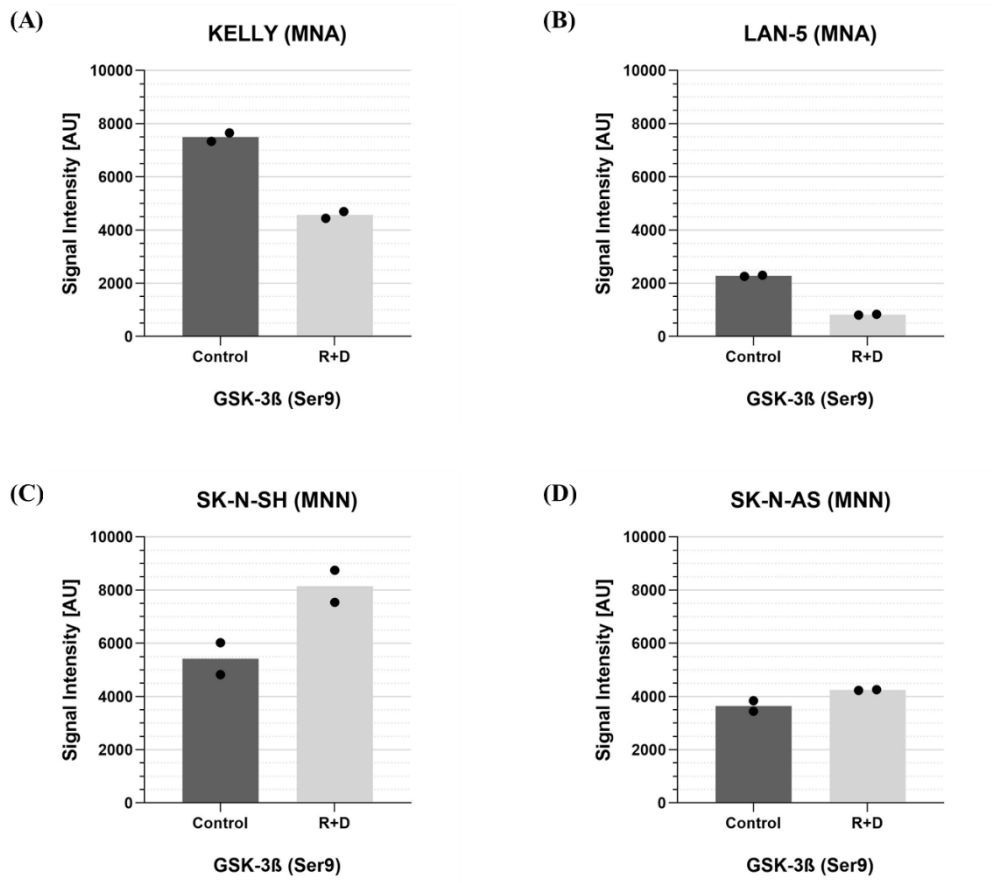


**Figure 26: Phosphorylation Status of Glycogen Synthase Kinase 3β in Control- and Rapamycin Plus Dasatinib-Treated Neuroblastoma Cell Lines**

Phosphorylation status of glycogen synthase kinase 3β (GSK-3β) at serine 9 (Ser9) after 72 hours of treatment with rapamycin plus dasatinib (R+D) compared to control (DMSO vehicle)-treated cells of the MycN-amplified (MNA) neuroblastoma (NB) cell lines KELLY **(A)** and LAN-5 **(B)**, and the MycN-non-amplified (MNN) NB cell lines SK-N-SH **(C)** and SK-N-AS **(D)** were analyzed utilizing the PathScan® AKT Signaling Array by Cell Signaling Technology. Data represents one array with duplicate target spots for each cell line. DMSO: dimethyl sulfoxide.AU (arbitrary unit): absolute pixel density values. Displayed bars are means.

Treatment with R+D showed a substantial decrease in phosphorylation of GSK-3β at Ser9 in the MNA cell lines KELLY and LAN-5 (*Figure 26 A and B*). Additionally, an independently performed array showed a decreasing tendency for KELLY, albeit much less profound (*Appendix*, *Figure 74 A*).

No decrease in phosphorylation was measurable in the MNN cell lines SK-N-SH and SK-N-AS; in fact, the arrays showed an increase in relative phosphorylation at Ser9 especially in SK-N-SH *(Figure 26 C and D*). No confirmational arrays were available.

GSK-3α/β phosphorylation at serine 21/9 (Ser21/Ser9) was also analyzed utilizing the Proteome Profiler™ Array. The array did not distinguish between GSK-3α (Ser21) and GSK-3β (Ser9). Results of the PathScan® arrays could be confirmed for the cell lines KELLY (MNA,

noticeable decrease in phosphorylation) (*Appendix*, *Figure 75 A)* and SK-N-AS (MNN, no distinct change) (*Appendix*, *Figure 75 B*).

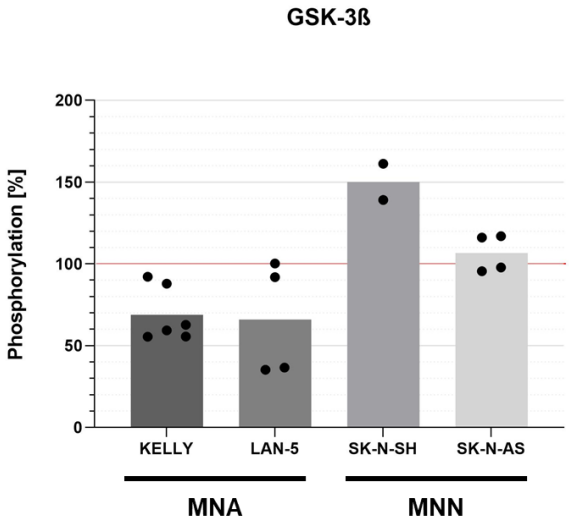


**Figure 27: Reduced Serine 9 Phosphorylation of Glycogen Synthase Kinase 3β in MycN-Amplified Compared to MycN-non-Amplified Neuroblastoma Cell Lines After Rapamycin Plus Dasatinib-Treatment**

Phosphorylation status (%) of glycogen synthase kinase 3β (GSK-3β) at serine 9 (Ser9) in rapamycin plus dasatinib (R+D)-treated cells relative to control (DMSO-vehicle)-treated cells (100 %, red line). Data represents three arrays for KELLY, two arrays each for LAN-5 and SK-N-AS, and one array for SK-N-SH with duplicate target spots per array. DMSO: dimethyl sulfoxide, MNA: MycN-amplified, MNN: MycN-non-amplified. Displayed bars are means.

Taken together, *Figure 27* strongly suggests that the molecularly targeted R+D treatment inhibits the phosphorylation of GSK-3β in MNA cell lines but not in MNN cell lines.

#### 3.2.2.6. Tumor Suppressor PTEN

The phosphatase PTEN functions as a tumor suppressor (39-41, 48). It negatively regulates the activation of the PI3K/AKT/mTOR pathway by dephosphorylating $PIP_3$ to $PIP_2$, thus preventing the activation of downstream targets (39-41, 48). Phosphorylation at residues serine 380 (Ser380), among others, is thought to be a mechanism of inactivation resulting in the activation of the PI3K/AKT/mTOR pathway (174). Thus, dephosphorylation of PTEN at Ser380 is a sign of inhibition of the PI3K/AKT/mTOR pathway.

The change in phosphorylation of PTEN at Ser380 after the treatment with R+D treatment was analyzed in the MNA cell lines KELLY and LAN-5, and the MNN cell lines SK-N-SH and SK-N-AS utilizing the PathScan® AKT Signaling Array. *Figure 28* shows the phosphorylation

status as absolute pixel density values (AU) after 72 hours of treatment with the molecularly targeted combinatorial treatment R+D compared to control (DMSO vehicle)-treated cells.

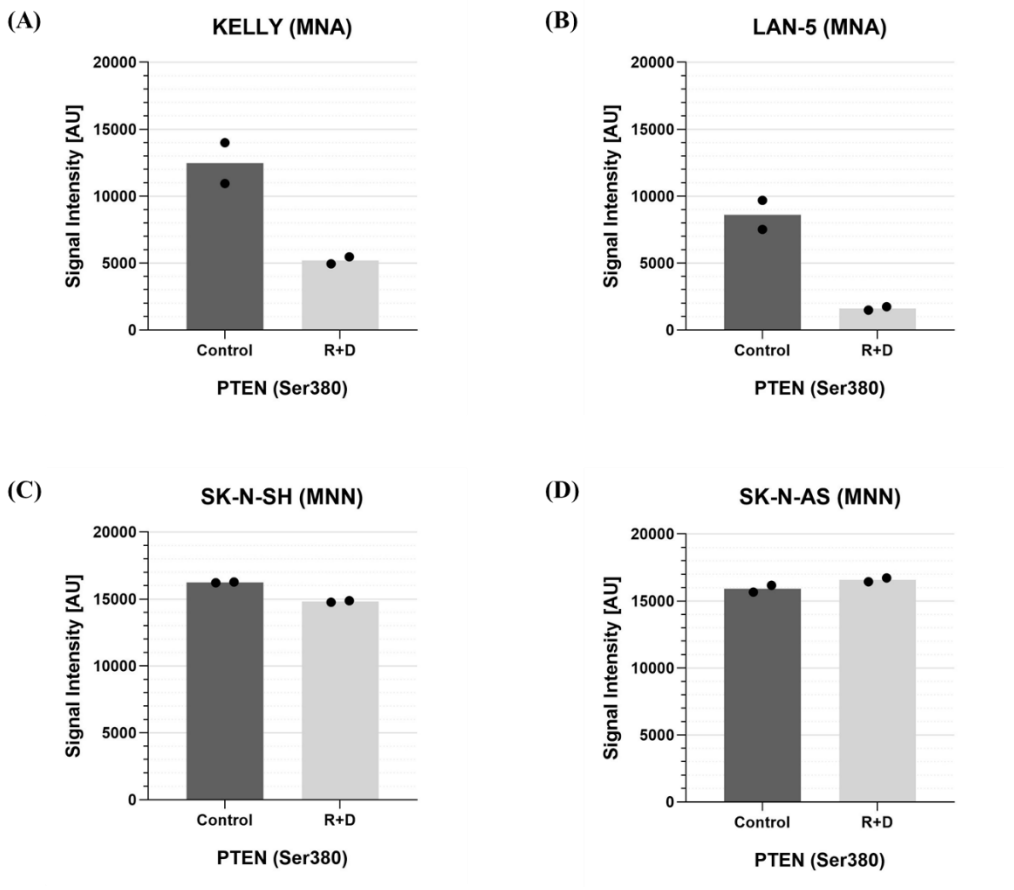


**Figure 28: Phosphorylation Status of Phosphatase and Tensin Homolog in Control- and Rapamycin plus Dasatinib-Treated Neuroblastoma Cell Lines**

Phosphorylation status of phosphatase and tensin homolog (PTEN) at serine 380 (Ser380) after 72 hours of treatment with rapamycin plus dasatinib (R+D) compared to control (DMSO-vehicle)-treated cells of the MycN-amplified (MNA) neuroblastoma (NB) cell lines KELLY **(A)** and LAN-5 **(B)**, and the MycN-non-amplified (MNN) NB cell lines SK-N-SH **(C)** and SK-N-AS **(D)** were analyzed utilizing the PathScan® AKT Signaling Array by Cell Signaling Technology. Data represents one array with duplicate target spots for each cell line. DMSO: dimethyl sulfoxide. AU (arbitrary unit): absolute pixel density values. Displayed bars are means.

Treatment with R+D showed a distinct decrease in phosphorylation of PTEN at Ser380 in the MNA cell lines KELLY and LAN-5 (*Figure 28 A and B*). Independently performed arrays confirmed a decrease in both cell lines (*Appendix, Figure 76 A and B).*

Treatment with R+D showed a slight decrease in phosphorylation levels of PTEN at Ser380 in the MNN cell line SK-N-SH (*Figure 28 C*), although to a much lesser extent than in the MNA cell lines. No profound change in phosphorylation levels of PTEN at Ser380 was detected in the MNN cell line SK-N-AS (*Figure 28 D*). No confirmational arrays were available for SK-N-SH and SK-N-AS.

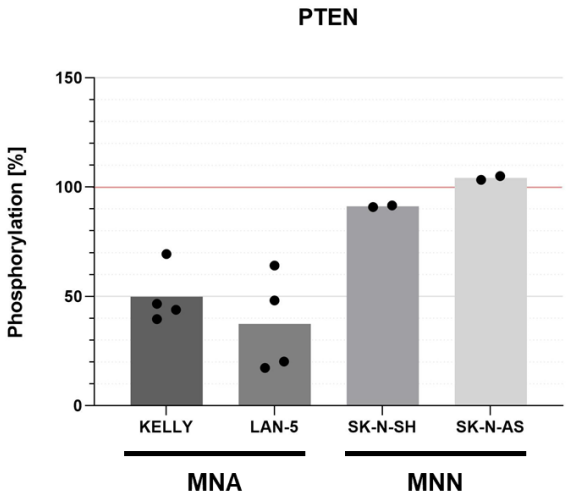


**Figure 29: Phosphorylation Status of Phosphatase and Tensin Homolog at Serine 380 is More Reduced in MycN-Amplified Compared to MycN-non-Amplified Neuroblastoma Cell Lines**

Phosphorylation status (%) of phosphatase and tensin homolog (PTEN) in rapamycin plus dasatinib (R+D)-treated cells relative to control (DMSO-vehicle)-treated cells (100 %, red line). Data represents two arrays per MycN-amplified (MNA) cell line and one array per MycN-non-amplified (MNN) cell line with duplicate target spots per array. DMSO: dimethyl sulfoxide, MNA: MycN-amplified, MNN: MycN-non-amplified. Displayed bars are means.

Taken together, *Figure 29* shows the results indicating a greater effect of the molecularly targeted R+D treatment in MNA cell lines than in MNN cell lines regarding the activation of the tumor suppressor PTEN due to reduced phosphorylation at Ser380.

### 3.2.3. Evidence for Greater Inhibition of the MAPK/ERK Pathway in MycN-Amplified Neuroblastoma Cell Lines

#### 3.2.3.1. Src and SKFs

Activity of the dual Abl/Src-kinase inhibitor dasatinib was confirmed by analyzing the phosphorylation of Src and SFKs as well as targets of the MAPK/ERK pathway. The tyrosine kinase Src is activated via phosphorylation or binding to specific tyrosine autophosphorylation sites in ligand-stimulated RTKs through its SH2 domain, leading to conformational change (91, 175). This allows the autophosphorylation of tyrosine 419 (Tyr419) within the activation loop and the stabilization of its active conformation (91, 175). Tyr419 may also be a target for other tyrosine kinases, resulting in Src activation (175).

The SFKs are comprised of nine members – Src, Yes, Fyn, Lyn, Lck, Hck, Fgr, Blk, and Yrk (83) – which are similar in their structure and function but whose expression levels vary depending on tissue type (86). While Src, Fyn, and Yes are ubiquitously expressed, Lyn is mainly expressed in hematopoietic cells and neuronal tissues, whereas Hck is primarily expressed in myeloid cells (83).

The change in phosphorylation of Src after the treatment with R+D was analyzed for the MNA cell lines KELLY and LAN-5, and the MNN cell lines SK-N-SH and SK-N-AS utilizing the PathScan® RTK Signaling Array. *Figure 30 A-D* shows the phosphorylation status as absolute pixel density values (AU) after 72 hours of treatment with the combinatorial R+D treatment compared to control (DMSO vehicle)-treated cells.

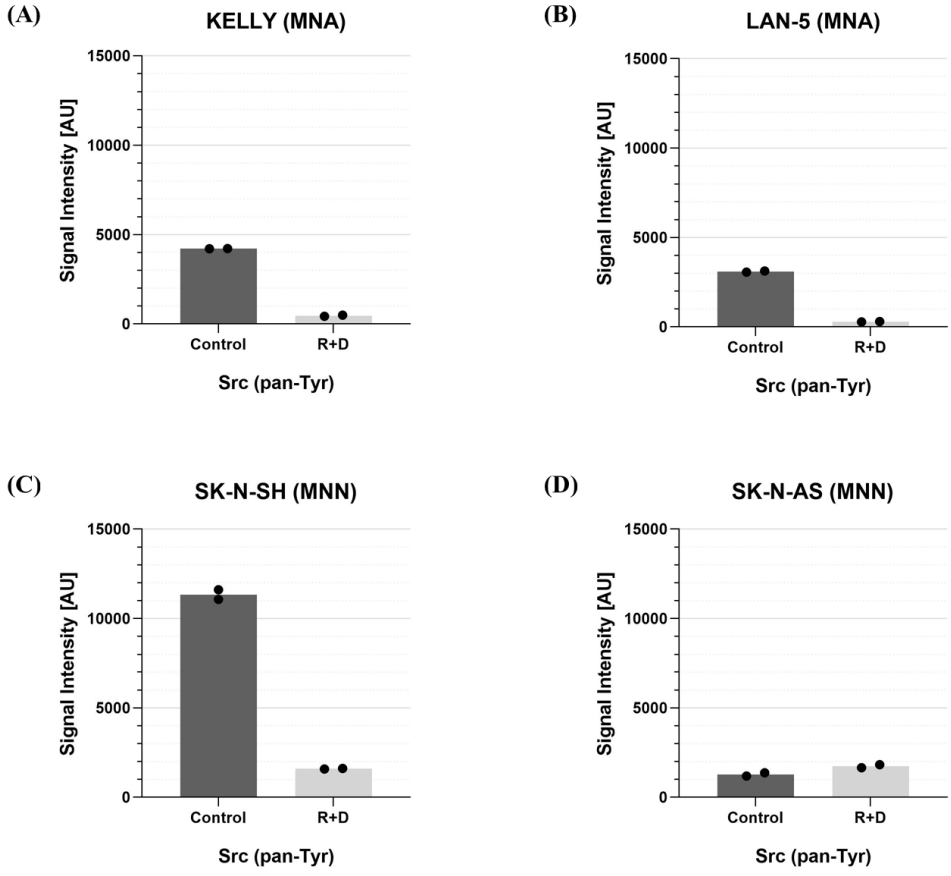


**Figure 30: Phosphorylation Status of Sarcoma Kinase in Control- and Rapamycin Plus Dasatinib-Treated Neuroblastoma Cell Lines**

Phosphorylation status of sarcoma kinase (Src) after 72 hours of treatment with rapamycin plus dasatinib (R+D) compared to control (DMSO vehicle)-treated cells of the MycN-amplified (MNA) neuroblastoma (NB) cell lines KELLY **(A)** and LAN-5 **(B)**, and the MycN-non-amplified (MNN) NB cell lines SK-N-SH **(C)** and SK-N-AS **(D)** were analyzed utilizing the PathScan® RTK Signaling Array by Cell Signaling Technology. Data represents one array with duplicate target spots for each cell line. DMSO: dimethyl sulfoxide. AU (arbitrary unit): absolute pixel density values. Displayed bars are means.

Treatment with R+D led to a marked decrease in phosphorylation of Src applying a pan-Tyr antibody (detection of general phosphorylation) in the MNA cell lines KELLY and LAN-5 (*Figure 30 A and B*), as well as in the MNN cell line SK-N-SH (*Figure 30 C*), but not in the MNN cell line SK-N-AS (*Figure 30 D*). However, signals in the SK-N-AS arrays were low compared to signals of the other cell lines. In addition, confirmational arrays were available for KELLY (MNA) and SK-N-SH (MNN), showing similar results for KELLY and also a decrease, albeit to a lesser extent, for SK-N-SH (MNN) *(Appendix, Figure 77 A and B).*

The Proteome Profiler™ Human Phospho-Kinase Array was used to analyze Src and SFK phosphorylation for the cell lines KELLY (MNA) and SK-N-AS (MNN). *Figure 31 A and B* shows the phosphorylation status as absolute pixel density values (AU) after 72 hours of treatment with the combinatorial R+D treatment compared to control (DMSO vehicle)-treated cells.

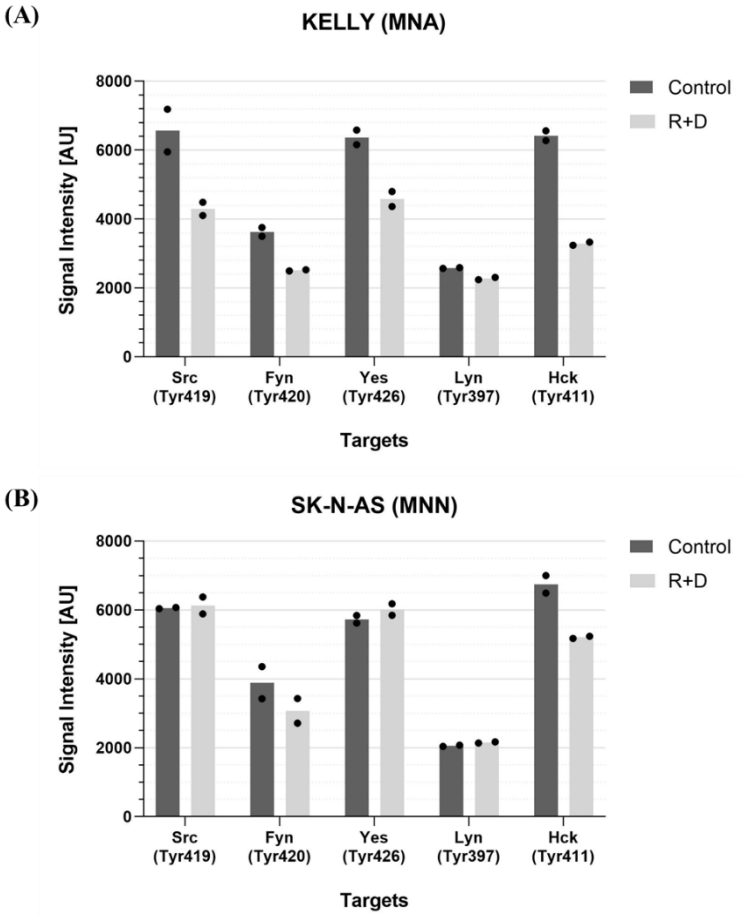


**Figure 31: Phosphorylation Status of Sarcoma Kinase and Related Sarcoma Kinase Family Kinases in Control- and Rapamycin Plus Dasatinib-Treated Neuroblastoma Cell Lines**

Phosphorylation status of sarcoma kinase (Src) at tyrosine 419 (Tyr419) and the related Src family kinases (SFKs) Fyn, Yes, Lyn, and Hck at their corresponding phosphorylation sites after 72 hours of treatment with rapamycin plus dasatinib (R+D) compared to control (DMSO vehicle)-treated cells of the MycN-amplified (MNA) neuroblastoma (NB) cell line KELLY **(A)** and the MycN-non-amplified (MNN) NB cell line SK-N-AS **(B)** were analyzed utilizing the Proteome Profiler™ Human Phospho-Kinase Array by R&D Systems. Data represents one array with duplicate target spots for each cell line. DMSO: dimethyl sulfoxide. AU (arbitrary unit): absolute pixel density values. Displayed bars are means.

Treatment with R+D showed a distinct decrease in phosphorylation of Src at Tyr419 in the MNA cell line KELLY (*Figure 31 A*) but not in the MNN cell line SK-N-AS (*Figure 31 B*), confirming results from the PathScan® array. Treatment with R+D also noticeably decreased the relative phosphorylation of three (Fyn at Tyr420, Yes at Tyr426, Hck at Tyr411) out of four SFKs (Lyn at Tyr397 was relatively unaffected) in the MNA cell line KELLY (*Figure 31 A*). On the contrary, only the SFK Hck at Tyr411 (and to a lesser extend Fyn at Tyr240) also showed a decrease in phosphorylation in the MNN cell line SK-N-AS (*Figure 31 B*).

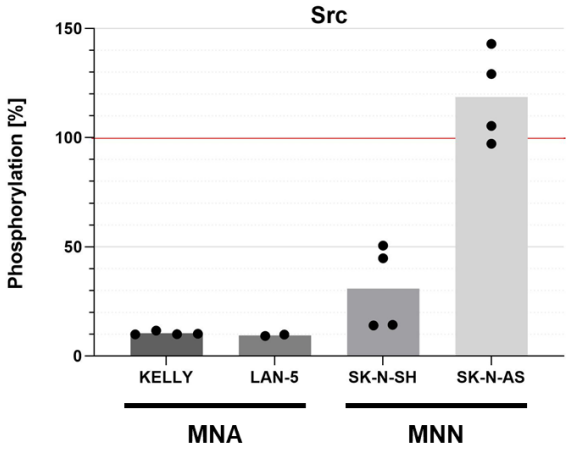


**Figure 32: Reduced Phosphorylation of Sarcoma Kinase in Three out of Four Neuroblastoma Cell Lines**

Phosphorylation status (%) of sarcoma kinase (Src) in rapamycin plus dasatinib (R+D)-treated cells relative to control (DMSO vehicle)-treated cells (100 %, red line). Data represents two arrays each for KELLY and SK-N-SH and one array each for LAN-5 and SK-N-AS with duplicate target spots per array. DMSO: dimethyl sulfoxide, MNA: MycN-amplified, MNN: MycN-non-amplified. Displayed bars represent means.

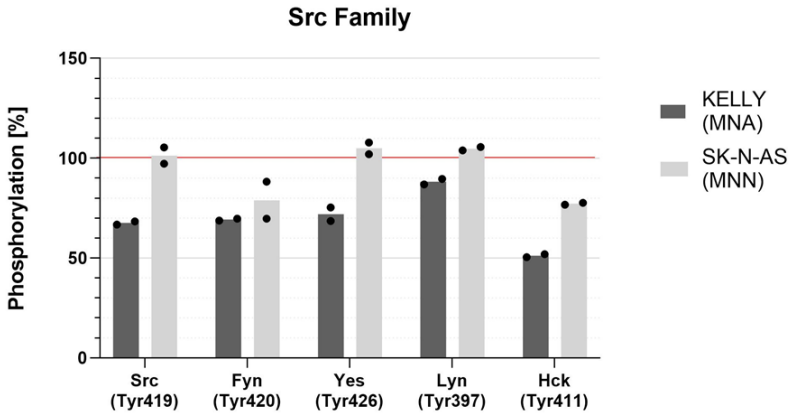


**Figure 33: Reduced Phosphorylation of Sarcoma Kinase and Sarcoma Kinase Family Kinases in KELLY Compared to SK-N-AS Cells After Rapamycin Plus Dasatinib-Treatment**

Phosphorylation status (%) of sarcoma kinase (Src) and related Src family kinases (SFKs) Fyn, Yes, Lyn and Hck in rapamycin plus dasatinib (R+D)-treated cells relative to control (DMSO vehicle)-treated cells (100 %, red line). Data represents one array for KELLY and one array for SK-N-AS with duplicate target spots per array. DMSO: dimethyl sulfoxide, MNA: MycN-amplified, MNN: MycN-non-amplified. Displayed bars represent means.

Taken together, *Figures 32 and 33* show that treatment with R+D led to a greater decrease in phosphorylation of Src and Src family kinases in the cell lines KELLY, LAN-5, and SK-N-SH compared to the cell line SK-N-AS, suggesting that the inhibition of the Src kinase family was efficient in most of the NB cell lines tested and independent of the MycN status.

#### 3.2.3.2. ERK 1/2, MSK 1/2, and RSK 1/2/3

ERK 1 and 2, MSK 1 and 2, and RSK 1, 2, and 3 are all kinases within the MAPK/ERK pathway (69, 76). Phosphorylation at threonine 202 and tyrosine 204 (Thr202/Tyr204) and threonine 185 and tyrosine 187 (Thr185/Tyr187) activates ERK 1 and 2, respectively (69, 76), which in turn activates RSK via a series of sequential phosphorylation, including at serine 380 (Ser380) (78). MSK 1/2 is activated via phosphorylation of ERK at serine 360 (Ser360), while autophosphorylation at serine 377 (Ser377) is important for its activity (176).

The change in phosphorylation of ERK, MSK, and RSK at their respective phosphorylation sites after the treatment with R+D was analyzed for the MNA cell lines KELLY and LAN-5, and the MNN cell lines SK-N-SH and SK-N-AS utilizing the PathScan® RTK Signaling Array. *Figure 34 A-D* shows the phosphorylation status of ERK as absolute pixel density values (AU) after 72 hours of treatment with the combinatorial R+D treatment compared to control (DMSO vehicle)-treated cells.

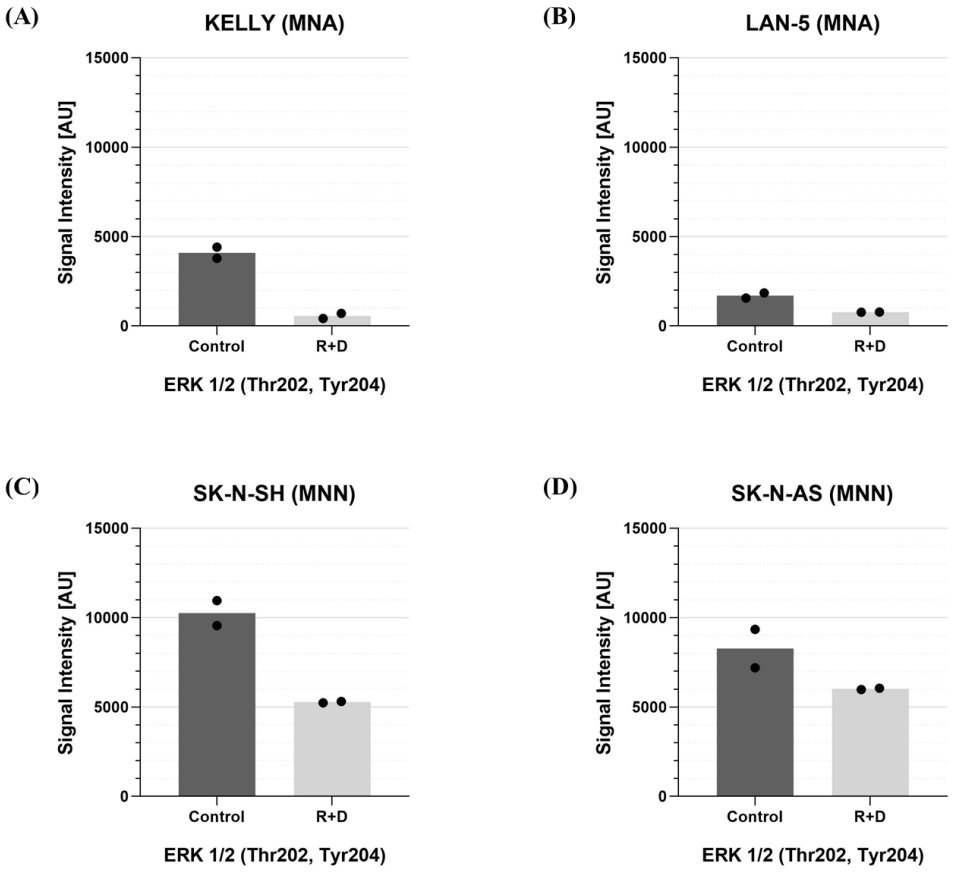


**Figure 34: Phosphorylation Status of Extracellular Signal-Regulated Kinases 1 and 2 in Control- and Rapamycin Plus Dasatinib-Treated Neuroblastoma Cell Lines**

Phosphorylation status of extracellular signal-regulated kinases 1 and 2 (ERK 1/2) at threonine 202 (Thr202) and tyrosine 204 (Tyr204), respectively, after 72 hours of treatment with rapamycin plus dasatinib (R+D) compared to control (DMSO vehicle)-treated cells of the MycN-amplified (MNA) neuroblastoma (NB) cell lines KELLY **(A)** and LAN-5 **(B)**, and the MycN-non-amplified (MNN) NB cell lines SK-N-SH **(C)** and SK-N-AS **(D)** were analyzed utilizing the PathScan® RTK Signaling Array by Cell Signaling Technology. Data represents one array with duplicate target spots for each cell line. DMSO: dimethyl sulfoxide. AU (arbitrary unit): absolute pixel density values. Displayed bars are means.

Treatment with R+D led to a clear decrease in phosphorylation of ERK 1 and 2 (ERK 1/2) at Thr202 and Tyr204 in the MNA cell lines KELLY and LAN-5 (*Figure 34 A and B*) as well as the MNN cell line SK-N-SH (*Figure 34 C*), but to a lesser extent in the MNN cell line SK-N-AS (*Figure 34 D*). Results could be confirmed in a second independently performed array for the cell lines KELLY (MNA) and SK-N-SH (MNN) *(Appendix, Figure 78 A and B)*. However, the reduction in phosphorylation was less profound in these arrays for both cell lines. The phosphorylation status of ERK was also analyzed for the cell lines KELLY (MNA) and SK-N-AS (MNN) with the Proteome Profiler™ Array (*Appendix, Figure 79 A and B)*. Results confirm the observations made in the PathScan® arrays, showing a noticeable reduction in phosphorylation after treatment with R+D for the cell line KELLY (MNA) but much less for the cell line SK-N-AS (MNN).

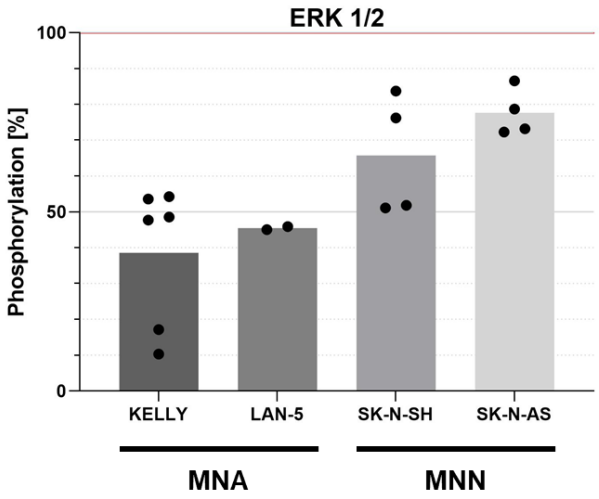


**Figure 35: Reduced Phosphorylation of Extracellular Signal-Regulated Kinases 1/2 at Threonine 202 and Tyrosine 204 in Neuroblastoma Cell Lines**

Phosphorylation status (%) of extracellular signal-regulated kinase 1 and 2 in rapamycin plus dasatinib (R+D)-treated cells relative to control (DMSO vehicle)-treated cells (100 %, red line). Data represents three arrays for KELLY, two arrays each for SK-N-SH and SK-N-AS, and one array for LAN-5 with duplicate target spots per array. DMSO: dimethyl sulfoxide, MNA: MycN-amplified, MNN: MycN-non-amplified. Displayed bars are means.

Taken together, the results in *Figure 35* suggest that treatment with R+D leads to a more profound decrease in phosphorylation of ERK 1/2 in the MNA cell lines KELLY and LAN-5 compared to the MNN cell lines SK-N-SH and SK-N-AS; however, the treatment is also effective to a certain extend in the MNN cell lines, especially SK-N-SH, as shown in *Figure 35.* The scatter of results of different test kits have to also be taken into account and results should be verified in future studies.

The change in phosphorylation of the ERK downstream targets MSK 1/2 at Ser376 and Ser360 and RSK 1/2/3 at Ser380, Ser386, and Ser377 after the treatment with R+D was analyzed for the MNA cell line KELLY and the MNN cell line SK-N-AS only utilizing the Proteome Profiler™ Array. *Figure 36 A-D* shows the phosphorylation status as absolute pixel density values (AU) after 72 hours of treatment with R+D compared to control (DMSO vehicle)-treated cells.

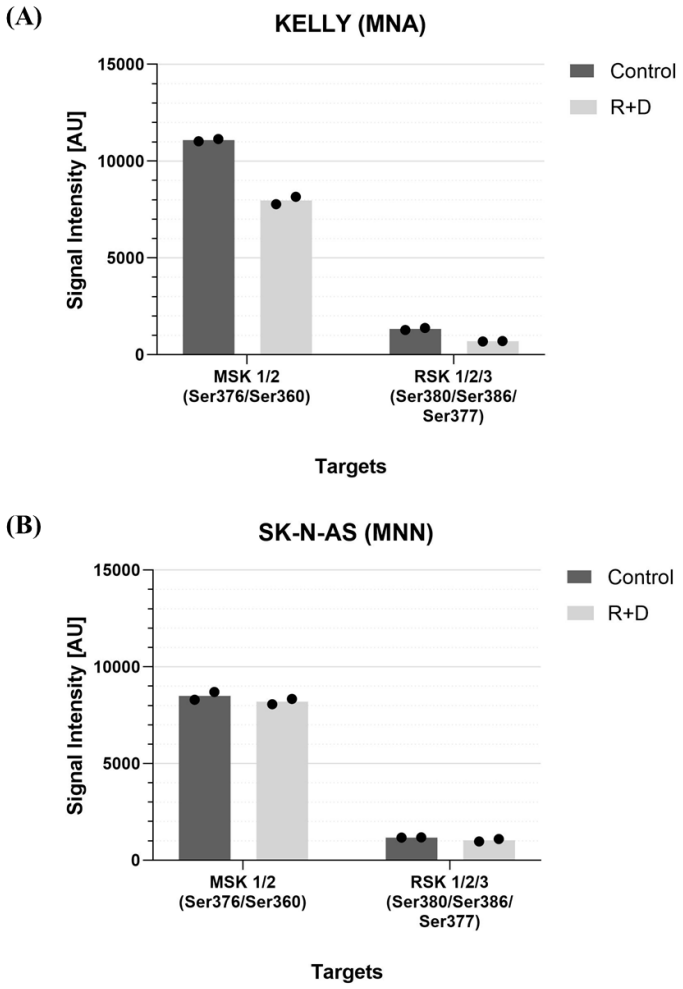


**Figure 36: Phosphorylation Status of Mitogen-and Stress-Activated Kinases 1 and 2 and p90 Ribosomal S6 Kinases 1, 2 and 3 in Control- and Rapamycin Plus Dasatinib-Treated Neuroblastoma Cell Lines**

Phosphorylation status of mitogen- and stress-activated kinases 1 and 2 (MSK 1/2) at serine 376 (Ser376) and serine 360 (Ser360), respectively, and p90 ribosomal kinase 1, 2 and 3 (RSK 1/2/3) at serine 380 (Ser380)/ serine 386 (Ser386)/ serine 377 (Ser377) after 72 hours of treatment with rapamycin plus dasatinib (R+D) compared to control (DMSO vehicle)-treated cells of the MycN-amplified (MNA) neuroblastoma (NB) cell line KELLY **(A)** and the MycN-non-amplified (MNN) NB cell line SK-N-AS **(B)** were analyzed utilizing the Proteome Profiler™ Human Phospho-Kinase Array by R&D Systems. Data represents one array with duplicate target spots for each cell line. DMSO: dimethyl sulfoxide. AU (arbitrary unit): absolute pixel density values. Displayed bars are means.

Treatment with R+D led to a noticeable decrease in phosphorylation of MSK 1/2 at Ser376 and Ser360 and RSK 1/2/3 at Ser380, Ser386, and Ser377 in the MNA cell line KELLY but only minimal change in phosphorylation in the MNN cell line SK-N-AS. However, signals for RKS are very low and might not be conclusive.

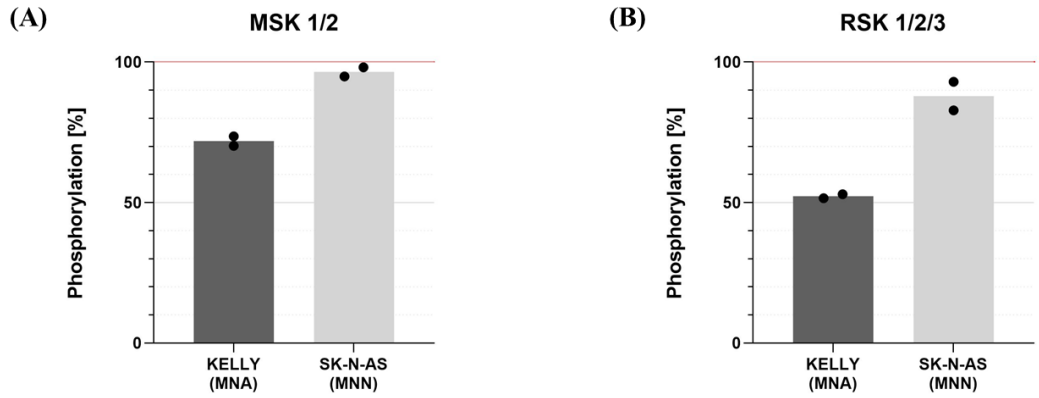


**Figure 37: Greater Reduction of Phosphorylation of Mitogen- and Stress-Regulated Kinases 1/2 and p90 Ribosomal S6 Kinases 1/2/3 in KELLY Compared to SK-N-AS Cells After Rapamycin Plus Dasatinib-Treatment**

Phosphorylation status (%) of mitogen- and stress-regulated kinases 1/2 (MSK 1/2) and p90 ribosomal S6 kinases 1/2/3 (RSK 1/2/3) in rapamycin plus dasatinib (R+D)-treated cells relative to control (DMSO vehicle)-treated cells (100 %, red line). Data represents one array with duplicate target spots for each cell line. DMSO. Dimethyl sulfoxide, MNA: MycN-amplified, MNN: MycN-non-amplified. Displayed bars are means.

In conclusion, *Figure 37* suggests that R+D treatment also leads to a reduction in phosphorylation of ERK downstream targets MSK and RSK in MNA cell line KELLY but much less in MNN cell line SK-N-AS.

#### 3.2.3.3. CREB

Phosphorylation of transcription factor CREB at serine 133 (Ser133) by growth factor signaling via receptor tyrosine kinase signaling through the MAPK/ERK pathway occurs in a stimulus-inducible manner (74, 75, 80). Together with other modifications and co-activator proteins, phosphorylation at Ser133 subsequently triggers gene expression (74, 75, 80). While CREB is essential for cellular functions, increased CREB expression and activation are associated with tumor progression and drug resistance (75).

The change in phosphorylation of CREB at Ser133 after the treatment with R+D was analyzed for the MNA cell line KELLY and the MNN cell line SK-N-AS only utilizing the Proteome Profiler™ Array. *Figure 38 A and B* shows the phosphorylation status as absolute pixel density values (AU) after 72 hours of treatment with the combinatorial R+D treatment compared to control (DMSO vehicle)-treated cells.

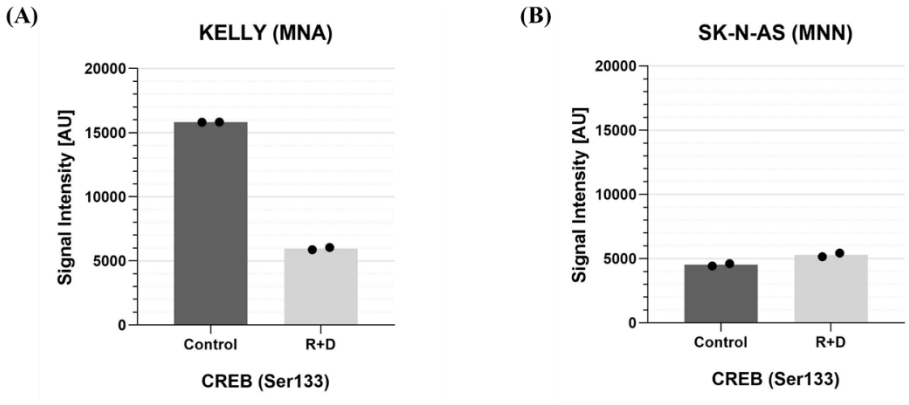


**Figure 38: Phosphorylation Status of cAMP Response Element Binding Protein in Control- and Rapamycin Plus Dasatinib-Treated Neuroblastoma Cell Lines**

Phosphorylation status of cAMP response element binding protein at serine 133 (Ser133) after 72 hours of treatment with rapamycin plus dasatinib (R+D) compared to control (DMSO vehicle)-treated cells of the MycN-amplified (MNA) neuroblastoma (NB) cell line KELLY**(A)** and the MycN-non-amplified (MNN) NB cell line SK-N-AS **(B)** were analyzed utilizing the Proteome Profiler™ Human Phospho-Kinase Array by R&D Systems. Data represents one array with duplicate target spots for each cell line. DMSO: dimethyl sulfoxide. AU (arbitrary unit): absolute pixel density values. Displayed bars are means.

Treatment with R+D led to a substantial decrease in phosphorylation of CREB at Ser133 in the MNA cell line KELLY (*Figure 38 A*) and even showed a slight increase in phosphorylation in the MNN cell line SK-N-AS (*Figure 38 B*). It is also noteworthy that CREB was phosphorylated to a greater extent in the control-treated cell population of KELLY (MNA) than in that of SK-N-AS (MNN).

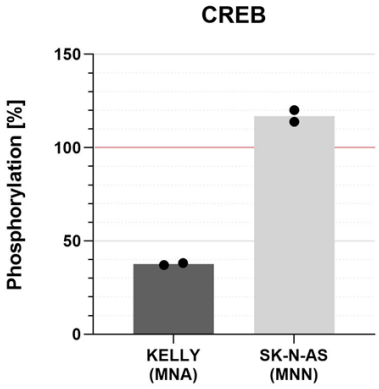


**Figure 39: Reduced Serine 133 Phosphorylation of cAMP Response Element Binding Protein in KELLY Compared to SK-N-AS Cells After Rapamycin Plus Dasatinib-Treatment**

Phosphorylation status (%) of cAMP response element binding protein (CREB) at serine 133 (Ser133) in rapamycin plus dasatinib (R+D)-treated cells relative to control (DMSO vehicle)-treated cells (100 %, red line). Data represents one array with duplicate target spots for each cell line. DMSO: dimethyl sulfoxide, MNA: MycN-amplified, MNN: MycN-non-amplified. Displayed bars are means.

Taken together, *Figure 39* shows that R+D treatment leads to a marked reduction of CREB phosphorylation in the MNA cell line KELLY but not in the MNN cell line SK-N-AS.

### 3.2.4. Additional Targets

#### 3.2.4.1. HSP60 Protein Levels

Heat shock protein 60 (HSP60) belongs to the family of heat shock proteins, mainly a group of molecular chaperones, and is essential for cell functionality and survival (177). Abnormal expression of HSP60 has been implicated in many cancers, including neuroblastoma (177).

The total protein level of HSP60 after the treatment with R+D was analyzed for the MNA cell line KELLY and the MNN cell line SK-N-AS utilizing the Proteome Profiler™ Array. *Figure 40 A and B* shows the absolute pixel density values in total protein level after 72 hours of R+D treatment compared to control (DMSO vehicle)-treated cells of the MNA cell line KELLY (*Figure 40 A*) and the MNN cell line SK-N-AS (*Figure 40 B*).

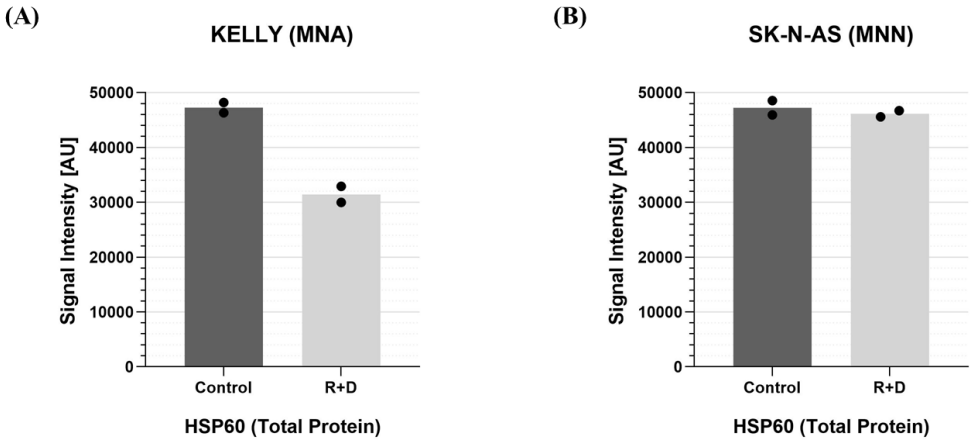


**Figure 40: Total Protein Level of Heat Shock Protein 60 in Control- and Rapamycin Plus Dasatinib-Treated Neuroblastoma Cell Lines**

Total protein level of heat shock protein 60 (HSP60) after 72 hours of treatment with rapamycin plus dasatinib (R+D) compared to control (DMSO vehicle)-treated cells of the MycN-amplified (MNA) neuroblastoma (NB) cell line KELLY **(A)** and the MycN-non-amplified (MNN) NB cell line SK-N-AS **(B)** were analyzed utilizing the Proteome Profiler™ Human Phospho-Kinase Array by R&D Systems. Data represents one array with duplicate target spots for each cell line. DMSO: dimethyl sulfoxide. AU (arbitrary unit): absolute pixel density values. Displayed bars are means.

As summarized in *Figure 41*, the results show a distinct decrease in the protein level of HSP60 induced by R+D treatment in the MNA cell line KELLY, while treatment did not noticeably affect the HSP60 protein level in the MNN cell line SK-N-AS.

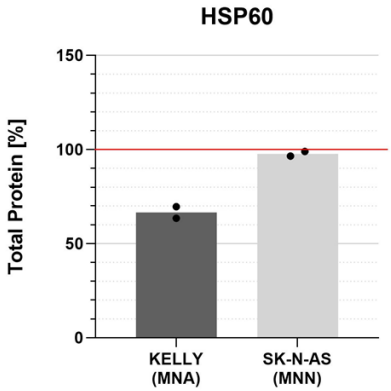


**Figure 41: Reduced Protein Level of Heat Shock Protein 60 in KELLY Compared to SK-N-AS Cells After Rapamycin Plus Dasatinib-Treatment**

Total protein level (%) of heat shock protein 60 (HSP60) in rapamycin plus dasatinib (R+D)-treated cells relative to control (DMSO vehicle)-treated cells (100%, red line). Data represents one array with duplicate target spots for each cell line. DMSO: dimethyl sulfoxide, MNA: MycN-amplified, MNN: MycN-non-amplified. Displayed bars are means.

#### 3.2.4.2. WNK

The with no lysine kinase (WNK) pathway, mainly known for regulating ion transport, is also implicated in cancer progression and angiogenesis (73). The phosphorylation site at threonine 60 (Thr60) of WNK 1 is phosphorylated by AKT and is often used as a readout for WNK activity (73).

The change in phosphorylation of WNK at Thr60 after the treatment with R+D was analyzed for the MNA cell line KELLY and the MNN cell line SK-N-AS utilizing the Proteome Profiler™ Array. *Figure 42 A and B* shows the absolute pixel density values in phosphorylation of WNK1 at Thr60 after 72 hours of R+D treatment compared to control (DMSO vehicle)-

treated cells of the MNA cell line KELLY (*Figure 42 A*) and the MNN cell line SK-N-AS (*Figure 42 B*).

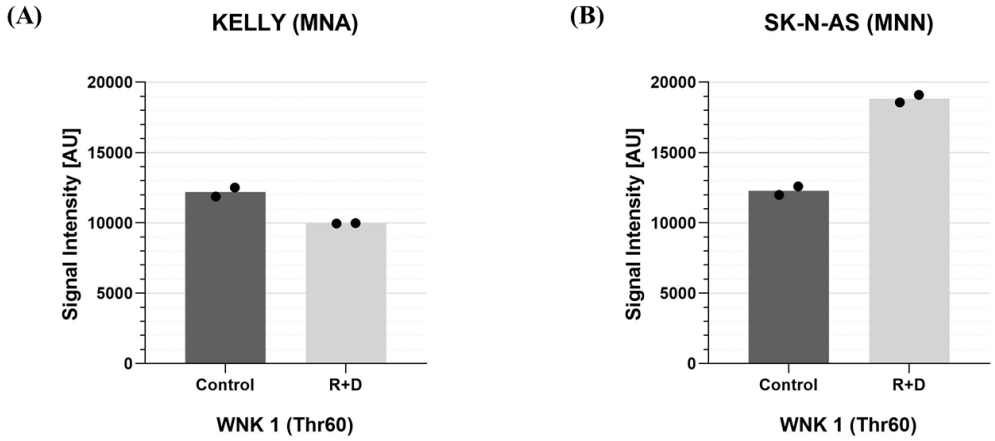


**Figure 42: Phosphorylation Status of With no Lysine Kinase 1 in Control- and Rapamycin Plus Dasatinib-Treated Neuroblastoma Cell Lines**

Phosphorylation status of with no lysine kinase 1 (WNK 1) at threonine 60 (Thr60) after 72 hours of treatment with rapamycin plus dasatinib (R+D) compared to control (DMSO vehicle)-treated cells of the MycN-amplified (MNA) neuroblastoma (NB) cell line KELLY **(A)**, and the MycN-non-amplified (MNN) NB cell line SK-N-AS **(B)** were analyzed utilizing the Proteome Profiler™ Human Phospho-Kinase Array by R&D Systems. Data represents one array with duplicate target spots for each cell line. DMSO: dimethyl sulfoxide. AU (arbitrary unit): absolute pixel density values. Displayed bars are means.

In summary, *Figure 43* shows a decrease in phosphorylation of WNK 1 at phosphorylation site Thr60 in the MNA cell line KELLY. In comparison, the treatment led to a noticeable increase in phosphorylation in the MNN cell line SK-N-AS.

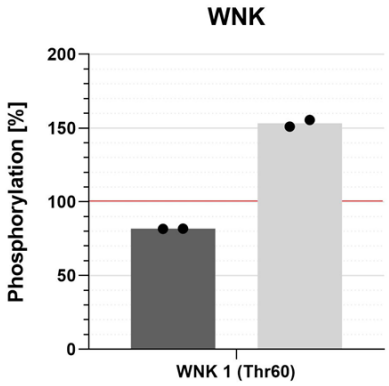


**Figure 43: Slightly Reduced Threonine 60 Phosphorylation of With no Lysine Kinase in KELLY Compared to Increased Phosphorylation in SK-N-AS Cells After Rapamycin Plus Dasatinib-Treatment**

Phosphorylation status (%) of with no lysine kinase 1 (WNK 1) at threonine 60 (Thr60) in rapamycin plus dasatinib (R+D)-treated cells relative to control (DMSO vehicle)-treated cells (100 %, red line). Data represents one array with duplicate target spots for each cell line. DMSO: dimethyl sulfoxide, MNA: MycN-amplified, MNN: MycN-non-amplified. Displayed bars are means.

# 4. Discussion

## 4.1. Greater Efficacy of RIST in MycN-Amplified Cell Lines

This study aimed to analyze if the combinatorial treatment of the molecularly targeted drugs rapamycin (mTOR inhibitor) plus dasatinib (TKI) with chemotherapeutic drugs irinotecan plus temozolomide, as designed in the RIST therapy, has an advantage in treating MNA NB compared to MNN NB in an *in vitro* model of NB. The RIST therapy is based on the hypothesis that the pre-treatment with molecularly targeted agents will synchronize the cell cycle and sensitize cells for the following chemotherapy. Additionally, it is hypothesized that in MNA NB, the PI3K/AKT/mTOR pathway is overly activated. Therefore, treatment with the mTOR inhibitor rapamycin in combination with the TKI dasatinib is believed to present an advantage in treating these mTOR-driven tumor entities. During extensive studies prior to the present study, *J. Leister* could already show that a greater reduction in cell viability in NB cell lines harboring the unfavorable MycN amplification (KELLY, LAN-5) could be achieved compared to cell lines without MycN amplification (SK-N-SH, SK-N-AS) when treating the cells with the multimodal RIST therapy (128). In addition, a dose reduction for the chemotherapeutics could be archived in the MNA cell lines by pre-treatment with R+D compared to the non-amplified cell lines (128).

For this present study, the individual cell line-specific approximate $IC_{50}$ concentrations established for the RIST therapy in our laboratory were used to evaluate the induction of apoptosis via AV/FITC and PI-staining assays in four NB cell lines with distinct genetic markers. Two MNA cell lines (KELLY, LAN-5) and two MNN cell lines (SK-N-SH, SK-N-AS) were compared. It could be shown that the molecularly targeted combinatorial treatment R+D alone successfully induces apoptosis in all NB cell lines tested. Greater efficacy of the molecularly targeted treatment could be demonstrated in MNA cell lines compared to the MNN cell line SK-N-AS, albeit only resulting in statistically significant results for the MNA cell line LAN-5. However, due to data sets not following a normal distribution, a non-parametric Mann-Whitney-U test was performed which has much less power than a parametric test in samples with small sample size. Compared to the MNN cell line SK-N-SH the molecularly targeted therapy alone showed no greater efficacy in MNA cell lines. The treatment proved to be more efficient in inducing apoptosis in the MNN cell line SK-N-SH compared to the MNN cell line

SK-N-AS. Regarding the chemotherapeutic treatment consisting of I+T, the treatment was more efficient in inducing apoptosis in the MNA NB cell lines than in the MNN cell line SK-N-AS. Compared to the MNN cell line SK-N-SH, the chemotherapy only showed more efficiency in the MNA cell line LAN-5 but not the MNA cell line KELLY. Greater apoptosis was induced by the chemotherapy treatment in the MNN cell line SK-N-SH compared to the MNN cell line SK-N-AS. When comparing the cell lines regarding the RIST therapy, a more significant induction of apoptosis could be demonstrated for both MNA cell lines compared to all MNN cell lines, suggesting a greater efficacy of the RIST therapy in MNA NB. Also, a greater sensitivity towards the RIST therapy could be shown for the MNN cell line SK-N-SH compared to the MNN cell line SK-N-AS, suggesting possible underlying genetic markers other than MycN that also impact susceptibility to treatment with RIST.

In line with these results, *Johnsen et al.* could also show mTOR inhibitor activity in NB cell lines with a dependence of sensitivity towards rapamycin or the mTOR inhibitor CCI-779 on the expression of MycN in the MycN-regulatable cell line Tet21N (58). *Segerström et al.* could show a greater sensitivity towards the dual PI3K/mTOR inhibitor PI103 plus the PDK-1 inhibitor OSU03012 in MycN-ON-cells of the Tet21N cell line (68). On the contrary, these results could not be replicated by *R. Wätzig*, who also used the Tet21N cell line and rapamycin; however, in a slightly differing experimental set-up regarding the induction of MycN expression in the Tet21N cells, which might explain the conflicting results (58, 129, 130). While *Johnsen et al.* cultivated cells in tetracycline-free media (MycN-ON cells) until 24 hours prior to experiments when the expression was suppressed by adding tetracycline for MycN-OFF cell experiments, *Wätzig et al.* cultivated cells in tetracycline-containing media (MycN-OFF cells) until 24 and 72 hours prior to experiments, respectively, when MycN expression was induced for MycN-ON cell experiments by removing tetracycline; which might have led to differences in the stability of MycN expression (58, 129, 130). *Vaughan et al*. showed an increased sensitivity of MNA cell lines compared to MNN cell lines as well as for cell lines engineered to contain MycN amplification (SHEP), compared to their MNN parental cell line, for several PI3K/mTOR inhibitors, including the allosteric mTOR inhibitor rapamycin and the ATP-competitive mTOR inhibitor Torin 1 in a panel of NB cell lines including KELLY, SK-N-SH, and SK-N-AS (65). In several of these studies, there was a positive correlation between the extent of proliferation inhibition and the level of MycN amplification and expression of MycN protein, showing a greater inhibition of proliferation in NB containing MycN amplification and high MycN protein expression (65, 68). *Kling et al.* could show a greater sensitivity of MNA

NB cell lines (IMR-32, SK-N-BE2, SK-N-DZ) toward the combinatorial treatment of the rapalog temsirolimus plus a BET inhibitor compared to MNN NB cell lines (SK-N-SH, SK-N-AS) (127). Furthermore, treatment with temsirolimus resulted in apoptosis induction detected via AV/FITC assays in MNA and MNN cell lines and led to greater apoptosis in MNA cell lines (SK-N-BE2, SK-N-DZ) compared to SK-N-AS (MNN) (127). *Vaughan et al.* could show apoptosis induction in the MNA cell line KELLY induced by the ATP-competitive mTOR inhibitor Torin 1 via a Caspase-Glo 3/7 cleavage assay and Cell Death ELISA (Roche™) (65). *Johnsen et al*. showed the induction of apoptosis in several MNN NB cell lines treated with rapamycin or the mTOR inhibitor CCI-779, including SK-N-AS, by demonstrating the activation of caspase-3 and subsequent cleavage of poly (ADP)-ribose polymerase (PARP) via Western blot analysis (58). These results support the apoptosis induction in MNA and MNN NB cell lines observed in the present study after treatment with R+D. However, neither *Vaughan et al.* nor *Johnsen et al.* directly compared apoptosis induction of MNA and MNN NB cells. *R. Wätzig* could only detect PARP cleavage products by Western blot analysis in the MNA NB cell line IMR-32 treated with dasatinib plus either rapamycin or Torin-2 but not KELLY at the determined $IC_{50}$ concentrations for the combinatorial treatment (129, 130), in contrary to the apoptosis induction shown in the present study. For treatment with rapamycin at concentrations above $IC_{50}$ concentrations for single treatment but not $IC_{50}$ concentrations, PARP cleavage could be detected (129, 130). Differences in the detection of apoptosis in NB cell lines, even though the same concentration of mTOR inhibitor and TKI were applied, could be due to variations in techniques detecting various stages of apoptosis as a marker like AV detects early stages of apoptosis and PARP cleavage occurs at later apoptotic stages. Further investigations are needed to identify the exact underlying mechanisms of apoptosis induction shown within the present study.

To this day, MycN amplification is the most important genetic prognostic marker in the risk stratification of NB in clinical use. Aberrant MycN expression is associated with high-risk disease, poor prognosis, and frequent therapy-refractory relapse (8). The increased sensitivity of MycN-expressing NB cells to the RIST therapy is of great importance as this could significantly improve the targeted treatment of patients with MNA tumors, for whom effective treatment options remain limited (36).

## 4.2. Greater Inhibition of mTOR Signaling in MycN-Amplified Cell Lines

In a second step, semiquantitative multiplex antibody assays were performed to identify therapy-relevant targets and signaling pathways through which the RIST therapy inhibits tumor cell growth. Cells were treated with R+D in their respective $IC_{50}$ values (as shown in *Table 9*) in order to be able to compare the effect on a molecular level. The phosphorylation status of several tyrosine kinases and other signaling nodes were evaluated in control (DMSO vehicle)-treated and drug-treated cells in the four NB cell lines as mentioned above. The effect of the allosteric mTOR inhibitor rapamycin is mainly attributed to its inhibition of the mTORC1 complex. Inhibition of mTORC2 only occurs cell line-specific after prolonged rapamycin treatment (178). Additionally, there is evidence that some mTORC1 functions may be resistant to rapamycin (179-181). In the present study, it could be shown that the combinatorial molecularly targeted treatment with R+D successfully inhibited the mTOR pathway. A reduction in phosphorylation of mTOR at Ser2448 as well as a reduction in phosphorylation and, thereby, activation of PRAS40 at Thr246, could be shown. Rapamycin also induced a reduction in phosphorylation of key downstream targets S6K (Thr389, Thr421/Ser424) and its effector rpS6 (Ser235/Ser236). MNA cell lines (KELLY, LAN-5) showed a greater reduction in phosphorylation of key targets mTOR, PRAS40, and S6K1 (Thr389) compared to MNN cell lines (SK-N-SH, SK-N-AS). No difference in effectiveness could be shown for S6K1 (Thr421/Ser424) and rpS6 (Ser235/236) since all of those phosphorylation sites were strongly affected by R+D treatment in all NB cell lines tested, independent of the MycN status.

Inhibition of the mTOR pathway could also be shown in various NB cell lines, including KELLY and SK-N-AS, by Western blot analysis of phospho-proteins compared to total protein levels for key targets mTOR (Ser2448), S6K1 (Thr389) and to a lesser extent 4E-BP1 (Ser65) by *Johnsen et al*. (58) and *R. Wätzig* (129, 130), respectively, in line with results of the phosphorylation assays of the present study. mTOR pathway inhibition was thereby achieved by *Johnsen et al.* with the treatment of either mTOR inhibitors rapamycin or CCI-779 (58). *Wätzig et al.* used the combinatorial treatment of either R+D (as used in the present study) or the ATP-competitive mTOR inhibitor Torin I plus dasatinib to achieve mTOR pathway inhibition (129, 130). However, no direct comparison between MycN-amplified and non-amplified cell lines has been done in these studies. *Kaess et al.* could show reduced phosphorylation of the key mTOR pathway targets S6K1 and 4E-BP1 as well as the tyrosine

kinase Src following treatment with R+D in the 2D and 3D cultures of MNN cell line SK-N-AS and the MNN cell line SK-N-BE2 using Western blot analysis, however using much higher dasatinib concentrations (182).

The differential inhibition of S6K1 phosphorylation sites Thr389 and Thr421/Ser424 in KELLY versus SK-N-AS may lie in a difference in rapamycin sensitivity or specificity of the phosphorylation sites. Thr389 phosphorylation is known to be blocked by rapamycin and correlates with its activity (183), whereas phosphorylation sites Thr421/Ser424 lie in a pseudo-substrate region and are thought to activate S6K by relieving pseudo-substrate suppression as an early step within S6K activation (53). Thus, a more accurate read-out for effective mTORC1 inhibition by rapamycin might be the phosphorylation site Thr389, which shows a greater reduction in phosphorylation after R+D-treatment in MycN-amplified cell lines in the present study.

rpS6 is a substrate of S6K and has been used as a readout for mTOR activity (47). The phosphorylation at Ser235/Ser236 represents two major phosphorylation sites responsible for its activation which are phosphorylated by S6K; however also RSK (53). RSK lies downstream of Src kinases and ERK within the MAPK/ERK signaling cascade (76-78). *Roux et al.* demonstrated that while S6K phosphorylates rpS6 at all known phosphorylation sites (Ser235, Ser236, Ser240, Ser244 Ser247), RSK exclusively phosphorylates Ser 235/236 *in vitro* and *in vivo* via an mTOR-independent mechanism (172). The reduction in phosphorylation that occurs in this study after treatment with R+D might, in part, be a dasatinib-mediated effect as RSK lays downstream of Src kinases and ERK within the MAPK/ERK signaling cascade. This may also explain why the reduction in phosphorylation is equally profound regardless of MycN status.

## 4.3.Feedback Inhibition Only in MycN-Amplified Cell Lines

In the present study, the phosphorylation status of AKT at Thr308 and Ser473 was also analyzed. It is known that treatment with rapamycin leads to feedback activation of the PI3K/AKT pathway due to suppression of the negative feedback loop mediated through S6K and IRS-1 upregulation and activation of AKT (*Figure 1*) (46, 49, 54, 184). As mentioned above, rapamycin may inhibit mTORC2 in a cell line-specific manner after prolonged treatment (178). Here, it could be shown that the PI3K-mediated phosphorylation of Thr308, as well as

the mTORC2-mediated phosphorylation at Ser473, could be inhibited with the 72-hour treatment of R+D in MNA NB cell lines. In contrast, hyperphosphorylation at both phosphorylation sites was shown for MNN cell lines in most assays. In line with observations by *Sarbassov et al.*, there seems to be cell line-specific sensitivity toward the ability of rapamycin to block mTORC2 during prolonged treatment (178). Results suggest that a prolonged treatment (72 hours) with rapamycin may be differentially able to suppress mTORC2 function in MNA cell lines used in this study. The occurring hyperphosphorylation of AKT in the MNN cell lines can probably be attributed to the feedback activation, as mentioned above. Contrary to this, *R. Wätzig* was not able to show a reduction in phosphorylation of AKT at Ser473 as a readout for mTORC2 inhibition via Western blot analysis in the cell line KELLY and even showed hyperphosphorylation after six hours of R+D treatment (129, 130). Additionally, after inhibition of phosphorylation at Thr308, reinduction and hyperphosphorylation were observed after 24 hours of treatment (129, 130). However, in the MNA cell line IMR-32 she showed a reduction in phosphorylation at AKT (Ser473) after prolonged treatment (24 hours) with R+D (129). Effects might be cell-line specific. Another potential reason might be the shorter duration of treatment. While *Sarbassov et al.* showed mTORC2 inhibition in several cell lines after 24 hours of rapamycin treatment, they also showed a lasting effect of this inhibition at 48 and 72 hours, respectively (178). Additionally, *Yori et al.* showed that combined SFK plus mTOR inhibition prevented rapamycin-mediated feedback activation in several breast cancer cell lines (122). The combinatorial treatment with dasatinib in the present study might therefore also be responsible for the AKT suppression, however intriguingly only in the MNA NB cell lines used and in contrary to experiments conducted by *R. Wätzig* with the same cell line and treatment combination (however analysis by *R. Wätzig* was done after 24 hours of treatment only) (129, 130). Nevertheless, this effect warrants further testing, as an unintended feedback activation dampens therapy efficacy and may be one reason why MNN tumors respond less to RIST within the present study but is also a potential risk factor regarding MNA tumors. A possible option to sidestep this problem could be the use of ATP-competitive mTOR inhibitors. The drawbacks of rapamycin and its rapalogs have led to the development of ATP-competitive inhibitors such as Torin 2, which inhibit mTORC 1 and 2 and are thought to circumvent the dilemma of feedback activation of PI3K/AKT (185). These dual mTOR inhibitors have also been shown to be superior to rapalogs in blocking proliferation and inducing apoptosis (185). In further studies, *R. Wätzig* has successfully demonstrated the effectiveness and a more sufficient AKT suppression of a modified RIST therapy substituting rapamycin for Torin 2 (TIST) in two MNA neuroblastoma

cell lines (129, 130). Several dual mTOR inhibitors are currently in clinical trials (98). Further studies with the modified RIST therapy should be performed in a panel of MNN tumor cell lines in order to test if the combination of an ATP-competitive mTOR inhibitor plus dasatinib is sufficient to circumvent AKT feedback activation in this subset of NB. However, *Rodrik-Outmezguine et al.* have shown in breast cancer cell lines that treatment with the dual mTORC1/2 inhibitor AZD8055 initiates an RTK-driven feedback loop, which ultimately leads to rebound accumulation of activated AKT (186). Another potential drug to consider might be the recently developed third-generation bivalent mTOR inhibitors, called "RapaLinks," combining rapamycin with an mTOR kinase inhibitor (187), which have shown promising results in several cancers in *in vitro* and *in vivo* studies and circumvent the development of drug resistance seen in prolonged therapy with mTOR inhibitors (188, 189).

While the present study shows the efficacy of the R+D treatment within the RIST therapy in MycN-amplified NB cell lines used, the treatment with the allosteric mTOR inhibitor rapamycin carries the risk of the feedback activation of the PI3K/AKT/mTOR pathway via mTORC2. A modified RIST therapy model utilizing either an ATP-competitive mTOR inhibitor such as Torin 2 or the newly developed RapaLinks may be desirable to overcome this drawback.

## 4.4.Activation of GSK-3β in MycN-Amplified NB Cell Lines

Within the scope of this study, other targets participating in the PI3K/AKT/mTOR pathway were also analyzed, such as serine-threonine protein kinase GSK-3β. Phosphorylation of GSK-3β at Ser9 via phosphorylation by AKT, among others inhibits its kinase activity (190). In its unphosphorylated and thereby activated state, GSK-3β phosphorylates MycN at Thr58 and cyclin D1 at Thr286 and subsequently facilitates their degradation (65, 191). Inhibition is reversed by the protein phosphatase PP2A (190). PP2A is phosphorylated and thereby inactivated by mTORC1, which leads to the accumulation of double-phosphorylated, activated MycN (19). mTORC inhibition by rapamycin may therefore lead to disinhibition of PP2A (192) and subsequent activation of GSK-3β by dephosphorylation with the following degradation of MycN and cyclin D1. Downregulation of cyclin D1 (193, 194) and a reduction in MycN (58, 65) have been shown in several NB cell lines after treatment with rapamycin. *Vaughan et al.* theorized that mTORC2 inhibition and the following disinhibition of GSK-3β is vital for MycN degradation (65).

In the present study, results show reduced phosphorylation at Ser9 of GSK-3β after treatment with R+D in MNA cell lines, supporting the abovementioned hypothesis. In line with other results in this study, this effect is only seen in MNA NB cell lines compared to MNN NB cell lines. Rapamycin seems to be able to block mTORC2 functions after prolonged treatment cell line-specific in MNA NB cell lines (within this study) as discussed above, and therefore activation of GSK-3β can be seen.

In support of the present findings, *R. Wätzig* showed a decrease in GSK-3β phosphorylation via Western blot analysis in MycN-amplified NB cell lines KELLY and IMR-32 treated with R+D. However, a reduction in MycN levels could only be shown for the MycN-amplified NB cell line IMR-32, not for KELLY, which is used in the present study. A cyclin D1 reduction could be demonstrated in both NB cell lines treated with R+D (129, 130). *Dong et al.* were able to show an increase in GSK-3β activity and subsequent degradation of cyclin D1 in rapamycin-sensitive breast cancer cell lines *in vitro* and *in vivo*, though independent of the phosphorylation status of Ser9 (193). However, these effects seem to be cell line-specific, and evidence suggests that GSK-3β can act as a tumor suppressor or promote cell proliferation in a cell type-specific context (195). Furthermore, while several studies indicate that active GSK-3β reduces MycN protein (19, 62), *Duffy et al.* show that several GSK-3 inhibitors reduced MycN mRNA levels by likely altering mRNA stability, which subsequently also led to reduced MycN protein levels (196). GSK-3 inhibition with the GSK-3 inhibitors lithium chloride (in much higher doses than those used for its neuroprotective effects) and BIO-acetoxime led to decreased NB viability in a time- and concentration-dependent manner, including in the cell line KELLY, and effects on viability seemed to be primarily apoptosis-mediated (196). A correlation between loss of viability and MycN amplification level could be shown in that MNA NB cell lines with greater MycN amplification fold (including KELLY) showed greater loss of viability compared to low-fold MycN amplification cell lines (196). According to *Duffy et al.*, the effects of lithium chloride or BIO-acetoxime treatment were comparable with those of the dual PI3K/mTOR inhibitor NVP-BZ235 (196). *Duffy et al.* hypothesized, that active GSK-3 reduces MycN protein (19, 62) while stabilizing MycN mRNA level (196) and that therefore GSK-3 inhibition may be beneficial for the treatment of NB (196). *Dickey et al.* utilized SB415286, a selective GSK-3β inhibitor, to show reduced cell survival and the induction of apoptosis following treatment, including in the cell line SK-N-SH, which is also used in the present study (197). These results suggest that not just GSK-3 activation but also its inhibition plays a role in NB survival.

The effect of rapamycin may vary with the activity of the PI3K/AKT/mTOR pathway or other signaling pathways not further investigated here within each cell line or experimental model. Additionally, the underlying mechanisms by which rapamycin leads to GSK-3β activation are not entirely clear. The present study and Western blot analysis by *R. Wätzig* suggest reduced phosphorylation at Ser9 as one component of GSK-3β activation. However, others show GSK-3β activation in the presence of rapamycin independent of phosphorylation at Ser9 or no activation of GSK-3β at all. GSK-3β may therefore be regulated by other mechanisms not identified within this study. Additionally, complex bi-directional cell type-specific interactions between GSK-3 and AKT exist (195). While GSK activation seems to reduce NB cell viability, GSK inhibition is also implicated in other studies to attenuate NB growth. Its complex role in NB therefore remains elusive and deserves further analysis.

## 4.5. Activation of Tumor Suppressor PTEN in MycN-Amplified Cell Lines

Yet another target analyzed was the phosphatase PTEN, which functions as a tumor suppressor gene (198, 199). PTEN, which is activated upon dephosphorylation (174), negatively regulates the activation of the PI3K/AKT/mTOR pathway by dephosphorylating $PIP_3$ to $PIP_2$, thus preventing the activation of downstream targets (200, 201). PTEN inactivation has been implicated in many cancers (40, 199, 201). PTEN activity is regulated by a variety of mechanisms, including phosphorylation (202). Phosphorylation within the PTEN tail (C2 domain), including Ser380, affects its phosphatase activity, subcellular location, and protein stability (202-204). It has been proposed that phosphorylation of the carboxyterminal site results in a decrease in PTEN activity (202), which may lead to a decrease or loss of its tumor suppressor function. Dysregulated PTEN phosphorylation of residues Ser380, Thr382, and Thr383 has been shown to promote cell survival through the PI3K/AKT/mTOR pathway and is implicated in the carcinogenesis of several cancers (174, 205-207).

In the present study, treatment with R+D led to reduced PTEN phosphorylation (and thereby activation) mainly in MNA cells and, to a much lesser extent, in the MNN cell line SK-N-SH. Dephosphorylation of PTEN occurs at least in part via PP2A (204). PP2A is phosphorylated and inactivated by mTORC1 (19). mTORC1 inhibition by rapamycin may therefore lead to the disinhibition of PP2A and its subsequent dephosphorylation of PTEN, as seen in the present study.

In line with other results in the present study and the notion that the RIST therapy is more effective in MNA NB cell lines than in those not amplified, treatment with R+D led to PTEN dephosphorylation (activation) mainly in MNA cells and to a much lesser extend in the MNN cell lines SK-N-SH whereas no change was detected for SK-N-AS.

## 4.6.Efficacy of Dasatinib

The efficacy of the multikinase inhibitor dasatinib could be shown by the effective inhibition of Src and ERK1/2 in both MNA and MNN NB cell lines. However, the effect is only mild and, in the case of some targets, not detectable in the MNN cell line SK-N-AS.

In line with these results, *Timeus et al.* and *Vitali et al.* showed anti-proliferative and anti-migratory effects in NB cell lines treated with dasatinib (103, 104). Treatment of several NB cell lines resulted in reduced phosphorylation of Src, AKT, and ERK1/2 as shown by Western blot analysis done by *Vitali et al.* and *R. Wätzig* (104, 129, 130). As shown by *Vitali et al.*, dasatinib exerted its effects via heterogeneous mechanisms, inducing senescence in one NB cell line while other cell lines underwent apoptosis without any sign of senescence (104). In contrast to these results, *Timeus et al.* could not show the induction of apoptosis at all in the NB cell lines used (103). Dasatinib seems to exert its effects in a cell type- and cell line-specific manner. Besides the inhibition of Src kinases, dasatinib also inhibits a variety of other serine/threonine kinases, some of which may be responsible for the heterogeneous effects when treating NB but have not been further evaluated within the scope of this study. Some of these kinases may also be functionally altered within certain NB cell lines, which may also account for the differential behavior. Within the present study, the cell line SK-N-AS only showed mild response to a 72-hour treatment with R+D. However, *Kaess et al.* clearly showed a reduction in phosphorylated Src by Western blot analysis in the cell line SK-N-AS after treatment with R+D, although with much higher dasatinib concentrations than used within this study and shorter treatment duration (24 hours) (182). *Vitali et al.* also showed an effective reduction in cell viability of the NB cell line SK-N-AS via MTT assay after 72 hours of dasatinib treatment (104). However, *Vitali et al.* used a 10-fold higher concentration of dasatinib in a single drug treatment set-up compared to the dual treatment employed within this study, which may account in part for the discrepancy of effects.

Extensive crosstalk between the PI3K/AKT/mTOR pathway and the MAPK/ERK pathway, among others, occurs. It has been shown that selective mTORC1 inhibition enhances RTK signaling, not only to PI3K/AKT via the aforementioned feedback activation but also to ERK 1/2 (92, 93, 208), which limits the overall therapeutic effect and results in the persistence of protein synthesis despite rapamycin treatment (41). Therefore, a combined treatment with rapamycin and the multi-kinase inhibitor dasatinib might help to overcome these limitations. The combinatorial molecularly targeted treatment R+D has been tested in NB cell lines, breast cancer cell lines, and NSCLC cell lines by *J. Leister, Park, et al.,* and *Chen et al.*, respectively, and shown to be superior to single drug treatment (120, 121, 128). Furthermore, dasatinib treatment might be responsible for suppressing the feedback activation following rapamycin treatment, which leads to activation of the PI3K/AKT pathway due to suppression of the negative feedback loop mediated through S6K and IRS-1 upregulation and activation of AKT, as shown by *Yori et al*. (122). As mentioned above, the combinatorial treatment of R+D within this study may therefore also be responsible for the demonstrated feedback inhibition in the MNA cell lines KELLY and LAN-5.

## 4.7. Other Targets

### 4.7.1. HSP60

Heat shock protein HSP 60, a highly conserved protein of the family of molecular chaperones, is induced by cells under physiological stress or pathological conditions (177). HSP60 has been implicated in tumor cell metastasis, inhibition of apoptosis, and drug resistance in a cell type-specific context (177). The present study shows a reduction in HSP60 protein levels upon treatment with R+D in the MNA cell line KELLY but not in the MNN cell line SK-N-AS.

In NB, HSP60 overexpression has been linked to high expressions of survivin, a member of the inhibitor of apoptosis (IAP) family (209). Additionally, a decrease in HSP60 leads to the instability and degradation of mitochondrial survivin, which in turn results in the loss of mitochondrial membrane integrity and the induction of apoptosis (210, 211). Survivin has been associated with high-risk NB and unfavorable prognosis in NB (212, 213). Down-regulation of HSP60 in glioblastoma cells has suppressed proliferation via the mTOR pathway network (211). Rapamycin, dasatinib, and other multikinase inhibitors have been shown to downregulate survivin in several types of cancer, at least in part via inhibition of the mTOR pathway network

(214-216). However, one study showed increased survivin expression upon rapamycin treatment in NB cell lines (217). In the present study, lowering effects of R+D treatment on HSP60 protein levels have only been seen in the MNA cell line KELLY, which is also more sensitive to mTOR inhibition via the RIST therapy. The exact underlying mechanisms and pathways in which HSP60 levels are affected and their precise role in NB remain to be examined but were not within the scope of the present study.

### 4.7.2. WNK1

Another novel finding within the present study was the reduction in phosphorylation of WNK1 (Thr60) upon R+D treatment in the MNA cell line KELLY but not in the MNN cell line SK-N-AS.

The with no lysine kinase (WNK) pathway, mainly known for regulating ion transport across membranes, is also implicated in cancer progression and angiogenesis (73). The phosphorylation of WNK1 at Thr60 by AKT is often used as a readout for WNK activity (73). In line with the hypothesis that RIST therapy or R+D, respectively, is effective in downregulation of the PI3K/AKT/mTOR pathway in MNA NB, downregulation of AKT subsequently leads to a reduction of phosphorylation of WNK1 by AKT. The exact role of this post-translational modification, its effects on WNK activity, and its implicated role in cell migration remain to be seen (73).

## 4.8.Cell Line-Specific Effects

While some cancers are characterized by a unique constitutive aberrant activation of an oncogene or inactivation of a tumor suppressor gene, which makes these mutations ideal targets for targeted cancer therapy (218), a single such targetable “addictive” oncogene has not been found for NB. The mutation rate is low compared to adult cancers, and a general targeted approach geared towards commonly aberrant pathways remains challenging (219). Few somatic alterations of significance have been identified, including ALK, PTPN11, ATRX, MycN, and NRAS (219), which present themselves as putative candidates for a molecularly targeted therapeutic approach, more so as an individualized approach based on the identification of targets in subsets of patients, rather than as a generalized approach.

A subset of NB is characterized by the genomically amplified MycN oncogene associated with dismal outcome (2, 16, 17). The transcription factor MycN itself, associated with dysregulation of the PI3K/AKT/mTOR pathway, is deemed "undruggable" (20). However, several strategies are being pursued to directly or indirectly target MycN, for example, by targeting its transcription via BET inhibitors or its oncogenic stabilization, e.g., by inhibiting the PI3K/AKT/mTOR pathway (21, 63).

The present study hypothesized that targeting the PI3K/AKT/mTOR pathway with the molecularly targeted drug combination R+D (allosteric mTOR inhibitor, multikinase inhibitor), and thereby indirectly targeting MycN, is superior in MycN-driven NB.

Data from the present study as well as the results of others as outlined above indicate that the RIST therapy is a successful strategy in treating NB and is especially effective in MNA NB, defining MycN as Weinstein's so-called "Achilles' heel of cancer" (218) in this subset of NB.

In those tumors where mTORC1 is the likely downstream effector of oncogenic activity, blockage of mTORC1 seems to be a feasible strategy, and evidence from this study suggests that in combination with dasatinib, it does not necessarily seem to induce AKT activation in MNA but in MNN cell lines via suppression of the negative feedback loop. However, as some functions of mTORC1 are rapamycin-resistant (179-181, 220) and a possibility of unintended indirect activation of the PI3K/AKT/mTOR pathway may occur, substituting rapamycin for an ATP-competitive dual mTORC1/2 inhibitor may be desirable as consequently all mTOR activities including AKT activation via phosphorylation at Ser473 are blocked (179, 181, 220). In a follow-up study, *R. Wätzig* has shown the efficacy of the dual mTORC1/2 inhibitor Torin 2 as a promising possible substitution for rapamycin in the RIST therapy regimen (129, 130). By suppressing rapamycin-resistant mTORC1 and mTORC2 functions, ATP-competitive mTOR inhibitors lead to a more profound and durable suppression of proliferation (179, 181) and may be a promising substitute candidate for rapamycin within the RIST therapy.

One additional mechanism to consider as to why MNA tumors seem to be especially susceptible to the RIST therapy may be that susceptibility may, in part, be mediated through metabolic reprogramming by co-amplified genes such as DDX1, a family of genes that encode for DEAD box proteins, putative ATP-dependent RNA helicases implicated in several cellular processes (221). In MNA NB, DDX1 is often co-amplified (222-225), and some studies implicate a more aggressive phenotype in DDX1-MycN co-amplified tumors (224). No DDX1 amplification was observed in NB tumors or cell lines lacking MycN amplification (222-225). A recent study

found that co-amplification of MycN and DDX1 does not influence tumor initiation or progression, nor did it alter tumorigenic properties or show differences in overall survival compared to MycN-only amplified tumors (221). However, DDX1-MycN co-amplified NB cell lines were associated with a high dependency on mTORC1, and DDX1 co-amplification was implicated in mTOR pathway activation in this subset of NB (221). When treated with the mTOR inhibitor rapamycin, DDX1-MycN co-amplified NB was significantly more sensitive to mTOR inhibition than MycN-only amplified NB in cell line and zebrafish models (221). The MNA NB cell line LAN-5 within the present study also harbors DDX1 co-amplification, whereas the MNA cell line KELLY does not (221-223). Within the apoptosis assays, the cell line LAN-5 was most sensitive to pre-treatment with R+D alone, but no significant difference between the two MNA cell lines was detected when treated with the complete RIST therapy protocol. However, these results might indicate the above-hypothesized sensitivity toward mTOR inhibition alone in co-amplified NB. It might be of interest to test in a preclinical and clinical setting whether NB patients with DDX1 co-amplification respond better to RIST than MycN-only amplified NB.

In the present study, both MNA NB cell lines responded similarly to the RIST therapy. However, it is noteworthy that higher dosages of rapamycin and dasatinib are necessary for the cell line KELLY, and in the study done by *R. Wätzig* on KELLY and another MNA cell line, MycN expression in the cell line KELLY was not affected, despite responsiveness to RIST (129, 130). These results might be due to the coexistence of an ALK mutation or potential differences in the expression of protein kinases such as Aurora A kinase (129, 130) or Polo-like kinase 1 (226, 227).

MNA NB cells evade regulation of MycN degradation in order to sustain high MycN activity necessary for proliferation and survival via a variety of mechanisms, including overexpression of the protein kinase Aurora A (228, 229). Overexpression of Aurora A is associated with advanced stage, poor prognosis, and disease relapse (228, 229). In these cells, Aurora A interferes with MycN degradation (but not c-Myc degradation) via a kinase-independent protein-protein interaction, rendering these cells less dependent on active PI3K/AKT/mTOR signaling but on high Aurora A levels to sustain high MycN levels (228, 229). Within the present study, no determination of Aurora A expression in the cell lines used has been done. It might be of interest to examine Aurora A expression in a panel of MNA NB treated with RIST and its effects on MycN levels as well as a possible combination of RIST with an Aurora A inhibitor.

Polo-like kinase 1 (PLK1) is another serine/threonine kinase with elevated expression levels in high-risk NB, which has been linked to poor outcome in these patients (226, 230). PLK1 counteracts ubiquitination and degradation of MycN. MycN, in turn, activates PLK1 transcription resulting in a positive feedforward loop driving the oncogenic potential of MycN (227) and might be part of an escape mechanism in subsets with high PLK1 expression. Elevated PLK1 expression has also been linked to poor outcome in MNN NB, and preclinical *in vitro* and *in vivo* studies showed antitumor effects of a PLK1 inhibitor, including in the cell lines KELLY and SK-N-AS, regardless of MycN status (226, 230). Therefore, PLK1 inhibitors might be a viable treatment option, potentially in combination with RIST, for less responsive MNA NB or MNN NB alike, and it might be of interest to examine its expression and therapeutic effects in combination with RIST in a suitable panel of NB cell lines in the future.

Yet another potential mechanism for the differential response in MycN expression might be the presence of an ALK mutation. In the present study, both MNA NB cell lines harbor an activating ALK mutation (F1174L and R1275Q, respectively). ALK is known to reduce phosphorylation at Thr58 of MycN, thereby enhancing its stability (60). ALK mutations such as ALK F1174L in KELLY are associated with advanced disease stages (61), lead to the overactivation of the PI3K/AKT/mTOR and MAPK pathways, and potentiate the oncogenic activity of MycN (60). Treatment combination with an ALK inhibitor such as crizotinib might be another option and should be further tested in a panel of MNA/ALK mutated and MNA/ ALK wildtype NB cell lines to examine the importance of additional ALK mutations in treating MNA NB with RIST and to examine possible effects of a combination with an ALK inhibitor. However, it is of note that the mutation ALK F1174L causes intrinsic resistance to crizotinib in ALK-mutated tumors (60). Nevertheless, a combination of the ATP-competitive mTOR inhibitor Torin 2 and crizotinib overcame resistance and led to the induction of apoptosis and tumor regression (60), and might therefore be a promising combination in treating this subset of double-mutated NB.

High-risk NB without MycN amplification may also be clinically aggressive, and a subset of these tumors also lead to therapy resistance and poor outcome, suggesting factors other than high MycN levels that influence tumor behavior. In the present study, MNN NB cell lines responded less to the RIST therapy than MNA cell lines, which might be due to the fact that the PI3K/AKT/mTOR pathway is overly activated in MNA NB and these cells are “addicted” to this overactivation and are thus more susceptible to interference of this pathway. Other potential mechanisms of therapy resistance, including the differential expression of several protein

kinases such as PLK1, which not only influences the stability of MycN but also c-Myc or the presence of activating ALK mutations, have been discussed and might also play a role in MNN NB.

Other potential mechanisms of therapy resistance and oncogenic aggressiveness include c-Myc as a potential oncogene in a subset of high-risk NB lacking amplification of MycN (231-234). In recent studies, a subset of high-risk NB patients lacking MycN amplification/high levels of MycN protein but instead expressing high levels of c-Myc protein was correlated with poor outcome (231, 232).

The MNN NB cell line SK-N-AS used in the present study has been shown to contain high levels of c-Myc (235). When disrupting Myc expression in KELLY (MNA) and SK-N-AS (MNN) using a CRISPR/Cas9 approach, *Zimmerman et al.* were able to show a loss in cell viability and reduced colony formation in SK-N-AS (MNN, elevated c-Myc) but not KELLY (MNA), which is MycN-driven and contains minimal c-Myc, thereby proving the dependency of SK-N-AS on c-Myc (235). This might explain why especially the NB cell line SK-N-AS is relatively unresponsive to the RIST therapy. Inhibition of ubiquitin-specific protease 28, a deubiquitinase, which plays a role in the stabilization of MycN as well as c-Myc, has shown to be effective in MNA and c-Myc-driven NB (SK-N-AS, SK-N-SH) cell lines alike (235). *Zimmerman et al.* showed that aberrantly elevated levels of c-Myc are driven by focal amplification of enhancer elements and hijacking of (super-) enhancers, where chromosomal translocations result in rearrangements that juxtapose Myc with super-enhancers from partner chromosomes, leading to elevated c-Myc (235). In the cell line SK-N-AS, for example, the translocation t(4;8) (q34;q24) led to the repositioning of a super-enhancer in the vicinity of Myc regulatory sequences (235). It is of note that in *Zimmerman et al*., in the cell line SH-SY5Y (t(7;8) (q33;q24)), a super-enhancer within chromosome 7 is translocated just downstream from the Myc transcriptional start site (235). The same translocation could be detected by DNA PCR in the parental cell line of SH-SY5Y, SK-N-SH. However, the activity of enhancer marks (H3K27ac) was much higher in SH-SY5Y than in its parental cell line SK-N-SH (235). Another subclone of SK-N-SH (SHEP) also harboring the translocation does not show any enhancer activity or high levels of c-Myc (235). Additionally, focal amplification of the specific enhancer region could be detected, especially in SH-SY5Y and, to a much lesser extent, in SK-N-SH (235). Therefore, it is likely that c-Myc levels in SK-N-SH are much lower compared to SK-N-AS and the cell line SK-N-SH may not be as dependent upon c-Myc. This might be, in part, why the SK-N-SH cell line is more susceptible than SK-N-AS to the RIST therapy within the

present study, as SK-N-SH may lack the oncogenic drive of high c-Myc levels displayed by SK-N-AS and may thus possess a less aggressive and chemo-resistant phenotype.

Other mechanisms by which MNN NB might be driven is via a deregulated WNT/β-catenin signaling pathway (21, 236), resulting in transactivation of Myc and other target genes, leading to a more aggressive and chemo-resistant NB phenotype (236). *Liu et al.* found upregulated β-catenin target gene expression in primary NB without MycN amplification and elevated expression of c-Myc and β-catenin levels in NB cell lines in the absence of MycN amplification, including NB cell lines SK-N-SH and SK-N-AS (236). In this study, SK-N-AS expresses higher levels of β-catenin than SK-N-SH (236), suggesting a possibly more aggressive and chemo-resistant phenotype. While no NB cell line tested showed specific β-catenin transactivation, evidence for relative β-catenin target gene upregulation was demonstrated (236). In the cell line SK-N-AS, one study showed that WNT signaling drives proliferation rather than differentiation, as shown in other NB cell lines tested, suggesting cell line-specific fates (237). Several studies implicate that interference with the WNT pathway leads to a reduction in the proliferation and migration of NB (21, 238).

Additionally, a candidate tumor suppressor gene p73 mapping to 1p36.33 has been identified, which is deleted in the cell line SK-N-AS (156). p73 has structural and functional homologies to p53 (156). Transfection of p73 into the SK-N-AS cell line suppresses its tumorigenic phenotype (156). Therefore, this might add to the more chemo-resistant behavior seen in the present study.

Taken together, the RIST therapy is effective in treating NB cell lines, especially in MNA NB cell lines. It is crucial to identify collateral vulnerabilities such as DDX1 co-amplification or potential escape mechanisms such as Aurora A kinase overexpression in order to define likely therapy responders and patients for which additional targeted therapeutic agents might be beneficial.

## 4.9. Limitations of This Study

As described by *J. Leister*, the $IC_{50}$ concentrations of the used drugs are in line with published data from other studies for single treatments and could be reduced substantially when used in combination (128). Combinations of the drugs were applied at $IC_{50}$ concentrations individualized for the cell lines to make the cell lines comparable in terms of their $IC_{50}$ and to

compare responses of the RIST therapy in the dosage relevant for each cell line. In a clinical setting, however, standardized uniform dosages will be used, which should be taken into account for future studies. It is also of note that dosages of the molecularly targeted drugs for the MNA cell line KELLY are greater than that of the other cell lines used, potentially due to the existence of the above-discussed escape mechanisms, however within this cell line, the greatest dose reduction of the drugs could be archived compared to the other cell lines tested when used in combination (128), underscoring the effectiveness of RIST in this MNA cell line. In the present study, individual $IC_{50}$ concentrations have also been used to examine changes within each cell line in their respective effective dose. Within the present study, a lower dosage of dasatinib has been used for SK-N-AS than has been established as $IC_{50}$ dosage by *J. Leister*; however, experiments in our lab by *M. Matthes* confirmed the used dosages are still within the $IC_{50}$ range.

As with all *in vitro* studies, the present study has limitations when it comes to translating *in vitro* findings into an *in vivo* or clinical setting. It is difficult to establish an *in vivo* relevant *in vitro* system as isolated and cultivated cells differ strongly from the corresponding cell type within an organism, and it is challenging to recreate an analog tumor microenvironment where gene regulation occurs the same as it would in *in vivo* conditions. Additionally, interactions between different cell types are not considered, and xenobiotic metabolism is challenging to recreate and predict in *in vitro* settings. Due to the complex structure and organization of organisms, it is also challenging to account for recompensating mechanisms of stress situations and to consider these when testing substances *in vitro*, and promising pre-clinical results can often not be translated into clinical settings (239).

Nevertheless, the presented results provide substantial evidence for the efficacy of the RIST therapy in high-risk relapsed and refractory NB, especially when MycN-amplified, and warrant further studies. One option to overcome the limitations of two-dimensional monolayer cancer cell models, and to resemble *in vivo* tumor biology and architecture more closely, is to use three-dimensional culture models (239). In a follow-up study, *C. Kaess* successfully established a three-dimensional spheroid culture of NB and has proven RIST to be effective in this experimental set-up as well (182).

Additionally, the recently published results of the prospective randomized RIST trial (RIST-rNB-2011) are consistent with the pre-clinical results of this study. Progress-free survival (PFS) and overall survival (OS) were significantly better in the RIST arm vs. the control arm

(irinotecan/temozolomide only) in the intention to treat (ITT) population as well as in the per-protocol (PP) population (240). Further subgroup analysis shows a selective effect in MNA NB patients. PFS and median OS were significantly better in MNA NB patients treated with RIST compared to control arm treatment, whereas MNN NB patients showed no differences neither in PFS nor in OS between the two treatment protocols (240).

## 4.10. Outlook

The results presented here provide important insights into the molecular mechanisms of the RIST therapy and lay the groundwork for further follow-up studies. To gain a deeper understanding and confirmation of the findings obtained herein, these should be validated in further studies, e.g., utilizing Western blot analysis. Several molecular targets and pathways, such as the exact role of GSK-3β, PTEN, or HSP60 should be further evaluated to gain a deeper understanding of their relevance in the molecular mechanisms of the RIST therapy. To sidestep the possibility of unwanted AKT induction by incomplete mTOR inhibition, further studies should evaluate the replacement of rapamycin with ATP-competitive mTOR inhibitors in a preclinical *in vitro* (as done already by *R. Wätzig*) and *in vivo* as well as in a clinical setting. Further experimental set-ups should take into account the heterogenicity of NB aside from MycN-amplification and the co-existence of resistance or escape mechanisms such as the presence of aberrantly expressed Aurora A kinase or Polo-like kinase or relevant co-amplifications such as the helicase DDX1. A precise understanding of the genetic complexity of NB is necessary in order to identify subgroups of patients based on their genetic predisposition. This could lead to the identification of prognostic tumor markers and a more accurate prediction of their likelihood of therapy response to targeted treatments. Additional testing of the RIST therapy in representative NB panels to identify subgroups that might benefit from additional molecularly targeted drugs in combination with RIST, such as ALK or Aurora A kinase inhibitors, might be helpful to tailor molecular targeted combinatorial treatments toward patients' needs. Future testing should be done in a more physiologically relevant, robust, and technically reproducible model such as three-dimensional spheroid cultures or the use of, e.g., zebra fish models in order to provide a better representation of tumor biology and microenvironment and to test drugs and therapy regiments under more relevant conditions.

# 5. Appendix

## 5.1. Additional Figures: Phosphorylation Status Profiling

### 5.1.1. Proteome Profiler™ Human Phospho-Kinase Array Kit

| Membrane/ Coordinate | Target/Control | Phosphorylation Site | DuoSet® IC (Total) ELISA Development System | DuoSet® IC (Phospho) ELISA Development System |
|---|---|---|---|---|
| A-A1, A2 | Reference Spot | — | — | — |
| A-A3, A4 | p38α | T180/Y182 | DYC8691B | DYC869B |
| A-A5, A6 | ERK1/2 | T202/Y204, T185/ Y187 | — | DYC1018B |
| A-A7, A8 | JNK 1/2/3 | T183/Y185, T221/ Y223 | DYC1205 | DYC1387 |
| A-A9, A10 | GSK-3α/β | S21/S9 | DYC2157 | DYC2630 |
| B-A13, A14 | p53 | S392 | DYC1043 | DYC2996 |
| B-A17, A18 | Reference Spot | — | — | — |
| A-B3, B4 | EGF R | Y1086 | DYC1854 | — |
| A-B5, B6 | MSK1/2 | S376/S360 | — | — |
| A-B7, B8 | AMPKα1 | T183 | DYC3197 | DYC3528 |
| A-B9, B10 | Akt 1/2/3 | S473 | — | DYC887B |
| B-B11, B12 | Akt 1/2/3 | T308 | — | — |
| B-B13, B14 | p53 | S46 | DYC1043 | DYC1489 |
| A-C1, C2 | TOR | S2448 | — | DYC1665 |
| A-C3, C4 | CREB | S133 | — | DYC2510 |
| A-C5, C6 | HSP27 | S78/S82 | DYC1580 | DYC2314 |
| A-C7, C8 | AMPKα2 | T172 | — | — |
| A-C9, C10 | β-Catenin | — | DYC1329 | — |
| B-C11, C12 | p70 S6 Kinase | T389 | DYC8962 | DYC896 |
| B-C13, C14 | p53 | S15 | DYC1043 | DYC1839 |
| B-C15, C16 | c-Jun | S63 | — | — |
| A-D1, D2 | Src | Y419 | — | DYC2685 |
| A-D3, D4 | Lyn | Y397 | — | DYC3936 |
| A-D5, D6 | Lck | Y394 | — | — |
| A-D7, D8 | STAT2 | Y689 | — | — |
| A-D9, D10 | STAT5a | Y694 | — | — |
| B-D11, D12 | p70 S6 Kinase | T421/S424 | DYC8962 | DYC8965 |
| B-D13, D14 | RSK1/2/3 | S380/S386/S377 | — | DYC889B |
| B-D15, D16 | eNOS | S1177 | — | — |

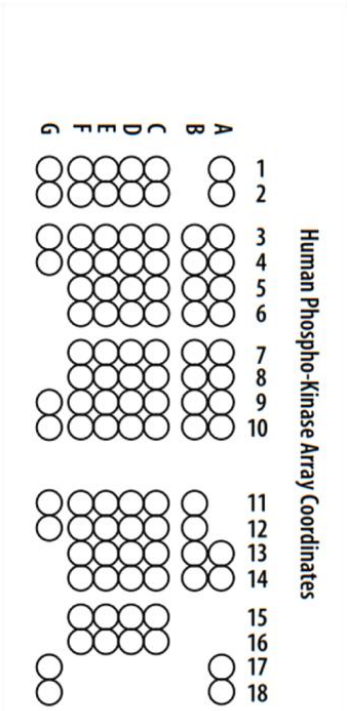


| Membrane/ Coordinate | Target/Control | Phosphorylation Site | DuoSet® IC (Total) ELISA Development System | DuoSet® IC (Phospho) ELISA Development System |
|---|---|---|---|---|
| A-E1, E2 | Fyn | Y420 | — | — |
| A-E3, E4 | Yes | Y426 | — | DYC3929 |
| A-E5, E6 | Fgr | Y412 | — | — |
| A-E7, E8 | STAT6 | Y641 | — | — |
| A-E9, E10 | STAT5b | Y699 | — | — |
| B-E11, E12 | STAT3 | Y705 | — | DYC4607B |
| B-E13, E14 | p27 | T198 | DYC2256 | — |
| B-E15, E16 | PLC-γ1 | Y783 | — | — |
| A-F1, F2 | Hck | Y411 | — | — |
| A-F3, F4 | Chk-2 | T68 | — | DYC1626 |
| A-F5, F6 | FAK | Y397 | DYC4467 | DYC4528 |
| A-F7, F8 | PDGF Rβ | Y751 | DYC385 | DYC3096 |
| A-F9, F10 | STAT5a/b | Y694/Y699 | — | — |
| B-F11, F12 | STAT3 | S727 | — | — |
| B-F13, F14 | WNK1 | T60 | — | DYC4720 |
| B-F15, F16 | PYK2 | Y402 | — | — |
| A-G1, G2 | Reference Spot | — | — | — |
| A-G3, G4 | PRAS40 | T246 | — | DYC6890 |
| A-G9, G10 | PBS (Negative Control) | — | — | — |
| B-G11, G12 | HSP60 | — | DYC1800 | — |
| B-G17, G18 | PBS (Negative Control) | — | — | — |

**Figure 44: Target Map of the Proteome Profiler™ Human Phospho-Kinase Array Kit by R&D Systems**

Target map of the Proteome Profiler™ Human Phospho-Kinase Array Kit as outlined in the provided protocol for the Proteome Profiler™ Human Phospho-Kinase Array Kit by R&D Systems (#ARY003B).

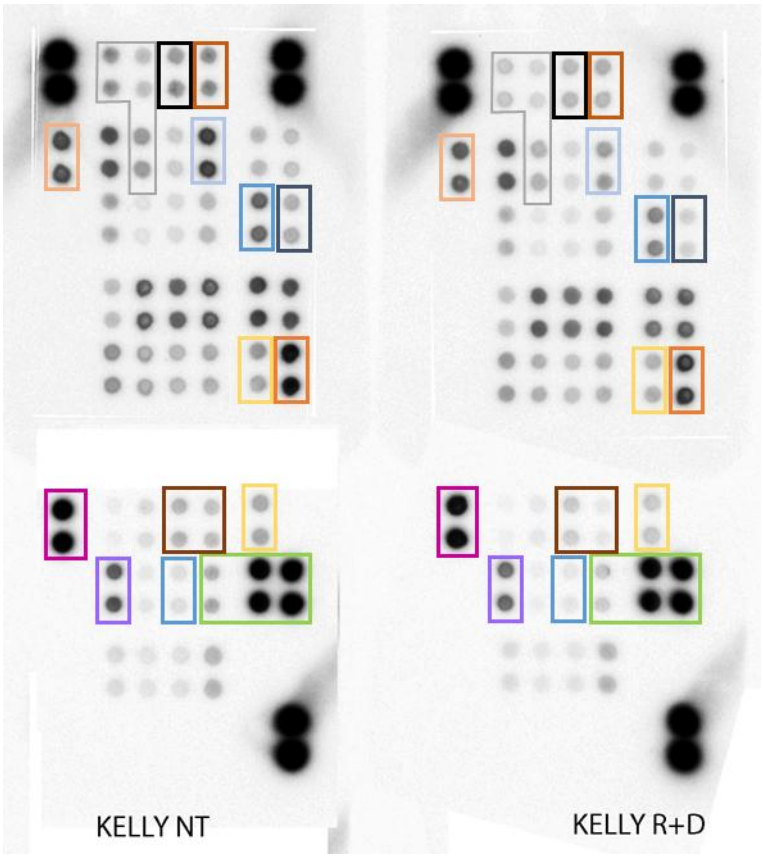


**Figure 45: Proteome Profiler™ Human Phospho-Kinase Arrays by R&D Systems for the MycN-Amplified Neuroblastoma Cell Line KELLY**

Relative phosphorylation levels of 43 phosphorylation sites of human kinases and 2 total protein levels of control (DMSO vehicle)-treated cells and cells after 72 hours of treatment with the molecularly targeted combinatorial treatment rapamycin plus dasatinib (R+D) were analyzed utilizing the Proteome Profiler™ Human Phospho-Kinase Kit by R&D Systems (#ARY003B) for the MycN-amplified (MNA) neuroblastoma (NB) cell line KELLY. Data represents one array with duplicate target spots for control (DMSO vehicle)-treated cells (NT) and cells after 72 hours of treatment with R+D.
Target-specific capture antibodies have been spotted in duplicate onto nitrocellulose-coated glass slides and cell lysates of control- (DMSO vehicle)-treated (NT) or R+D-treated cells were incubated, followed by a biotinylated detection antibody cocktail. Streptavidin-conjugated reagents were used to visualize the bound detection antibody by chemiluminescence. Images were captured with the ImageQuant LAS 4000 Mini.

Targets used for further analysis: **Src (Tyr419)**, **Src Family – Fyn (Tyr420), Yes (Tyr426), Hck (Tyr411)**, **ERK1/2 (Thr202/Tyr204, Thr185/Tyr187)**, **MSK1/2 (Ser376/Ser360)**, **RSK 1/2/3 (Ser380, Ser386/Ser377)**, **CREB (Ser133)** **AKT 1/2/3 (Ser473/Thr308)**, **TOR (Ser2448)**, **PRAS40 (Thr246)**, **S6K1 (Thr389, Thr421/Ser424)**, **GSK-3α/β (Ser21/Ser9)**, **p53 (Ser392, Ser46, Ser15)**, **WNK1 (Thr60)**, **HSP60 (Protein Level)**.

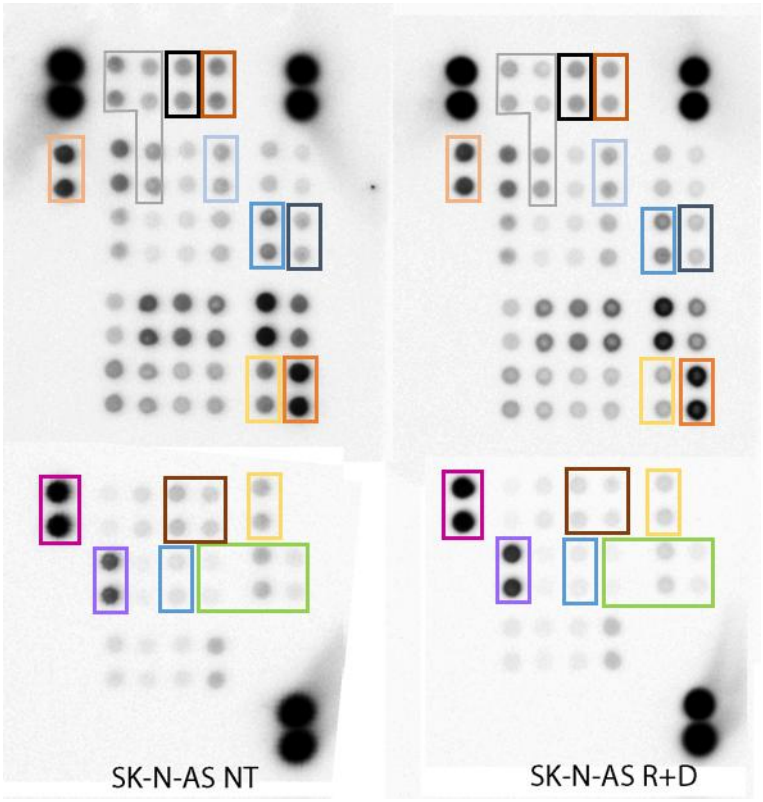


**Figure 46: Proteome Profiler™ Human Phospho-Kinase Arrays by R&D Systems for the MycN-non-Amplified Neuroblastoma Cell Line SK-N-AS**

Relative phosphorylation levels of 43 phosphorylation sites of human kinases and 2 total protein levels of control (DMSO vehicle)-treated cells and cells after 72 hours of treatment with the molecularly targeted combinatorial treatment rapamycin plus dasatinib (R+D) were analyzed utilizing the Proteome Profiler™ Human Phospho-Kinase Kit by R&D Systems (#ARY003B) for the MycN-non-amplified (MNN) neuroblastoma (NB) cell line SK-N-AS. Data represents one array with duplicate target spots for control (DMSO vehicle)-treated cells (NT) and cells after 72 hours of treatment with R+D.
Target-specific capture antibodies have been spotted in duplicate onto nitrocellulose-coated glass slides and cell lysates of control- (DMSO vehicle)-treated (NT) and R+D-treated cells were incubated, followed by a biotinylated detection antibody cocktail. Streptavidin-conjugated reagents were used to visualize the bound detection antibody by chemiluminescence. Images were captured with the ImageQuant LAS 4000 Mini.

Targets used for further analysis: **Src (Tyr419),** **Src Family – Fyn (Tyr420), Yes (Tyr426), Hck (Tyr411),** **ERK1/2 (Thr202/Tyr204, Thr185/Tyr187),** **MSK1/2 (Ser376/Ser360),** **RSK 1/2/3 (Ser380, Ser386/Ser377),** **CREB (Ser133)** **AKT 1/2/3 (Ser473/Thr308),** **TOR (Ser2448),** **PRAS40 (Thr246),** **S6K1 (Thr389, Thr421/Ser424),** **GSK-3α/β (Ser21/Ser9),** **p53 (Ser392, Ser46, Ser15),** **WNK1 (Thr60),** **HSP60 (Protein Level).**

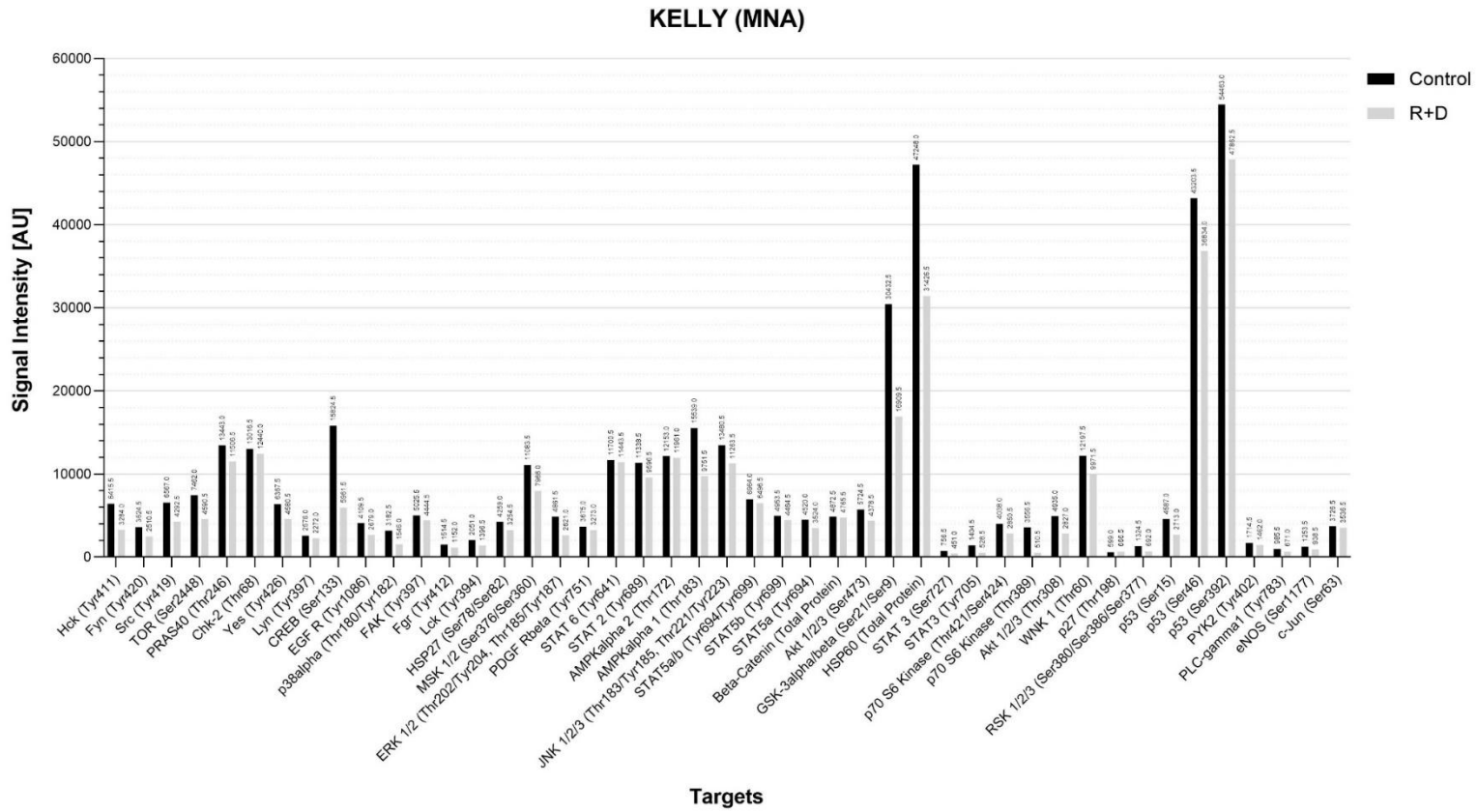


**Figure 47: Proteome Profiler™ Human Phospho-Kinase Arrays by R&D Systems of the MycN-Amplified Neuroblastoma Cell Line KELLY**

Relative phosphorylation levels of 43 target proteins and 2 total protein levels of control (DMSO vehicle)-treated cells and cells after 72 hours of treatment with the molecularly targeted combinatorial treatment rapamycin plus dasatinib (R+D) of the MycN-amplified (MNA) neuroblastoma (NB) cell line KELLY were analyzed utilizing the Proteome Profiler™ Human Phospho-Kinase Kit by R&D Systems (#ARY003B). Data represents one array with duplicate target spots for control (DMSO vehicle)-treated cells and cells after 72 hours of treatment with R+D.
Target-specific capture antibodies have been spotted in duplicate onto nitrocellulose-coated glass slides and cell lysates of control (DMSO vehicle)-treated (NT) and R+D-treated cells were incubated, followed by a biotinylated detection antibody cocktail. Chemiluminescent detection reagents were used to visualize the results. Images were captured with the ImageQuant LAS 4000 Mini. Target spot intensities were visualized using the array signaling analysis software ImageStudio Lite by Licor, and statistical and graphical analysis was done in Microsoft Excel and GraphPad Prism. Signal values were exported into an Excel spreadsheet file. An average background signal derived from the negative control spots was subtracted from each target spot signal value. Corresponding signals from control and R+D-treated arrays were graphed in GraphPad Prism for comparison. AU (arbitrary unit): absolute pixel density values, displayed values are means.

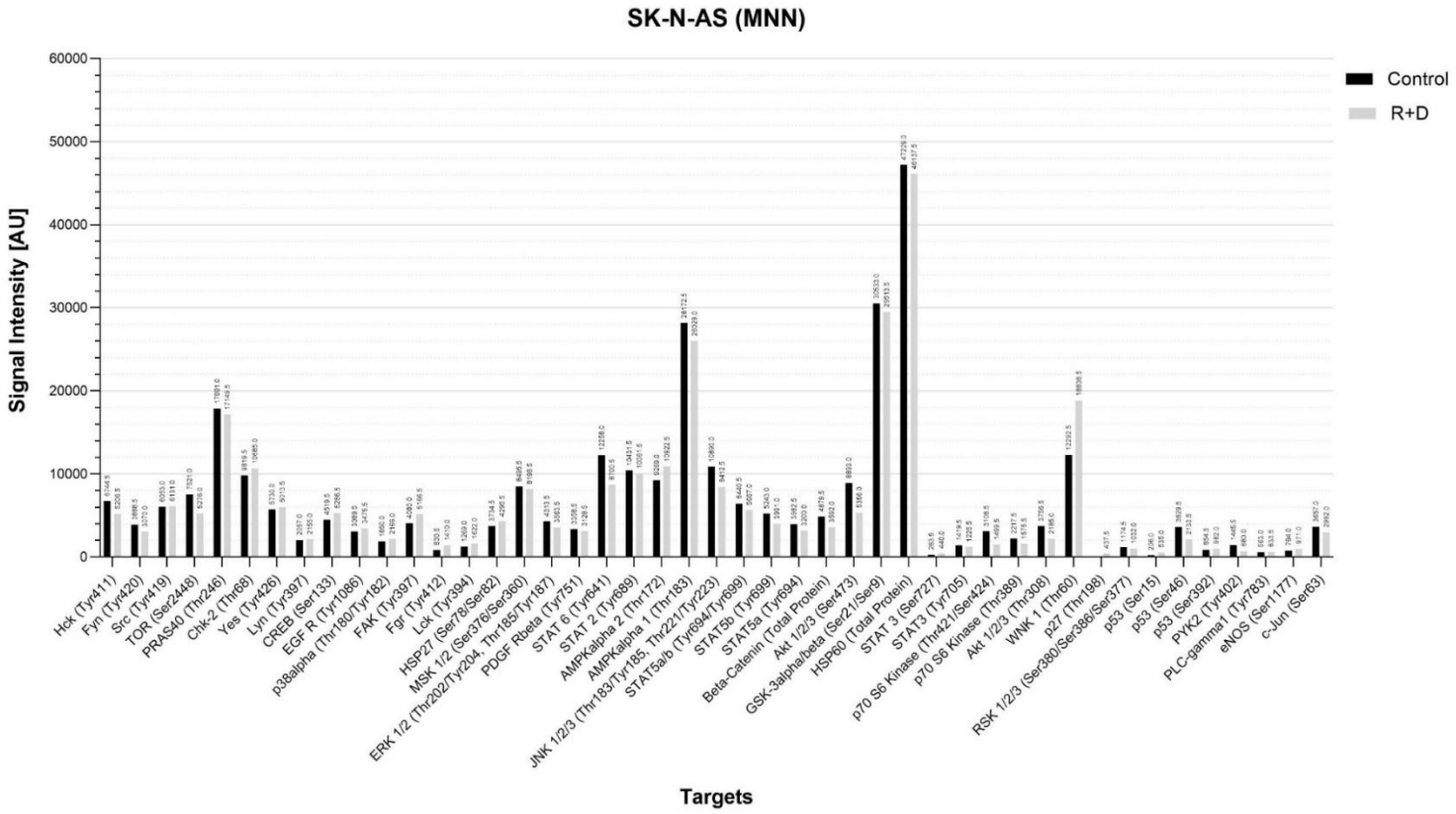


**Figure 48: Proteome Profiler™ Human Phospho-Kinase Arrays by R&D Systems of the MycN-non-Amplified Neuroblastoma Cell Line SK-N-AS**

Relative phosphorylation levels of 43 target proteins and 2 total protein levels of control (DMSO vehicle)-treated cells and cells after 72 hours of treatment with the molecularly targeted combinatorial treatment rapamycin plus dasatinib (R+D) of the MycN-non-amplified (MNN) neuroblastoma (NB) cell line SK-N-AS were analyzed utilizing the Proteome Profiler™ Human Phospho-Kinase Kit by R&D Systems (#ARY003B). Data represents one array with duplicate target spots for control (DMSO vehicle)-treated cells and cells after 72 hours of treatment with R+D. Target-specific capture antibodies have been spotted in duplicate onto nitrocellulose-coated glass slides and cell lysates of control (DMSO vehicle)-treated and R+D-treated cells were incubated, followed by a biotinylated detection antibody cocktail. Chemiluminescent detection reagents were used to visualize the results. Images were captured with the ImageQuant LAS 4000 Mini. Target spot intensities were visualized using the array signaling analysis software ImageStudio Lite by Licor, and statistical and graphical analysis was done in Microsoft Excel and GraphPad Prism. Signal values were exported into an Excel spreadsheet file. An average background signal derived from the negative control spots was subtracted from each target spot signal value. Corresponding signals from control and R+D-treated arrays were graphed in GraphPad Prism for comparison. AU (arbitrary unit): absolute pixel density values, displayed values are means.

### 5.1.2. PathScan® Akt Signaling Antibody Array Kit

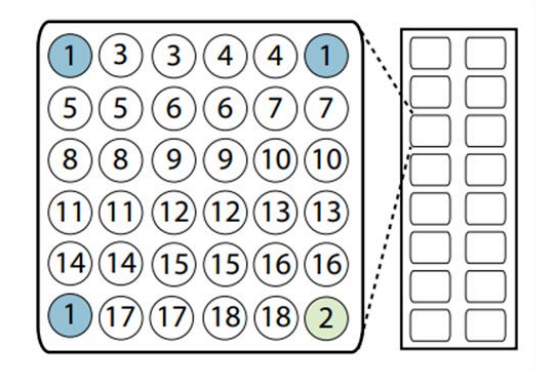


**Akt Signaling**

| | Target | Phosphorylation Site |
|---|---|---|
| 1 | Positive Control | N/A |
| 2 | Negative Control | N/A |
| 3 | Akt | Thr308 |
| 4 | Akt | Ser473 |
| 5 | S6 Ribosomal Protein | Ser235/236 |
| 6 | AMPKα | Thr172 |
| 7 | PRAS40 | Thr246 |
| 8 | mTOR | Ser2481 |
| 9 | GSK-3α | Ser21 |
| 10 | GSK-3β | Ser9 |
| 11 | p70 S6 Kinase | Thr389 |
| 12 | p70 S6 Kinase | Thr421/Ser424 |
| 13 | Bad | Ser112 |
| 14 | RSK1 | Thr421/Ser424 |
| 15 | PTEN | Ser380 |
| 16 | PDK 1 | Ser241 |
| 17 | Erk1/2 | Thr202/Tyr204 |
| 18 | 4E-BP1 | Thr37/46 |

**Figure 49: Target Map of the PathScan® Akt Signaling Antibody Array Kit (Chemiluminescent Readout) by Cell Signaling Technology**

Target map of the PathScan® Akt Signaling Antibody Array Kit (Chemiluminescent Readout) as outlined in the provided protocol for the PathScan® Akt Signaling Antibody Array Kit (Chemiluminescent Readout) by Cell Signaling Technology (#9474).

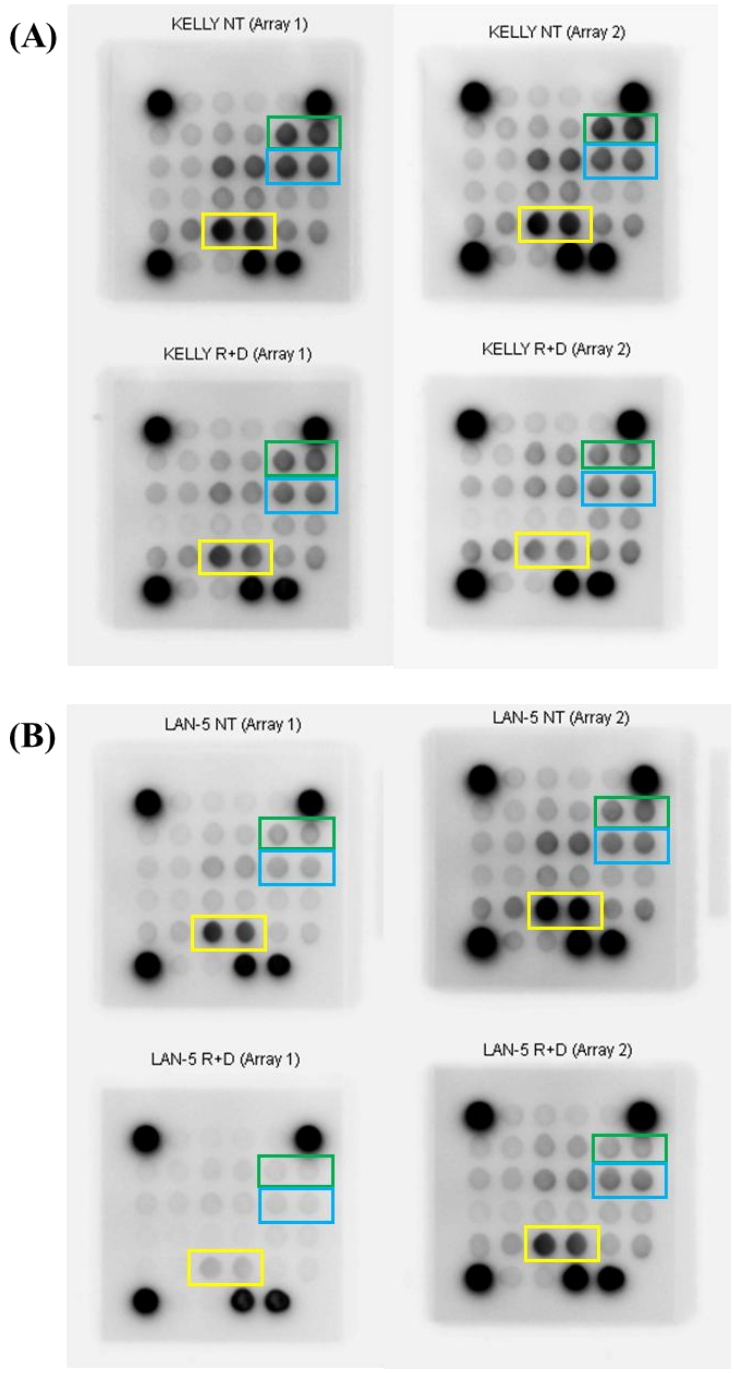


**Figure 50: PathScan® AKT Signaling Arrays by Cell Signaling Technology for the MycN-Amplified Neuroblastoma Cell Lines KELLY and LAN-5**

Relative phosphorylation levels of 16 phosphorylation sites of targets predominantly belonging to the AKT signaling network were analyzed utilizing the PathScan® AKT Signaling Array (Chemiluminescent Readout) (#9474) by Cell Signaling Technology. Relative phosphorylation levels of control (DMSO vehicle)-treated cells and cells after 72 hours of treatment with the molecularly targeted combinatorial treatment rapamycin plus dasatinib (R+D) of the MycN-amplified (MNA) neuroblastoma (NB) cell lines KELLY **(A)** and LAN-5 **(B)** were analyzed. Data represents two independent arrays per cell line with duplicate target spots for control (DMSO vehicle)-treated cells (NT) and cells after 72 hours of treatment with R+D. Target-specific capture antibodies have been spotted in duplicate onto nitrocellulose-coated glass slides and cell lysates of control (DMSO vehicle)-treated (NT) and R+D-treated cells were incubated, followed by a biotinylated detection antibody cocktail. Streptavidin-conjugated reagents were used to visualize the bound detection antibody by chemiluminescence. Images were captured with the ImageQuant LAS 4000 Mini.

Targets used for further analysis: PRAS40 Thr246, GSK-3β Ser9, PTEN Ser380.

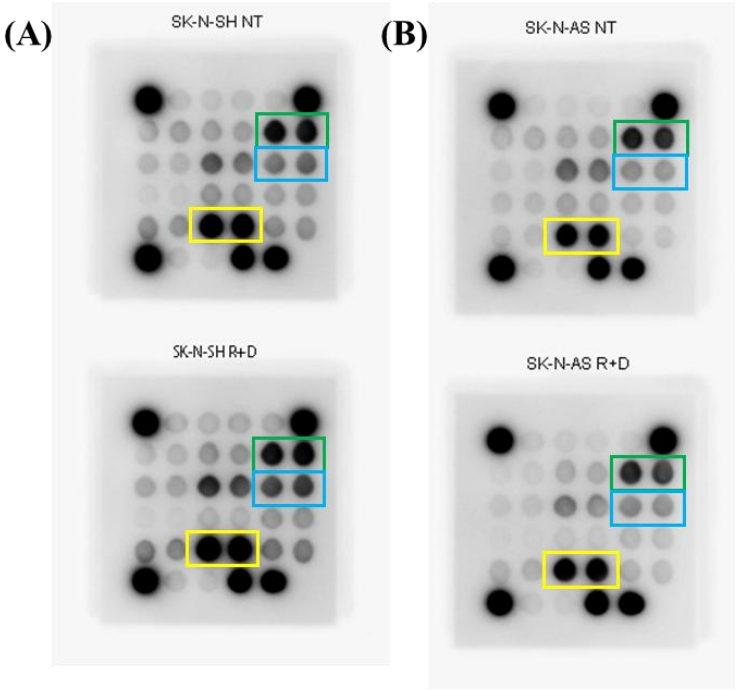


**Figure 51: PathScan® AKT Signaling Arrays by Cell Signaling Technology for the MycN-non-Amplified Neuroblastoma Cell Lines SK-N-SH and SK-N-AS**

Relative phosphorylation levels of 16 phosphorylation sites of targets predominantly belonging to the AKT signaling network were analyzed utilizing the PathScan® AKT Signaling Array (Chemiluminescent Readout) (#9474) by Cell Signaling Technology. Relative phosphorylation levels of control (DMSO vehicle)-treated cells and cells after 72 hours of treatment with the molecularly targeted combinatorial treatment rapamycin plus dasatinib (R+D) of the MycN-non-amplified (MNN) neuroblastoma (NB) cell lines SK-N-SH **(A)** and SK-N-AS **(B)** were analyzed. Data represents one array per cell line with duplicate target spots for control (DMSO vehicle)-treated cells (NT) and cells after 72 hours of treatment with R+D.
Target-specific capture antibodies have been spotted in duplicate onto nitrocellulose-coated glass slides and cell lysates of control- (DMSO vehicle)-treated (NT) and R+D-treated cells were incubated, followed by a biotinylated detection antibody cocktail. Streptavidin-conjugated reagents were used to visualize the bound detection antibody by chemiluminescence. Images were captured with the ImageQuant LAS 4000 Mini.

Targets used for further analysis: PRAS40 Thr246, GSK-3β Ser9, PTEN Ser380.

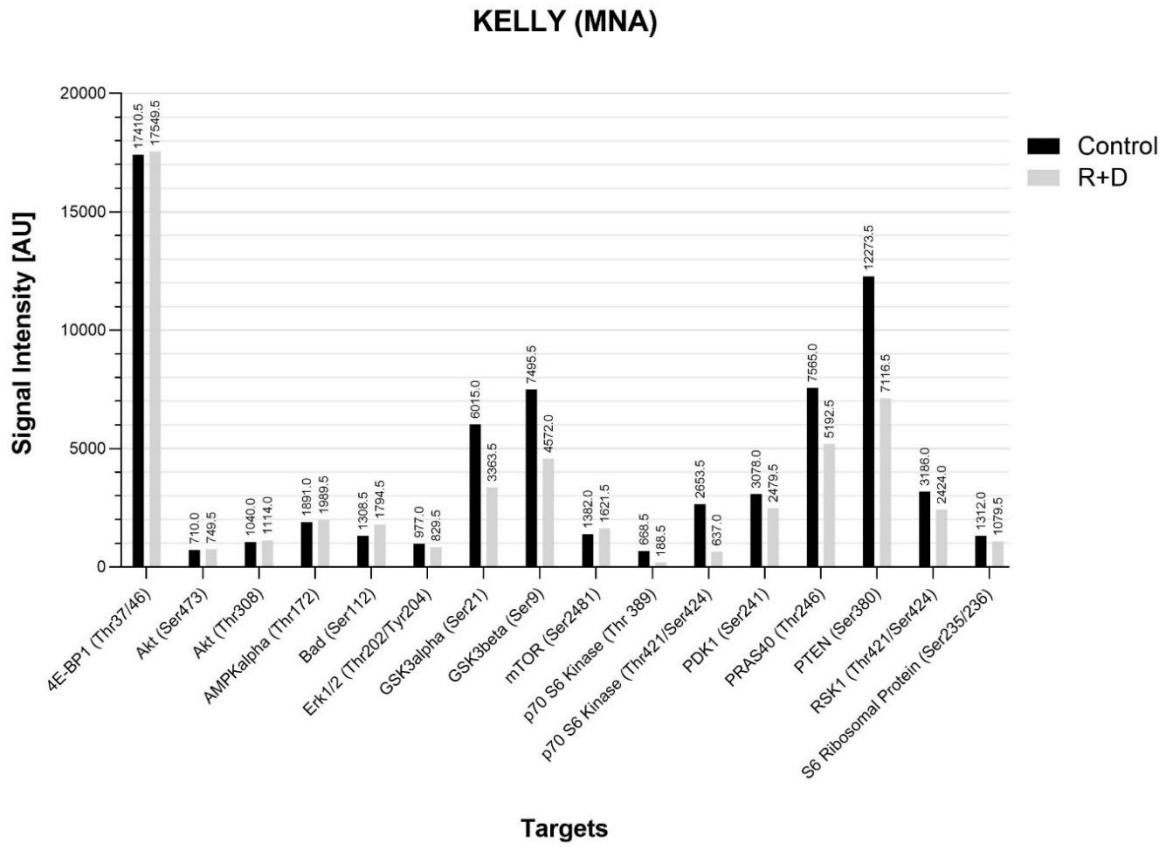


**Figure 52: PathScan® AKT Signaling Array by Cell Signaling Technology of the MycN-Amplified Neuroblastoma Cell Line KELLY**

Relative phosphorylation levels of 16 phosphorylation sites of targets predominantly belonging to the AKT signaling network were analyzed utilizing the PathScan® AKT Signaling Array (Chemiluminescent Readout) (#9474) by Cell Signaling Technology. Data represents one array with duplicate target spots for control (DMSO vehicle)-treated cells and cells after 72 hours of treatment of rapamycin plus dasatinib (R+D) of the MycN-amplified (MNA) neuroblastoma (NB) cell line KELLY. Data represents the results of the array displayed in *Figure 50A, Array 1*.
Target-specific capture antibodies have been spotted in duplicate onto nitrocellulose-coated glass slides and cell lysates of control (DMSO vehicle)-treated and rapamycin plus dasatinib (R+D)-treated cells were incubated, followed by a biotinylated detection antibody cocktail. Chemiluminescent detection reagents were used to visualize the results. Images were captured with the ImageQuant LAS 4000 Mini. Target spot intensities were visualized using the array signaling analysis software ImageStudio Lite by Licor, and statistical and graphical analysis was done in Microsoft Excel and GraphPad Prism. Signal values were exported into an Excel spreadsheet file. An average background signal derived from the negative control spots was subtracted from each target spot signal value. Corresponding signals from control and R+D-treated arrays were graphed in GraphPad Prism for comparison. AU (arbitrary unit): absolute pixel density values, displayed values are means.

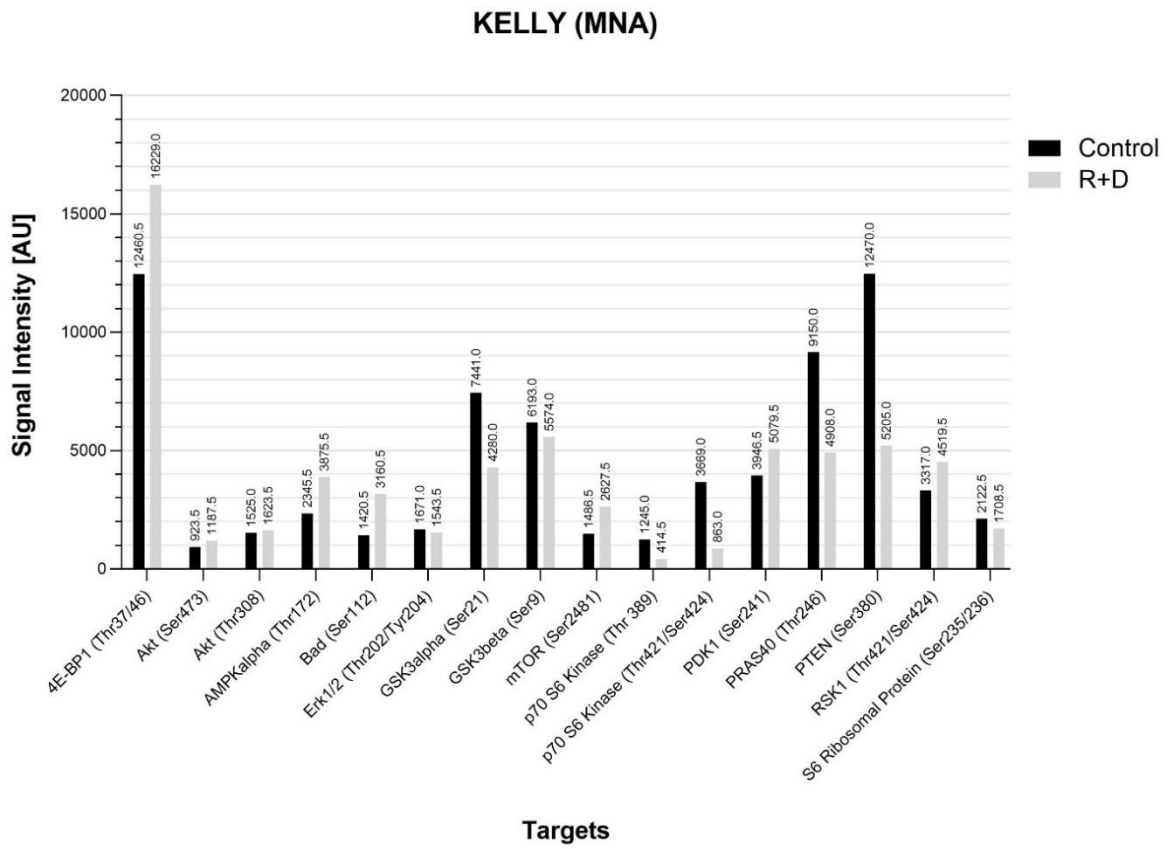


**Figure 53: PathScan® AKT Signaling Array by Cell Signaling Technology of the MycN-Amplified Neuroblastoma Cell Line KELLY**

Relative phosphorylation levels of 16 phosphorylation sites of targets predominantly belonging to the AKT signaling network were analyzed utilizing the PathScan® AKT Signaling Array (Chemiluminescent Readout) (#9474) by Cell Signaling Technology. Data represents one array with duplicate target spots for control (DMSO vehicle)-treated cells and cells after 72 hours of treatment of rapamycin plus dasatinib (R+D) of the MycN-amplified (MNA) neuroblastoma (NB) cell line KELLY. Data represents the results of the array displayed in *Figure 50A, Array 2*.
Target-specific capture antibodies have been spotted in duplicate onto nitrocellulose-coated glass slides and cell lysates of control (DMSO vehicle)-treated and rapamycin plus dasatinib (R+D)-treated cells were incubated, followed by a biotinylated detection antibody cocktail. Chemiluminescent detection reagents were used to visualize the results. Images were captured with the ImageQuant LAS 4000 Mini. Target spot intensities were visualized using the array signaling analysis software ImageStudio Lite by Licor, and statistical and graphical analysis was done in Microsoft Excel and GraphPad Prism. Signal values were exported into an Excel spreadsheet file. An average background signal derived from the negative control spots was subtracted from each target spot signal value. Corresponding signals from control and R+D-treated arrays were graphed in GraphPad Prism for comparison. AU (arbitrary unit): absolute pixel density values, displayed values are means.

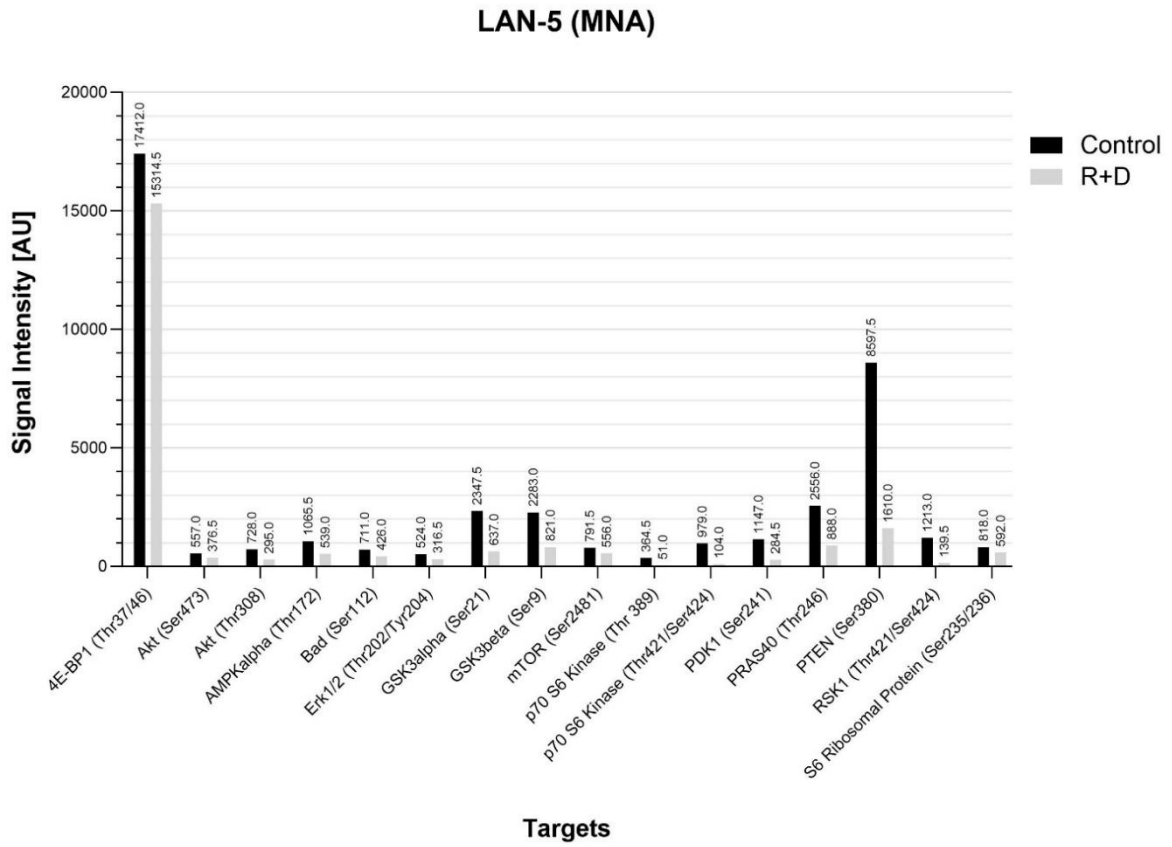


**Figure 54: PathScan® AKT Signaling Array by Cell Signaling Technology of the MycN-Amplified Neuroblastoma Cell Line LAN-5**

Relative phosphorylation levels of 16 phosphorylation sites of targets predominantly belonging to the AKT signaling network were analyzed utilizing the PathScan® AKT Signaling Array (Chemiluminescent Readout) (#9474) by Cell Signaling Technology. Data represents one array with duplicate target spots for control (DMSO vehicle)-treated cells and cells after 72 hours of treatment of rapamycin plus dasatinib (R+D) of the MycN-amplified (MNA) neuroblastoma (NB) cell line LAN-5. Data represents the results of the array displayed in *Figure 50B, Array 1*.
Target-specific capture antibodies have been spotted in duplicate onto nitrocellulose-coated glass slides and cell lysates of control (DMSO vehicle)-treated and rapamycin plus dasatinib (R+D)-treated cells were incubated, followed by a biotinylated detection antibody cocktail. Chemiluminescent detection reagents were used to visualize the results. Images were captured with the ImageQuant LAS 4000 Mini. Target spot intensities were visualized using the array signaling analysis software ImageStudio Lite by Licor, and statistical and graphical analysis was done in Microsoft Excel and GraphPad Prism. Signal values were exported into an Excel spreadsheet file. An average background signal derived from the negative control spots was subtracted from each target spot signal value. Corresponding signals from control and R+D-treated arrays were graphed in GraphPad Prism for comparison. AU (arbitrary unit): absolute pixel density values, displayed values are means.

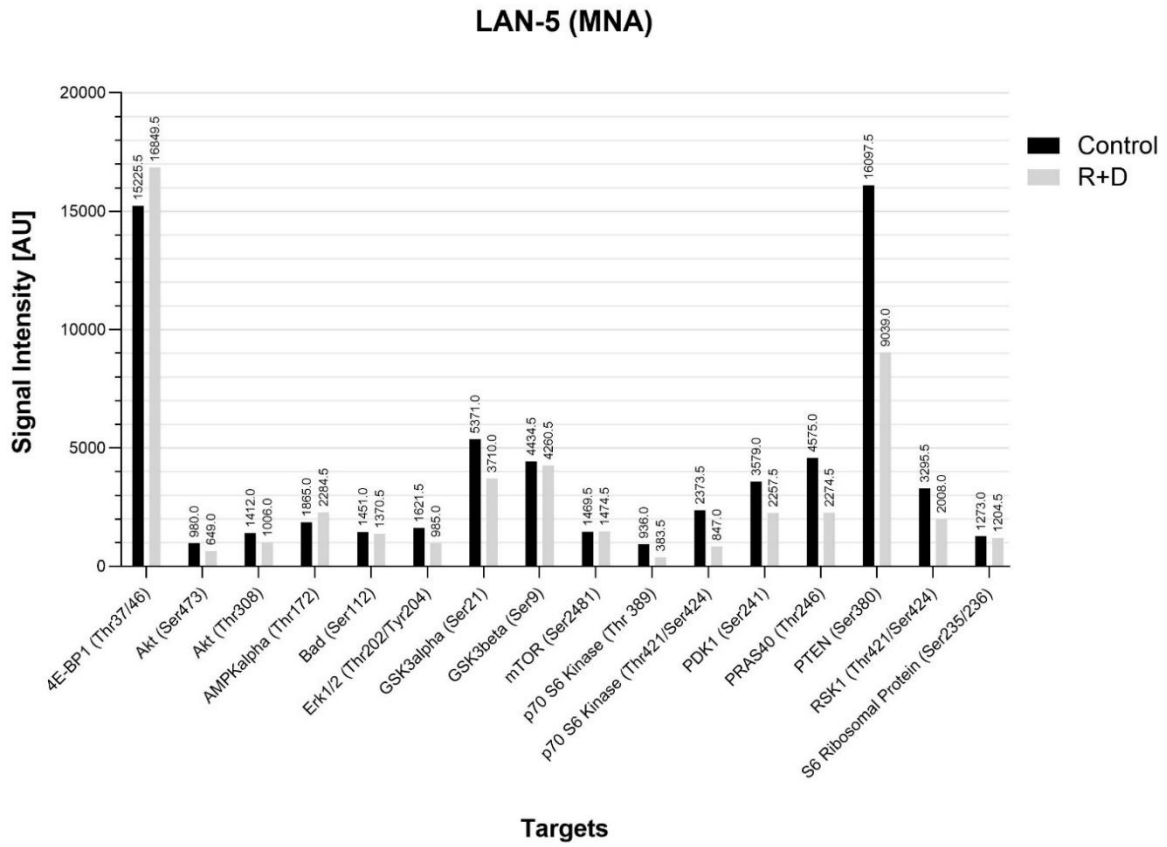


**Figure 55: PathScan® AKT Signaling Array by Cell Signaling Technology of the MycN-Amplified Neuroblastoma Cell Line LAN-5**

Relative phosphorylation levels of 16 phosphorylation sites of targets predominantly belonging to the AKT signaling network were analyzed utilizing the PathScan® AKT Signaling Array (Chemiluminescent Readout) (#9474) by Cell Signaling Technology. Data represents one array with duplicate target spots for control (DMSO vehicle)-treated cells and cells after 72 hours of treatment of rapamycin plus dasatinib (R+D) of the MycN-amplified (MNA) neuroblastoma (NB) cell line LAN-5. Data represents the results of the array displayed in *Figure 50B, Array 2*.
Target-specific capture antibodies have been spotted in duplicate onto nitrocellulose-coated glass slides and cell lysates of control (DMSO vehicle)-treated and rapamycin plus dasatinib (R+D)-treated cells were incubated, followed by a biotinylated detection antibody cocktail. Chemiluminescent detection reagents were used to visualize the results. Images were captured with the ImageQuant LAS 4000 Mini. Target spot intensities were visualized using the array signaling analysis software ImageStudio Lite by Licor, and statistical and graphical analysis was done in Microsoft Excel and GraphPad Prism. Signal values were exported into an Excel spreadsheet file. An average background signal derived from the negative control spots was subtracted from each target spot signal value. Corresponding signals from control and R+D-treated arrays were graphed in GraphPad Prism for comparison. AU (arbitrary unit): absolute pixel density values, displayed values are means.

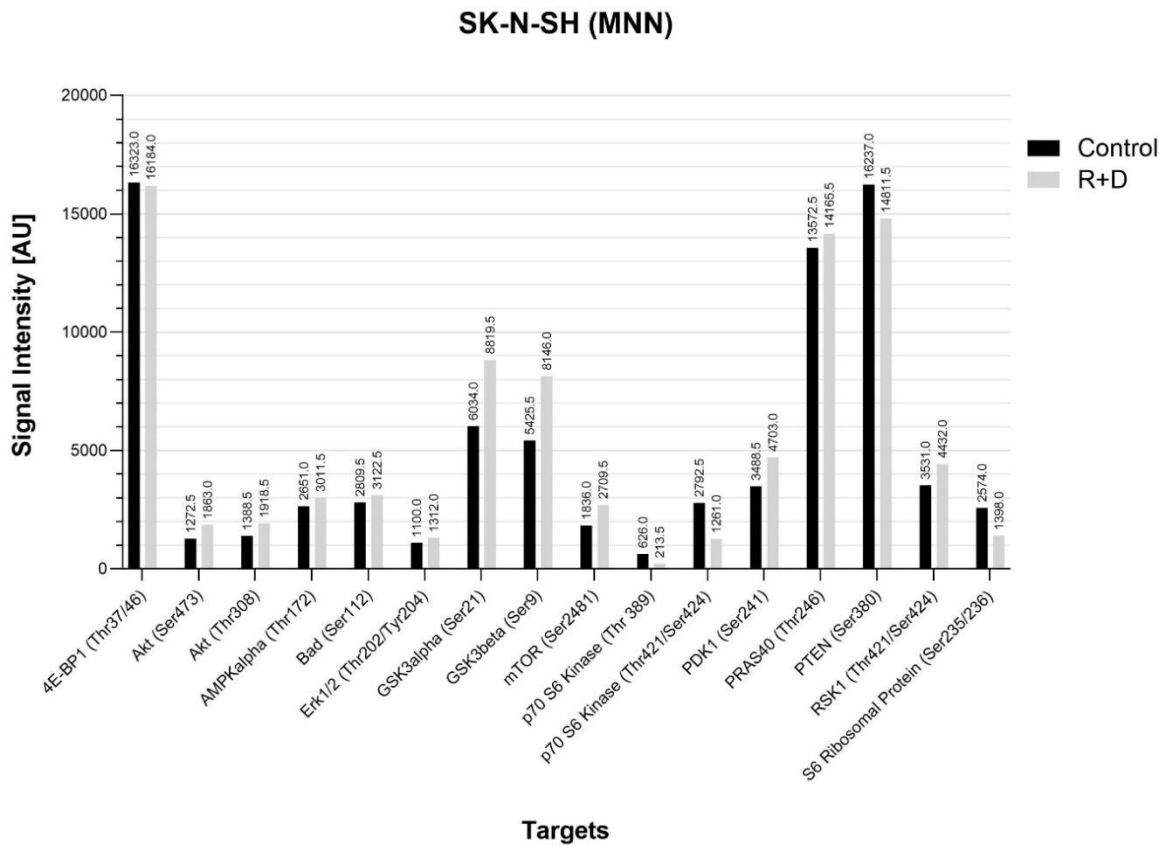


**Figure 56: PathScan® AKT Signaling Array by Cell Signaling Technology of the MycN-non-Amplified Neuroblastoma Cell Line SK-N-SH**

Relative phosphorylation levels of 16 phosphorylation sites of targets predominantly belonging to the AKT signaling network were analyzed utilizing the PathScan® AKT Signaling Array (Chemiluminescent Readout) (#9474) by Cell Signaling Technology. Data represents one array with duplicate target spots for control (DMSO vehicle)-treated cells and cells after 72 hours of treatment of rapamycin plus dasatinib (R+D) of the MycN-non-amplified (MNN) neuroblastoma (NB) cell line SK-N-SH. Data represents the results of the array displayed in *Figure 51A*.
Target-specific capture antibodies have been spotted in duplicate onto nitrocellulose-coated glass slides and cell lysates of control (DMSO vehicle)-treated and rapamycin plus dasatinib (R+D)-treated cells were incubated, followed by a biotinylated detection antibody cocktail. Chemiluminescent detection reagents were used to visualize the results. Images were captured with the ImageQuant LAS 4000 Mini. Target spot intensities were visualized using the array signaling analysis software ImageStudio Lite by Licor, and statistical and graphical analysis was done in Microsoft Excel and GraphPad Prism. Signal values were exported into an Excel spreadsheet file. An average background signal derived from the negative control spots was subtracted from each target spot signal value. Corresponding signals from control and R+D-treated arrays were graphed in GraphPad Prism for comparison. AU (arbitrary unit): absolute pixel density values, displayed values are means.

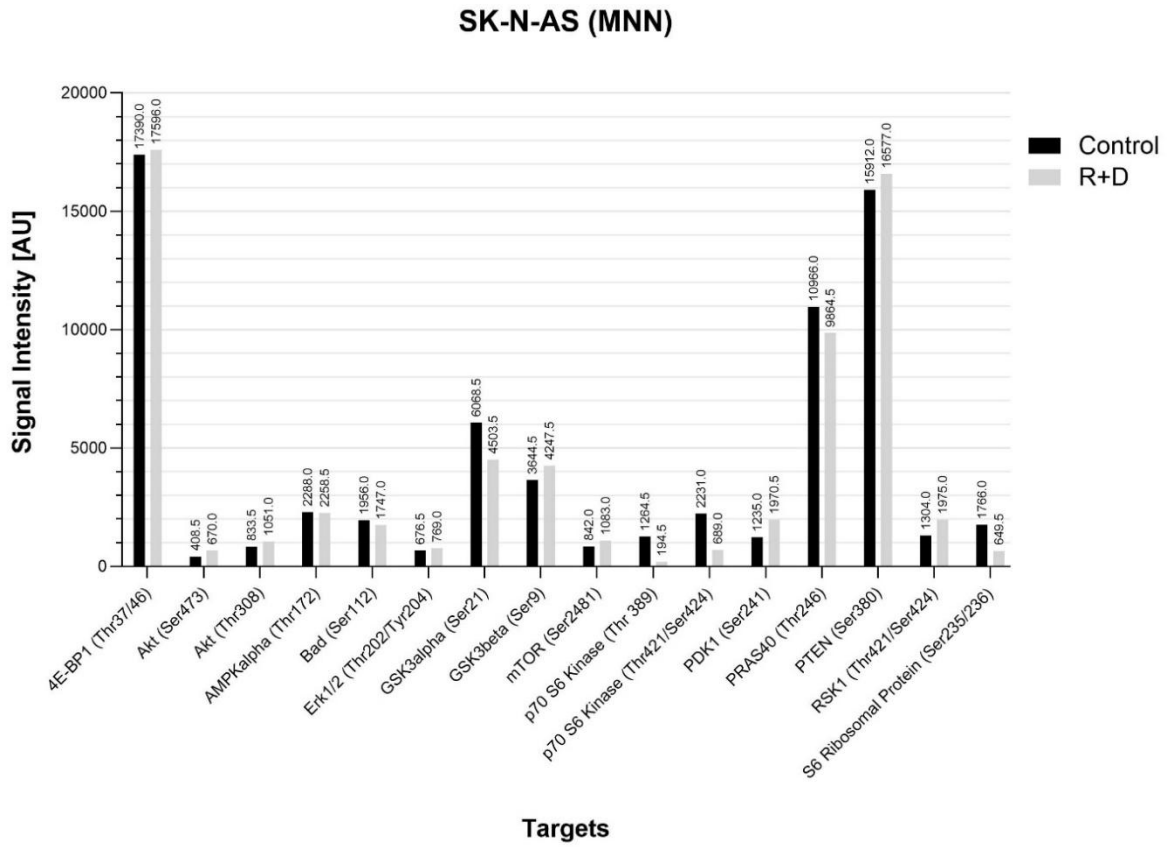


**Figure 57: PathScan® AKT Signaling Array by Cell Signaling Technology of the MycN-non-Amplified Neuroblastoma Cell Line SK-N-AS**

Relative phosphorylation levels of 16 phosphorylation sites of targets predominantly belonging to the AKT signaling network were analyzed utilizing the PathScan® AKT Signaling Array (Chemiluminescent Readout) (#9474) by Cell Signaling Technology. Data represents one array with duplicate target spots for control (DMSO vehicle)-treated cells and cells after 72 hours of treatment of rapamycin plus dasatinib (R+D) of the MycN-non-amplified (MNN) neuroblastoma (NB) cell line SK-N-AS. Data represents the results of the array displayed in *Figure 51B*.
Target-specific capture antibodies have been spotted in duplicate onto nitrocellulose-coated glass slides and cell lysates of control (DMSO vehicle)-treated and rapamycin plus dasatinib (R+D)-treated cells were incubated, followed by a biotinylated detection antibody cocktail. Chemiluminescent detection reagents were used to visualize the results. Images were captured with the ImageQuant LAS 4000 Mini. Target spot intensities were visualized using the array signaling analysis software ImageStudio Lite by Licor, and statistical and graphical analysis was done in Microsoft Excel and GraphPad Prism. Signal values were exported into an Excel spreadsheet file. An average background signal derived from the negative control spots was subtracted from each target spot signal value. Corresponding signals from control and R+D-treated arrays were graphed in GraphPad Prism for comparison. AU (arbitrary unit): absolute pixel density values, displayed values are means.

### 5.1.3. PathScan® RTK Signaling Antibody Array Kit

**Receptor Tyrosine Kinases**

| | Target | Phosphorylation Site | Family |
|---|---|---|---|
| 1 | EGFR/ErbB1 | pan-Tyr | EGFR |
| 2 | HER2/ErbB2 | pan-Tyr | EGFR |
| 3 | HER3/ErbB3 | pan-Tyr | EGFR |
| 4 | FGFR1 | pan-Tyr | FGFR |
| 5 | FGFR3 | pan-Tyr | FGFR |
| 6 | FGFR4 | pan-Tyr | FGFR |
| 7 | InsR | pan-Tyr | Insulin R |
| 8 | IGF-IR | pan-Tyr | Insulin R |
| 9 | TrkA/NTRK1 | pan-Tyr | NGFR |
| 10 | TrkB/NTRK2 | pan-Tyr | NGFR |
| 11 | Met/HGFR | pan-Tyr | HGFR |
| 12 | Ron/MST1R | pan-Tyr | HGFR |
| 13 | Ret | pan-Tyr | Ret |
| 14 | ALK | pan-Tyr | LTK |
| 15 | PDGFR | pan-Tyr | PDGFR |
| 16 | c-Kit/SCFR | pan-Tyr | PDGFR |
| 17 | FLT3/Flk2 | pan-Tyr | PDGFR |
| 18 | M-CSFR/CSF-1R | pan-Tyr | PDGFR |
| 19 | EphA1 | pan-Tyr | EphR |
| 20 | EphA2 | pan-Tyr | EphR |
| 21 | EphA3 | pan-Tyr | EphR |
| 22 | EphB1 | pan-Tyr | EphR |
| 23 | EphB3 | pan-Tyr | EphR |
| 24 | EphB4 | pan-Tyr | EphR |
| 25 | Tyro3/Dtk | pan-Tyr | Axl |
| 26 | Axl | pan-Tyr | Axl |
| 27 | Tie2/TEK | pan-Tyr | Tie |
| 28 | VEGFR2/KDR | pan-Tyr | VEGFR |

**Signaling Nodes**

| | Target | Phosphorylation Site | Family |
|---|---|---|---|
| 29 | Akt/PKB/Rac | Thr308 | Akt |
| 30 | Akt/PKB/Rac | Ser473 | Akt |
| 31 | p44/42 MAPK (ERK1/2) | Thr202/Tyr204 | MAPK |
| 32 | S6 Ribosomal Protein | Ser235/236 | RSK |
| 33 | c-Abl | pan-Tyr | Abl |
| 34 | IRS-1 | pan-Tyr | IRS |
| 35 | Zap-70 | pan-Tyr | Zap-70 |
| 36 | Src | pan-Tyr | Src |
| 37 | Lck | pan-Tyr | Src |
| 38 | Stat1 | Tyr701 | Stat |
| 39 | Stat3 | Tyr705 | Stat |

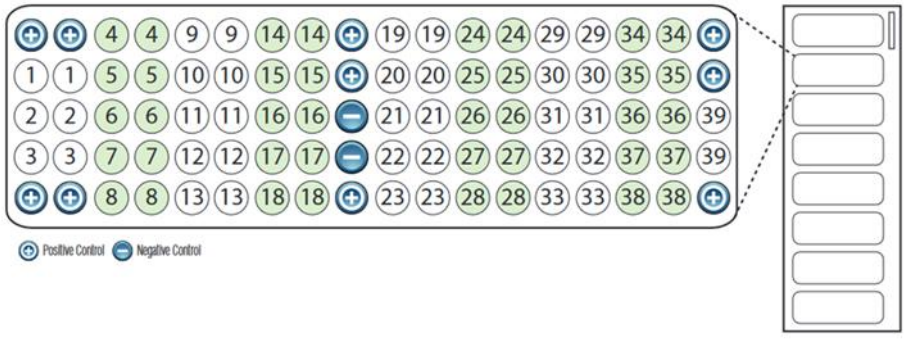


**Figure 58: Target Map of the PathScan® RTK Signaling Antibody Array Kit (Chemiluminescent Readout) by Cell Signaling Technology**

Target map of the PathScan® RTK Signaling Antibody Array Kit (Chemiluminescent Readout) as outlined in the provided protocol for the PathScan® RTK Signaling Antibody Array Kit (Chemiluminescent Readout) by Cell Signaling Technology (#7982).

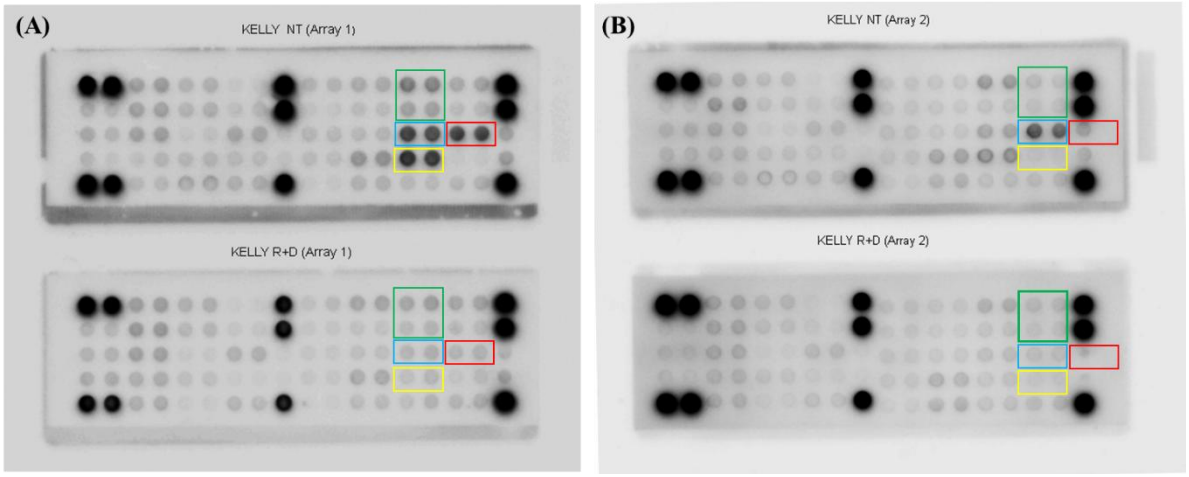


**Figure 59: PathScan® RTK Signaling Arrays by Cell Signaling Technology for the MycN-Amplified Neuroblastoma Cell Line KELLY**

Relative phosphorylation levels of 39 receptor tyrosine kinases (RTKs) and signaling node phosphorylation sites were analyzed utilizing the PathScan® RTK Signaling Array (Chemiluminescent Readout) (#7982) by Cell Signaling Technology. Relative phosphorylation levels of control (DMSO vehicle)-treated cells (NT) and cells after 72 hours of treatment with the molecularly targeted combinatorial treatment rapamycin plus dasatinib (R+D) of the MycN-amplified (MNA) neuroblastoma (NB) cell line KELLY were analyzed. Data represents two independent arrays (**A** and **B**) with duplicate target spots for control (DMSO vehicle)-treated cells (NT) and cells after 72 hours of treatment with R+D.
Target-specific capture antibodies have been spotted in duplicate onto nitrocellulose-coated glass slides and cell lysates of control (DMSO vehicle)-treated (NT) and R+D-treated cells were incubated, followed by a biotinylated detection antibody cocktail. Streptavidin-conjugated reagents were used to visualize the bound detection antibody by chemiluminescence. Images were captured with the ImageQuant LAS 4000 Mini.
Targets used for further analysis: AKT Ser473/Thr308, ERK1/2 Thr202/Tyr204, Src (pan-Tyr), rpS6 Ser 235/236.

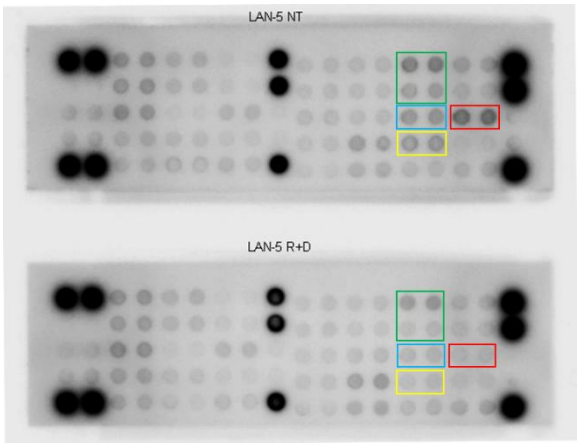


**Figure 60: PathScan® RTK Signaling Arrays by Cell Signaling Technology for the MycN-Amplified Neuroblastoma Cell Line LAN-5**

Relative phosphorylation levels of 39 receptor tyrosine kinases (RTKs) and signaling node phosphorylation sites were analyzed utilizing the PathScan® RTK Signaling Array (Chemiluminescent Readout) (#7982) by Cell Signaling Technology. Relative phosphorylation levels of control (DMSO vehicle)-treated cells (NT) and cells after 72 hours of treatment with the molecularly targeted combinatorial treatment rapamycin plus dasatinib (R+D) of the MycN-amplified (MNA) neuroblastoma (NB) cell line LAN-5 were analyzed. Data represents one array with duplicate target spots for control (DMSO vehicle)-treated cells (NT) and cells after 72 hours of treatment with R+D.
Target-specific capture antibodies have been spotted in duplicate onto nitrocellulose-coated glass slides and cell lysates of control (DMSO vehicle)-treated (NT) and R+D-treated cells were incubated, followed by a biotinylated detection antibody cocktail. Streptavidin-conjugated reagents were used to visualize the bound detection antibody by chemiluminescence. Images were captured with the ImageQuant LAS 4000 Mini.
Targets used for further analysis: AKT Ser473/Thr308, ERK1/2 Thr202/Tyr204, Src (pan-Tyr), rpS6 Ser 235/236.

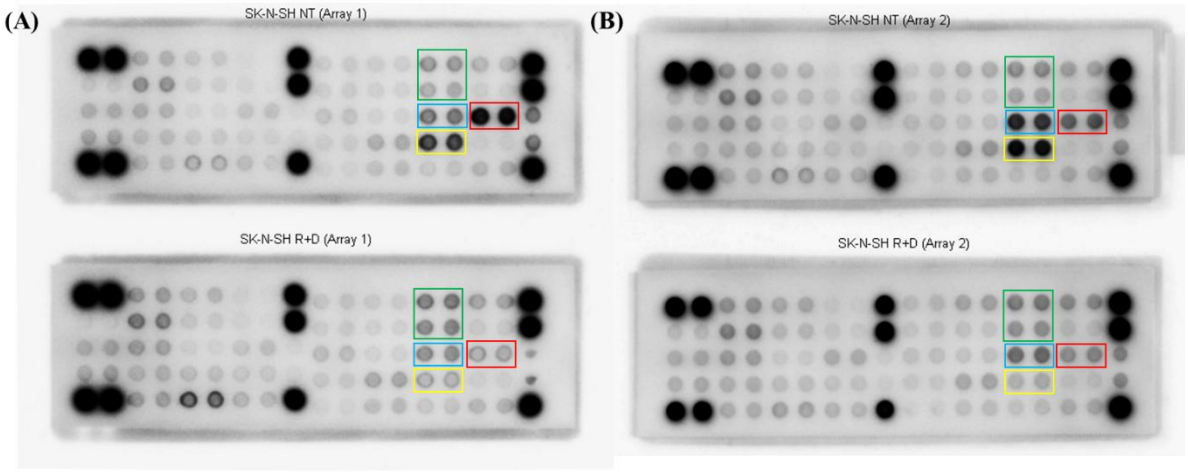


**Figure 61: PathScan® RTK Signaling Arrays by Cell Signaling Technology for the MycN- non-Amplified Neuroblastoma Cell Line SK-N-SH**

Relative phosphorylation levels of 39 receptor tyrosine kinases (RTKs) and signaling node phosphorylation sites were analyzed utilizing the PathScan® RTK Signaling Array (Chemiluminescent Readout) (#7982) by Cell Signaling Technology. Relative phosphorylation levels of control (DMSO vehicle)-treated cells (NT) and cells after 72 hours of treatment with the molecularly targeted combinatorial treatment rapamycin plus dasatinib (R+D) of the MycN-non-amplified (MNN) neuroblastoma (NB) cell line SK-N-SH were analyzed. Data represents two independent arrays (**A** and **B**) with duplicate target spots for control (DMSO vehicle)-treated cells (NT) and cells after 72 hours of treatment with R+D.
Target-specific capture antibodies have been spotted in duplicate onto nitrocellulose-coated glass slides and cell lysates of control (DMSO vehicle)-treated (NT) and R+D-treated cells were incubated, followed by a biotinylated detection antibody cocktail. Streptavidin-conjugated reagents were used to visualize the bound detection antibody by chemiluminescence. Images were captured with the ImageQuant LAS 4000 Mini.
Targets used for further analysis: AKT Ser473/Thr308, ERK1/2 Thr202/Tyr204, Src (pan-Tyr), rpS6 Ser 235/236.

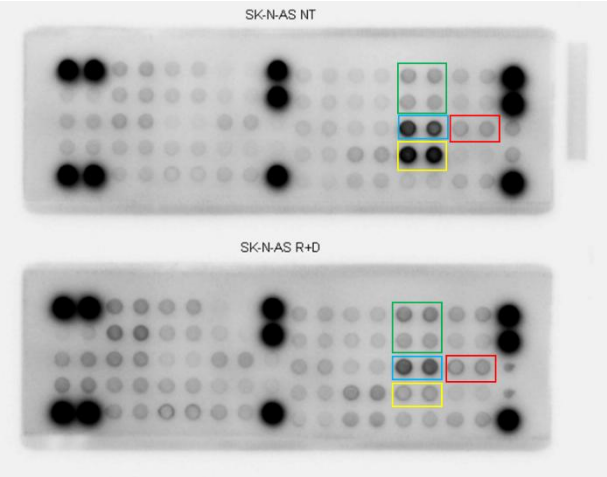


**Figure 62: PathScan® RTK Signaling Arrays by Cell Signaling Technology for the MycN- non-Amplified Neuroblastoma Cell Line SK-N-AS**

Relative phosphorylation levels of 39 receptor tyrosine kinases (RTKs) and signaling node phosphorylation sites were analyzed utilizing the PathScan® RTK Signaling Array (Chemiluminescent Readout) (#7982) by Cell Signaling Technology. Relative phosphorylation levels of control (DMSO vehicle)-treated cells (NT) and cells after 72 hours of treatment with the molecularly targeted combinatorial treatment rapamycin plus dasatinib (R+D) of the MycN-non-amplified (MNN) neuroblastoma (NB) cell line SK-N-AS were analyzed. Data represents one array with duplicate target spots for control (DMSO vehicle)-treated cells (NT) and cells after 72 hours of treatment with R.D.
Target-specific capture antibodies have been spotted in duplicate onto nitrocellulose-coated glass slides and cell lysates of control (DMSO vehicle)-treated (NT) and R+D-treated cells were incubated, followed by a biotinylated detection antibody cocktail. Streptavidin-conjugated reagents were used to visualize the bound detection antibody by chemiluminescence. Images were captured with the ImageQuant LAS 4000 Mini.
Targets used for further analysis: AKT Ser473/Thr308, ERK1/2 Thr202/Tyr204, Src (pan-Tyr), rpS6 Ser 235/236.

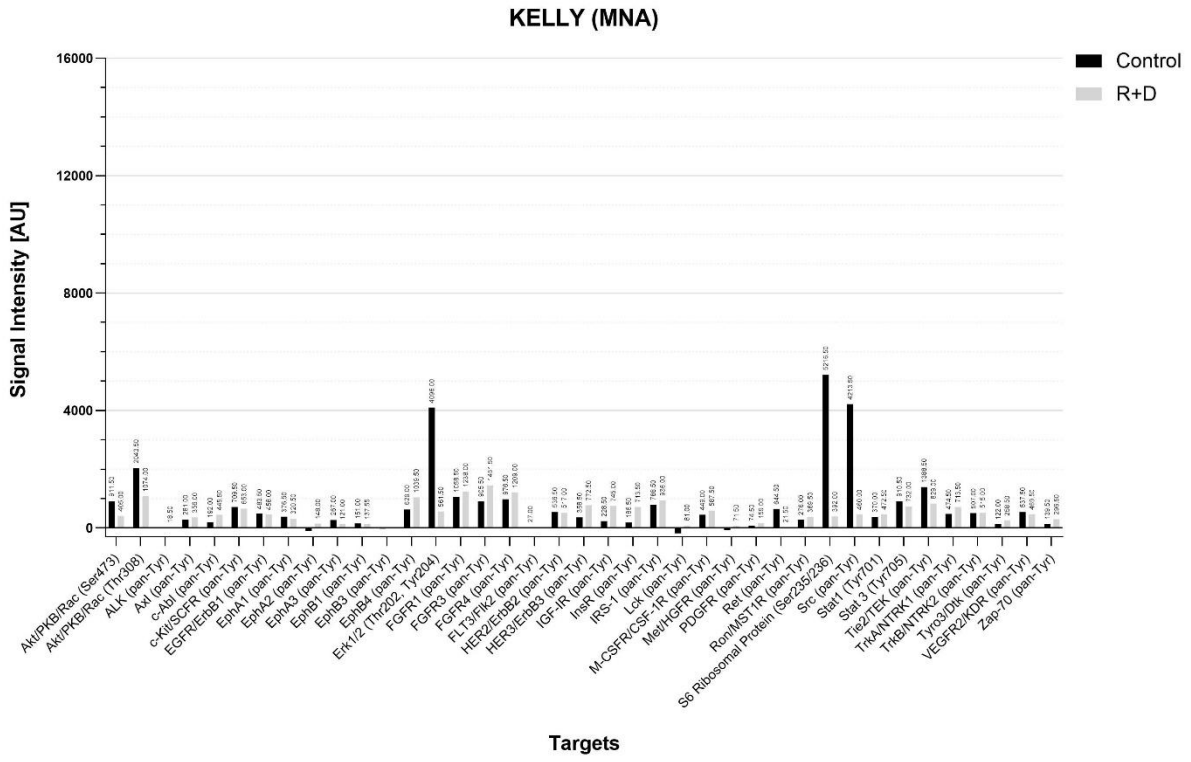


**Figure 63: PathScan® RTK Signaling Arrays of the MycN-Amplified Neuroblastoma Cell Line KELLY**

Relative phosphorylation levels of 39 receptor tyrosine kinases (RTKs) and signaling node phosphorylation sites were analyzed utilizing the PathScan® RTK Signaling Array (Chemiluminescent Readout) (#7982) by Cell Signaling Technology. Data represents one array with duplicate target spots of control (DMSO vehicle)-treated cells and cells after 72 hours of treatment of rapamycin plus dasatinib (R+D) of the MycN-amplified (MNA) neuroblastoma (NB) cell line KELLY. Data represents the results of the array displayed in *Figure 59A*.
Target-specific capture antibodies have been spotted in duplicate onto nitrocellulose-coated glass slides and cell lysates of control (DMSO vehicle)-treated and R+D-treated cells were incubated, followed by a biotinylated detection antibody cocktail. Chemiluminescent detection reagents were used to visualize the results. Images were captured with the ImageQuant LAS 4000 Mini. Target spot intensities were visualized using the array signaling analysis software ImageStudio Lite by Licor,and statistical and graphical analysis was done in Microsoft Excel and GraphPad Prism. Signal values were exported into an Excel spreadsheet file. An average background signal derived from the negative control spots was subtracted from each target spot signal value. Corresponding signals from control and R+D-treated arrays were graphed in GraphPad Prism for comparison. AU (arbitrary unit): absolute pixel density values, displayed values are means.

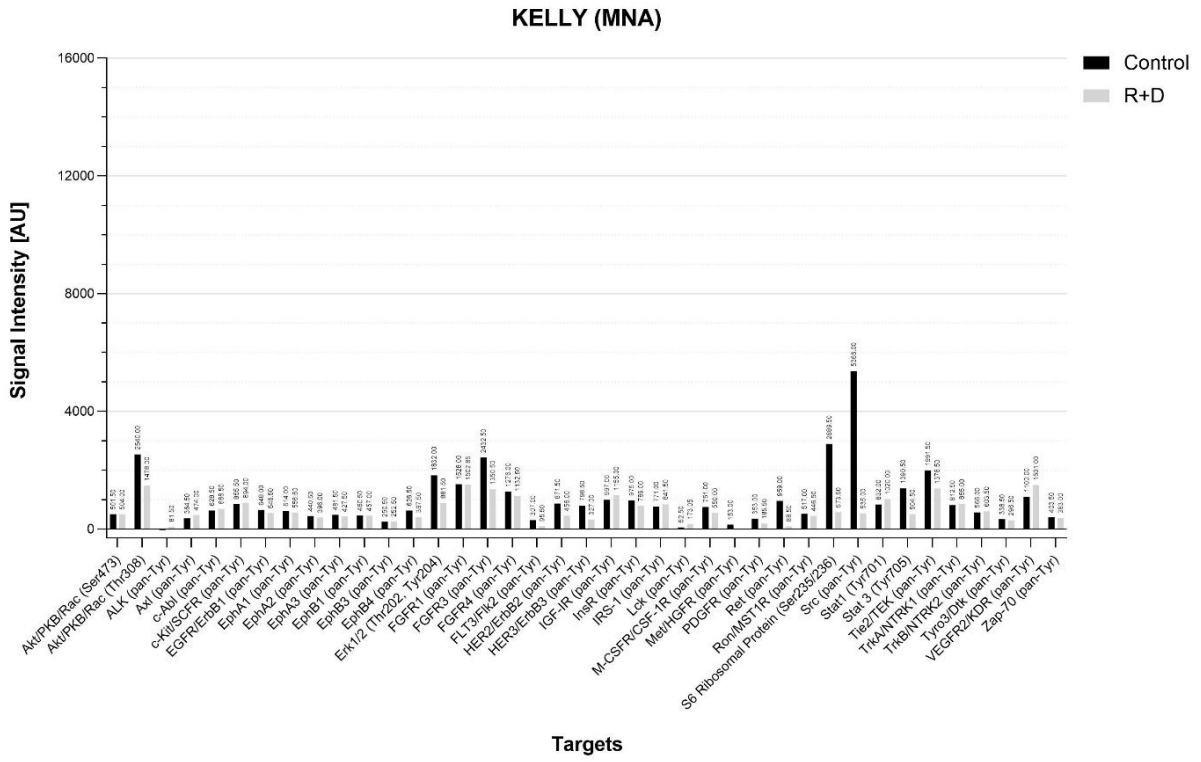


**Figure 64: PathScan® RTK Signaling Arrays of the MycN-Amplified Neuroblastoma Cell Line KELLY**

Relative phosphorylation levels of 39 receptor tyrosine kinases (RTKs) and signaling node phosphorylation sites were analyzed utilizing the PathScan® RTK Signaling Array (Chemiluminescent Readout) (#7982) by Cell Signaling Technology. Data represents one array with duplicate target spots of control (DMSO vehicle)-treated cells and cells after 72 hours of treatment of rapamycin plus dasatinib (R+D) of the MycN-amplified (MNA) neuroblastoma (NB) cell line KELLY. Data represents the results of the array displayed in *Figure 59B*.
Target-specific capture antibodies have been spotted in duplicate onto nitrocellulose-coated glass slides and cell lysates of control (DMSO vehicle)-treated and R+D-treated cells were incubated, followed by a biotinylated detection antibody cocktail. Chemiluminescent detection reagents were used to visualize the results. Images were captured with the ImageQuant LAS 4000 Mini. Target spot intensities were visualized using the array signaling analysis software ImageStudio Lite by Licor, and statistical and graphical analysis was done in Microsoft Excel and GraphPad Prism. Signal values were exported into an Excel spreadsheet file. An average background signal derived from the negative control spots was subtracted from each target spot signal value. Corresponding signals from control and R+D-treated arrays were graphed in GraphPad Prism for comparison. AU (arbitrary unit): absolute pixel density values, displayed values are means.

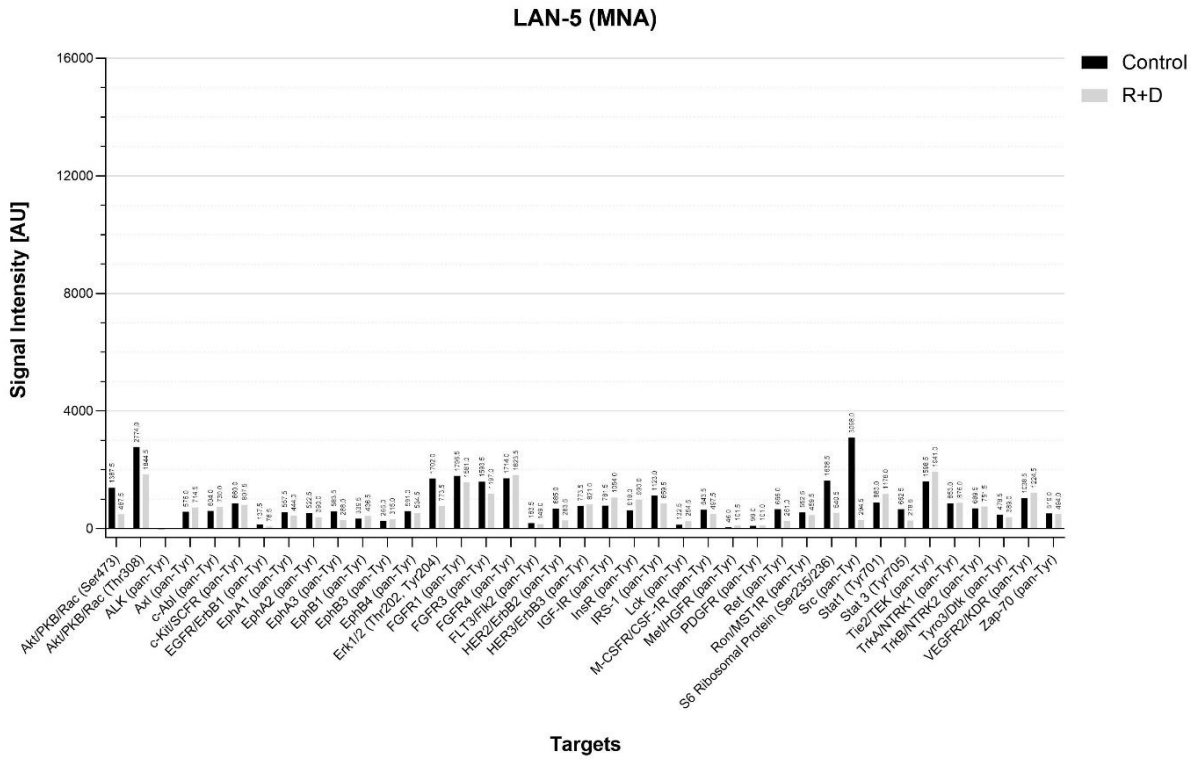


**Figure 65: PathScan® RTK Signaling Arrays of the MycN-Amplified Neuroblastoma Cell Line LAN-5**

Relative phosphorylation levels of 39 receptor tyrosine kinases (RTKs) and signaling node phosphorylation sites were analyzed utilizing the PathScan® RTK Signaling Array (Chemiluminescent Readout) (#7982) by Cell Signaling Technology. Data represents one array with duplicate target spots of control (DMSO vehicle)-treated cells and cells after 72 hours of treatment of rapamycin plus dasatinib (R+D) of the MycN-amplified (MNA) neuroblastoma (NB) cell line LAN-5. Data represents the results of the array displayed in *Figure 60*.
Target-specific capture antibodies have been spotted in duplicate onto nitrocellulose-coated glass slides and cell lysates of control (DMSO vehicle)-treated and R+D-treated cells were incubated, followed by a biotinylated detection antibody cocktail. Chemiluminescent detection reagents were used to visualize the results. Images were captured with the ImageQuant LAS 4000 Mini. Target spot intensities were visualized using the array signaling analysis software ImageStudio Lite by Licor, and statistical and graphical analysis was done in Microsoft Excel and GraphPad Prism. Signal values were exported into an Excel spreadsheet file. An average background signal derived from the negative control spots was subtracted from each target spot signal value. Corresponding signals from control and R+D-treated arrays were graphed in GraphPad Prism for comparison. AU (arbitrary unit): absolute pixel density values, displayed values are means.

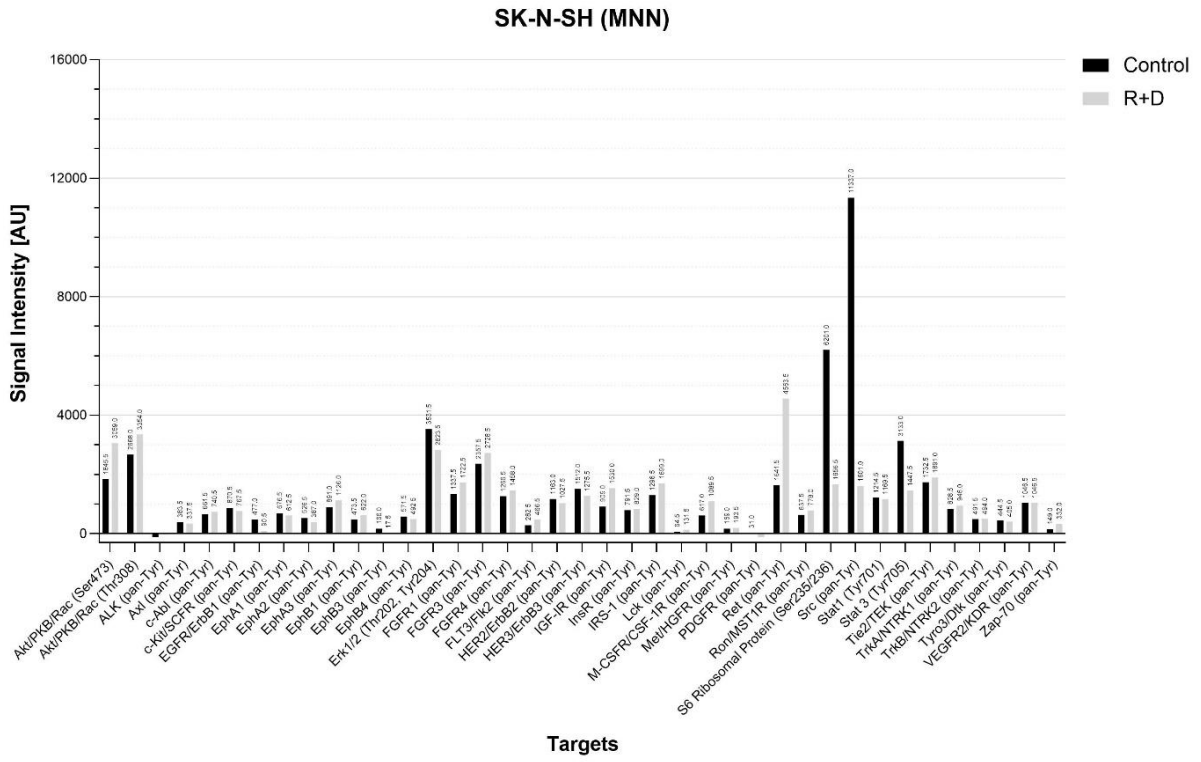


**Figure 66: PathScan® RTK Signaling Arrays of the MycN-non-Amplified Neuroblastoma Cell Line SK-N-SH**

Relative phosphorylation levels of 39 receptor tyrosine kinases (RTKs) and signaling node phosphorylation sites were analyzed utilizing the PathScan® RTK Signaling Array (Chemiluminescent Readout) (#7982) by Cell Signaling Technology. Data represents one array with duplicate target spots of control (DMSO vehicle)-treated cells and cells after 72 hours of treatment of rapamycin plus dasatinib (R+D) of the MycN-non-amplified (MNN) neuroblastoma (NB) cell line SK-N-SH. Data represents the results of the array displayed in *Figure 61A*.
Target-specific capture antibodies have been spotted in duplicate onto nitrocellulose-coated glass slides and cell lysates of control (DMSO vehicle)-treated and R+D-treated cells were incubated, followed by a biotinylated detection antibody cocktail. Chemiluminescent detection reagents were used to visualize the results. Images were captured with the ImageQuant LAS 4000 Mini. Target spot intensities were visualized using the array signaling analysis software ImageStudio Lite by Licor, and statistical and graphical analysis was done in Microsoft Excel and GraphPad Prism. Signal values were exported into an Excel spreadsheet file. An average background signal derived from the negative control spots was subtracted from each target spot signal value. Corresponding signals from control and R+D-treated arrays were graphed in GraphPad Prism for comparison. AU (arbitrary unit): absolute pixel density values, displayed values are means.

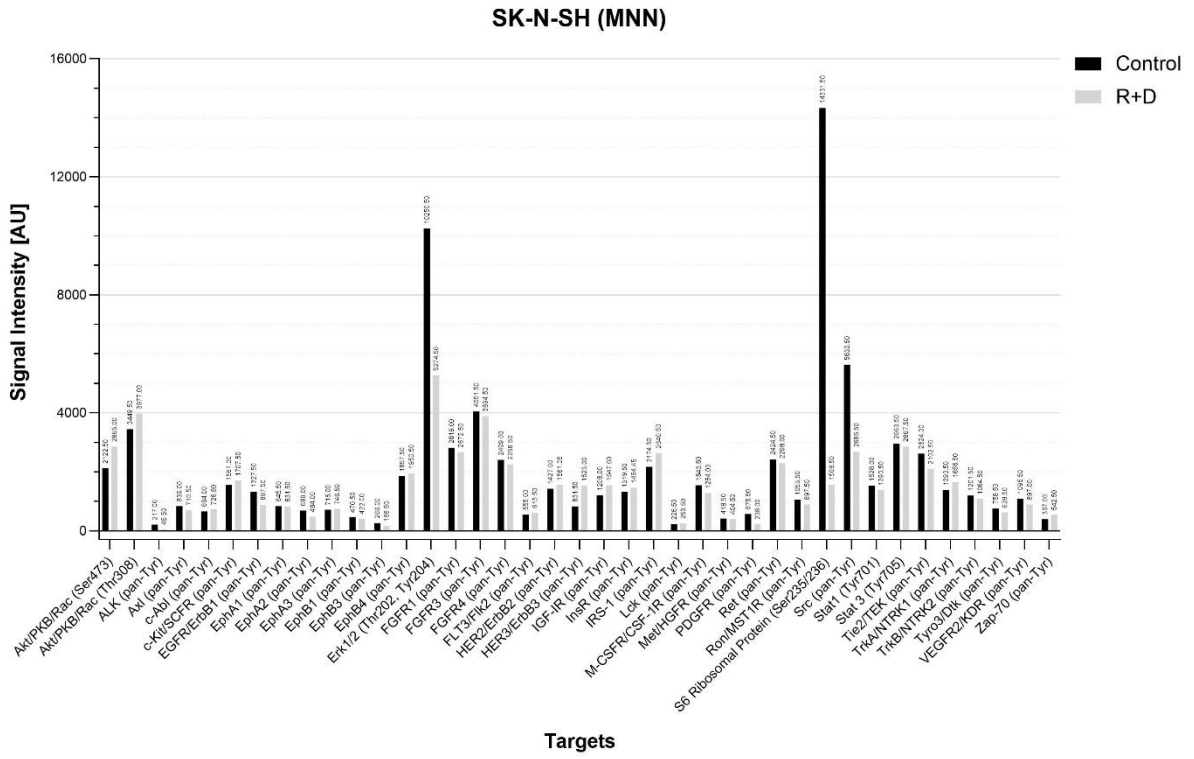


**Figure 67: PathScan® RTK Signaling Arrays of the MycN-non-Amplified Neuroblastoma Cell Line SK-N-SH**

Relative phosphorylation levels of 39 receptor tyrosine kinases (RTKs) and signaling node phosphorylation sites were analyzed utilizing the PathScan® RTK Signaling Array (Chemiluminescent Readout) (#7982) by Cell Signaling Technology. Data represents one array with duplicate target spots of control (DMSO vehicle)-treated cells and cells after 72 hours of treatment of rapamycin plus dasatinib (R+D) of the MycN-non-amplified (MNN) neuroblastoma (NB) cell line SK-N-SH. Data represents the results of the array displayed in *Figure 61B*.
Target-specific capture antibodies have been spotted in duplicate onto nitrocellulose-coated glass slides and cell lysates of control (DMSO vehicle)-treated and R+D-treated cells were incubated, followed by a biotinylated detection antibody cocktail. Chemiluminescent detection reagents were used to visualize the results. Images were captured with the ImageQuant LAS 4000 Mini. Target spot intensities were visualized using the array signaling analysis software ImageStudio Lite by Licor, and statistical and graphical analysis was done in Microsoft Excel and GraphPad Prism. Signal values were exported into an Excel spreadsheet file. An average background signal derived from the negative control spots was subtracted from each target spot signal value. Corresponding signals from control and R+D-treated arrays were graphed in GraphPad Prism for comparison. AU (arbitrary unit): absolute pixel density values, displayed values are means.

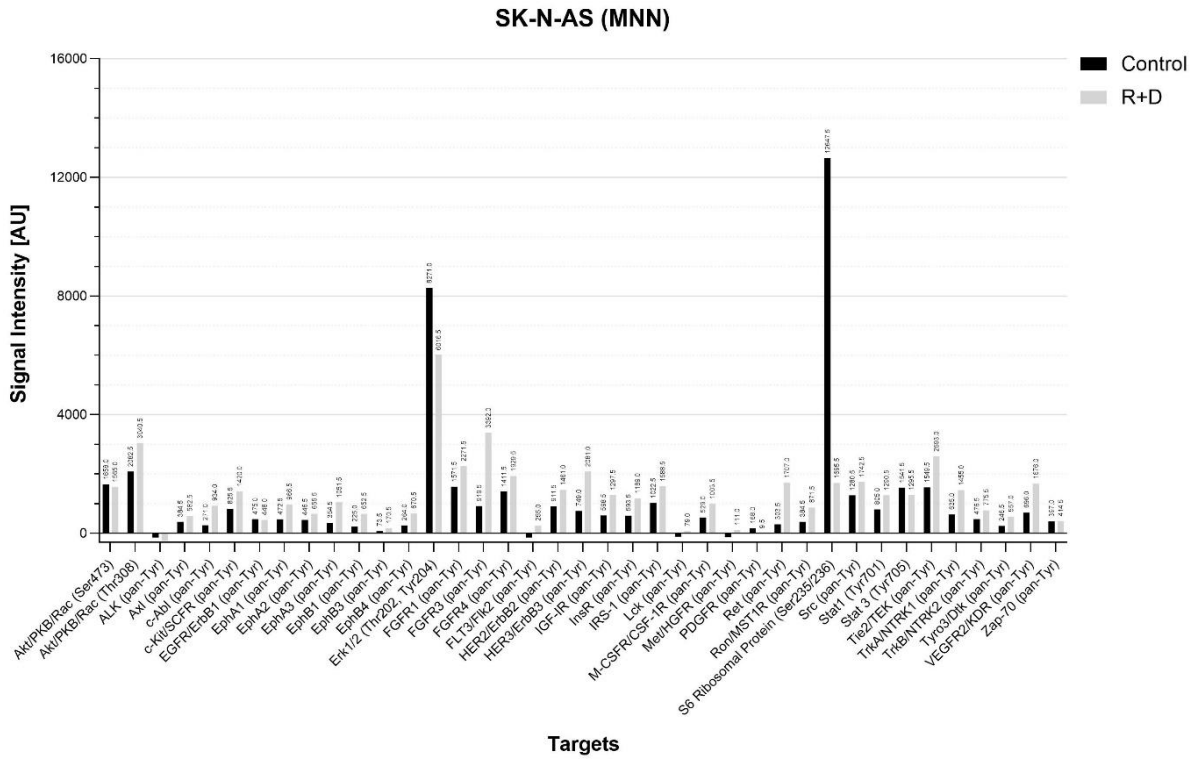


**Figure 68: PathScan® RTK Signaling Arrays of the MycN-non-Amplified Neuroblastoma Cell Line SK-N-AS**

Relative phosphorylation levels of 39 receptor tyrosine kinases (RTKs) and signaling node phosphorylation sites were analyzed utilizing the PathScan® RTK Signaling Array (Chemiluminescent Readout) (#7982) by Cell Signaling Technology. Data represents one array with duplicate target spots of control (DMSO vehicle)-treated cells and cells after 72 hours of treatment of rapamycin plus dasatinib (R+D) of the MycN-non-amplified (MNN) neuroblastoma (NB) cell line SK-N-AS. Data represents the results of the array displayed in *Figure 62*.
Target-specific capture antibodies have been spotted in duplicate onto nitrocellulose-coated glass slides and cell lysates of control (DMSO vehicle)-treated and R+D-treated cells were incubated, followed by a biotinylated detection antibody cocktail. Chemiluminescent detection reagents were used to visualize the results. Images were captured with the ImageQuant LAS 4000 Mini. Target spot intensities were visualized using the array signaling analysis software ImageStudio Lite by Licor, and statistical and graphical analysis was done in Microsoft Excel and GraphPad Prism. Signal values were exported into an Excel spreadsheet file. An average background signal derived from the negative control spots was subtracted from each target spot signal value. Corresponding signals from control and R+D-treated arrays were graphed in GraphPad Prism for comparison. AU (arbitrary unit): absolute pixel density values, displayed values are means.

### 5.1.4. PRAS40

Change in phosphorylation of PRAS40 at Thr246 after the treatment with R+D was analyzed for the MNA cell lines KELLY and LAN-5, and the MNN cell lines SK-N-SH and SK-N-AS utilizing the PathScan® ATK Signaling Array and utilizing the Proteome Profiler™ Human Phospho-Kinase Array for KELLY (MNA) and SK-NAS (MNN). The following figures show additional arrays not displayed in the main results section and show the phosphorylation status as absolute pixel density values (AU) after 72 hours of treatment with R+D compared to control (DMSO vehicle)-treated cells.

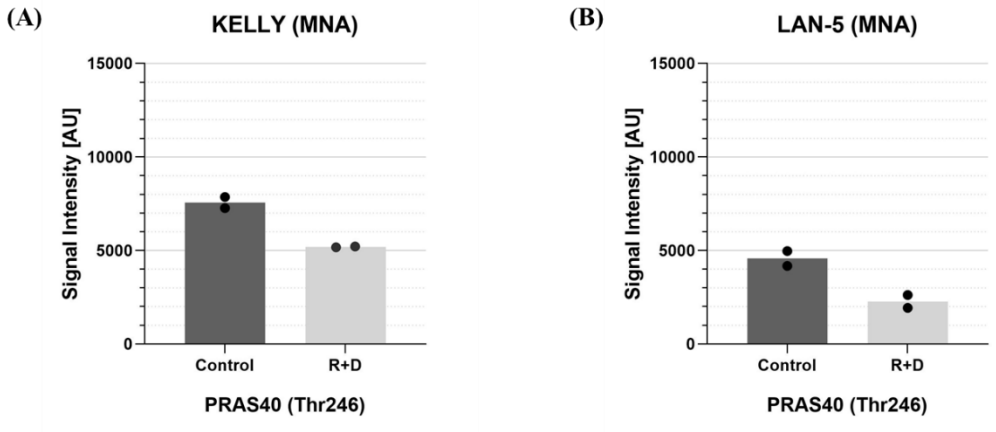


**Figure 69: Phosphorylation Status of Proline-Rich AKT Substrate of 40 kDa in Control- and Rapamycin Plus Dasatinib-Treated Neuroblastoma Cell Lines**

Phosphorylation status of proline-rich AKT substrate of 40 kDa (PRAS40) at threonine 246 (Thr246) after 72 hours of treatment with rapamycin plus dasatinib (R+D) compared to control (DMSO vehicle)-treated cells of the MycN-amplified (MNA) neuroblastoma (NB) cell lines KELLY **(A)** and LAN-5 **(B)** were analyzed utilizing the PathScan® AKT Signaling Array by Cell Signaling Technology. Data represents one array with duplicate target spots for each cell line. DMSO: dimethyl sulfoxide. AU (arbitrary unit): absolute pixel density values. Displayed bars are means.

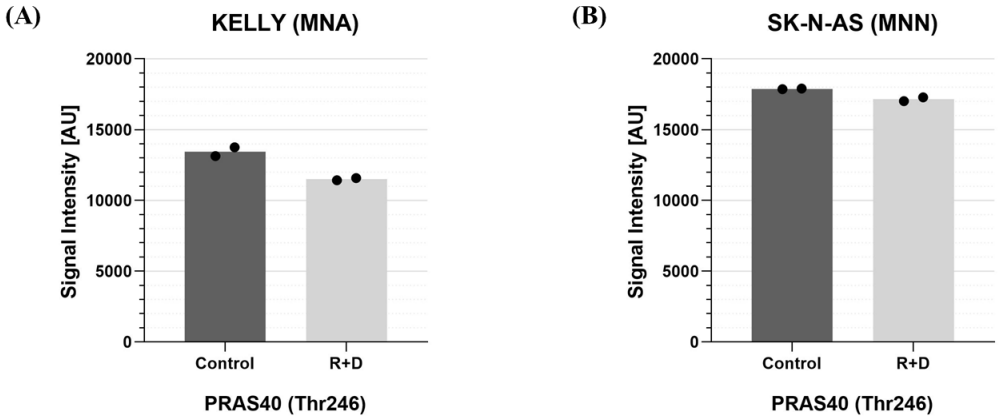


**Figure 70: Phosphorylation Status of Proline-Rich AKT Substrate of 40 kDA in Control- and Rapamycin Plus Dasatinib-Treated Neuroblastoma Cell Lines**

Phosphorylation status of proline-rich AKT substrate of 40 kDa (PRAS40) at threonine 246 (Thr246) after 72 hours of treatment with rapamycin plus dasatinib (R+D) compared to control (DMSO vehicle)-treated cells of the MycN-amplified (MNA) neuroblastoma (NB) cell line KELLY **(A)** and the MycN-non-amplified (MNN) NB cell line SK-N-AS **(B)** were analyzed utilizing the Proteome Profiler™ Human Phospho-Kinase Array by R&D Systems. Data represents one array with duplicate target spots for each cell line. DMSO: dimethyl sulfoxide. AU (arbitrary unit): absolute pixel density values. Displayed bars represent means.

### 5.1.5. S6 Ribosomal Protein

Change in phosphorylation of rpS6 at Ser235/236 after treatment with R+D was analyzed for the MNA cell lines KELLY and LAN-5, and the MNN cell lines SK-N-SH and SK-N-AS utilizing the PathScan® RTK Signaling Array. The following figure shows additional arrays for the cell lines KELLY (MNA) and SK-NSH (MNN) not displayed in the main results section and shows the phosphorylation status as absolute pixel density values (AU) after 72 hours of treatment with R+D compared to control (DMSO vehicle)-treated cells.

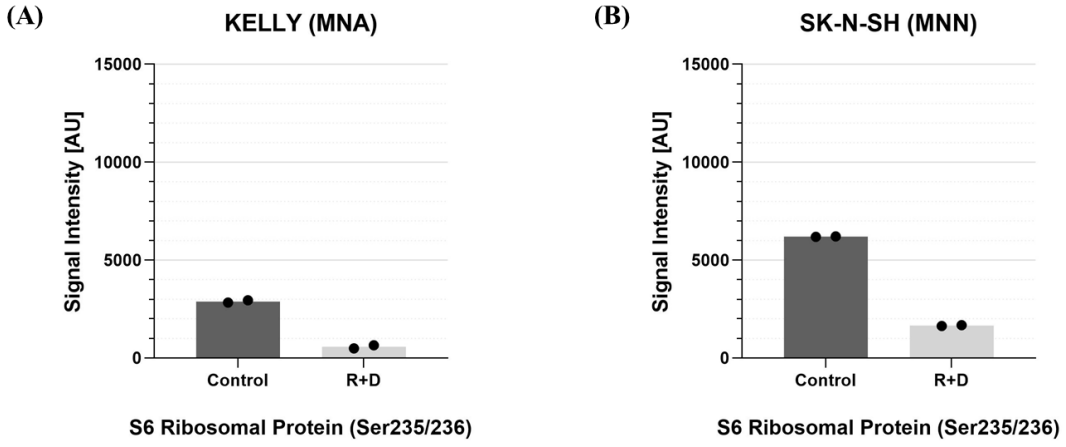


**Figure 71: Phosphorylation Status of S6 Ribosomal Protein at Serine 235/236 in Control- and Rapamycin Plus Dasatinib-Treated Neuroblastoma Cell Lines**

Phosphorylation status of S6 ribosomal protein (rpS6) at serine 235/236 (Ser235/236) after 72 hours of treatment with rapamycin plus dasatinib (R+D) compared to control (DMSO vehicle)-treated cells of the MycN-amplified (MNA) neuroblastoma (NB) cell line KELLY **(A)** and the MycN-non-amplified (MNN) NB cell line SK-N-SH **(B)** were analyzed utilizing the PathScan® RTK Signaling Array by Cell Signaling Technology. Data represents one array with duplicate target spots for each cell line. DMSO: dimethyl sulfoxide. AU: absolute pixel density values. Displayed bars represent means.

### 5.1.6. AKT

Change in phosphorylation of AKT at Thr308 and Ser473 after the treatment with R+D was analyzed for the MNA cell lines KELLY and LAN-5, and the MNN cell lines SK-N-SH and SK-N-AS utilizing the PathScan® RTK Signaling Array and utilizing the Proteome Profiler™ Human Phospho-Kinase Array for KELLY (MNA) and SK-NAS (MNN). The following figures show additional arrays not displayed in the main results section and show the phosphorylation status as absolute pixel density values (AU) after 72 hours of treatment with R+D compared to control (DMSO vehicle)-treated cells.

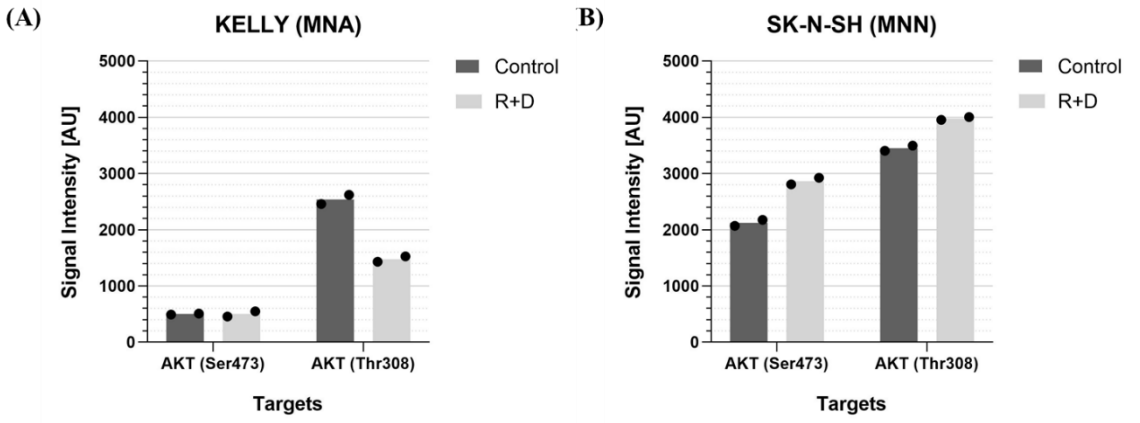


**Figure 72: Phosphorylation Status of Protein Kinase B (AKT) at Serine 473 and Threonine 308 in Control- and Rapamycin Plus Dasatinib-Treated Neuroblastoma Cell Lines**

Phosphorylation status of protein kinase B (AKT) at serine 473 (Ser473) and threonine 308 (Thr308) after 72 hours of treatment with rapamycin plus dasatinib (R+D) compared to control (DMSO-vehicle)-treated cells of the MycN-amplified (MNA) neuroblastoma (NB) cell line KELLY **(A)** and the MycN-non-amplified (MNN) NB cell line SK-N-SH **(B)** were analyzed utilizing the PathScan® RTK Signaling Array by Cell Signaling Technology. Data represents one array with duplicate target spots for each cell line. AU (arbitrary unit): absolute pixel density values. Displayed bars represent means.

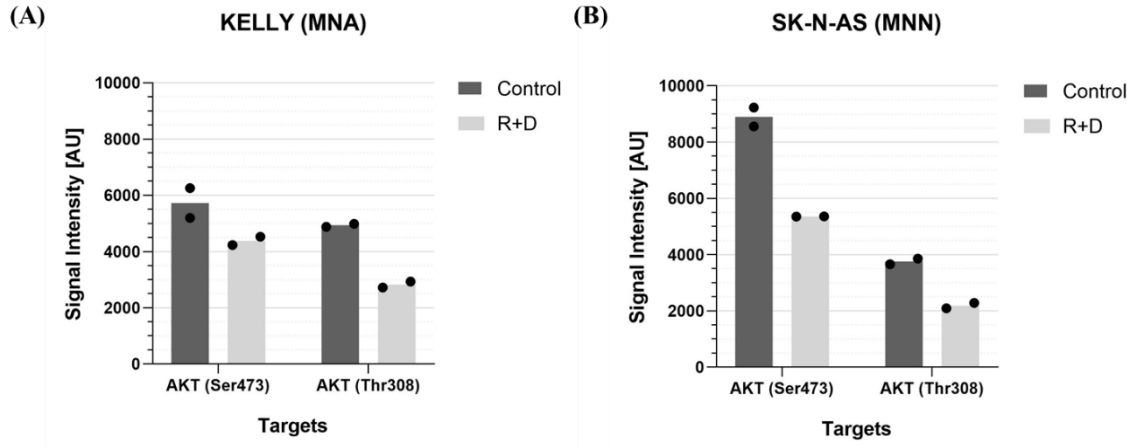


**Figure 73: Phosphorylation Status of Protein Kinase B (AKT) at Serine 473 and Threonine 308 in Control- and Rapamycin Plus Dasatinib-Treated Neuroblastoma Cell Lines**

Phosphorylation status of protein kinase B (AKT) at serine 473 (Ser473) and threonine 308 (Thr308) after 72 hours of treatment with rapamycin plus dasatinib (R+D) compared to control (DMSO-vehicle)-treated cells of the MycN-amplified (MNA) neuroblastoma (NB) cell line KELLY **(A)** and the MycN-non-amplified (MNN) NB cell line SK-N-AS **(B)** were analyzed utilizing the Proteome Profiler™ Human Phospho-Kinase Array by R&D Systems. Data represents one array with duplicate target spots for each cell line. AU (arbitrary unit): absolute pixel density values. Displayed bars represent means.

### 5.1.7. GSK-3β

The change in phosphorylation of GSK-3β at Ser9 after the treatment with R+D was analyzed for the MNA cell lines KELLY and LAN-5, and the MNN cell lines SK-N-SH and SK-N-AS utilizing the PathScan® AKT Signaling Array and utilizing the Proteome Profiler™ Human Phospho-Kinase Array for KELLY (MNA) and SK-NAS (MNN). That array did not distinguish between GSK-3α (Ser21) and GSK-3β (Ser9). The following figures show additional arrays not displayed in the main results section and show the phosphorylation status as absolute pixel density values (AU) after 72 hours of treatment with R+D compared to control (DMSO vehicle)-treated cells.

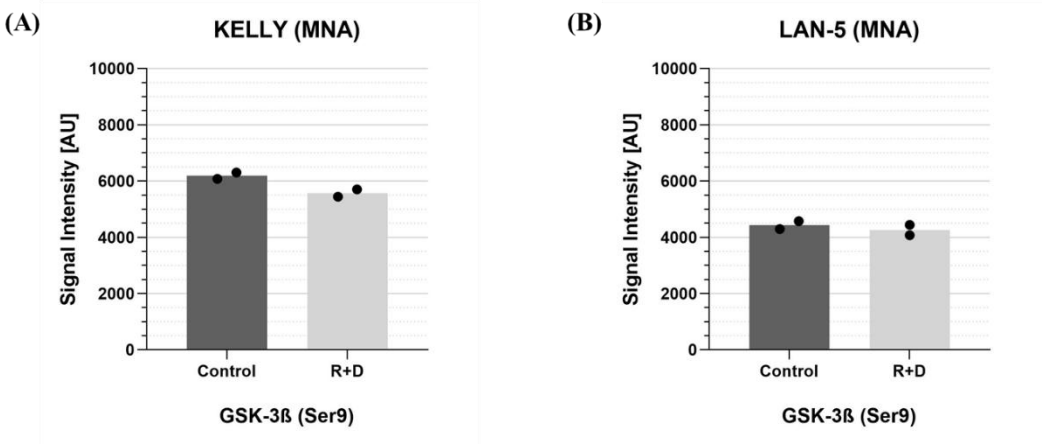


**Figure 74: Phosphorylation Status of Glycogen Synthase Kinase 3β in Control- and Rapamycin Plus Dasatinib-Treated Neuroblastoma Cell Lines**

Phosphorylation status of glycogen synthase kinase 3β (GSK-3β) at serine 9 (Ser9) after 72 hours of treatment with rapamycin plus dasatinib (R+D) compared to control (DMSO vehicle)-treated cells of the MycN-amplified (MNA) neuroblastoma (NB) cell lines KELLY **(A)** and LAN-5 **(B)** were analyzed utilizing the PathScan® AKT Signaling Array by Cell Signaling Technology. Data represents one array with duplicate target spots for each cell line. DMSO: dimethyl sulfoxide. AU (arbitrary unit): absolute pixel density values. Displayed bars represent means.

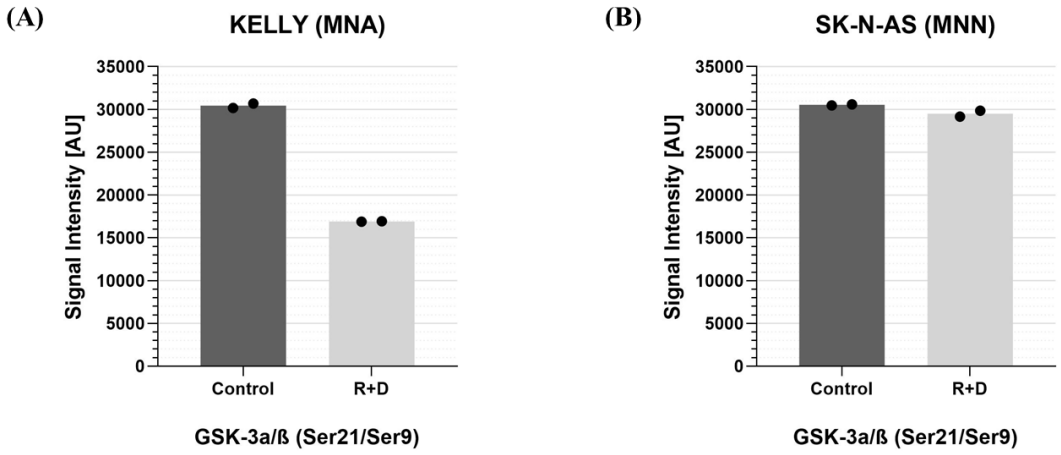


**Figure 75: Phosphorylation Status of Glycogen Synthase Kinase 3α/β in Control- and Rapamycin Plus Dasatinib-Treated Neuroblastoma Cell Lines**

Phosphorylation status of glycogen synthase kinase 3α/β (GSK-3α/β) at serine 21/serine 9 (Ser21/Ser9) after 72 hours of treatment with rapamycin plus dasatinib (R+D) compared to control (DMSO vehicle)-treated cells of the MycN-amplified (MNA) neuroblastoma (NB) cell line KELLY **(A)** and the MycN-non-amplified (MNN) NB cell line SK-N-AS **(B)** were analyzed utilizing the Proteome Profiler™ Human Phospho-Kinase Array by R&D Systems. Data represents one array with duplicate target spots for each cell line. DMSO: dimethyl sulfoxide. AU (arbitrary unit): absolute pixel density values. Displayed bars represent means.

### 5.1.8. PTEN

The change in phosphorylation of PTEN at Ser380 after the treatment with R+D treatment was analyzed in the MNA cell lines KELLY and LAN-5, and the MNN cell lines SK-N-SH and SK-N-AS utilizing the PathScan® AKT Signaling Array. The following figure shows additional arrays not displayed in the main results section and shows the phosphorylation status as absolute pixel density values (AU) after 72 hours of treatment with R+D compared to control (DMSO vehicle)-treated cells.

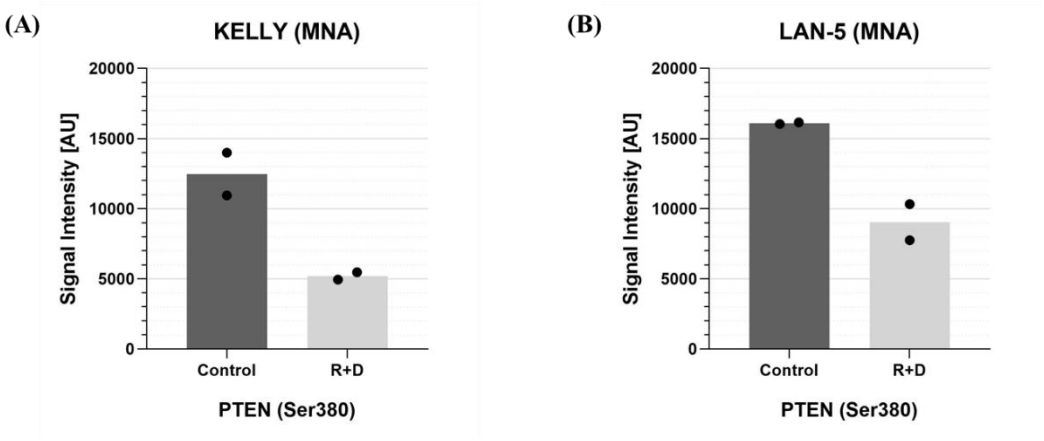


**Figure 76: Phosphorylation Status of Phosphatase and Tensin Homolog in Control- and Rapamycin plus Dasatinib-Treated Neuroblastoma Cell Lines**

Phosphorylation status of phosphatase and tensin homolog /PTEN) at serine 380 (Ser380) after 72 hours of treatment with rapamycin plus dasatinib (R+D) compared to control (DMSO-vehicle)-treated cells of the MycN-amplified (MNA) neuroblastoma (NB) cell lines KELLY **(A)** and LAN-5 **(B)** were analyzed utilizing the PathScan® AKT Signaling Array by Cell Signaling Technology. Data represents one array with duplicate target spots for each cell line. DMSO: dimethyl sulfoxide. AU (arbitrary unit): absolute pixel density values. Displayed bars represent means.

### 5.1.9. Src

Change in phosphorylation of Src after the treatment with R+D was analyzed for the MNA cell lines KELLY and LAN-5, and the MNN cell lines SK-N-SH and SK-N-AS utilizing the PathScan® RTK Signaling Array. The following figure shows additional arrays not displayed in the main results section and shows the phosphorylation status as absolute pixel density values (AU) after 72 hours of treatment with R+D compared to control (DMSO vehicle)-treated cells.

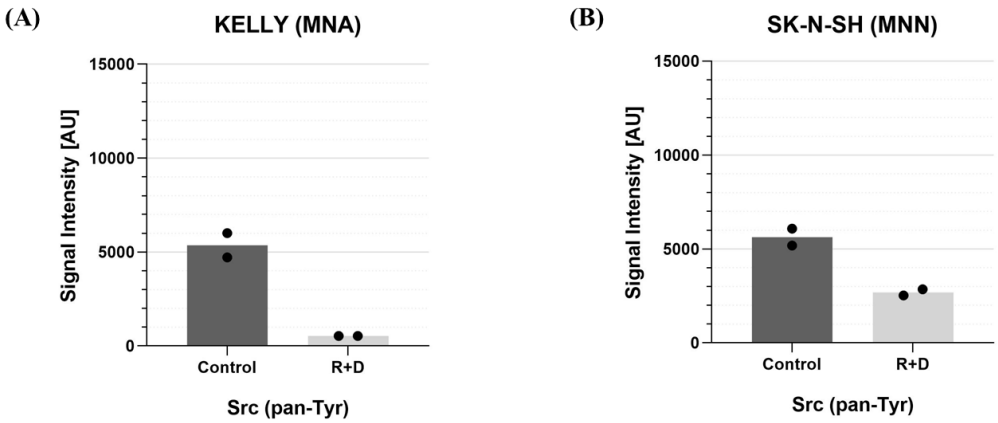


**Figure 77: Phosphorylation Status of Sarcoma Kinase in Control- and Rapamycin Plus Dasatinib-Treated Neuroblastoma Cell Lines**

Phosphorylation status of sarcoma kinase (Src) after 72 hours of treatment with rapamycin plus dasatinib (R+D) compared to control (DMSO vehicle)-treated cells of the MycN-amplified (MNA) neuroblastoma (NB) cell line KELLY **(A)** and the MycN-non-amplified (MNN) NB cell line SK-N-SH **(B)** were analyzed utilizing the PathScan® RTK Signaling Array by Cell Signaling Technology. Data represents one array with duplicate target spots for each cell line. DMSO: dimethyl sulfoxide. AU (arbitrary unit): absolute pixel density values. Displayed bars represent means.

### 5.1.10. ERK 1/2

Change in phosphorylation of ERK 1/2 at threonine 202 (Thr202) and tyrosine 204 (Tyr204) after the treatment with R+D was analyzed for the MNA cell lines KELLY and LAN-5, and the MNN cell lines SK-N-SH and SK-N-AS utilizing the PathScan® RTK Signaling Array and utilizing the Proteome Profiler™ Human Phospho-Kinase Array for KELLY (MNA) and SK-NAS (MNN). The following figures show additional arrays not displayed in the main results section and show the phosphorylation status as absolute pixel density values (AU) after 72 hours of treatment with R+D compared to control (DMSO vehicle)-treated cells.

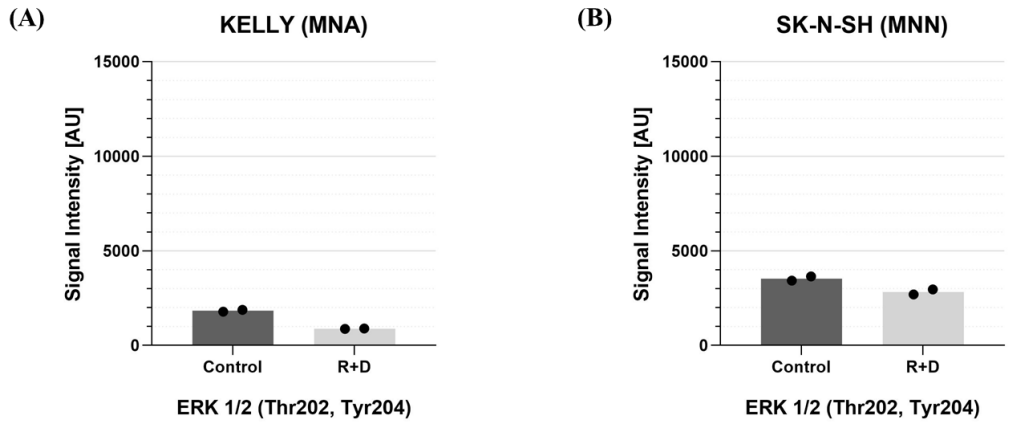


**Figure 78: Phosphorylation Status of Extracellular Signal-Regulated Kinases 1 and 2 in Control- and Rapamycin Plus Dasatinib-Treated Neuroblastoma Cell Lines**

Phosphorylation status of extracellular signal-regulated kinases 1 and 2 (ERK 1/2) at threonine 202 (Thr202) and tyrosine 204 (Tyr204), respectively, after 72 hours of treatment with rapamycin plus dasatinib (R+D) compared to control (DMSO vehicle)-treated cells of the MycN-amplified (MNA) neuroblastoma (NB) cell line KELLY **(A)** and the MycN-non-amplified (MNN) NB cell line SK-N-SH **(B)** were analyzed utilizing the PathScan® RTK Signaling Array by Cell Signaling Technology. Data represents one array with duplicate target spots for each cell line. DMSO: dimethyl sulfoxide. AU (arbitrary unit): absolute pixel density values. Displayed bars represent means.

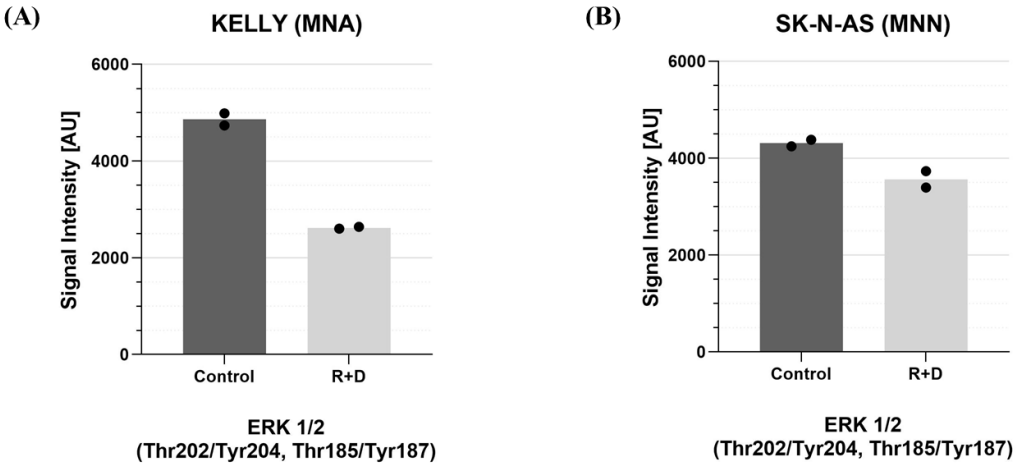


**Figure 79: Phosphorylation Status of Extracellular Signal-Regulated Kinases 1 and 2 in Control- and Rapamycin Plus Dasatinib-Treated Neuroblastoma Cell Lines**

Phosphorylation status of extracellular signal-regulated kinases 1 and 2 (ERK 1/2) at threonine 202/ tyrosine 204 (Thr202/Tyr204) and threonine 185/ tyrosine187 (Thr185/Tyr187), respectively, after 72 hours of treatment with rapamycin plus dasatinib (R+D) compared to control (DMSO vehicle)-treated cells of the MycN-amplified (MNA) neuroblastoma (NB) cell line KELLY **(A)** and the MycN-non-amplified (MNN) NB cell line SK-N-AS **(B)** were analyzed utilizing the Proteome Profiler™ Human Phospho-Kinase Array by R&D Systems. Data represents one array with duplicate target spots for each cell line. DMSO: dimethyl sulfoxide. AU (arbitrary unit): absolute pixel density values. Displayed bars represent means.

# 6. References


1. Louis CU, Shohet JM. Neuroblastoma: molecular pathogenesis and therapy. Annu Rev Med. 2015;66:49-63.
2. Brodeur GM. Neuroblastoma: biological insights into a clinical enigma. Nat Rev Cancer. 2003;3(3):203-16.
3. Gurney JG, Ross JA, Wall DA, Bleyer WA, Severson RK, Robison LL. Infant cancer in the U.S.: histology-specific incidence and trends, 1973 to 1992. J Pediatr Hematol Oncol. 1997;19(5):428-32.
4. Ries LAG SM, Gurney JG, Linet M, Tamra T, Young JL, Bunin GR (eds). Cancer Incidence and Survival among Children and Adolescents: United States SEER Program 1975-1995. Statistical Report. Bethesda, MD, 1999: National Cancer Institute, SEER Program; 1999.
5. Ward E, DeSantis C, Robbins A, Kohler B, Jemal A. Childhood and adolescent cancer statistics, 2014. CA Cancer J Clin. 2014;64(2):83-103.
6. Siegel RL, Miller KD, Fuchs HE, Jemal A. Cancer Statistics, 2021. CA Cancer J Clin. 2021;71(1):7-33.
7. Erdmann F KP, Grabow D, Spix C. German Childhood Cancer Registry - Annual Report 2019 (1980-2018). Statistical Report. Institute of Medical Biostatistics, Epidemiology and Informatics (IMBEI) at the University Medical Centerof the Johannes Gutenberg University Mainz; 2020.
8. Brodeur GM, Hogarty MD, Mosse YP, Maris JM. Neuroblastoma. 2011 2011/01/01. In: Principles and Practice of Pediatric Oncology [Internet]. Lippincott Williams & Wilkins. 6th_Edition. [886-922].
9. Maris JM, Hogarty MD, Bagatell R, Cohn SL. Neuroblastoma. Lancet. 2007;369(9579):2106-20.
10. Mosse YP, Laudenslager M, Longo L, Cole KA, Wood A, Attiyeh EF, et al. Identification of ALK as a major familial neuroblastoma predisposition gene. Nature. 2008;455(7215):930-5.
11. Janoueix-Lerosey I, Lequin D, Brugieres L, Ribeiro A, de Pontual L, Combaret V, et al. Somatic and germline activating mutations of the ALK kinase receptor in neuroblastoma. Nature. 2008;455(7215):967-70.
12. D'Angio GJ, Evans AE, Koop CE. Special pattern of widespread neuroblastoma with a favourable prognosis. Lancet. 1971;1(7708):1046-9.
13. Nickerson HJ, Matthay KK, Seeger RC, Brodeur GM, Shimada H, Perez C, et al. Favorable biology and outcome of stage IV-S neuroblastoma with supportive care or minimal therapy: a Children's Cancer Group study. J Clin Oncol. 2000;18(3):477-86.
14. Cohn SL, Pearson AD, London WB, Monclair T, Ambros PF, Brodeur GM, et al. The International Neuroblastoma Risk Group (INRG) classification system: an INRG Task Force report. J Clin Oncol. 2009;27(2):289-97.

15. Monclair T, Brodeur GM, Ambros PF, Brisse HJ, Cecchetto G, Holmes K, et al. The International Neuroblastoma Risk Group (INRG) staging system: an INRG Task Force report. J Clin Oncol. 2009;27(2):298-303.
16. Brodeur GM, Seeger RC, Schwab M, Varmus HE, Bishop JM. Amplification of N-myc in untreated human neuroblastomas correlates with advanced disease stage. Science. 1984;224(4653):1121-4.
17. Seeger RC, Brodeur GM, Sather H, Dalton A, Siegel SE, Wong KY, et al. Association of multiple copies of the N-myc oncogene with rapid progression of neuroblastomas. N Engl J Med. 1985;313(18):1111-6.
18. Caron H, van Sluis P, de Kraker J, Bokkerink J, Egeler M, Laureys G, et al. Allelic loss of chromosome 1p as a predictor of unfavorable outcome in patients with neuroblastoma. N Engl J Med. 1996;334(4):225-30.
19. Gustafson WC, Weiss WA. Myc proteins as therapeutic targets. Oncogene. 2010;29(9):1249-59.
20. Hogarty MD, Maris JM. PI3King on MYCN to improve neuroblastoma therapeutics. Cancer Cell. 2012;21(2):145-7.
21. Zafar A, Wang W, Liu G, Wang X, Xian W, McKeon F, et al. Molecular targeting therapies for neuroblastoma: Progress and challenges. Med Res Rev. 2021;41(2):961-1021.
22. Kholodenko IV, Kalinovsky DV, Doronin, II, Deyev SM, Kholodenko RV. Neuroblastoma Origin and Therapeutic Targets for Immunotherapy. J Immunol Res. 2018;2018:7394268.
23. Attiyeh EF, London WB, Mosse YP, Wang Q, Winter C, Khazi D, et al. Chromosome 1p and 11q deletions and outcome in neuroblastoma. N Engl J Med. 2005;353(21):2243-53.
24. Guo C, White PS, Weiss MJ, Hogarty MD, Thompson PM, Stram DO, et al. Allelic deletion at 11q23 is common in MYCN single copy neuroblastomas. Oncogene. 1999;18(35):4948-57.
25. Mosse YP, Diskin SJ, Wasserman N, Rinaldi K, Attiyeh EF, Cole K, et al. Neuroblastomas have distinct genomic DNA profiles that predict clinical phenotype and regional gene expression. Genes Chromosomes Cancer. 2007;46(10):936-49.
26. Maris JM, Guo C, White PS, Hogarty MD, Thompson PM, Stram DO, et al. Allelic deletion at chromosome bands 11q14-23 is common in neuroblastoma. Med Pediatr Oncol. 2001;36(1):24-7.
27. Bown N, Cotterill S, Lastowska M, O'Neill S, Pearson AD, Plantaz D, et al. Gain of chromosome arm 17q and adverse outcome in patients with neuroblastoma. N Engl J Med. 1999;340(25):1954-61.
28. Plantaz D, Mohapatra G, Matthay KK, Pellarin M, Seeger RC, Feuerstein BG. Gain of chromosome 17 is the most frequent abnormality detected in neuroblastoma by comparative genomic hybridization. Am J Pathol. 1997;150(1):81-9.
29. Hartmann O BF. Treatment of advanced neuroblastoma: the European Experience. In: Brodeur GM ST, Tsuchida Y, et al., editors. , editor. Neuroblastoma. Amsterdam: Elsevier Press; 2000. p. p417-36.

30. Matthay KK CR. Treatment of advanced neuroblastoma: the U.S. Experience. In: Brodeur GM ST, Tsuchida Y, et al., editors., editor. Neuroblastoma. Amsterdam: Elsevier Press; 2000. p. 414-36.
31. Tsuchida Y KM. Treatment of advanced neuroblastoma: the Japanese Experience. In: Brodeur GM ST, Tsuchida Y, et al., editors., editor. Neuroblastoma. Amsterdam: Elsevier Press; 2000. p. 417-36.
32. Deutsche Gesellschaft für Kinder- und Jugendheilkunde (DGKJ); Deutsche Gesellschaft für Pädiatrische Onkologie und Hämatologie (GPOH) ea. S1-Leitlinie: Neuroblastom [Leitlinie]. AWMF; 2019 [updated 07.2019]. Available from: https://www.awmf.org/uploads/tx_szleitlinien/025-008l_S1_Neuroblastom_2019-07_01.pdf.
33. London WB, Bagatell R, Weigel BJ, Fox E, Guo D, Van Ryn C, et al. Historical time to disease progression and progression-free survival in patients with recurrent/refractory neuroblastoma treated in the modern era on Children's Oncology Group early-phase trials. Cancer. 2017;123(24):4914-23.
34. London WB, Castel V, Monclair T, Ambros PF, Pearson AD, Cohn SL, et al. Clinical and biologic features predictive of survival after relapse of neuroblastoma: a report from the International Neuroblastoma Risk Group project. J Clin Oncol. 2011;29(24):3286-92.
35. Friedman DN, Henderson TO. Late Effects and Survivorship Issues in Patients with Neuroblastoma. Children (Basel). 2018;5(8).
36. Zage PE. Novel Therapies for Relapsed and Refractory Neuroblastoma. Children (Basel). 2018;5(11).
37. Corbacioglu S. Multimodal Molecular Targeted Therapy to Treat Relapsed or Refractory High-risk Neuroblastoma: RIST-rNB-2011-Studienprotokoll [Web Page]. ClinicalTrials.gov: U.S. National Library of Medicine. Available from: https://clinicaltrials.gov/ct2/show/NCT01467986?cond=Neuroblastoma&cntry=DE&city=Regensburg&draw=2&rank=1.
38. Vogelstein B, Papadopoulos N, Velculescu VE, Zhou S, Diaz LA, Jr., Kinzler KW. Cancer genome landscapes. Science. 2013;339(6127):1546-58.
39. Vivanco I, Sawyers CL. The phosphatidylinositol 3-Kinase AKT pathway in human cancer. Nat Rev Cancer. 2002;2(7):489-501.
40. Cully M, You H, Levine AJ, Mak TW. Beyond PTEN mutations: the PI3K pathway as an integrator of multiple inputs during tumorigenesis. Nat Rev Cancer. 2006;6(3):184-92.
41. King D, Yeomanson D, Bryant HE. PI3King the lock: targeting the PI3K/Akt/mTOR pathway as a novel therapeutic strategy in neuroblastoma. J Pediatr Hematol Oncol. 2015;37(4):245-51.
42. Yang J, Nie J, Ma X, Wei Y, Peng Y, Wei X. Targeting PI3K in cancer: mechanisms and advances in clinical trials. Mol Cancer. 2019;18(1):26.
43. Bjornsti MA, Houghton PJ. The TOR pathway: a target for cancer therapy. Nat Rev Cancer. 2004;4(5):335-48.

44. Engelman JA. Targeting PI3K signalling in cancer: opportunities, challenges and limitations. Nat Rev Cancer. 2009;9(8):550-62.
45. Zoncu R, Efeyan A, Sabatini DM. mTOR: from growth signal integration to cancer, diabetes and ageing. Nat Rev Mol Cell Biol. 2011;12(1):21-35.
46. Huang K, Fingar DC. Growing knowledge of the mTOR signaling network. Semin Cell Dev Biol. 2014;36:79-90.
47. Ma XM, Blenis J. Molecular mechanisms of mTOR-mediated translational control. Nat Rev Mol Cell Biol. 2009;10(5):307-18.
48. Manning BD, Toker A. AKT/PKB Signaling: Navigating the Network. Cell. 2017;169(3):381-405.
49. Saxton RA, Sabatini DM. mTOR Signaling in Growth, Metabolism, and Disease. Cell. 2017;169(2):361-71.
50. Reiling JH, Sabatini DM. Stress and mTORture signaling. Oncogene. 2006;25(48):6373-83.
51. Yorimitsu T, Klionsky DJ. Autophagy: molecular machinery for self-eating. Cell Death Differ. 2005;12 Suppl 2(Suppl 2):1542-52.
52. Mathiassen SG, De Zio D, Cecconi F. Autophagy and the Cell Cycle: A Complex Landscape. Front Oncol. 2017;7:51.
53. Magnuson B, Ekim B, Fingar DC. Regulation and function of ribosomal protein S6 kinase (S6K) within mTOR signalling networks. Biochem J. 2012;441(1):1-21.
54. Harrington LS, Findlay GM, Gray A, Tolkacheva T, Wigfield S, Rebholz H, et al. The TSC1-2 tumor suppressor controls insulin-PI3K signaling via regulation of IRS proteins. J Cell Biol. 2004;166(2):213-23.
55. Treins C, Warne PH, Magnuson MA, Pende M, Downward J. Rictor is a novel target of p70 S6 kinase-1. Oncogene. 2010;29(7):1003-16.
56. Dibble CC, Asara JM, Manning BD. Characterization of Rictor phosphorylation sites reveals direct regulation of mTOR complex 2 by S6K1. Mol Cell Biol. 2009;29(21):5657-70.
57. Opel D, Poremba C, Simon T, Debatin KM, Fulda S. Activation of Akt predicts poor outcome in neuroblastoma. Cancer Res. 2007;67(2):735-45.
58. Johnsen JI, Segerstrom L, Orrego A, Elfman L, Henriksson M, Kagedal B, et al. Inhibitors of mammalian target of rapamycin downregulate MYCN protein expression and inhibit neuroblastoma growth in vitro and in vivo. Oncogene. 2008;27(20):2910-22.
59. Izycka-Swieszewska E, Drozynska E, Rzepko R, Kobierska-Gulida G, Grajkowska W, Perek D, et al. Analysis of PI3K/AKT/mTOR signalling pathway in high risk neuroblastic tumours. Pol J Pathol. 2010;61(4):192-8.
60. Berry T, Luther W, Bhatnagar N, Jamin Y, Poon E, Sanda T, et al. The ALK(F1174L) mutation potentiates the oncogenic activity of MYCN in neuroblastoma. Cancer Cell. 2012;22(1):117-30.
61. Chen Y, Takita J, Choi YL, Kato M, Ohira M, Sanada M, et al. Oncogenic mutations of ALK kinase in neuroblastoma. Nature. 2008;455(7215):971-4.

62. Chesler L, Schlieve C, Goldenberg DD, Kenney A, Kim G, McMillan A, et al. Inhibition of phosphatidylinositol 3-kinase destabilizes Mycn protein and blocks malignant progression in neuroblastoma. Cancer Res. 2006;66(16):8139-46.
63. Barone G, Anderson J, Pearson AD, Petrie K, Chesler L. New strategies in neuroblastoma: Therapeutic targeting of MYCN and ALK. Clin Cancer Res. 2013;19(21):5814-21.
64. Schramm A, Koster J, Marschall T, Martin M, Schwermer M, Fielitz K, et al. Next-generation RNA sequencing reveals differential expression of MYCN target genes and suggests the mTOR pathway as a promising therapy target in MYCN-amplified neuroblastoma. Int J Cancer. 2013;132(3):E106-15.
65. Vaughan L, Clarke PA, Barker K, Chanthery Y, Gustafson CW, Tucker E, et al. Inhibition of mTOR-kinase destabilizes MYCN and is a potential therapy for MYCN-dependent tumors. Oncotarget. 2016;7(36):57525-44.
66. Bender A, Opel D, Naumann I, Kappler R, Friedman L, von Schweinitz D, et al. PI3K inhibitors prime neuroblastoma cells for chemotherapy by shifting the balance towards pro-apoptotic Bcl-2 proteins and enhanced mitochondrial apoptosis. Oncogene. 2011;30(4):494-503.
67. Chanthery YH, Gustafson WC, Itsara M, Persson A, Hackett CS, Grimmer M, et al. Paracrine signaling through MYCN enhances tumor-vascular interactions in neuroblastoma. Sci Transl Med. 2012;4(115):115ra3.
68. Segerstrom L, Baryawno N, Sveinbjornsson B, Wickstrom M, Elfman L, Kogner P, et al. Effects of small molecule inhibitors of PI3K/Akt/mTOR signaling on neuroblastoma growth in vitro and in vivo. Int J Cancer. 2011;129(12):2958-65.
69. Guo YJ, Pan WW, Liu SB, Shen ZF, Xu Y, Hu LL. ERK/MAPK signalling pathway and tumorigenesis. Exp Ther Med. 2020;19(3):1997-2007.
70. Schlessinger J. Cell signaling by receptor tyrosine kinases. Cell. 2000;103(2):211-25.
71. McKay MM, Morrison DK. Integrating signals from RTKs to ERK/MAPK. Oncogene. 2007;26(22):3113-21.
72. Dhillon AS, Hagan S, Rath O, Kolch W. MAP kinase signalling pathways in cancer. Oncogene. 2007;26(22):3279-90.
73. Gallolu Kankanamalage S, Karra AS, Cobb MH. WNK pathways in cancer signaling networks. Cell Commun Signal. 2018;16(1):72.
74. Lonze BE, Ginty DD. Function and regulation of CREB family transcription factors in the nervous system. Neuron. 2002;35(4):605-23.
75. Steven A, Seliger B. Control of CREB expression in tumors: from molecular mechanisms and signal transduction pathways to therapeutic target. Oncotarget. 2016;7(23):35454-65.
76. Lavoie H, Gagnon J, Therrien M. ERK signalling: a master regulator of cell behaviour, life and fate. Nat Rev Mol Cell Biol. 2020;21(10):607-32.

77. Romeo Y, Zhang X, Roux PP. Regulation and function of the RSK family of protein kinases. Biochem J. 2012;441(2):553-69.
78. Anjum R, Blenis J. The RSK family of kinases: emerging roles in cellular signalling. Nat Rev Mol Cell Biol. 2008;9(10):747-58.
79. Sears R, Nuckolls F, Haura E, Taya Y, Tamai K, Nevins JR. Multiple Ras-dependent phosphorylation pathways regulate Myc protein stability. Genes Dev. 2000;14(19):2501-14.
80. Naqvi S, Martin KJ, Arthur JS. CREB phosphorylation at Ser133 regulates transcription via distinct mechanisms downstream of cAMP and MAPK signalling. Biochem J. 2014;458(3):469-79.
81. Kim LC, Song L, Haura EB. Src kinases as therapeutic targets for cancer. Nat Rev Clin Oncol. 2009;6(10):587-95.
82. Parsons SJ, Parsons JT. Src family kinases, key regulators of signal transduction. Oncogene. 2004;23(48):7906-9.
83. Thomas SM, Brugge JS. Cellular functions regulated by Src family kinases. Annu Rev Cell Dev Biol. 1997;13:513-609.
84. Yeatman TJ. A renaissance for SRC. Nat Rev Cancer. 2004;4(6):470-80.
85. Stokoe D, McCormick F. Activation of c-Raf-1 by Ras and Src through different mechanisms: activation in vivo and in vitro. EMBO J. 1997;16(9):2384-96.
86. Irby RB, Yeatman TJ. Role of Src expression and activation in human cancer. Oncogene. 2000;19(49):5636-42.
87. Summy JM, Gallick GE. Treatment for advanced tumors: SRC reclaims center stage. Clin Cancer Res. 2006;12(5):1398-401.
88. Bjelfman C, Hedborg F, Johansson I, Nordenskjold M, Pahlman S. Expression of the neuronal form of pp60c-src in neuroblastoma in relation to clinical stage and prognosis. Cancer Res. 1990;50(21):6908-14.
89. Bolen JB, Rosen N, Israel MA. Increased pp60c-src tyrosyl kinase activity in human neuroblastomas is associated with amino-terminal tyrosine phosphorylation of the src gene product. Proc Natl Acad Sci U S A. 1985;82(21):7275-9.
90. Montero JC, Seoane S, Ocana A, Pandiella A. Inhibition of SRC family kinases and receptor tyrosine kinases by dasatinib: possible combinations in solid tumors. Clin Cancer Res. 2011;17(17):5546-52.
91. Martellucci S, Clementi L, Sabetta S, Mattei V, Botta L, Angelucci A. Src Family Kinases as Therapeutic Targets in Advanced Solid Tumors: What We Have Learned so Far. Cancers (Basel). 2020;12(6).
92. Mendoza MC, Er EE, Blenis J. The Ras-ERK and PI3K-mTOR pathways: cross-talk and compensation. Trends Biochem Sci. 2011;36(6):320-8.

93. De Luca A, Maiello MR, D'Alessio A, Pergameno M, Normanno N. The RAS/RAF/MEK/ERK and the PI3K/AKT signalling pathways: role in cancer pathogenesis and implications for therapeutic approaches. Expert Opin Ther Targets. 2012;16 Suppl 2:S17-27.
94. Corbacioglu S. Molecular-Targeted Therapy in Refractory or Relapsed Neuroblastoma. In: Christiansen H, Christiansen NM, editors. Progressive Neuroblastoma: Innovation and Novel Therapeutic Strategies. 20. Basel: Karger; 2015.
95. Nonnenmacher L, Westhoff MA, Fulda S, Karpel-Massler G, Halatsch ME, Engelke J, et al. RIST: a potent new combination therapy for glioblastoma. Int J Cancer. 2015;136(4):E173-87.
96. Sehgal SN. Sirolimus: its discovery, biological properties, and mechanism of action. Transplant Proc. 2003;35(3 Suppl):7S-14S.
97. Sehgal SN, Baker H, Vezina C. Rapamycin (AY-22,989), a new antifungal antibiotic. II. Fermentation, isolation and characterization. J Antibiot (Tokyo). 1975;28(10):727-32.
98. Mao B, Zhang Q, Ma L, Zhao DS, Zhao P, Yan P. Overview of Research into mTOR Inhibitors. Molecules. 2022;27(16).
99. Bahmad HF, Mouhieddine TH, Chalhoub RM, Assi S, Araji T, Chamaa F, et al. The Akt/mTOR pathway in cancer stem/progenitor cells is a potential therapeutic target for glioblastoma and neuroblastoma. Oncotarget. 2018;9(71):33549-61.
100. Lombardo LJ, Lee FY, Chen P, Norris D, Barrish JC, Behnia K, et al. Discovery of N-(2-chloro-6-methyl- phenyl)-2-(6-(4-(2-hydroxyethyl)- piperazin-1-yl)-2-methylpyrimidin-4-ylamino)thiazole-5-carboxamide (BMS-354825), a dual Src/Abl kinase inhibitor with potent antitumor activity in preclinical assays. J Med Chem. 2004;47(27):6658-61.
101. Hantschel O, Rix U, Superti-Furga G. Target spectrum of the BCR-ABL inhibitors imatinib, nilotinib and dasatinib. Leuk Lymphoma. 2008;49(4):615-9.
102. Rix U, Hantschel O, Durnberger G, Remsing Rix LL, Planyavsky M, Fernbach NV, et al. Chemical proteomic profiles of the BCR-ABL inhibitors imatinib, nilotinib, and dasatinib reveal novel kinase and nonkinase targets. Blood. 2007;110(12):4055-63.
103. Timeus F, Crescenzio N, Fandi A, Doria A, Foglia L, Cordero di Montezemolo L. In vitro antiproliferative and antimigratory activity of dasatinib in neuroblastoma and Ewing sarcoma cell lines. Oncol Rep. 2008;19(2):353-9.
104. Vitali R, Mancini C, Cesi V, Tanno B, Piscitelli M, Mancuso M, et al. Activity of tyrosine kinase inhibitor Dasatinib in neuroblastoma cells in vitro and in orthotopic mouse model. Int J Cancer. 2009;125(11):2547-55.
105. Chabot GG. Clinical pharmacokinetics of irinotecan. Clin Pharmacokinet. 1997;33(4):245-59.
106. Komuro H, Li P, Tsuchida Y, Yokomori K, Nakajima K, Aoyama T, et al. Effects of CPT-11 (a unique DNA topoisomerase I inhibitor) on a highly malignant xeno-transplanted neuroblastoma. Med Pediatr Oncol. 1994;23(6):487-92.

107. Vassal G, Pondarre C, Cappelli C, Terrier-Lacombe MJ, Boland I, Morizet J, et al. DNA-topoisomerase I, a new target for the treatment of neuroblastoma. Eur J Cancer. 1997;33(12):2011-5.
108. Vassal G, Terrier-Lacombe MJ, Bissery MC, Venuat AM, Gyergyay F, Benard J, et al. Therapeutic activity of CPT-11, a DNA-topoisomerase I inhibitor, against peripheral primitive neuroectodermal tumour and neuroblastoma xenografts. Br J Cancer. 1996;74(4):537-45.
109. Furman WL, Stewart CF, Poquette CA, Pratt CB, Santana VM, Zamboni WC, et al. Direct translation of a protracted irinotecan schedule from a xenograft model to a phase I trial in children. J Clin Oncol. 1999;17(6):1815-24.
110. Blaney S, Berg SL, Pratt C, Weitman S, Sullivan J, Luchtman-Jones L, et al. A phase I study of irinotecan in pediatric patients: a pediatric oncology group study. Clin Cancer Res. 2001;7(1):32-7.
111. Bomgaars LR, Bernstein M, Krailo M, Kadota R, Das S, Chen Z, et al. Phase II trial of irinotecan in children with refractory solid tumors: a Children's Oncology Group Study. J Clin Oncol. 2007;25(29):4622-7.
112. Vassal G, Giammarile F, Brooks M, Geoerger B, Couanet D, Michon J, et al. A phase II study of irinotecan in children with relapsed or refractory neuroblastoma: a European cooperation of the Societe Francaise d'Oncologie Pediatrique (SFOP) and the United Kingdom Children Cancer Study Group (UKCCSG). Eur J Cancer. 2008;44(16):2453-60.
113. Thomas A, Tanaka M, Trepel J, Reinhold WC, Rajapakse VN, Pommier Y. Temozolomide in the Era of Precision Medicine. Cancer Res. 2017;77(4):823-6.
114. Newlands ES, Stevens MF, Wedge SR, Wheelhouse RT, Brock C. Temozolomide: a review of its discovery, chemical properties, pre-clinical development and clinical trials. Cancer Treat Rev. 1997;23(1):35-61.
115. De Sio L, Milano GM, Castellano A, Jenkner A, Fidani P, Dominici C, et al. Temozolomide in resistant or relapsed pediatric solid tumors. Pediatr Blood Cancer. 2006;47(1):30-6.
116. Rubie H, Chisholm J, Defachelles AS, Morland B, Munzer C, Valteau-Couanet D, et al. Phase II study of temozolomide in relapsed or refractory high-risk neuroblastoma: a joint Societe Francaise des Cancers de l'Enfant and United Kingdom Children Cancer Study Group-New Agents Group Study. J Clin Oncol. 2006;24(33):5259-64.
117. Yap TA, Omlin A, de Bono JS. Development of therapeutic combinations targeting major cancer signaling pathways. J Clin Oncol. 2013;31(12):1592-605.
118. Bayat Mokhtari R, Homayouni TS, Baluch N, Morgatskaya E, Kumar S, Das B, et al. Combination therapy in combating cancer. Oncotarget. 2017;8(23):38022-43.
119. Al-Lazikani B, Banerji U, Workman P. Combinatorial drug therapy for cancer in the post-genomic era. Nat Biotechnol. 2012;30(7):679-92.

120. Park BJ, Whichard ZL, Corey SJ. Dasatinib synergizes with both cytotoxic and signal transduction inhibitors in heterogeneous breast cancer cell lines--lessons for design of combination targeted therapy. Cancer Lett. 2012;320(1):104-10.
121. Chen B, Xu X, Luo J, Wang H, Zhou S. Rapamycin Enhances the Anti-Cancer Effect of Dasatinib by Suppressing Src/PI3K/mTOR Pathway in NSCLC Cells. PLoS One. 2015;10(6):e0129663.
122. Yori JL, Lozada KL, Seachrist DD, Mosley JD, Abdul-Karim FW, Booth CN, et al. Combined SFK/mTOR inhibition prevents rapamycin-induced feedback activation of AKT and elicits efficient tumor regression. Cancer Res. 2014;74(17):4762-71.
123. Laukkanen S, Veloso A, Yan C, Oksa L, Alpert EJ, Do D, et al. Therapeutic targeting of LCK tyrosine kinase and mTOR signaling in T-cell acute lymphoblastic leukemia. Blood. 2022;140(17):1891-906.
124. Mohi MG, Boulton C, Gu TL, Sternberg DW, Neuberg D, Griffin JD, et al. Combination of rapamycin and protein tyrosine kinase (PTK) inhibitors for the treatment of leukemias caused by oncogenic PTKs. Proc Natl Acad Sci U S A. 2004;101(9):3130-5.
125. Corbacioglu S, Kilic M, Westhoff MA, Reinhardt D, Fulda S, Debatin KM. Newly identified c-KIT receptor tyrosine kinase ITD in childhood AML induces ligand-independent growth and is responsive to a synergistic effect of imatinib and rapamycin. Blood. 2006;108(10):3504-13.
126. Li Z, Yan S, Attayan N, Ramalingam S, Thiele CJ. Combination of an allosteric Akt Inhibitor MK-2206 with etoposide or rapamycin enhances the antitumor growth effect in neuroblastoma. Clin Cancer Res. 2012;18(13):3603-15.
127. Kling MJ, Griggs CN, McIntyre EM, Alexander G, Ray S, Challagundla KB, et al. Synergistic efficacy of inhibiting MYCN and mTOR signaling against neuroblastoma. BMC Cancer. 2021;21(1):1061.
128. Leister JE. Multimodale molekulare Therapieansätze in einem in-vitro-Modell des Neuroblastoma. Regensburg: Universität Regensburg; 2019.
129. Wätzig RB. Testung verschiedener mTOR-Inhibitoren zur Verbesserung der RIST-Therapie in einem in-vitro-Modell des Neuroblastoms. Regensburg: Universität Regensburg; 2021.
130. Waetzig R, Matthes M, Leister J, Penkivech G, Heise T, Corbacioglu S, et al. Comparing mTOR inhibitor Rapamycin with Torin-2 within the RIST molecular-targeted regimen in neuroblastoma cells. Int J Med Sci. 2021;18(1):137-49.
131. Kushner BH, Kramer K, Modak S, Cheung NK. Irinotecan plus temozolomide for relapsed or refractory neuroblastoma. J Clin Oncol. 2006;24(33):5271-6.
132. Bagatell R, London WB, Wagner LM, Voss SD, Stewart CF, Maris JM, et al. Phase II study of irinotecan and temozolomide in children with relapsed or refractory neuroblastoma: a Children's Oncology Group study. J Clin Oncol. 2011;29(2):208-13.
133. Kerbel RS, Kamen BA. The anti-angiogenic basis of metronomic chemotherapy. Nat Rev Cancer. 2004;4(6):423-36.

134. Hanahan D, Bergers G, Bergsland E. Less is more, regularly: metronomic dosing of cytotoxic drugs can target tumor angiogenesis in mice. J Clin Invest. 2000;105(8):1045-7.
135. Browder T, Butterfield CE, Kraling BM, Shi B, Marshall B, O'Reilly MS, et al. Antiangiogenic scheduling of chemotherapy improves efficacy against experimental drug-resistant cancer. Cancer Res. 2000;60(7):1878-86.
136. Geidel P, Tauer JT, Steinbronn N, Jung R, Leuschner I, Strasser RH, et al. Cardiac Failure In Juvenile Rats Caused By Continuous Long-Term Exposure To The Tyrosine Kinase Inhibitor Dasatinib Can Be Circumvented By An Intermittent Application Schedule. Blood. 2013;122(21):3984-.
137. La Rosee P, Martiat P, Leitner A, Klag T, Muller MC, Erben P, et al. Improved tolerability by a modified intermittent treatment schedule of dasatinib for patients with chronic myeloid leukemia resistant or intolerant to imatinib. Ann Hematol. 2013;92(10):1345-50.
138. Saito K, Matsumoto S, Yasui H, Devasahayam N, Subramanian S, Munasinghe JP, et al. Longitudinal imaging studies of tumor microenvironment in mice treated with the mTOR inhibitor rapamycin. PLoS One. 2012;7(11):e49456.
139. Qayum N, Im J, Stratford MR, Bernhard EJ, McKenna WG, Muschel RJ. Modulation of the tumor microvasculature by phosphoinositide-3 kinase inhibition increases doxorubicin delivery in vivo. Clin Cancer Res. 2012;18(1):161-9.
140. Zhou Q, Gallo JM. Differential effect of sunitinib on the distribution of temozolomide in an orthotopic glioma model. Neuro Oncol. 2009;11(3):301-10.
141. Kieran MW, Turner CD, Rubin JB, Chi SN, Zimmerman MA, Chordas C, et al. A feasibility trial of antiangiogenic (metronomic) chemotherapy in pediatric patients with recurrent or progressive cancer. J Pediatr Hematol Oncol. 2005;27(11):573-81.
142. Corbacioglu S, Steinbach D, Lode HN, Gruhn B, Fruehwald M, Broeckelmann M, et al. The RIST design: A molecularly targeted multimodal approach for the treatment of patients with relapsed and refractory neuroblastoma. Journal of Clinical Oncology. 2013;31(15_suppl):10017-.
143. ECACC. ECACC General Cell Collection Datasheet: KELLY (ECACC 92110411).
144. DSMZ. Data Sheet LAN-5 (DSMZ no. ACC 673).
145. Thiele CJ. Neuroblastoma Cell Lines. In: Masters J, editor. Human Cell Culture. 1. Lancaster, UK: Kluwer Academic Publishers; 1998. p. 21-53.
146. ATCC. Product Sheet SK-N-SH (ATCC HTB-11).
147. Biedler JL, Helson L, Spengler BA. Morphology and growth, tumorigenicity, and cytogenetics of human neuroblastoma cells in continuous culture. Cancer Res. 1973;33(11):2643-52.
148. ATCC. Product Sheet SK-N-AS (ATCC CRL-2137).
149. Lodrini M, Sprussel A, Astrahantseff K, Tiburtius D, Konschak R, Lode HN, et al. Using droplet digital PCR to analyze MYCN and ALK copy number in plasma from patients with neuroblastoma. Oncotarget. 2017;8(49):85234-51.

150. Peitz C, Sprussel A, Linke RB, Astrahantseff K, Grimaldi M, Schmelz K, et al. Multiplexed Quantification of Four Neuroblastoma DNA Targets in a Single Droplet Digital PCR Reaction. J Mol Diagn. 2020;22(11):1309-23.
151. Harenza JL, Diamond MA, Adams RN, Song MM, Davidson HL, Hart LS, et al. Transcriptomic profiling of 39 commonly-used neuroblastoma cell lines. Sci Data. 2017;4:170033.
152. Valencia-Sama I, Ladumor Y, Kee L, Adderley T, Christopher G, Robinson CM, et al. NRAS Status Determines Sensitivity to SHP2 Inhibitor Combination Therapies Targeting the RAS-MAPK Pathway in Neuroblastoma. Cancer Res. 2020;80(16):3413-23.
153. De Brouwer S, De Preter K, Kumps C, Zabrocki P, Porcu M, Westerhout EM, et al. Meta-analysis of neuroblastomas reveals a skewed ALK mutation spectrum in tumors with MYCN amplification. Clin Cancer Res. 2010;16(17):4353-62.
154. Duijkers FA, Gaal J, Meijerink JP, Admiraal P, Pieters R, de Krijger RR, et al. Anaplastic lymphoma kinase (ALK) inhibitor response in neuroblastoma is highly correlated with ALK mutation status, ALK mRNA and protein levels. Cell Oncol (Dordr). 2011;34(5):409-17.
155. Van Maerken T, Rihani A, Dreidax D, De Clercq S, Yigit N, Marine JC, et al. Functional analysis of the p53 pathway in neuroblastoma cells using the small-molecule MDM2 antagonist nutlin-3. Mol Cancer Ther. 2011;10(6):983-93.
156. Kaghad M, Bonnet H, Yang A, Creancier L, Biscan JC, Valent A, et al. Monoallelically expressed gene related to p53 at 1p36, a region frequently deleted in neuroblastoma and other human cancers. Cell. 1997;90(4):809-19.
157. Rothe G. Technische und methodische Grundlagen der Durchflusszytometrie. In: Sack U.; Tamok A. RG, editor. Zelluläre Diagnostik Grundlagen, Methoden und klinische Anwendungen der Durchflusszytometrie. Basel: Karger; 2007. p. 27-70.
158. Biotec M. MACSQuant Analyzer Instrument specifications [Web Page]. [02.02.2023]. Available from: https://www.miltenyibiotec.com/upload/assets/IM0011348.PDF.
159. Taylor RC, Cullen SP, Martin SJ. Apoptosis: controlled demolition at the cellular level. Nat Rev Mol Cell Biol. 2008;9(3):231-41.
160. Koopman G, Reutelingsperger CP, Kuijten GA, Keehnen RM, Pals ST, van Oers MH. Annexin V for flow cytometric detection of phosphatidylserine expression on B cells undergoing apoptosis. Blood. 1994;84(5):1415-20.
161. Fadok VA, Voelker DR, Campbell PA, Cohen JJ, Bratton DL, Henson PM. Exposure of phosphatidylserine on the surface of apoptotic lymphocytes triggers specific recognition and removal by macrophages. J Immunol. 1992;148(7):2207-16.
162. Vermes I, Haanen C, Steffens-Nakken H, Reutelingsperger C. A novel assay for apoptosis. Flow cytometric detection of phosphatidylserine expression on early apoptotic cells using fluorescein labelled Annexin V. J Immunol Methods. 1995;184(1):39-51.

163. Martin SJ, Reutelingsperger CP, McGahon AJ, Rader JA, van Schie RC, LaFace DM, et al. Early redistribution of plasma membrane phosphatidylserine is a general feature of apoptosis regardless of the initiating stimulus: inhibition by overexpression of Bcl-2 and Abl. J Exp Med. 1995;182(5):1545-56.
164. Biotec M. Fluorescent Dyes [Web Page]. [Available from: https://www.miltenyibiotec.com/DE-en/resources/macs-handbook/macs-technologies/flow-cytometry/fluorescence-dyes.html.
165. Shapiro HM. Practical Flow Cytometry. 4th ed. Hoboken, New Jersey: Wiley & Sons; 2003. 43-4 p.
166. Poon IK, Lucas CD, Rossi AG, Ravichandran KS. Apoptotic cell clearance: basic biology and therapeutic potential. Nat Rev Immunol. 2014;14(3):166-80.
167. Pietkiewicz S, Schmidt JH, Lavrik IN. Quantification of apoptosis and necroptosis at the single cell level by a combination of Imaging Flow Cytometry with classical Annexin V/propidium iodide staining. J Immunol Methods. 2015;423:99-103.
168. Smith PK, Krohn RI, Hermanson GT, Mallia AK, Gartner FH, Provenzano MD, et al. Measurement of protein using bicinchoninic acid. Anal Biochem. 1985;150(1):76-85.
169. Sekulic A, Hudson CC, Homme JL, Yin P, Otterness DM, Karnitz LM, et al. A direct linkage between the phosphoinositide 3-kinase-AKT signaling pathway and the mammalian target of rapamycin in mitogen-stimulated and transformed cells. Cancer Res. 2000;60(13):3504-13.
170. Chiang GG, Abraham RT. Phosphorylation of mammalian target of rapamycin (mTOR) at Ser-2448 is mediated by p70S6 kinase. J Biol Chem. 2005;280(27):25485-90.
171. Wiza C, Nascimento EB, Ouwens DM. Role of PRAS40 in Akt and mTOR signaling in health and disease. Am J Physiol Endocrinol Metab. 2012;302(12):E1453-60.
172. Roux PP, Shahbazian D, Vu H, Holz MK, Cohen MS, Taunton J, et al. RAS/ERK signaling promotes site-specific ribosomal protein S6 phosphorylation via RSK and stimulates cap-dependent translation. J Biol Chem. 2007;282(19):14056-64.
173. Sutherland C, Leighton IA, Cohen P. Inactivation of glycogen synthase kinase-3 beta by phosphorylation: new kinase connections in insulin and growth-factor signalling. Biochem J. 1993;296 ( Pt 1)(Pt 1):15-9.
174. Yang Z, Xie C, Xu W, Liu G, Cao X, Li W, et al. Phosphorylation and inactivation of PTEN at residues Ser380/Thr382/383 induced by Helicobacter pylori promotes gastric epithelial cell survival through PI3K/Akt pathway. Oncotarget. 2015;6(31):31916-26.
175. Levin VA. Basis and importance of Src as a target in cancer. Cancer Treat Res. 2004;119:89-119.
176. McCoy CE, Campbell DG, Deak M, Bloomberg GB, Arthur JS. MSK1 activity is controlled by multiple phosphorylation sites. Biochem J. 2005;387(Pt 2):507-17.
177. Sun B, Li G, Yu Q, Liu D, Tang X. HSP60 in cancer: a promising biomarker for diagnosis and a potentially useful target for treatment. J Drug Target. 2022;30(1):31-45.

178. Sarbassov DD, Ali SM, Sengupta S, Sheen JH, Hsu PP, Bagley AF, et al. Prolonged rapamycin treatment inhibits mTORC2 assembly and Akt/PKB. Mol Cell. 2006;22(2):159-68.
179. Thoreen CC, Kang SA, Chang JW, Liu Q, Zhang J, Gao Y, et al. An ATP-competitive mammalian target of rapamycin inhibitor reveals rapamycin-resistant functions of mTORC1. J Biol Chem. 2009;284(12):8023-32.
180. Choo AY, Yoon SO, Kim SG, Roux PP, Blenis J. Rapamycin differentially inhibits S6Ks and 4E-BP1 to mediate cell-type-specific repression of mRNA translation. Proc Natl Acad Sci U S A. 2008;105(45):17414-9.
181. Feldman ME, Apsel B, Uotila A, Loewith R, Knight ZA, Ruggero D, et al. Active-site inhibitors of mTOR target rapamycin-resistant outputs of mTORC1 and mTORC2. PLoS Biol. 2009;7(2):e38.
182. Kaess C, Matthes M, Gross J, Waetzig R, Heise T, Corbacioglu S, et al. Evaluating the RIST Molecular-Targeted Regimen in a Three-Dimensional Neuroblastoma Spheroid Cell Culture Model. Cancers (Basel). 2023;15(6).
183. Burnett PE, Barrow RK, Cohen NA, Snyder SH, Sabatini DM. RAFT1 phosphorylation of the translational regulators p70 S6 kinase and 4E-BP1. Proc Natl Acad Sci U S A. 1998;95(4):1432-7.
184. O'Reilly KE, Rojo F, She QB, Solit D, Mills GB, Smith D, et al. mTOR inhibition induces upstream receptor tyrosine kinase signaling and activates Akt. Cancer Res. 2006;66(3):1500-8.
185. Zheng Y, Jiang Y. mTOR Inhibitors at a Glance. Mol Cell Pharmacol. 2015;7(2):15-20.
186. Rodrik-Outmezguine VS, Chandarlapaty S, Pagano NC, Poulikakos PI, Scaltriti M, Moskatel E, et al. mTOR kinase inhibition causes feedback-dependent biphasic regulation of AKT signaling. Cancer Discov. 2011;1(3):248-59.
187. Rodrik-Outmezguine VS, Okaniwa M, Yao Z, Novotny CJ, McWhirter C, Banaji A, et al. Overcoming mTOR resistance mutations with a new-generation mTOR inhibitor. Nature. 2016;534(7606):272-6.
188. Fan Q, Aksoy O, Wong RA, Ilkhanizadeh S, Novotny CJ, Gustafson WC, et al. A Kinase Inhibitor Targeted to mTORC1 Drives Regression in Glioblastoma. Cancer Cell. 2017;31(3):424-35.
189. Kuroshima K, Yoshino H, Okamura S, Tsuruda M, Osako Y, Sakaguchi T, et al. Potential new therapy of Rapalink-1, a new generation mammalian target of rapamycin inhibitor, against sunitinib-resistant renal cell carcinoma. Cancer Sci. 2020;111(5):1607-18.
190. Cross DA, Alessi DR, Cohen P, Andjelkovich M, Hemmings BA. Inhibition of glycogen synthase kinase-3 by insulin mediated by protein kinase B. Nature. 1995;378(6559):785-9.
191. Diehl JA, Cheng M, Roussel MF, Sherr CJ. Glycogen synthase kinase-3beta regulates cyclin D1 proteolysis and subcellular localization. Genes Dev. 1998;12(22):3499-511.
192. Peterson RT, Desai BN, Hardwick JS, Schreiber SL. Protein phosphatase 2A interacts with the 70-kDa S6 kinase and is activated by inhibition of FKBP12-rapamycinassociated protein. Proc Natl Acad Sci U S A. 1999;96(8):4438-42.

193. Dong J, Peng J, Zhang H, Mondesire WH, Jian W, Mills GB, et al. Role of glycogen synthase kinase 3beta in rapamycin-mediated cell cycle regulation and chemosensitivity. Cancer Res. 2005;65(5):1961-72.
194. Gera JF, Mellinghoff IK, Shi Y, Rettig MB, Tran C, Hsu JH, et al. AKT activity determines sensitivity to mammalian target of rapamycin (mTOR) inhibitors by regulating cyclin D1 and c-myc expression. J Biol Chem. 2004;279(4):2737-46.
195. Beurel E, Grieco SF, Jope RS. Glycogen synthase kinase-3 (GSK3): regulation, actions, and diseases. Pharmacol Ther. 2015;148:114-31.
196. Duffy DJ, Krstic A, Schwarzl T, Higgins DG, Kolch W. GSK3 inhibitors regulate MYCN mRNA levels and reduce neuroblastoma cell viability through multiple mechanisms, including p53 and Wnt signaling. Mol Cancer Ther. 2014;13(2):454-67.
197. Dickey A, Schleicher S, Leahy K, Hu R, Hallahan D, Thotala DK. GSK-3beta inhibition promotes cell death, apoptosis, and in vivo tumor growth delay in neuroblastoma Neuro-2A cell line. J Neurooncol. 2011;104(1):145-53.
198. Steck PA, Pershouse MA, Jasser SA, Yung WK, Lin H, Ligon AH, et al. Identification of a candidate tumour suppressor gene, MMAC1, at chromosome 10q23.3 that is mutated in multiple advanced cancers. Nat Genet. 1997;15(4):356-62.
199. Li J, Yen C, Liaw D, Podsypanina K, Bose S, Wang SI, et al. PTEN, a putative protein tyrosine phosphatase gene mutated in human brain, breast, and prostate cancer. Science. 1997;275(5308):1943-7.
200. Maehama T, Dixon JE. The tumor suppressor, PTEN/MMAC1, dephosphorylates the lipid second messenger, phosphatidylinositol 3,4,5-trisphosphate. J Biol Chem. 1998;273(22):13375-8.
201. Stambolic V, Suzuki A, de la Pompa JL, Brothers GM, Mirtsos C, Sasaki T, et al. Negative regulation of PKB/Akt-dependent cell survival by the tumor suppressor PTEN. Cell. 1998;95(1):29-39.
202. Vazquez F, Ramaswamy S, Nakamura N, Sellers WR. Phosphorylation of the PTEN tail regulates protein stability and function. Mol Cell Biol. 2000;20(14):5010-8.
203. Vazquez F, Matsuoka S, Sellers WR, Yanagida T, Ueda M, Devreotes PN. Tumor suppressor PTEN acts through dynamic interaction with the plasma membrane. Proc Natl Acad Sci U S A. 2006;103(10):3633-8.
204. Bermudez Brito M, Goulielmaki E, Papakonstanti EA. Focus on PTEN Regulation. Front Oncol. 2015;5:166.
205. Yang Z, Yuan XG, Chen J, Luo SW, Luo ZJ, Lu NH. Reduced expression of PTEN and increased PTEN phosphorylation at residue Ser380 in gastric cancer tissues: a novel mechanism of PTEN inactivation. Clin Res Hepatol Gastroenterol. 2013;37(1):72-9.
206. van Ree JH, Jeganathan KB, Fierro Velasco RO, Zhang C, Can I, Hamada M, et al. Hyperphosphorylated PTEN exerts oncogenic properties. Nat Commun. 2023;14(1):2983.

207. Nakahata S, Ichikawa T, Maneesaay P, Saito Y, Nagai K, Tamura T, et al. Loss of NDRG2 expression activates PI3K-AKT signalling via PTEN phosphorylation in ATLL and other cancers. Nat Commun. 2014;5:3393.
208. Carracedo A, Ma L, Teruya-Feldstein J, Rojo F, Salmena L, Alimonti A, et al. Inhibition of mTORC1 leads to MAPK pathway activation through a PI3K-dependent feedback loop in human cancer. J Clin Invest. 2008;118(9):3065-74.
209. Kim W, Ryu J, Kim JE. CCAR2/DBC1 and Hsp60 Positively Regulate Expression of Survivin in Neuroblastoma Cells. Int J Mol Sci. 2019;20(1).
210. Ghosh JC, Dohi T, Kang BH, Altieri DC. Hsp60 regulation of tumor cell apoptosis. J Biol Chem. 2008;283(8):5188-94.
211. Tang H, Li J, Liu X, Wang G, Luo M, Deng H. Down-regulation of HSP60 Suppresses the Proliferation of Glioblastoma Cells via the ROS/AMPK/mTOR Pathway. Sci Rep. 2016;6:28388.
212. Azuhata T, Scott D, Takamizawa S, Wen J, Davidoff A, Fukuzawa M, et al. The inhibitor of apoptosis protein survivin is associated with high-risk behavior of neuroblastoma. J Pediatr Surg. 2001;36(12):1785-91.
213. Islam A, Kageyama H, Takada N, Kawamoto T, Takayasu H, Isogai E, et al. High expression of Survivin, mapped to 17q25, is significantly associated with poor prognostic factors and promotes cell survival in human neuroblastoma. Oncogene. 2000;19(5):617-23.
214. Chen B, Yuping S, Ni J. Rapamycin decreases survivin expression to induce NSCLC cell apoptosis under hypoxia through inhibiting HIF-1alpha induction. Mol Biol Rep. 2012;39(1):185-91.
215. Kim YS, Jin HO, Seo SK, Woo SH, Choe TB, An S, et al. Sorafenib induces apoptotic cell death in human non-small cell lung cancer cells by down-regulating mammalian target of rapamycin (mTOR)-dependent survivin expression. Biochem Pharmacol. 2011;82(3):216-26.
216. Tabata M, Tsubaki M, Takeda T, Tateishi K, Tsurushima K, Imano M, et al. Dasatinib reverses drug resistance by downregulating MDR1 and Survivin in Burkitt lymphoma cells. BMC Complement Med Ther. 2020;20(1):84.
217. Samkari A, Cooper ZA, Holloway MP, Liu J, Altura RA. Rapamycin induces the anti-apoptotic protein survivin in neuroblastoma. Int J Biochem Mol Biol. 2012;3(1):28-35.
218. Weinstein IB. Cancer. Addiction to oncogenes--the Achilles heal of cancer. Science. 2002;297(5578):63-4.
219. Pugh TJ, Morozova O, Attiyeh EF, Asgharzadeh S, Wei JS, Auclair D, et al. The genetic landscape of high-risk neuroblastoma. Nat Genet. 2013;45(3):279-84.
220. Yu K, Toral-Barza L, Shi C, Zhang WG, Lucas J, Shor B, et al. Biochemical, cellular, and in vivo activity of novel ATP-competitive and selective inhibitors of the mammalian target of rapamycin. Cancer Res. 2009;69(15):6232-40.
221. Bei Y, Bramé L, Kirchner M, Fritsche-Guenther R, Kunz S, Bhattacharya A, et al. Amplicon structure creates collateral therapeutic vulnerability in cancer. bioRxiv. 2022:2022.09.08.506647.

222. Manohar CF, Salwen HR, Brodeur GM, Cohn SL. Co-amplification and concomitant high levels of expression of a DEAD box gene with MYCN in human neuroblastoma. Genes Chromosomes Cancer. 1995;14(3):196-203.
223. Godbout R, Packer M, Bie W. Overexpression of a DEAD box protein (DDX1) in neuroblastoma and retinoblastoma cell lines. J Biol Chem. 1998;273(33):21161-8.
224. George RE, Kenyon RM, McGuckin AG, Malcolm AJ, Pearson AD, Lunec J. Investigation of co-amplification of the candidate genes ornithine decarboxylase, ribonucleotide reductase, syndecan-1 and a DEAD box gene, DDX1, with N-myc in neuroblastoma. United Kingdom Children's Cancer Study Group. Oncogene. 1996;12(7):1583-7.
225. Squire JA, Thorner PS, Weitzman S, Maggi JD, Dirks P, Doyle J, et al. Co-amplification of MYCN and a DEAD box gene (DDX1) in primary neuroblastoma. Oncogene. 1995;10(7):1417-22.
226. Pajtler KW, Sadowski N, Ackermann S, Althoff K, Schonbeck K, Batzke K, et al. The GSK461364 PLK1 inhibitor exhibits strong antitumoral activity in preclinical neuroblastoma models. Oncotarget. 2017;8(4):6730-41.
227. Xiao D, Yue M, Su H, Ren P, Jiang J, Li F, et al. Polo-like Kinase-1 Regulates Myc Stabilization and Activates a Feedforward Circuit Promoting Tumor Cell Survival. Mol Cell. 2016;64(3):493-506.
228. Otto T. MYCN and Its Posttranslational Regulation in Neuroblastoma. In: H C, NM C, editors. Progressive Neuroblastoma: Innovation and Novel Therapeutic Strategies. 20. Basel: Karger; 2015. p. 47-58.
229. Otto T, Horn S, Brockmann M, Eilers U, Schuttrumpf L, Popov N, et al. Stabilization of N-Myc is a critical function of Aurora A in human neuroblastoma. Cancer Cell. 2009;15(1):67-78.
230. Ackermann S, Goeser F, Schulte JH, Schramm A, Ehemann V, Hero B, et al. Polo-like kinase 1 is a therapeutic target in high-risk neuroblastoma. Clin Cancer Res. 2011;17(4):731-41.
231. Wang LL, Teshiba R, Ikegaki N, Tang XX, Naranjo A, London WB, et al. Augmented expression of MYC and/or MYCN protein defines highly aggressive MYC-driven neuroblastoma: a Children's Oncology Group study. Br J Cancer. 2015;113(1):57-63.
232. Wang LL, Suganuma R, Ikegaki N, Tang X, Naranjo A, McGrady P, et al. Neuroblastoma of undifferentiated subtype, prognostic significance of prominent nucleolar formation, and MYC/MYCN protein expression: a report from the Children's Oncology Group. Cancer. 2013;119(20):3718-26.
233. Fredlund E, Ringner M, Maris JM, Pahlman S. High Myc pathway activity and low stage of neuronal differentiation associate with poor outcome in neuroblastoma. Proc Natl Acad Sci U S A. 2008;105(37):14094-9.
234. Westermann F, Muth D, Benner A, Bauer T, Henrich KO, Oberthuer A, et al. Distinct transcriptional MYCN/c-MYC activities are associated with spontaneous regression or malignant progression in neuroblastomas. Genome Biol. 2008;9(10):R150.

235. Zimmerman MW, Liu Y, He S, Durbin AD, Abraham BJ, Easton J, et al. MYC Drives a Subset of High-Risk Pediatric Neuroblastomas and Is Activated through Mechanisms Including Enhancer Hijacking and Focal Enhancer Amplification. Cancer Discov. 2018;8(3):320-35.
236. Liu X, Mazanek P, Dam V, Wang Q, Zhao H, Guo R, et al. Deregulated Wnt/beta-catenin program in high-risk neuroblastomas without MYCN amplification. Oncogene. 2008;27(10):1478-88.
237. Szemes M, Greenhough A, Melegh Z, Malik S, Yuksel A, Catchpoole D, et al. Wnt Signalling Drives Context-Dependent Differentiation or Proliferation in Neuroblastoma. Neoplasia. 2018;20(4):335-50.
238. Duffy DJ, Krstic A, Schwarzl T, Halasz M, Iljin K, Fey D, et al. Wnt signalling is a bi-directional vulnerability of cancer cells. Oncotarget. 2016;7(37):60310-31.
239. Nolan JC, Frawley T, Tighe J, Soh H, Curtin C, Piskareva O. Preclinical models for neuroblastoma: Advances and challenges. Cancer Lett. 2020;474:53-62.
240. Corbacioglu S, Lode HN, Jakob M, Suttorp M, Escherich G, Gruhn B, et al. Irinotecan and temozolomide combined with dasatinib and rapamycin for patients with relapsed or refractory neuroblastoma: Results of the prospective randomized RIST trial. Journal of Clinical Oncology. 2023;41(16_suppl):10001-.

# Acknowledgement

I am extremely grateful to Prof. Dr. Selim Corbacioglu for providing me with this very interesting topic of this thesis and his continuous support. The work on this thesis as well as my work in his department have opened up the world of pediatric oncology to me and have fostered my passion for this very multifaceted, fascinating and incredibly rewarding medical field.

This endeavor would not have been possible without my supervisors Dr. rer. nat. Muriel Malaisé and especially Dr. rer. nat. Gunhild Sommer. I could not have undertaken this journey without their support and guidance throughout this journey. Their trust and guidance have given me the opportunity to understand the work and value of basic scientific research. Their faith and constant encouragement gave me the opportunity and strength to follow this experimental work to the end through all ups and downs, setbacks, and successes. Without Dr. rer. nat. Gunhild Sommer and her unwavering faith in me and this work and her ability to always know when a little extra nudge or extrinsic motivation is needed, I would not be where I am today with this finished thesis before me.

I would like to extend my sincere thanks also to Marie Matthes for introducing me to the basics of laboratory work, always providing me with advice and support and who was always there to troubleshoot any potential lab problems. I would also like to thank Florian Zeman for his insights on biostatistics.

I thank my family for their support throughout this journey. Without the support of my parents, my studies and this doctorate would not have been possible. I also thank my husband and my kids for their endless patience and understanding and their willingness to always make some time in our busy life for me to continue working on this dissertation.

Last but not least I would like to thank my friend Manuela Weps who has been there for me throughout this whole journey – entertaining me throughout countless late-night hours of lab work, providing me with helpful insight and advice and for her constant assurances when I doubted myself.

# Declaration in Lieu of an Oath
# (Eidesstattliche Erklärung)

Ich erkläre hiermit, dass ich die vorliegende Arbeit ohne unzulässige Hilfe Dritter und ohne Benutzung anderer als der angegebenen Hilfsmittel angefertigt habe. Die aus anderen Quellen direkt oder indirekt übernommenen Daten und Konzepte sind unter Angabe der Quelle gekennzeichnet.

Insbesondere habe ich nicht die entgeltliche Hilfe von Vermittlungs- bzw. Beratungsdiensten (Promotionsberater oder andere Personen) in Anspruch genommen. Niemand hat von mir unmittelbar oder mittelbar geldwerte Leistungen für Arbeit erhalten, die im Zusammenhang mit dem Inhalt der vorgelegten Dissertation stehen.

Die Arbeit wurde bisher weder im In- noch im Ausland in gleicher oder ähnlicher Form einer anderen Prüfungsbehörde vorgelegt.

I hereby declare that I have written this thesis without unauthorized assistance from third parties and without the use of any aids other than those specified. Data and concepts taken directly or indirectly from other sources are marked and sources are specified.

In particular, I have not used the paid assistance of any advisory services (doctoral advisors or other persons). No one has directly or indirectly received any monetary benefits for work directly or indirectly related to the content of the dissertation.

The dissertation has not been submitted to another examination authority in the same or a similar form.

Regensburg, 08.01.2024

---

Ort, Datum Unterschrift (Gina Penkivech)